Understanding equine influenza pathogenesis within the respiratory tract of the horse

Andreu Masdefiol Garriga

Submitted in fulfilment of the requirements for the degree of

Doctor of Philosophy in Virology

Sgoil Leighis-sprèidh - School of Veterinary Medicine

Colaiste nan Saidheansan ann an Eòlas-leighis, Leigheas-sprèidh, agus Eolàs na Beatha - College of Medical, Veterinary & Life Sciences

Oilthigh Glaschu - University of Glasgow

June 2023

ABSTRACT

The pathogenesis of equine influenza in the horse has not been studied in depth. Equine influenza is a relevant, highly contagious viral respiratory disease of the horse that has notable sanitary and economic consequences. As a rarely lethal infection, research has not focused on describing lesions and understanding its pathogenesis, but on developing preventive tools (i.e., vaccines).

I used FFPE respiratory sections of EI-infected horses to describe and study viral spread, histological lesions and expression of specific proteins during the course of the infection, and image analysis software to quantify these lesions and immunostaining in sections from experimentally infected individuals stained with H&E and immunomarkers for viral antigens, innate immunity, apoptosis, mitosis, T and B lymphocytes and type II pneumocytes.

The results obtained showed that EIV spread throughout the entire respiratory tract by 2dpi and the viral nucleoprotein was detectable at least until 14dpi, in high amounts in the lung and intrapulmonary airways, including their surrounding smooth muscle and hyaline cartilage. A transient and fast activation of the innate immunity at 3dpi decelerated its spread for a limited time, although it likely contributed to the development of histological changes too, whereas at late timepoints an increase in T lymphocytes was highlighted, with no apparent direct effect on viral levels. Lesions were evident in the airways at 3dpi and became more severe at 7dpi, showing signs of recovery by 14dpi. On the other hand, infected horses developed pneumonia, likely of bacterial origin, that was identifiable at 7dpi, with extensive areas of oedema, inflammation, haemorrhage and type II pneumocyte proliferation that gained extension and severity at 14dpi.

This study showed that the initial disruption of the respiratory epithelia of the airways caused by EIV impairs the mucociliary system, which leads to the accumulation of mucus and debris that ultimately create the conditions for a secondary bacterial pneumonia to be developed.

TABLE OF CONTENTS

FIGURES

TABLES

Publications not included in this thesis:

Elevated temperature inhibits SARS-CoV-2 replication in respiratory epithelium independently of IFN-mediated innate immune defenses. Herder, V., Dee, K., Wojtus, J. K., Epifano, I., Goldfarb, D., Rozario, C., Gu, Q., da Silva Filipe, A., Nomikou, K., Nichols, J., Jarrett, R. F., Stevenson, A., McFarlane, S., Stewart, M. E., Szemiel, A. M., Pinto, R. M., Masdefiol Garriga, A., Davis, C., Allan, J., Graham, S. V., Murcia, P. R., Boutell, C. (2021). ***PLoS Biology*, *19*(12). https://doi.org/10.1371/journal.pbio.3001065**.

Lung influenza virus-specific memory CD4 T cell location and optimal cytokine production are dependent on interactions with lung antigen-presenting cells. Hargrave KE, Worrell JC, Pirillo C, Brennan E, Masdefiol Garriga A, Gray JI, Purnell T, Roberts EW, MacLeod MKL. **Mucosal Immunol. 2024 Jun 6:S1933-0219(24)00050-3. doi: 10.1016/j.mucimm.2024.06.001. Epub ahead of print. PMID: 38851589.**

Acknowledgements

Vull donar les gràcies a la Dra. Pamela Johnston i al Dr. Pablo Murcia, els meus supervisors, per guiar-me durant el desenvolupament del doctorat.

També a tota la gent del CVR que m'ha ajudat en diversos assumptes, com la Lynn Stevenson i el Frazer Bell, del laboratori d'histologia, i el Colin Loney, l"imaging manager" del centre.

Dono les gràcies al Dr. Akihiro Ochi i al Dr. Takashi Yamanaka, del Japan Racing Association, per enviar el material biològic que he necessitat per fer les anàlisis incloses en aquesta tesi, i als companys del grup del Dr. Murcia per a l'ajuda i l'assessorament que m'han donat sobre tècniques de laboratori.

Finalment, als amics que he fet durant aquests anys, el Daniel, l'Elihu, el John, el Julien, el Kieran i la Vanessa, sense els quals el doctorat hauria sigut una experiència molt menys positiva, entretinguda i divertida.

Declaration

I, Andreu Masdefiol, hereby certify that, except where explicit reference is made to the contribution of others, this thesis is the result of my own work and has not been submitted for any other degree at the University of Glasgow or any other institution. I acknowledge that the work undertaken for the completion of this PhD thesis was supported by of the University of Glasgow Vet Fund, with Dr Pamela Johnston as the recipient, and the Horseracing Betting Levy Board small grants funding scheme

Date: 3rd of June 2023

Signature:

Printed name: Andreu Masdefiol Garriga

ABBREVIATIONS

BALT	-	Bronchus-associated lymphoid tissue
BRALT	-	Bronchiole-associated lymphoid tissue
CC3	-	Cleaved caspase 3
CD138	-	Cluster of differentiation 138
CD3	-	Cluster of differentiation 3
CD38	-	Cluster of differentiation 38
CD66b	-	Cluster of differentiation 66b
CD68	-	Cluster of differentiation 68
CIV	-	Canine influenza virus
dpi	-	Day post infection
EI	-	Equine influenza
EID50	-	Egg 50% infectious dose
EIV	-	Equine influenza virus
ERS	-	Endoplasmic reticulum stress
FBS	-	Foetal Bovine Serum
FFPE	-	Formalin fixed paraffin embedded
H&E	-	Haematoxylin and eosin
H_2O	-	Water
HA	-	Haemagglutinin
IAV	-	Influenza A virus
Iba-1	-	Ionized calcium-binding adapter molecule 1
IF	-	Immunofluorescence
IFNγ	-	Gamma interferon
IgG	-	G immunoglobulin
IHC	-	Immunohistochemistry
IL-2	-	Interleukin 2
IL-2	-	Interleukin 4
ISH	-	In-situ hybridization
Log10	-	Logarithm base 10
LTALT	-	Laryngo-tracheal associated lymphoid tissue
M1	-	Matrix 1 protein
M2	-	Matrix 2 protein
MALT	-	Mucosa-associated lymphoid tissue
mRNA	-	Messenger RNA
MX1	-	Myxovirus resistance 1
NA	-	Neuraminidase
NALT	-	Nose-associated lymphoid tissue
NE	-	Neutrophil elastase
NP	-	Nucleoprotein
NS1	-	Non-structural protein 1
NS2	-	Non-structural protein 2
ºC	-	Degree Celsius

PA	-	Polymerase acidic
PA-X	-	Polymerase acidic-X
PAS	-	Periodic Acid Schiff
PAX5	-	Paired box gene 5
PB1	-	Polymerase basic protein 1
PB2	-	Polymerase basic protein 2
PBS	-	Phosphate buffered saline
PCNA	-	Proliferation cell nuclear antigen
PCR	-	Polymerase chain reaction
pi	-	Post infection
RNA	-	Ribonucleic acid
SARS-CoV-2	-	Severe acute respiratory syndrome coronavirus 2
TNF	-	Tumor necrosis factor
TNF-α	-	Tumor necrosis factor alfa
µL	-	Microliters

Chapter 1. Introduction

1.1 Generalities

Influenza viruses belong to the *Orthomyxoviridae* family, which is subgrouped into nine different genera: A (*Alphainfluenzavirus*), B (*Betainfluenzavirus*), C (*Gammainfluenzavirus*) and D (*Deltainfluenzavirus*), together with *Isavirus*, *Thogotovirus, Sardinovirus, Mykissvirus* and *Quaranjavirus* (ICTV, 2021). The first four genera infect mammals and birds, whereas *Isavirus* infect salmon (Raynard *et al*., 2001), *Sardinovirus* and *Mykissvirus* infect fish (ICTV, 2021), *Thogotoviruses* infect vertebrates and invertebrates (Jones and Nuttall, 1989) and *Quaranjaviruses* infect birds and invertebrates (Sameroff *et al*., 2021).

Orthomyxoviruses are spherical, sometimes filamentous, and range between 80 and 120 nanometers of diameter, containing negative sense, single stranded ribonucleic acid (RNA). Viral particles contain variable numbers of segments of RNA, depending on their genus: A and B influenza virus, *Mykissvirus*, *Sardinavirus* and *Isavirus* have eight, influenza C and D have seven and *Thogotovirus* and *Quaranjavirus* have six (ICTV, 2021, 2020). Equine influenza virus (EIV), the subject study of this thesis, belongs to the genera *Alphainfluenzavirus*, or influenza A virus (IAV).

Influenza A viruses are classified in subtypes depending on two of the surface proteins they carry, haemagglutinin (HA) and neuraminidase (NA), which can also have different subtypes. So far, 18 subtypes of NA and 11 of HA have been identified (CDC, 2019). Subtypes take the name of the combination of HA and NA they have. For example, if a virus carries a HA 2 protein and a NA 4 protein, it will be called A(H2N4). The nomenclature for each specific is completed with the species of the origin host, the place where the virus was isolated, the strain number and the year it was isolated. In the case of the virus used to infect the horses studied in this thesis, its complete name is A/equine/Ibaraki/1/2007(H3N8), although considering that only one subtype of equine influenza is circulating nowadays, the HA and NA combination is usually removed (CDC, 2019). Apart from HA and NA, the IAV genome encodes for several additional proteins: NP (nucleoprotein), M1 and M2 (matrix 1 and 2), NS1 and NS2 (non-structural 1 and 2) and PB1, PB2 and PA (polymerase basic 1, polymerase basic 2 and polymerase acidic). As said, IAVs include the etiological agent of equine influenza (EI), but also for influenza affecting other species, such as the dog (Klivleyeva *et al*., 2022a), the pig (Van Epps, 2006), the ferret, seals (Lang *et al*., 1981), mink, camels, cats, horses, donkeys, whales (Parrish and Kawaoka, 2005) and several birds (Perroncito, 1878), including waterfowl wild populations, especially those belonging to

Anseriformes and *Charadriiformes* orders, which are considered the main reservoirs (Easterday *et al*., 1968; Hinshaw *et al*., 1980). Humans are also affected by IAV, which include the influenza viruses that cause the annual flu and also flu pandemics, such as the "Spanish flu", in 1918, and the 2009 swine flu pandemic (Berche, 2022).

1.2 History of equine influenza

Equine influenza is the disease caused by equine influenza virus. It can be caused by at least two subtypes: H7N7 and H3N8. The first, commonly known as equine 1 virus, was isolated in Prague, in the former Czechoslovakia, in 1956, during a severe epidemic of a influenza-like disease, and was called A-equi/Praha/56 (Tumova and Fiserova-Sovinova, 1959). Regarding H3N8, or equine 2 virus, it was first isolated in Miami (United States of America) in 1963, during an outbreak in thoroughbreds imported from Argentina and called A2-equi/Miami/63 (Scholtens *et al*., 1964). Nevertheless, records of epidemics of "influenza" existed before 1956 and 1963. Doctor George Fleming described in (Fleming, 1891) several records of influenza causing disease in horses after or during human influenza outbreaks during the 18th and 19th centuries and pointed to a "serious and wide-spread disease among horses" in Yemen in 1328 as a possible EI outbreak. Morens and Taubenberger, in their review from 2010, pulled this first time further back to 1299, when it was documented that, at the same time a human influenza epidemic was spreading around Europe, an equine epizootic was seen, with horses infected "carrying his head drooping, eating nothing and running from the eyes" (Morens and Taubenberger, 2010). They also mention in their review several older claimed cases, like the one described in Homer's *The Iliad*, in which horses, dogs and men would have been affected by a 9-day long epidemic at the beginning of the Trojan War (around 1194 BC). This outbreak has been considered to be produced by influenza by some 19th and 20th century observers. Another interesting one is the case of the veterinary physician Absyrtus, who described a claimed equine influenza epizootic in 330. Both cases, though, have to be considered cautiously, given the lack of details and description of the symptoms and epidemiological characteristics. After the first fairly documented episode that nowadays could be explained by equine influenza, in 1299, equine influenza outbreak descriptions have been found throughout the history, often linked to human influenza epidemics. In 1989, an important outbreak, caused by a virus distantly related to the equine influenza H3N8 that was circulating by that time, was described in Jilin, People's Republic of China, involving equine herds in which the mortality was around 20%. This new Equine/Jilin/89 (H3N8) was attributed to have avian origin (Guo *et al*., 1992). Nowadays, equine influenza has been described in the entire world, with the exception of

New Zealand and Iceland, and is only absent in these two countries plus Australia (American Association of Equine Practitioners, 2017). However, only H3N8 still circulates, since H7N7 was isolated for the last time in 1980 and, thus, is considered to be extinct (Lewis *et al*., 2011; Webster, 1993).

As explained, Australia is considered at the moment a country where equine influenza is eradicated, although cases of the disease were reported once, in 2007. In August of that year, thirteen horses travelled to the country from Japan and shortly after, once in the quarantine facilities, some of them started showing pyrexia and respiratory symptoms. They were sampled and diagnosed of equine influenza by polymerase chain reaction (PCR). Some days after, EI was diagnosed outside of the quarantine premises, and after that it was found that the virus was widely distributed across two Australian states, New South Wales and Queensland (Watson *et al*., 2011). However, strict measures, such as movement restrictions and vaccination campaigns, were implemented to eradicate the virus, which was achieved in December 2007 (Cowled *et al*., 2009; Watson *et al*., 2011). The overall result of the outbreak were 70,000 horses infected (Sack *et al*., 2019), 150,000 vaccinated (Watson *et al*., 2011) and hundreds of millions (if not billions) of dollars of economic impact (Smyth *et al*., 2011). In Japan, very few days before some horses housed in quarantine facilities in Australia started showing respiratory symptoms (August 2007), nineteen horses stabled in 4 four different facilities showed acute pyrexia, and twelve of those were diagnosed for equine influenza some days after. Restriction of movements and massive testing of new febrile cases followed the positive detection, resulting in a rapid decrease in the number of new cases and the partial reopening of horse movements by early September 2007 (Yamanaka *et al*., 2008). The fact that Japan was not considered an EI-free country, differently from Australia, meant that vaccination was mandatory, which, together with containing measures, such as isolation of positive cases, quarantine of exposed animals and restriction of movements, resulted in a great reduction of the spread of the disease (Nishiura and Satou, 2010).

1.3 Epidemiology and clinical signs

EI is a respiratory disease that affects horses, but also donkeys and mules, causing sudden outbreaks in susceptible populations, affecting near 100% of the animals. It spreads by aerosols produced by cough and sneezes from infected individuals, wind, fomites and close contact between individuals (Myers and Wilson, 2006). The incubation period lasts between one and three days after the infection, although from the first day after infection virus can be detected in nasal secretions, whereas viremia can happen but is a rare finding (Myers and

Wilson, 2006). Shedding of virus lasts from five to ten days (Daly M. *et al*., 2004; Donis, 2017; Paillot *et al*., 2013; Radostits *et al*., 2003; Wattrang *et al*., 2003; Yamanaka *et al*., 2009). The initial symptomatology, which in uncomplicated cases will last for 1 to 5 days, includes sudden pyrexia, often biphasic, ranging between 39.1°C and 41.7°C (Mumford *et al*., 1990), anorexia and depression, as well as respiratory signs, such as nasal discharge and a distinctive nonproductive dry cough. Other less common signs after EI infection are epiphora, submandibular adenopathy, congestion of the conjunctival and nasal mucosa, tachycardia and tachypnea, muscle pain and limb oedema (Muranaka *et al*., 2012; Myers and Wilson, 2006). In case of viremia, signs can include myositis, myocarditis and encephalitis (Myers and Wilson, 2006). Although it has been studied, no EIV has been observed infecting the central nervous system. Similarly, neurological symptomatology has been seen in horses with equine influenza, although no evidence to make a clear link between the disease and the symptomatology that infected individuals displayed has been found (Daly *et al*., 2006). Complicated cases are more common in young foals and non-immunocompetent adults, and are characterized by the presence of pneumonia, normally caused by opportunistic bacteria like *Staphylococcus aureus, Haemophilus influenzae* and *Streptococcus zooepidemicus*. Horses that develop bacterial pneumonia display fever (second phase), wheezes and crackles on thoracic auscultation, increased respiratory effort, anxiety and reluctance to move, and, in especially severe cases, mainly foals and young adults, might die (Begg *et al*., 2011; Muranaka *et al*., 2012; Myers and Wilson, 2006; Patterson-Kane *et al*., 2008). In normal conditions, as explained, symptomatology can last for up to five days, with the exception of the cough, which can take between one and three weeks to disappear completely. On the other hand, the recovery has to consist in strict rest, for as many weeks as days of fever the animal had (Myers and Wilson, 2006), in a space with good ventilation. In case of racehorses, training can be reintroduced little by little (Dionísio *et al*., 2021).

1.4 Economic impact

Equine influenza is a notifiable disease of the World Organization for Animal Health – WOAH (formerly Organisation Internationale des Épizooties – OIE) list of diseases, which illustrates its importance. This list includes animal diseases of international concern and obligates countries to report any cases detected, as well as give annual information about the status of the disease in their territories. Furthermore, in the case of equine influenza, it gives recommendations about how to safely import horses from other countries and how to treat horse meat, as well as setting standards for diagnostic tests and vaccines (OIE-WOAH,

2011). Although regulations vary depending on the country, the standard measures in response to an EI outbreak are normally isolation of confirmed and suspected cases, restriction of movements and vaccination (or booster) (Equiflunet, 2022; OIE-WOAH, 2011). As said, equine influenza is rarely a life threat for healthy horses, and least of all for those who have received a vaccine. However, aforementioned measures to fight against the spread of EIV have a financial impact. As an example, the 2007's EI outbreak in Australia, in which 70,000 horses were infected between August and December, had an impact of 381 million Australian dollars, summing lack of income due to the cancellation of events, veterinary expenses and losses produced by animal deaths (Smyth *et al*., 2011). In 2019 Europe experienced several EI outbreaks, in France, Belgium, Germany and the UK (Paillot *et al*., 2019). In Great Britain, at least 412 animals were infected in 234 different equine facilities, causing the cancellation of different horse races and gatherings during February of that year (Whitlock *et al*., 2023).

1.5 The equine respiratory tract

1.5.1 Anatomy

The respiratory tract of the horse, similarly to the other mammals, is composed by a succession of tissues and organs, starting from the nasal cavity and ending in the alveoli, which are found in the lung. Its main function is to supply of oxygen to the blood circulation, by conducting the air from outside of the body to the alveoli and, once there, do the gas exchange, to allow the oxygen to enter the bloodstream and the carbon dioxide to leave it and be exhaled. Furthermore, in the respiratory tract, especially in the nasal cavity and the trachea, the inhaled air is warmed up, humidified and filtered, before continuing its way to the lung (Davis *et al*., 2006, 2002). Anatomically, the respiratory tract of the horse is divided into two main parts, the upper respiratory tract, including the nasal cavity, the pharynx and the larynx, and the lower respiratory tract, with the trachea and the lung within it.

Since horses are known to be one of the few mammals that are obligate nasal breathers, the oral airflow is very scarce (Holcombe *et al*., 2007). The nasal cavity is preceded by the nares, the nasal vestibule and the nasal valve, and its function is to humidify and warm the inhaled air. Caudally, after the nasal cavity, the respiratory tract continues with the pharynx, which connects the former with the oral cavity and the larynx. For this reason, it is anatomically divided into three regions: the nasopharynx, as the continuation of the nasal cavity, and the oropharynx, as the continuation of the oral cavity, divided by the soft palate, and the

laryngopharynx, which is the most caudal part and leads to the larynx. A particularity of *Equidae* is the existence of a pair of diverticulae of the Eustachian tubes (those that connect the middle ear with the pharynx) called guttural pouches, which are known to have important structures such as cranial nerves and blood vessels, although their function is under discussion.

Regarding the larynx, it is the continuation of the pharynx, and consists of a cartilaginous structure formed by four cartilages (epiglottis, thyroid, cricoid and arytenoid) and different muscles and ligaments that stabilize and move it. The most cranial cartilage is the epiglottis, which is positioned in the center of the tract and it blocks the larynx during swallowing, preventing food and water from going to the trachea. Forming the sides and the floor of the larynx, and caudally to the epiglottis, the thyroid cartilage can be found, covered by the arytenoid cartilages, 2 in total, which form the ceiling of the larynx. Finally, further caudally, and surrounding the cranial edge of the trachea, resides the cricoid cartilage (Caswell and Williams, 2007; König and Liebich, 2008).

The lower respiratory tract starts with the trachea, a flexible tube of 70 to 80 centimeters of length and between 3 and 4 of diameter (Carstens *et al*., 2009) which communicates the upper respiratory tract with the primary bronchi. It is supported by C-shaped hyaline cartilage rings (in a number between 48 and 60) and smooth muscle that closes the gap between the two ends of the ring. These originate from the lowest part of the trachea, in the carina, and continue to the two lungs, left and right, and further branch once inside of these, at the same time their diameter decreases, becoming segmental bronchi, bronchioles and terminal bronchioles before arriving to the lung parenchyma, where the oxygen will enter the blood circulation (König and Liebich, 2008). Lungs are covered by a thick serous membrane that reduces the friction between these and the thoracic wall during respiration, called pleura (Caswell and Williams, 2007), and divided into lobes, although in the case of the horse there is no evident anatomical delimitation among them. The left lung has an apical (cranial) and a diaphragmatic (caudal) lobe, whereas the right lung has, in addition to the two mentioned, an accessory lobe (Budras, *et al*., 2011; Lekeux, *et al*., 2014).

1.5.2 Histology

1.5.2.1 Nasal cavity

From rostral to caudal, the nasal cavity has 4 different epithelial types (stratified squamous, transitional, respiratory and olfactory) that seat on a basal membrane and a submucosa, which has mucus-producing glands, blood vessels, nose-associated lymphoid tissue (NALT) patches and innervation.

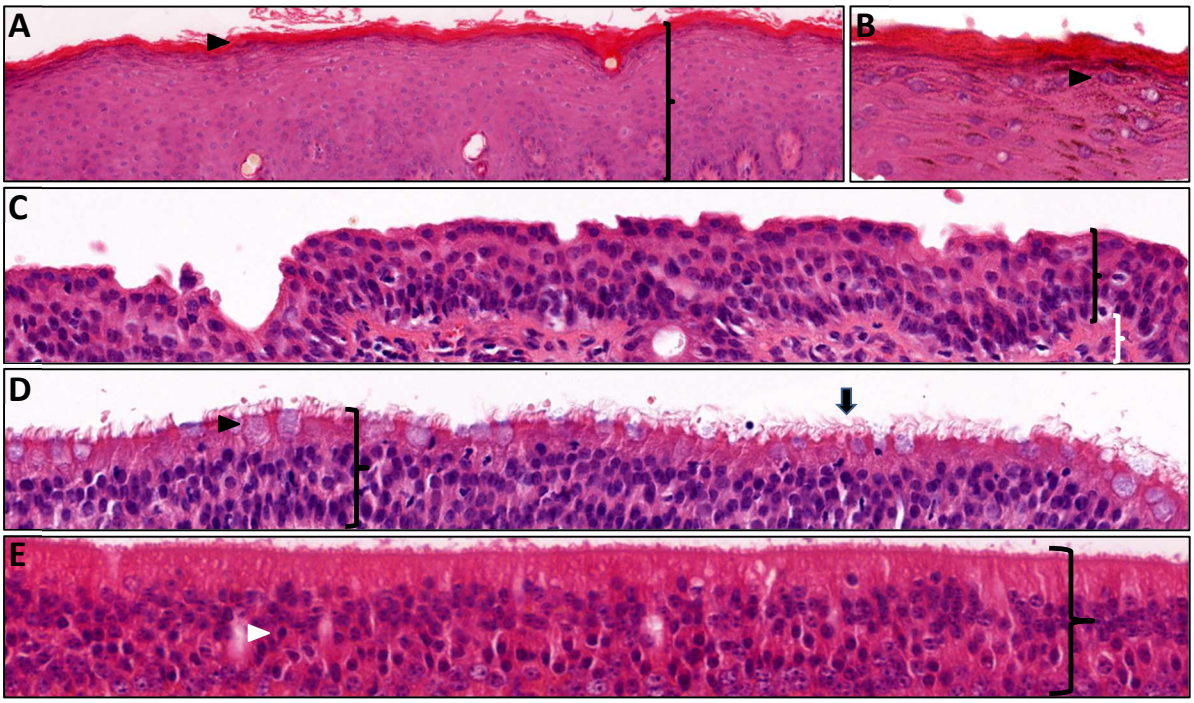

Figure 1-1: Representative images of the four epithelial types in the nasal cavity, stained with H&E (**A**) Stratified squamous epithelium. 15x. Arrowhead shows keratinized cells in the surface. Brace shows the thickness of the epithelium. (**B**) Magnification of (**A**). 25x. Arrowhead shows a squamous epithelial cell. (**C**) Transitional epithelium. Black brace shows the epithelium, white brace shows the submucosa. 25x. (**D**) Respiratory epithelium, with goblet cells (arrowhead) and cilia (arrow). Brace shows the thickness of the epithelium. 25x. (**E**) Olfactory epithelium, populated by olfactory receptor neurons (arrowhead). Brace shows the thickness of the epithelium. 25x.

The stratified squamous epithelium is the most rostral, and it covers the entrance of the nasal cavity. It is formed by layers of epithelial cells, that become flatter and keratinized while they get closer to the surface (Scherzad *et al*., 2019). As its name suggests, the transitional epithelium has a combination of characteristics from both the stratified squamous and the respiratory epithelia. It is located caudal to the former, and it is made of non-ciliated cuboidal to columnar cells. Caudally, the nasal cavity is covered by the respiratory epithelium and its main features are a pseudostratified columnar structure resting on a basal membrane, and presence of ciliated and goblet cells (Caswell and Williams, 2007). Goblet cells are secretory cells which produce mucins, a constituent of the mucus, whereas ciliated cells possess cilia, between 200 and 300 per cell, that beat synchronously. Together, they compose the

mucocilliary system, which is responsible for clearing pathogens and debris present in the inner surface of the respiratory tract (Tilley *et al*., 2015). Finally, the caudal and caudodorsal nasal cavity is lined by the olfactory epithelium, which is mainly made of neurons that transduce the olfactory information and supporting cells (Purves *et al*., 2001) (**Fig. 1-1**).

1.5.2.2 Nasopharynx and larynx

The nasopharynx is lined by three epithelial types that also cover the nasal cavity. These are the stratified squamous epithelium, the transitional epithelium and respiratory epithelium, with alike characteristics to those seen in the nasal cavity (Ali, 1965). Similarly, in the larynx two of these types alternate depending on the location; the stratified squamous epithelium and the respiratory epithelium (Caswell and Williams, 2007).

1.5.2.3 Trachea

The entire trachea is lined by respiratory epithelium. In the submucosa, abundant seromucous tubular glands can be found, as well as laryngo-tracheal associated lymphoid tissue (LTALT) (Mair *et al*., 1987).

1.5.2.4 Bronchi

As a continuation of the trachea, bronchi are also covered by respiratory epithelium. After a submucosa where bronchus-associated lymphoid tissue (BALT) is scarce (Mair *et al*., 1987), bronchi are surrounded by smooth muscle fibers and eccentrically by overlaying C-shaped pieces of hyaline cartilage. As bronchi branch and lose diameter, the amount and thickness of these cartilage rings decrease, as it does the number of ciliated and goblet cells in the surface of the respiratory epithelium (West and Luks, 2016).

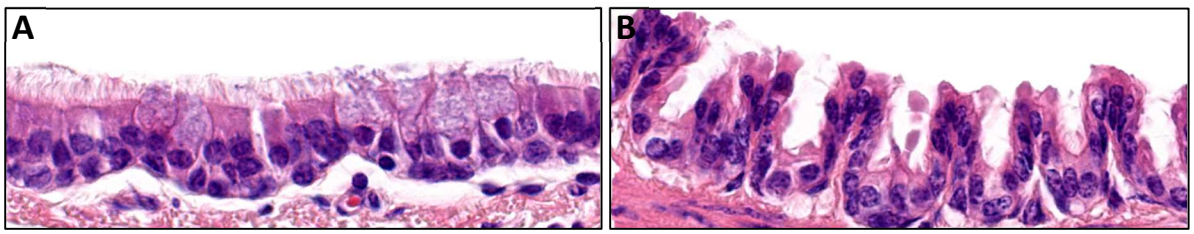

Figure 1-2: Representative images of bronchi stained with H&E. (**A**) Big bronchus (3 millimetres of diameter). (**B**) Small bronchus (150 micrometres of diameter). Note the difference in the amount of goblet cells and cilia. 30x.

1.5.2.5 Bronchioles

Bronchioles are the continuation of bronchi, although they have their specific characteristics. First of all, they lack hyaline cartilage surrounding them. Furthermore, their respiratory epithelium, which has now become cuboidal, is populated by club cells (formerly Clara cells), a unique bronchiole cell type that replaces goblet cells and develops stem cell, secretory and protective functions, among others (Khan and Lynch, 2019; Reynaud *et al*., 2021) (**Fig. 1-3**). Under the respiratory epithelia is common to find lymphoid aggregates, which in this location are called bronchiole associated lymphoid tissue (BRALT) (Mair *et al*., 1987). Within the bronchioles, those that are located in the most distal part of the conducting area of the respiratory tract are called terminal bronchioles.

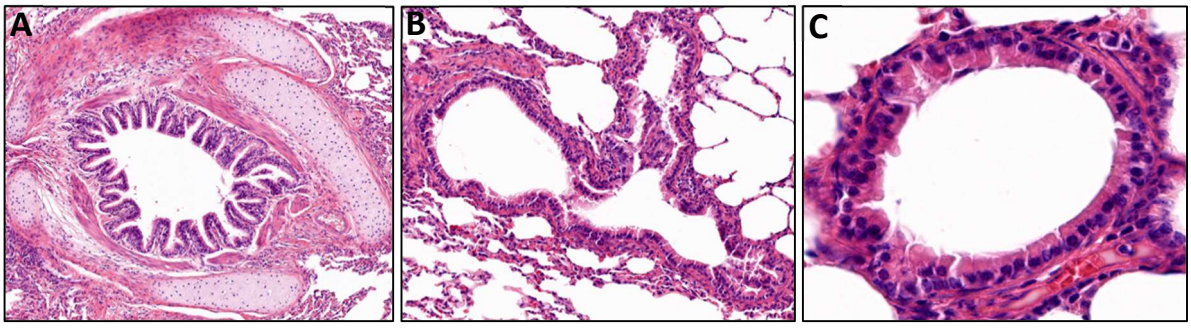

Figure 1-3: Representative images of intrapulmonary airways stained with H&E Note the difference between bronchi (A,10x) and bronchioles (B, 10x). (C) Image of a bronchiole stained with H&E. The cuboidal respiratory epithelium and the lack of goblet cells and hyaline cartilage can be seen in the bronchioles. 25x.

After the terminal bronchioles, the equine respiratory tract continues with the respiratory bronchioles, which are poorly developed compared to other mammals (Mclaughlin *et al*., 1961). Respiratory bronchioles are transitional areas between the non-respiratory terminal bronchioles and the alveoli, with the particularity that they include alveolar niches that emerge from their walls (**Fig. 1-4**).

1.5.2.6 Alveoli

The alveoli are the basic unit of gas exchange, in other words, where the inhaled oxygen enters the bloodstream and the carbon dioxide produced by the organism leaves it. The air is conducted from the respiratory bronchioles through the alveolar ducts to the alveoli, which are grouped in alveolar sacs (**Fig. 1-4**) (Caswell and Williams, 2007). As a highly specialized tissue, alveoli are populated by unique cell types, such as type I and type II pneumocytes. Type I pneumocytes are squamous cells that represent around 40% of the lining cells of the alveoli, although, thanks to their thin and extensive cytoplasm, they

cover at least 90% of the alveolar surface (Flieder, 2018). Their function is to facilitate the gas exchange.

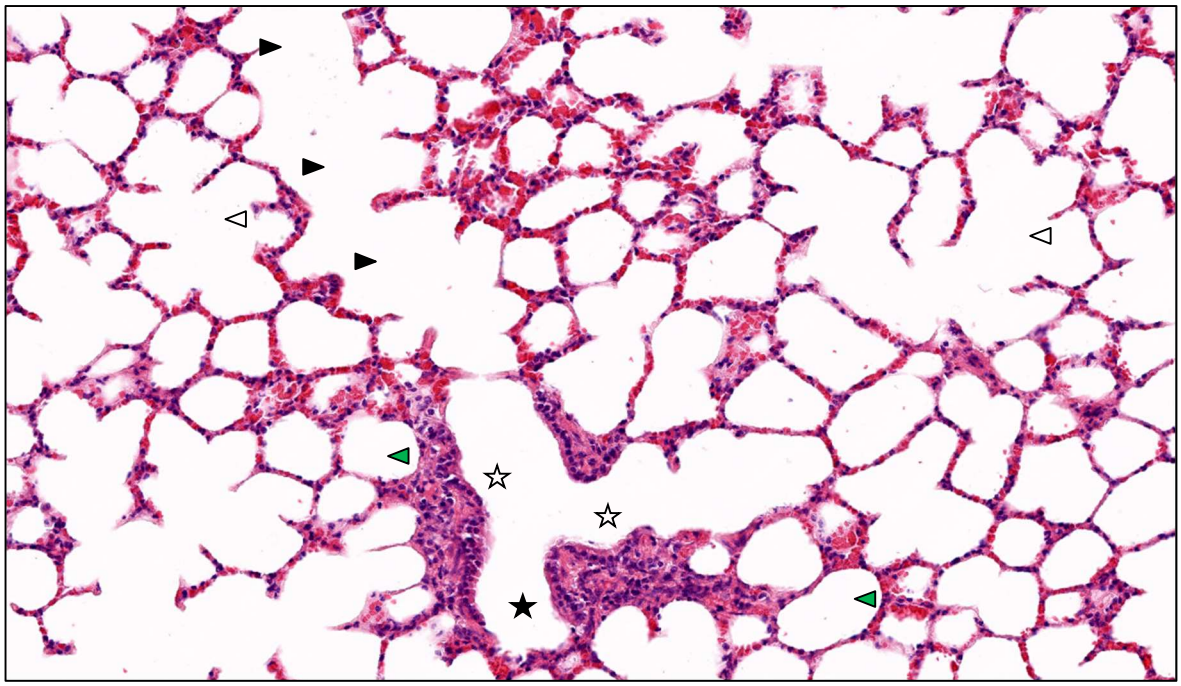

Figure 1-4: Landscape image of the equine lung architecture, stained with H&E. Black star shows a terminal bronchiole. White stars show respiratory bronchioles. Black arrowheads show an alveolar duct. White arrowheads show alveolar sacs. Green arrowheads show alveoli. 15x.

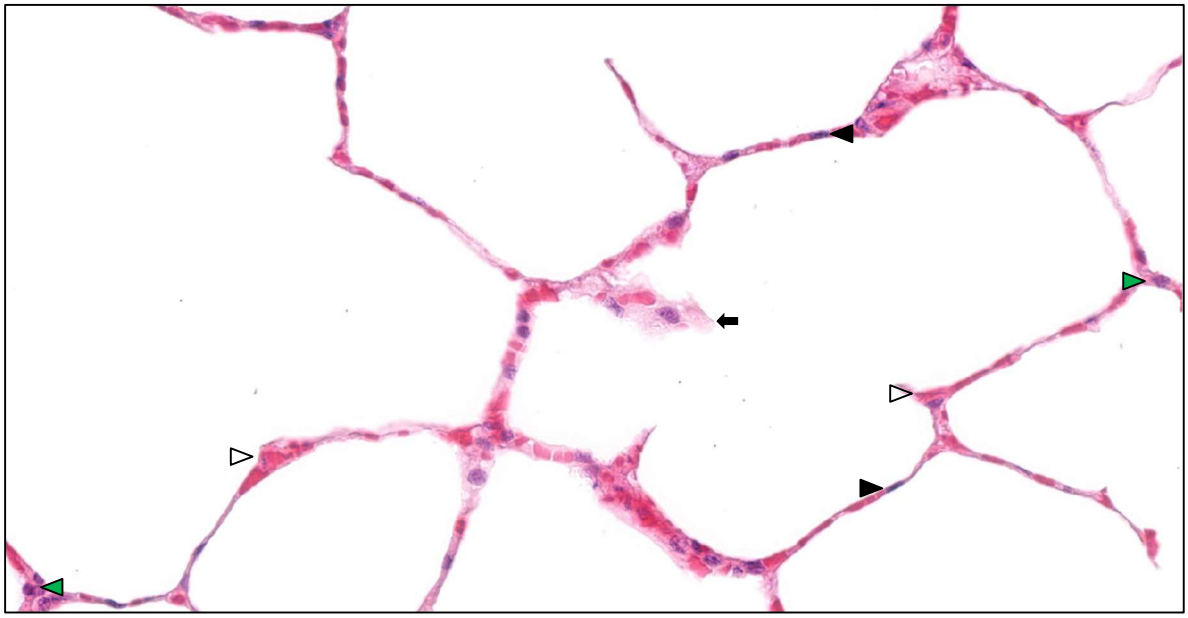

Figure 1-5: Landscape image of the equine lung architecture, stained with H&E. Black arrowheads show type I pneumocytes. White arrowheads show alveolar capillaries. Green arrowheads show type II pneumocytes. Black arrow shows an alveolar macrophage. 25x.

On the other hand, type II pneumocytes act as alveolar progenitor cells (since type I pneumocytes cannot divide) and secrete surfactant, which prevents the lung collapse during breathing, that they store in their lamellar bodies, located in the cytoplasm (Caswell and Williams, 2007). They represent the remaining 60% of the alveolar lining cells, although they cover less than 10% of its surface, being usually found in corners of the alveoli or

between capillaries. Type II pneumocytes have a characteristic cuboidal shape and basophilic round nucleus (Flieder, 2018). Another cell type of the alveoli are the alveolar macrophages, which phagocyte foreign particles and bacteria (**Fig. 1-5**).

The alveolar architecture is completed by alveolar capillaries, which supply blood to the lung parenchyma, and the interstitium, mainly populated by support cells, such as fibroblasts, myofibroblasts and pericytes, immunity cells, such as mast cells and histiocytes, and nerve terminals (Corrin and Nicholson, 2011; Takizawa *et al*., 1965).

1.6 Equine influenza pathogenesis

EIV is a pneumotropic virus which affects the upper and lower respiratory tract's respiratory epithelia. It infects and kills ciliated cells, where it also replicates, causing the impairment of the mucocilliary system, which leads to the lack of ability to clear foreign particles from the respiratory tract (Singh *et al*., 2018; van Maanen and Cullinane, 2002). The cell death pathway described as the one normally EIV induces is apoptosis (Hinshaw *et al*., 1994; Lam *et al*., 2008), although some authors have argued this statement (Liu *et al*., 2010; Zhirnov *et al*., 2002). The main lesions observed in this stage are epithelial degeneration, with loss of cilia and goblet cells, epithelial infiltration of inflammatory cells and hyperplasia and squamous metaplasia of the respiratory epithelia of the airways.

In uncomplicated cases these pathological alterations lead to a mild general and respiratory symptomatology, which lasts a few days. However, if the infection develops, which might occur depending on different factors, such as the animal's age, vaccination or natural exposure history and environmental factors (Timoney, 1996), the damage produced in the airways increases; the virus causes upregulation of the production of toxins, inducing epithelial and immunitary cells to necrosis (Conenello and Palese, 2007; Iverson *et al*., 2011). As a pro-inflammatory cell death pathway, necrosis triggers a cytokine storm which ultimately leads to host inflammation and tissular damage (Rock and Kono, 2007). Under these circumstances, the likelihood of individuals developing a pathological secondary bacterial infection increases. Secondary bacterial processes in horses infected with equine influenza are a common observation (Timoney, 1996), as they are in other species, such as humans (Morris *et al*., 2017), and they are usually produced by *Streptococcus zooepidemicus, Staphylococcus aureus,* or *Bacteroides/Actinobacillus*/*Pasteurella* spp (Gerber, 1970; López and Martinson, 2017), although not all of them produce pathological alterations that lead to the worsening of the symptomatology. Main risk factors for developing them are impaired immunitary mechanisms and lack of previous exposure to the

virus (López and Martinson, 2017; Timoney, 1996). In these cases, the main lesions are found in the lung, which develops a bronchopneumonia that leads, as explained, to a second wave of fever and an increase of intensity and variety of respiratory symptoms. As described by Begg *et al*. in 2007 and by Patterson-Kane *et al*. in 2008 on horses that died after being infected by equine influenza during the 2007's outbreak in Australia, bacterial bronchopneumonia (sometimes involving the alveolar interstitium) was the main finding in the lung. Hyperplasia, degeneration, necrosis, squamous metaplasia and neutrophilic infiltration of the respiratory epithelia of the intrapulmonary airways, with cell debris and mucus blocking their lumina, were reported, as well as alveolar necrosis and neutrophilic infiltration, fibrin exudation and type II pneumocyte proliferation (Begg *et al*., 2011; Patterson-Kane *et al*., 2008). Similarly, in their work with horses experimentally infected with equine influenza, Muranaka *et al*. described, in horses euthanized during the second febrile episode, degeneration, hyperplasia and squamous metaplasia of the respiratory epithelia of the airways, with frequent lymphocytes and neutrophils infiltrating them, and pulmonary oedema and haemorrhage, inflammatory infiltration and proliferation of type II pneumocytes in the alveoli (Muranaka *et al*., 2012).

1.7 Lesions described in tissues infected with EIV

Histological changes in response to EIV have been comprehensively described, as explained above. In this section, I used tissues derived from (Muranaka *et al*., 2012; Yamanaka *et al*., 2009) to illustrate the most commonly described lesions upon Equine Influenza infection in the literature.

1.7.1 Loss of cilia and goblet cells

As explained, cilia are present in the apical surface of ciliated cells. These are one of the main components of the respiratory epithelium of the airways of the horse. Their function is to move in a coordinated fashion to transport mucus rostrally to the nasopharynx. Loss of cilia and goblet cells is a specific lesion of influenza, as epithelial cells of the respiratory epithelium cells are the main target of EIV and many other influenza A viruses, and infection results in ciliostasis and cell lysis (Singh *et al*., 2018). Figure 3-1A shows a tracheal respiratory epithelium from an uninfected horse with cilia on its surface, as the black arrow shows, and Figure 3-1B shows a tracheal respiratory epithelium from a horse infected and euthanized at 7dpi without cilia. Goblet cells are another important cell type of the respiratory epithelium. They produce and secrete mucins, which are one of the central

components of the mucus. Due to their high mucin content, goblet cells are differentially stained with Periodic Acid Schiff (PAS) staining, which dyes them in dark pink (McManus, 1946). Goblet cells are also a target for influenza viruses (Van Riel *et al*., 2010) as both loss of cilia and loss of goblet cells have been described in horses infected with EI from the first stages of the disease, their reduction in numbers is considered a consequence of the direct effect of the virus on the respiratory epithelium of the airways. (Muranaka *et al*., 2012). In other species, the loss of cilia and goblet cells is well documented. For example, in dogs experimentally infected with canine H3N2, it is described to be especially severe between days 3 and 9 post infection (Jung *et al*., 2010), during the peak of viral shedding and after it (Song *et al*., 2008; Tangwangvivat *et al*., 2022). In air-liquid interface cultures of porcine airway epithelial cells experimentally infected with different human pandemic 2009 H1N1 strains, Fu *et al*. observed variable, sometimes severe, loss of the cilia coverage at day 8 post infection, although this was not correlated with the viral load at that time (Fu *et al*., 2019). Wu *et al*. experimentally infected porcine airway epithelial cell cultures with two different swine influenza viruses, a H1N1 and a H3N2, and determined that the loss of cilia coverage was around 80% in both infections, at 8dpi, when the virus loads were high and increasing (Wu *et al*., 2016).

Figure 1-6C and D display differences in the presence and distribution of goblet cells in uninfected (C) and infected (D) tracheas.

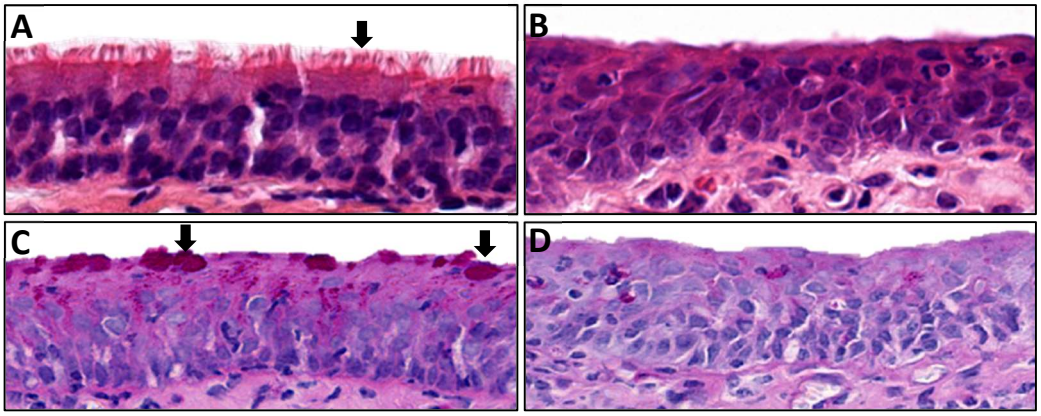

Figure 1-6*:* Representative images of trachea sections stained with H&E and PAS. Control (**A**) and 7dpi infected (**B**) horses showing loss of cilia (H&E). Black arrow shows cilia. Control (**C**) and 7dpi infected (**D**) horses showing loss of goblet cells (PAS). Black arrows show goblet cells, stained in dark pink. 25x.

1.7.2 Epithelial degeneration/necrosis

Degeneration either refers to a process by which a tissue degrades and loses functional activity, being eventually replaced by other types of tissue, or to the condition that this process has made on a tissue.

Regarding necrosis, although the word has another meaning when referred to a cell death pathway, at tissue/organ level it describes the death of a large number of cells (Aster *et al*., 2015a; Majno and Joris, 2004; Stevens *et al*., 2009; Woolf, 1998a).

The presence of epithelia undergoing degeneration and/or necrosis is a consequence of the aforementioned influenza tropism for the respiratory epithelium and, in the tissues I studied was common and observable during all the timepoints in which animals were euthanised and necropsied. It has also been described in the literature as a primary effect of the virus on the respiratory epithelium, since it can be seen from the very early stages of the infection, when viral levels are increasing.

Cynomolgus macaques experimentally infected with human H5N1 showed respiratory epithelial necrosis, being especially severe from day 4 to day 7 post infection, when virus was still detectable but in decreasing levels (Rimmelzwaan *et al*., 2003). Dogs experimentally inoculated with canine H3N2 displayed severe epithelial necrosis of the tracheal respiratory epithelium at day 3 post infection (Jung *et al*., 2010), coinciding with the time when viral levels have reached their peak (3dpi) and start declining (Song *et al*., 2008; Tangwangvivat *et al*., 2022).

Other species, such as the cotton rat, have been reported to show epithelial degeneration and necrosis from day 2 post experimental infection with human H3N2, when viral levels have started to decline (Ottolini *et al*., 2005). Tang and Chong experimentally infected Guinea pigs with human H1N1 and H3N2 influenza viruses, and discovered variable, widespread desquamation of the respiratory epithelium of the respiratory tract from 1dpi in animals that had received the H3N2 inoculum, matching the peak of viral load in these tissues (Tang and Chong, 2009). In their work with avian H5N1-experimentally inoculated ferrets, Zitzow *et al*. saw extensive bronchial epithelial necrosis at 3dpi, when the viral load was peaking in the respiratory tract (Zitzow *et al*., 2002). In a similar experiment with ferrets and human 1918 H1N1 influenza, Tumpey *et al*. observed bronchiolar necrosis at 3dpi, at the same time the viral loads peaked (Tumpey *et al*., 2007). Finally, Sreta *et al*. worked with experimentally infected pigs, which were inoculated swine influenza H1N1 or H3N2, and found bronchiolar attenuation, which is a lesion that is preceded by necrosis or degeneration of respiratory epithelial cells, that was particularly severe at 2dpi, when there was a detectable viral load and moderate at 4dpi, when there was no detectable virus (Sreta *et al*., 2009)

As **figure 1-7** shows, dead cells undergoing vacuolisation (white arrows) and nuclear fragments (yellow arrows) within the epithelium were seen. These findings were especially common in tissues from horses euthanized at 7dpi and 14dpi.

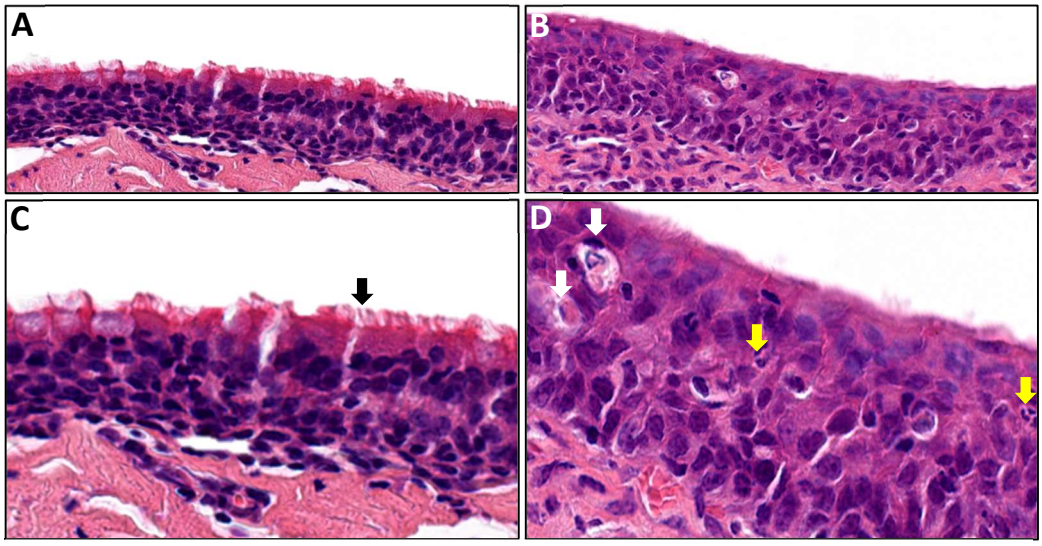

Figure 1-7: Representative images of tracheal sections stained with H&E from a noninfected horse (**A**, 12x) and the horse infected with EIV and euthanized at 7dpi (**B**, 12x). (**C**) Magnification of **Fig.3-2a**, showing cilia (black arrow). 25x. (**D**) Magnification of **Fig.3-2b**, showing vacuolised, dead cells (white arrows) and nuclear fragments (yellow arrows). 30x.

1.7.3 Hyperplasia of the respiratory epithelium

Epithelial hyperplasia is described as an increase in cell numbers conforming an epithelium, resulting in the increase in size of the organ or tissue in response to an injury (Mohan, 2005a; Woolf, 1998b), such as the loss of epithelial cells explained in the previous section. It is a reported finding in late, non-infectious stages of EI in horse (Muranaka *et al*., 2012). Epithelial hyperplasia has also been observed in dogs. On this regard, Jung et al. experimentally infected dogs with canine H3N2, and observed epithelial hyperplasia in the trachea at late stages of the infection (6-9dpi) (Jung *et al*., 2010), when very little or no virus is being shed (Song *et al*, 2008; Tangwangvivat *et al*., 2022). In pigs experimentally infected with human H1N1 Khatri *et al*. reported epithelial hyperplasia of the bronchial epithelium 3 days after the viral inoculation (Khatri *et al*., 2010), matching with the highest levels of virus, which in different studies have been established to happen also in the first days post infection. Khatri *et al*. studied the virus titers of nasal swabs and lungs from swine H1N1-experimentally infected pigs and reported the highest amounts of virus at days 1 and 3pi in the nasal cavity and at day 3pi in the lungs (Khatri *et al*., 2010). By doing IHC with an anti influenza A virus, Lyoo *et al*., detected a peak of staining at 4dpi in pigs experimentally infected with swine H1N1, H1N2 and H3N2 (Lyoo *et al*., 2014). Tumpey *et al.* experimentally infected ferrets with human 1918 H1N1 and observed alveolar epithelial hyperplasia at 3dpi, when the viral load was determined to be the highest along the infection (Tumpey *et al*., 2007). I observed it in the respiratory epithelium of the airways, at late timepoints (7dpi and 14dpi), once horses had stopped shedding virus (Muranaka *et al*., 2012; Yamanaka *et al*., 2009) and the tissue was regenerating (**Fig. 1-8**).

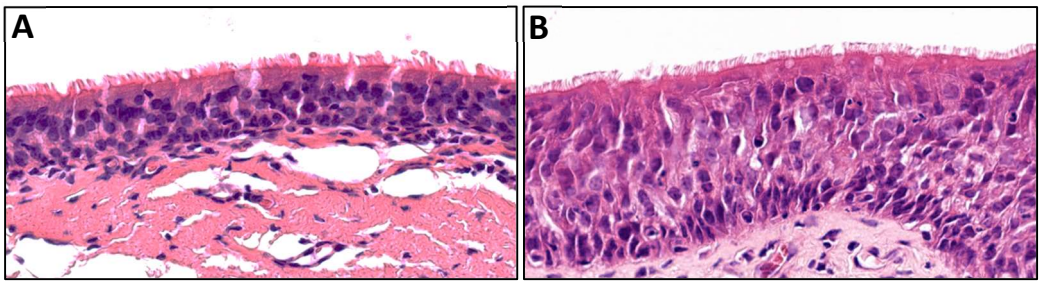

Figure 1-8*:* Representative images of trachea sections stained with H&E from noninfected horse (**A**) and a horse infected and euthanized at 14dpi (**B**) showing epithelial hyperplasia. 15x.

1.7.4 Squamous metaplasia of the respiratory epithelium

This lesion is described as a reversible change in the aspect of differentiated cells, often in response to chronic injury (=metaplasia), in which the cells become squamous or, in other words, thin and flat (Aster *et al*., 2015a; Mohan, 2005b). It is another epithelial response to the loss of ciliated and goblet cells in the respiratory epithelium of the airways. In the tissues I examined, this lesion was observed in the apical layer of the respiratory epithelium, once the loss of cilia and goblet cells exposed the epithelial cells to abnormal conditions (**Fig. 1-9**).

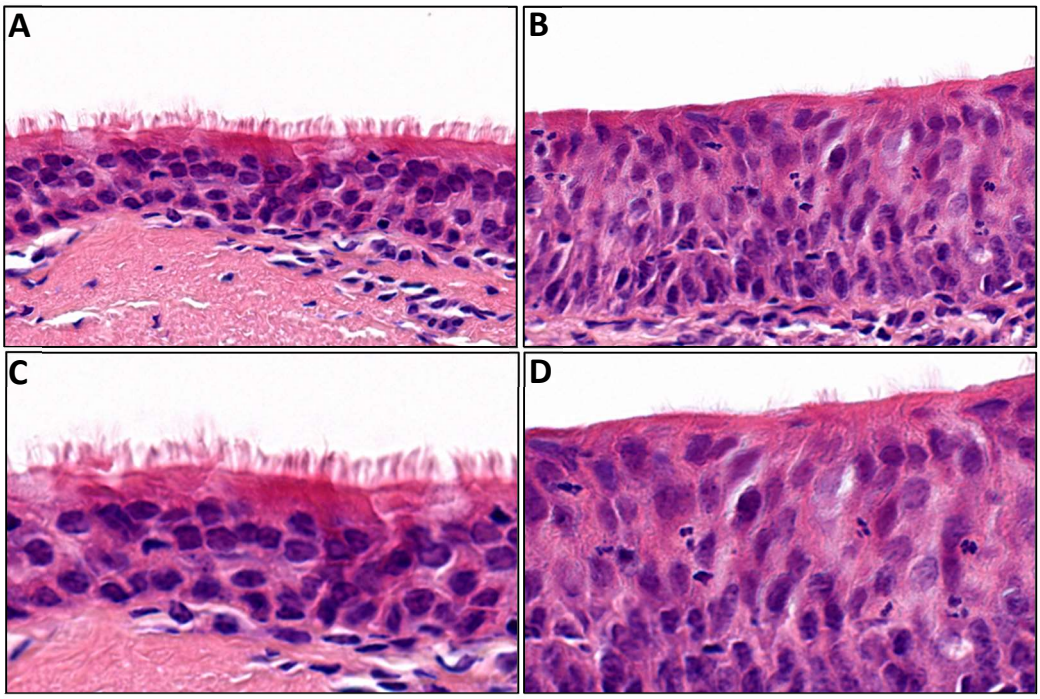

Figure 1-9*:* Representative images of tracheal sections stained with H&E from a noninfected horse (**A,** 25x) and the horse infected and euthanized at 7dpi (**B,** 25x) showing squamous metaplasia of the superficial layer of the respiratory epithelium. (**C**) Magnification of **Fig. 3-4a.** 30x. (**D**) Magnification of **Fig. 3-4b**, showing cells undergoing squamous metaplasia (arrows). 30x.

Squamous metaplasia has been described in H3N8 naturally-infected horses (Patterson-Kane *et al*., 2008; Muranaka *et al*., 2012) to be mild at 3dpi and moderate to severe at days 7 and 14pi, after horses have stopped being infectious. In dogs experimentally infected with canine

H3N2 influenza, it was described in the early stages of the disease by Watson *et al*. (Watson *et al*., 2017), although no specific timepoints are provided. Squamous metaplasia upon influenza infection has also been reported in mice. Baskerville *et al.* experimentally infected mice and golden hamsters with a human H1N1 strain and observed squamous metaplasia in the alveoli of hamsters, at 11dpi, and in the alveoli, bronchioles at days 12 and 14 post infection respectively (Baskerville *et al*., 1974). In their work with different strains of mice experimentally infected with a mouse adapted H1N1, Sell *et al.* described squamous metaplasia at late stages of the infection, between 3 and 4 weeks post infection in the alveoli and at 90dpi in the bronchial respiratory epithelium, in two immunodeficient mice strains (Sell *et al*., 2014), when the virus is not being shed anymore.

In other species infected with influenza viruses, such as the pig, it is described at 5dpi with swine H1N1 (Janke *B.H.,* 2013b). Interestingly, in this species squamous metaplasia is observed after the peak of infection with swine H1N1, known to be between 1 and 4dpi, depending on the tissue (Khatri *et al*., 2010; Lyoo *et al*., 2014).

1.7.5 Inflammation of the airways

Inflammation is a response triggered by damage in vascularized tissues consisting of the recruitment of cells and molecules of host defence from the circulation to the injured site, in order to eliminate the offending agents, and it can be generally divided into acute and chronic, depending on the immunological capacity that the host has and the duration of the response (Kumar *et al*., 2015a; Mohan, 2005c).

Acute inflammation is the initial and quick response, capable to developing in minutes and with a duration of up to few days. Its main features are the exudation of fluid and plasma proteins (=oedema) and the migration of polymorphonuclear neutrophils from blood vessels. Chronic inflammation has a longer duration and occurs when the agent that is causing acute inflammation remains for a long time (two weeks or more). It involves chronic inflammatory cells, such as macrophages, lymphocytes and plasma cells (Kumar *et al*., 2015b; Mohan, 2005c).

The inflammation of the airways is a common feature of EI-infected horses (Patterson-Kane *et al*., 2008), although it is not an influenza-specific lesion, as other pathogens, such as opportunistic bacteria, can also trigger it.

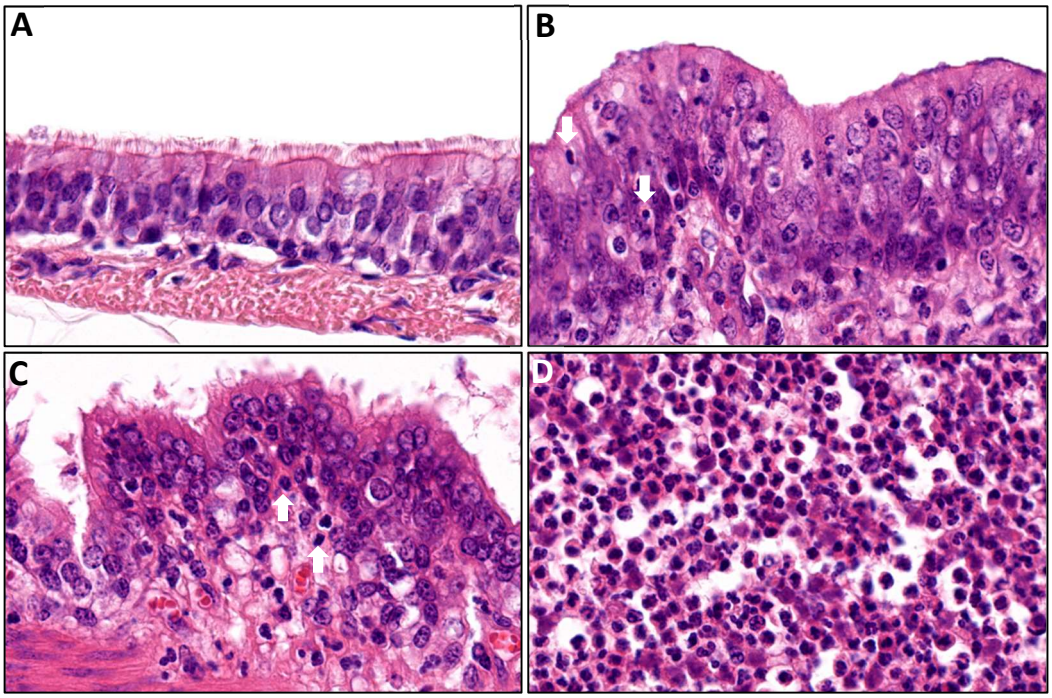

Figure 1-10*:* Representative images of lung sections stained with H&E. (**A**) Bronchial respiratory epithelium of an uninfected horse. (**B**) and (**C**) Bronchial respiratory epithelia of the horse infected and euthanized at 7dpi. (**D**) Inflammatory (neutrophils) and epithelial cells in the lumen of a bronchus of the horse infected and euthanized at 7dpi. Arrows show inflammatory cells infiltrating the mucosa and the submucosa. 25x.

It has been described in the literature as lymphocytic infiltration being present throughout the infection and a delayed neutrophilic presence from day 7pi onwards, when the virus is not being excreted by the animals (Muranaka *et al*., 2012). In the airways of respiratory sections from horses I studied, different inflammatory cell types, such as neutrophils, plasma cells, T lymphocytes and macrophages, were visualized infiltrating the submucosa and mucosa of the airways and in the alveoli, especially from 3dpi onwards. Abundant degenerated neutrophils and T lymphocytes were also seen in the airways' lumina at the beginning of the infection and until the end of it (**Fig. 1-10** and **11**). In dogs experimentally infected with H3N2 avian influenza, severe tracheitis, bronchitis and bronchiolitis have been observed at 3, 6 and 9dpi (Song *et al*., 2008), during the peak and posterior decline of viral shedding (Song *et al*., 2008; Tangwangvivat *et al*., 2022). In pigs experimentally infected with H1N1, the inflammation of the airways is a lesion described following spontaneous or experimental infection of IAV from the very first days after the infection, being initially more neutrophilic but rapidly shifting to mononuclear cells (Janke B.H., 2013b). In pigs experimentally infected with H1N1 following vaccination with human-like H1N2, Gauger *et al*. observed lymphocytic and suppurative inflammation in bronchi, bronchioles and alveoli at 5dpi (Gauger *et al*., 2011). Other study with swine H1N1-experimentally infected pigs described neutrophilic and mononuclear inflammation at 3dpi (Khatri *et al*., 2010). This inflammatory response matches with elevated viral levels in the tissues, which have been

observed between 1 and 4dpi in swine experimentally infected with H1N1, H1N2 and H3N2 (Khatri *et al*., 2010; Lyoo *et al*., 2014, De Vleeschauwer et a., 2009).

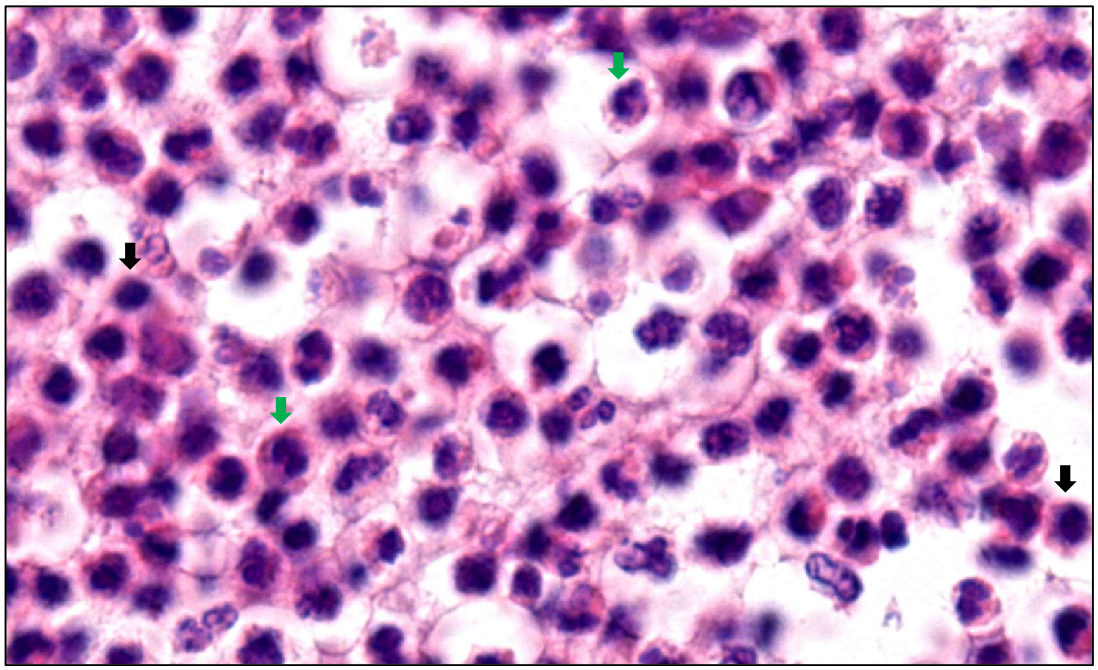

Figure 1-11*:* Magnification of **Figure 1-10d.** Black arrows show cells with characteristic features of T lymphocytes. Green arrows show cells with characteristic features of neutrophils. 60x.

In ferrets experimentally infected with different strains of highly pathogenic H5N1 avian influenza and H5N1 human influenza, bronchitis, bronchiolitis and pneumonia were observed as soon as 1dpi and until days 6 and 7pi (Govorkova *et al*., 2005; Zitzow *et al*., 2002), during the peak and posterior decline of viral excretion (Zitzow *et al*., 2002; Govorkova *et al*., 2005).

1.7.6 Epithelial, submucosal and alveolar oedema

Oedema is another unspecific lesion, that consists in abnormal accumulation of fluid in the extracellular space, as it can have different causes, being one of them, as mentioned above, an inflammatory response. In this case, the increased permeability of the blood vessels in order to allow inflammatory cells to reach the affected tissue results in spontaneous extravasation of fluid.

It can happen in any vascularized tissue, and grossly is appreciated as a separation of the extracellular matrix and slight cell swelling (Kumar *et al*., 2015b; Mohan, 2005d; Woolf, 1998c). Alveolar oedema can be detected by observing light pink, filamentous matter (belonging to plasma proteins) in the alveolar space (**Fig 1-12b**).

Oedema was present in all timepoints in the horses I studied, as expected considering that it is an unspecific change, although it was especially abundant in horses infected with EIV and euthanized at 7dpi and 14dpi, showing a multifocal pattern. On the other hand, epithelial and submucosal oedema could be seen extensively in infected horses, becoming especially severe at 7dpi, where its presence was generalised in most airways. It was revealed as the presence of blank space within the cells and collagen fibres (**Fig. 1-12d** and **f**). Pulmonary oedema was also found by Muranaka *et al*., in horses experimentally inoculated with equine H3N8 influenza, at different timepoints, being present from 3dpi (when viral levels are peaking) and particularly prominent at 7 and 14dpi, after viral shedding has finished (Muranaka *et al*., 2012).

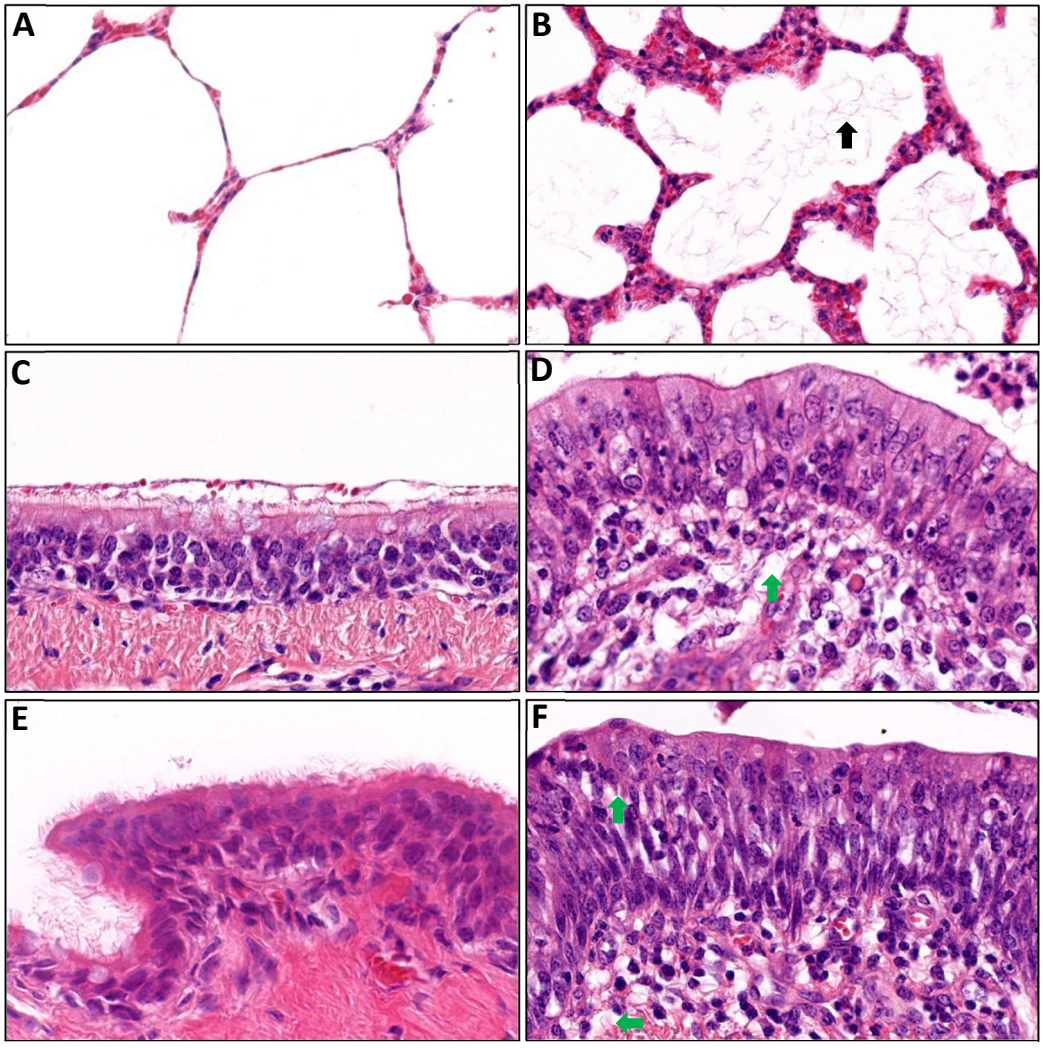

Figure 1-12: Representative images of lung sections stained with H&E. (**A**) Alveoli from a noninfected horse. 15x. (**B**) Alveoli from the horse infected and euthanized at 7dpi. Arrows show liquid (oedema) in the alveolar space. 15x. (**C**) Bronchial respiratory epithelium from a noninfected horse. 25x. (**D**) Bronchial respiratory epithelium from the horse infected and euthanized at 7dpi. Blank spaces in the submucosa, consistent with the presence of liquid, can be seen (arrow). 25x. (**E**) Bronchial respiratory epithelium from a noninfected horse. 25x. (**F**) Bronchial respiratory epithelium from the horse infected and euthanized at 7dpi. Blank spaces in the epithelium and the submucosa, consistent with the presence of liquid, can be seen (arrows). 25x.

In ferrets, alveolar edema is described at days 3 and 4pi in experimental infections with highly pathogenic avian and seasonal human H5N1 and human H1N1 influenza strains, coinciding with the highest values of viral shedding (van der Brand *et al*., 2010; Zitzow *et al*., 2002). In dogs, pulmonary oedema has been reported in individuals experimentally infected with canine H3N2 at 5, 9 and 14dpi (Jung *et al*., 2010; Kang *et al*., 2013; Tangwangvivat *et al*., 2022), when the peak of viral excretion has passed. Similarly, to ferrets, in pigs experimentally infected with swine H1N1, alveolar oedema is observed during the first days after the challenge (1-5dpi) (Gauger *et al*., 2011; Janke B.H., 2013b), when viral levels in respiratory tissues are peaking (Khatri *et al*., 2010; Lyoo *et al*., 2014, De Vleeschauwer et a., 2009).

1.7.7 Lumen blockage

Blockage of pulmonary airways is not a lesion by itself, but a consequence of other lesions aforementioned, such as epithelial degeneration, necrosis, inflammation and desquamation. It is observed as the presence of cells and debris in the lumen of the bronchi and bronchioles and is not an uncommon feature of the horses I studied. As **Fig. 1-13b** shows, in the horse infected and euthanized at 7dpi (and also at 14dpi) a high degree of blockage could be observed in the intrapulmonary airways, caused by inflammatory (mainly neutrophils) and epithelial detached cells and debris (shown in **Fig. 1-12**). It is also described in the literature as a lesion observed in horses naturally and experimentally infected with equine H3N8 (Begg *et al*., 2011; Muranaka *et al*., 2012) and, given its lack of specificity, it is reported to be present during different stages of the disease; however, it is described to be more prominent at the end of the disease, when animals do not shed virus anymore. In ferrets, the presence of necrotic debris and inflammatory cells in the lumen of the airways has also been reported during and after the peak of viral excretion: at 4dpi in experimental infection with seasonal human H5N1 influenza (van der Brand *et al*., 2010), and 3, 6 and 7dpi in experimental infection with highly pathogenic avian H5N1 and human H5N1 (Govorkova *et al*., 2005; Zitzow *et al*., 2002), In dogs, experimental infection with canine H3N2 resulted in suppurative inflammation in the lumina of the airways and consequent airway blockage during different phases of the disease, at days 3, 6 and 9 post infection (Song *et al*., 2008; Jung *et al*., 2010), in the peak and following decline of viral shedding (Song *et al*., 2008; Tangwangvivat *et al*., 2022). Similarly, pigs experimentally infected with different swine H1N1 strains and swine H3N2 showed a variable degree of luminal blockage and exudation of inflammatory cells and cell debris between 3 and 6dpi (Gauger *et al*., 2011; Khatri *et al*., 2010; Janke B.H., 2013a), during and after the peak of virus in the tissues, established to

happen in the first 3-4 days after infection (Khatri *et al*., 2010; Lyoo *et al*., 2014, De Vleeschauwer et a., 2009).

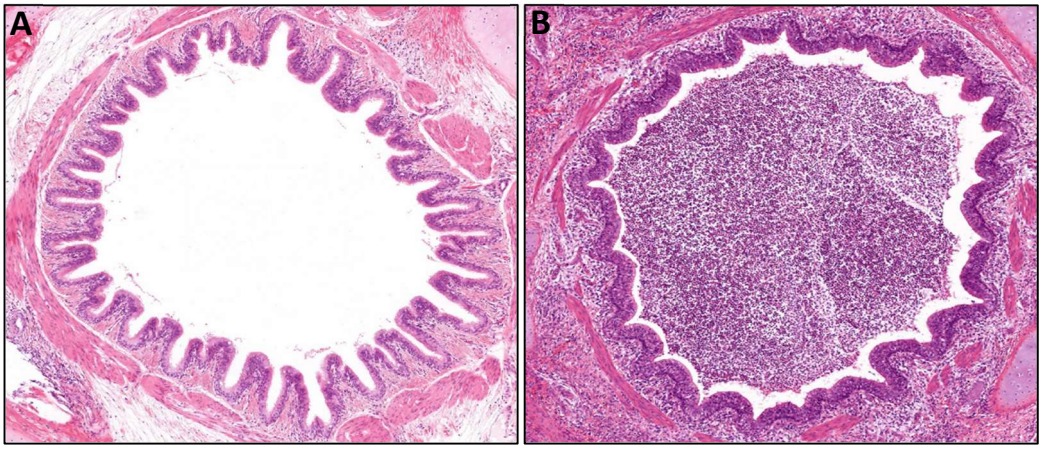

Figure 1-13: Representative images of lung sections stained with H&E from an uninfected horse (**A**) and the horse infected and euthanized at 7dpi (**B**), showing bronchi. Cell debris blocking the lumina can be seen in (**B**). 2x.

1.7.8 Type II pneumocytes proliferation

As explained, type II pneumocytes are one of the predominant cell types within the alveoli. These are cuboidal and have their nuclei in the centre of the cytoplasm (Plopper and Adams, 2006). Apart from secreting surfactant, these are reserve cells which proliferate when type I pneumocytes are injured (Mohan, 2005e). Influenza virus have been proved to infect type II pneumocytes in several species. In ferrets experimentally infected with human seasonal H1N1 and highly pathogenic avian H5N1, positive signal to influenza virus on IHC was found at 4dpi in type II pneumocytes, being more intense in the avian strain (van der Brand *et al*., 2010). Baskin *et al*. experimentally infected cynomolgus macaques with H5N1 human influenza and observed positive signal on IHC in type II pneumocytes at days 1, 2, 4 and 7 post infection (Baskin *et al*., 2009). Finally, in cats experimentally infected with human H7N7, van Riel *et al*. saw positive immunostaining against influenza in type II pneumocytes at 7dpi (van Riel *et al*., 2010). I observed type II pneumocytes proliferation in the lungs of the horses studied, as **Figure 1-14** shows, which had been described before in experimentally and naturally H3N8-infected animals (Muranaka *et al*., 2012; Patterson-Kane *et al*., 2008), being especially severe at late timepoints (7 and 14dpi), when animals are not shedding virus anymore. In ferrets experimentally infected with seasonal human H5N1 influenza, type II pneumocyte hyperplasia has been described at 4dpi (van der Brand *et al*., 2010). In dogs it is described as a chronic histological change, as in experimentally infected with canine H3N2, type II pneumocyte's numbers were reported to be increased at 7dpi (Tangwangvivat *et al*., 2022), when viral loads are minimal (Song *et al*., 2008; Tangwangvivat *et al*., 2022). In pigs infected with natural or experimental H1N1 swine influenza, marked type II

pneumocyte hyperplasia is a feature observed (Brockmeier *et al*., 2002, Grau-Roma and Segalés, 2007), although the timepoints in which this is observed have not been established. Finally, in cats, type II pneumocyte hyperplasia was seen in individuals experimentally infected with human H7N7 at 7dpi (van Riel *et al*., 2010).

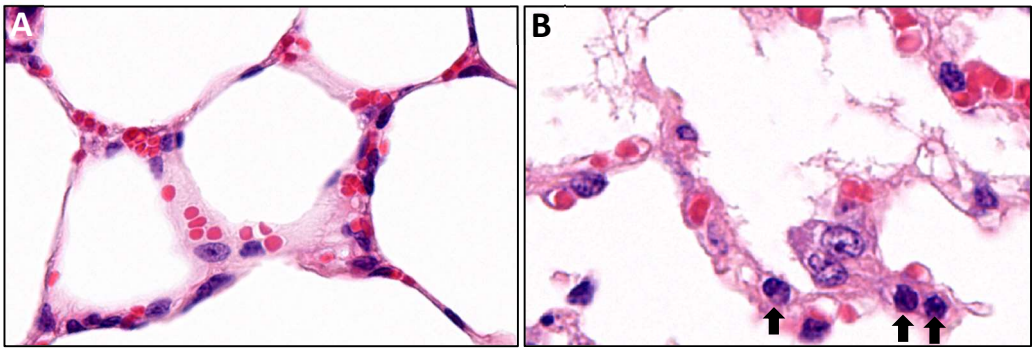

Figure 1-14*:* Representative images of lung sections stained with H&E from control (**A**) and 14dpi (**B**), showing alveoli. Arrow shows type II pneumocytes. 30x.

1.7.9 Haemorrhage

Haemorrhage is the leakage of blood from a blood vessel. It can happen in any vascularized tissue and has many possible causes, being one of them inflammatory lesions of the vessel wall (Mohan, 2005f). As it happens with oedema, in case of inflammation, the increased permeability of the blood vessels allows erythrocytes to escape the blood flow and move into the tissues. As a consequence, the presence of haemorrhage is not always a consequence of vascular damage. Given its unspecific nature, I observed haemorrhage in the submucosa of the airways and in the alveoli (**Fig. 1-15**). Other reports with EI in horses have described the presence of haemorrhage in respiratory tissues of horses, experimentally or naturally infected with H3N8, from early times post infection, when viral levels are peaking (2dpi) until late stages of the disease (14dpi), once viral shedding has finished (Begg *et al*., 2011; Muranaka *et al*., 2012). Van der Brand *et al*. described hemorrhage in the alveolar spaces and bronchiolar lumen at 4dpi in ferrets experimentally infected with human H5N1 influenza (van der Brand *et al*., 2010). Similarly, in dogs experimentally infected with canine H3N2, pulmonary hemorrhage was seen during all the phases of the infection (3dpi, 6dpi, 9dpi and 14dpi) including after the end of viral shedding (Song *et al*., 2008; Jung *et al*., 2010; Tangwangvivat *et al*., 2022). Finally, in pigs, pulmonary hemorrhages have been reported in the first days after infection, when viral levels are peaking. Specifically, after experimental infection with swine H1N1, H1N2 and H3N2, hemorrhages in the lung were seen at 2dpi (Lyoo *et al*., 2014), and in animals experimentally infected with swine H1N2; at 5dpi (Gauger *et al*., 2011).

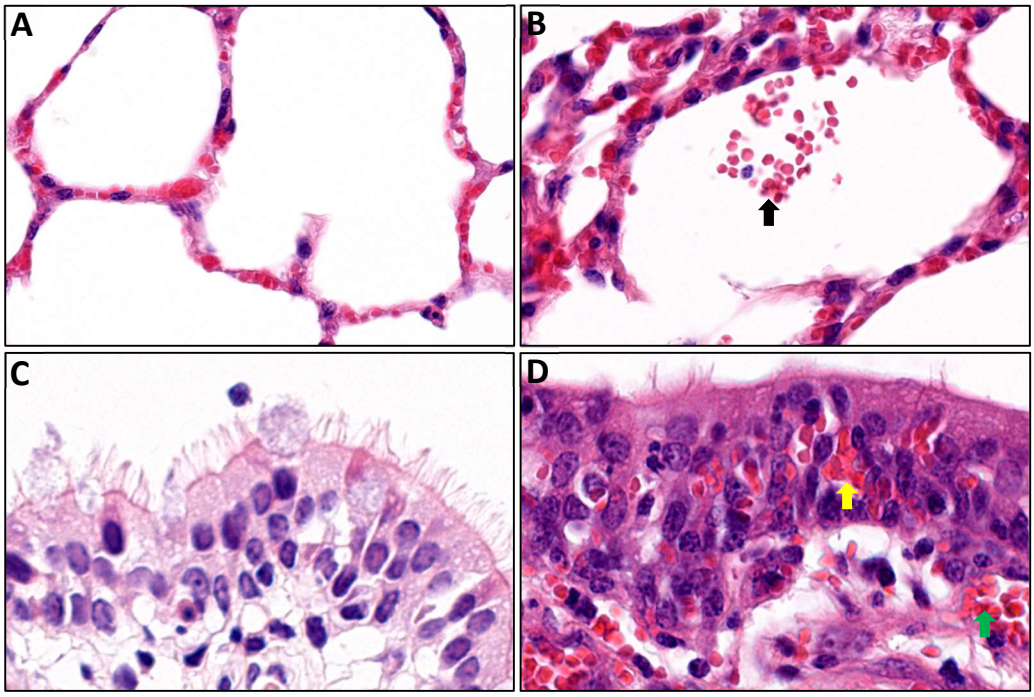

Figure 1-15*:* Representative images of lung sections stained with H&E. (**A**) Alveoli from a noninfected horse. (**B**) Alveoli from a horse infected and euthanized at 14dpi, showing red blood cells in the alveolar space (arrow). 25x. (**C**) Bronchial respiratory epithelium from a noninfected horse. (**D**) Bronchial respiratory epithelia and submucosa from the horse infected and euthanized at 7dpi. Red blood cells, coloured in strong red, in the alveoli (black arrow, **B**), respiratory epithelium of the bronchus (yellow arrow, **D**) and in its submucosa (green arrow, **D**) can be seen. 30x.

1.8 Temporal and anatomical dynamics of EIV infection

EIV is known as one of the fastest spreading virus among the agents causing respiratory disease in equines. As said, it can be detected in the entire respiratory tract after between 3 and 7 days post infection. A very reduced number of publications have worked on the dynamics of EIV in the equine respiratory tract. Sutton *et al*. infected ponies with H3N8 and performed immunocytochemistry on cytology brushes from pharynx, mid-trachea and right mainstem bronchus sampled on days 0, 3, 5, 7, 9 and 21 post infection and on bronchoalveolar lavages on days 0, 3, 7 and 21, observing the strongest viral signal to immunoperoxidase staining for EI antigen at days 3 in both types of samples. Samples of 5 and 7dpi had a decreasing level of positivity, whereas no signal was seen at 9dpi and very reduced in bronchoalveolar lavage obtained at 21dpi (Sutton *et al*., 1997). Similarly, Muranaka *et al*. and Yamanaka *et al*. infected horses with a H3N8 strain. Euthanasia of these animals at days 2,3 and 7pi, and 14dpi respectively was followed by immunostaining against human influenza A monoclonal antibody and posterior semi quantification, which showed high levels of EI antigen in the nasal mucosa, trachea and bronchi at days 2 and 3 post infection, with scarce signal from 7dpi onwards in these tissues and no signal later than 2dpi

in the bronchioles and in any timepoint in the alveoli (Yamanaka *et al*., 2009; Muranaka *et al*., 2012). In an *in vitro* setting, Amat *et al*. infected equine tracheal explants with two temporally distant H3N8 and observed a peak of NP positive staining at days 2 and 3 post infection in both virus, being the signal at days 1, 4 and 5pi much lower (Amat *et al*., 2021).

1.9 Influenza pathology in other species

1.9.1 Swine influenza

Swine influenza is caused by H1N1, H1N2, H2N1, H3N1, H3N2 and H2N3 and affects pigs in a similar way EI affects horses. It infects the respiratory epithelia of the airways, causing their denudation and the blockage of the airways due to the accumulation of cell debris (MacLachlan and Dubovi, 2011). Lesions described in the respiratory epithelia, mostly from animals experimentally infected with H1N1 (and H1N2 and H3N2 to a lesser extent) are hyperplasia, squamous metaplasia and inflammatory infiltration. Furthermore, in the lung it develops a bronchopneumonia, normally located cranioventrally, characterized by the necrosis and inflammation of the intrapulmonary airways and the alveoli, which can also look atelectatic (Janke B.H., 2013a; Rajao *et al*., 2014). Similarly, to horses, in cases secondary bacterial infections occur, the mentioned lesions will be extended, worsening the symptomatology, which in absence of complications is characterized by the presence of cough, pyrexia, rhinitis and sneezing that cease in approximately a week (Driskell, 2014).

1.9.2 Canine influenza

Canine influenza is produced by H3N8, believed to come from horses (Crawford *et al*., 2005a; Driskell, 2014), and H3N2, which has avian origin (Voorhees *et al*., 2017). It produces similar lesions and clinical outcome than EI. The most common presentation is the mild disease, characterized by cough, sneezes, nasal discharge and anorexia that last between 7 and 10 days (Driskell, 2014; Klivleyeva *et al*., 2022b). Disruption of respiratory epithelia, with loss of cilia, squamous metaplasia of the epithelial cells and infiltration of inflammatory cells, together with airway blockage due to the presence of detached epithelial and inflammatory cells, are the lesions that can be seen in experimental infections with H3N8 and H3N2 (Crawford *et al*., 2005b; Payungporn *et al*., 2008; Jung et al., 2010; Watson *et al*., 2017), although, differently from H3N8, experimental H3N2 infections have been reported not to cause extrapulmonary lesions (Jung *et al.,* 2010). In severe presentations of the disease, normally natural infections aggravated by opportunistic bacteria in the lungs, the

severity and extension of the lesions increases, involving in a higher degree the intrapulmonary airways and the alveoli, which show haemorrhages and inflammation (Crawford *et al*., 2005b; Jung *et al*., 2010; Klivleyeva *et al*., 2022b; Payungporn *et al*., 2008; Song *et al*., 2008; Watson et al., 2017).

1.9.3 Ferret influenza

Ferrets get infected by different influenza A viruses, including avian and zoonotic types, and display symptoms also seen in humans (Belser *et al*., 2020). For this reason, they are a model that has been deeply studied. The clinical presentation and pathology of ferret influenza is highly dependent on the virus subtype or strain (Kuiken *et al*., 2010). For example, 1918 human H1N1 experimental infection resulted in serious disease and high mortality, with the animals showing necrotizing bronchopneumonia with focal alveolar haemorrhage and oedema, hyperplasia of the alveolar respiratory epithelia and peribronchiolar inflammatory infiltrate (Tumpey *et al*., 2007). Different strains of H5N1 human influenza experimentally inoculated to ferrets have shown to cause in high lethality, neurological signs, high fever, diarrhoea, anorexia, weight loss and extreme lethargy in experimentally infected ferrets. Lesions described in these animals were bronchointerstitial pneumonia, epithelial necrosis, degeneration and hyperplasia in the alveoli and intrapulmonary airways. Furthermore, alveolar oedema and haemorrhage, as well as abundant mixed inflammatory infiltrate and exudate in the lung parenchyma and the airways are also reported (Boltz *et al*., 2008; Govorkova *et al*., 2005; Yen *et al*., 2007). Finally, experimental inoculation of 2009 pandemic H1N1 in ferrets resulted in bronchiolar multifocal necrosis with moderate infiltrates of neutrophils, multifocal peribronchiolar mixed inflammatory infiltration and moderate numbers of macrophages, neutrophils, and erythrocytes, mixed with fibrin, edema fluid, and cellular debris, in the lumen of the bronchioles, along with mixed inflammation of the bronchi (van den Brand *et al*., 2010).

On the other hand, highly pathogenic avian H5N1 influenza viruses have variable virulence on experimentally infected ferrets (Maines *et al*., 2005), being some of them highly lethal (Govorkova *et al*., 2005). Lesions described in ferrets infected with these are similar to those seen in 2009 H1N1 human influenza-inoculated ferrets, but with a lower degree of severity (Zitzow *et al.,* 2002; Maines *et al*., 2005; van den Brand *et al*., 2010).

1.10 Markers used for characterising EI pathogenesis

Equine influenza and its pathogenesis have not been studied in depth by the use of biomarkers in tissues either derived from horses that were infected in vivo or infected in vitro after euthanasia. However, there is literature describing cellular responses to EI. Amat *et al*. used tracheal explants infected *in vitro* to study viral spread throughout the respiratory epithelium of the trachea, as well as levels of apoptosis, mitosis and activation of the innate immune activation (Amat *et al*., 2021). Similarly, Gonzalez et al. infected canine tracheal explants with EIV and studied its spread and distribution and the apoptosis observed in epithelial cells in response to infection (Gonzalez *et al*., 2014). As a secondary objective of this thesis was to replicate the work done by Amat, Gonzalez and other people in Dr Pablo Murcia's group on tracheal explants, but on *in vivo* tissues, Cleaved Caspase 3, MX1 and Ki67 were used in a first instance. Immunomarkers for the quantification of specific cell types (T lymphocytes, B lymphocytes and type II pneumocytes) were used in a later stage to characterise the inflammatory response of the host and the regeneration of the alveolar tissue

1.10.1 Cleaved Caspase 3

Cleaved caspase 3 (CC3) is an important cellular marker for apoptosis, which has been traditionally considered detrimental for the spread of viral infections, although this statement has been recently challenged, since it has been discovered that some viruses facilitate their replication by using components of the apoptotic pathway (Best and Bloom, 2004). Even if they have been shown to differ in their capacity to induce apoptosis depending on the strain (Brydon *et al*., 2005), influenza A viruses have been widely described as apoptosis promoters, both *in vitro* and *in vivo*. As an example, Lam *et al*. experimentally transfected H292 human airway epithelial cells with an avian influenza A virus H5N1 NS1 plasmid, and observed DNA strand breakage, which is a hallmark of apoptosis. In another study, Takizawa *et al.* experimentally infected MDCK and Henrietta Lacks (HeLa) cells with human H3N2 and observed features characteristic of apoptosis, such as nuclear and DNA fragmentation and chromatin condensation (Takizawa *et al*., 1993). Sumikoshi *et al* infected human vascular endothelial cells (HUVEC) with different influenza strains (H1N1, H2N2 and two different H3N2) and found positive signal in cells that were also positive to the virus, at 48h post infection (Sumikoshi *et al*., 2008). Other studies, such as (Hinshaw *et al.,* 1994), also demonstrated that influenza A viruses induce apoptosis *in vitro*. Importantly,

Mori *et al*. experimentally infected mice with human H1N1 and demonstrated, by i*n situ* DNA labelling and IHC, that infection with influenza caused the respiratory epithelial cells to undergo morphological alterations and DNA fragmentation compatible with apoptosis *in vivo*, suggesting that this was triggered by influenza (Mori *et al.,* 1995a).

The link between apoptosis and influenza A viruses is controversial, although has been widely studied, as, differently to what was exposed earlier, it has been proved that influenza can also inhibit apoptosis. Zhirnov *et al*. demonstrated that human H1N1 virus with experimental deletion of NS1, one of the influenza proteins, caused earlier and more intensive apoptosis in vitro than wild-type virus, suggesting that NS1 has antiapoptotic potential that might be expressed in the earliest stages of the infection, to support viral replication (Zhirnov *et al*., 2002). Liu *et al*., working with different cell lines, demonstrated that avian H6N6 amd human H3N2 NS1 had an inhibitory effect on the complex Stribble, which is a multidomain scaffold protein of epithelial cells known to have proapoptotic capability (Liu *et al.,* 2010). In summary, according to the literature, it seems that apoptosis might be downregulated at the beginning of the infection, to promote viral replication, and upregulated later (Chen *et al*., 2001; Zhirnov *et al.,* 2002; Yeganeh *et al*., 2018).

CC3 has been proven to be a good apoptosis marker in immunohistochemistry (Gown and Willingham, 2002) and in equine tissues (Amat *et al*., 2021). It is expressed in the cytoplasm in any cells undergoing apoptosis that have reached the point of no return in the caspase cascade (Bressenot *et al*., 2009). Literature on CC3 expression in experimental infections with influenza is not abundant, and the few works on it coincide that the peak of CC3 expression and, therefore, of apoptosis, is shortly, but not immediately, after the experimental inoculation, as explained in the previous paragraph. In his work with equine tracheal explants experimentally infected with two different equine H3N8 viruses, Amat *et al*. observed a peak of CC3 at day 2 post infection, coinciding with the viral peak, and a posterior decrease (Amat et al., 2021). Kosai *et al*. observed a big increase of CC3 activity in the lung at 3dpi in a murine model of coinfection with mouse adapted H1N1 influenza and *Streptococcus pneumoniae* 48 hours later (Kosai *et al*., 2011), although the viral load was not estimated in this experiment. As explained in the previous paragraph, these results suggest that it is possible that influenza restricts apoptosis in the very first stages after infection, to allow its replication, and promotes it after this has happened.

1.10.2 Myxovirus resistance 1

Myxovirus resistance 1 (MX1) is a protein belonging to the Myxovirus resistance protein family, which are believed to be interferon-stimulated host restriction factors that can be

triggered independently by the innate immune system of individual cells to block the replication of different viruses, including A influenza viruses (Fatima *et al*., 2019; Haller *et al*., 1980; Staeheli, 1990). Overall, Mx1 is described to confer resistance to influenza virus infections by modulating the host's immune response. Cilloniz *et al* worked with two mice strains, one of them carrying a defective allele of the Mx1 resistance gene, experimentally infected with human 1918 H1N1 influenza, and observed that these had higher viral loads, higher weight loss and lower survival rate than the mice with normal Mx1 gene. As thoroughly explained in the paper, this was achieved by a widespread downregulation of genes associated with the inflammatory response (Cilloniz *et al*., 2011). In a similar setting, working with two mice strains and human 1918 H1N1 and highly lethal H5N1 viruses, Tumpey *et al*. saw higher weight loss and viral load and lower survival rate in the Mx1-deficient mice strain, compared to the competent one, although the mechanisms of protection conferred by Mx1 were not further investigated (Tumpey *et al*., 2007). Literature on whether and by which means equine Mx1 restricts the spread of influenza virus is limited to the work carried by Fatima *et al*. In it, they worked *in vitro* with two different cell lines and avian Zhejiang 2013 H7N9 and Jilin 1989 equine H3N8 and observed that only the substitution of Jilin 1989 H3N8 NP by the Zhejiang 2013 H7N9 NP resulted in a change of the polymerase activity of the virus, whereas changes in other influenza proteins, such as PB1, PB2 and PA did not translate into any modification of its activity, suggesting that the equine influenza NP was the target of Mx1 (Fatima *et al*., 2019). This result is aligned with what has been observed in other species, such as the mouse (Verhelst et al., 2012), and *in vitro* (Turan *et al*., 2004). Furthermore, Fatima *et al*. suggested that Mx1 might block viral replication of equine influenza by interacting with viral NP and preventing NP and PB2 from interacting with each other.

Although it is a well-studied gene, there are a few publications speaking about the distribution and temporal dynamics of Mx1 expression during influenza infection. Working with Syrian hamsters infected with human H3N2 influenza, SARS-CoV-2 or coinfected, Halfmann *et al*. saw a peak of positive staining to Mx1 in influenza-only infected animals at 3dpi (Halfmann *et al*., 2022), with the airways but also the alveoli and pulmonary interstitium heavily positive to anti-MX1 antibody. Amat *et al*. used two different equine H3N8 influenza to experimentally infect equine tracheal explants, and discovered that the most abundant signal of this ISG was at days 4-5 post infection, depending on the virus (Amat *et al.,* 2021). In an experimental inoculation of a Korean isolate of porcine respiratory reproductive virus on pigs, Chung *et al*. observed positive signal to Mx1 from day 1 post infection and until day 10 post infection, with a subpeak of positivity at day 3pi and a sudden

increase of the signal from 5 to 7dpi, in the alveolar septa and, with a lower intensity, in cells with features compatible with type II pneumocytes (Chung *et al.,* 2004).

1.10.3 Ki67

Ki67 is a well-known marker for mitosis, which is defined as the multiplication of somatic cells (Mohan, 2005b). Mitotic activity has been described in the respiratory epithelia of influenza-infected tissues (Tauenberger and Morens, 2008), although the relation between it and influenza virus is not fully understood. In their study with equine tracheal explants experimentally infected with two H3N8 equine influenza virus, Amat el al. showed a peak of mitotic division at days 3 and 4, whereas non-infected tracheal explants did not show any significant changes in mitosis levels (Amat el al., 2021). This finding suggests that upon influenza infection, the respiratory epithelium is in need of regeneration, presumably due to the pathogenic effect of the virus or the apoptotic response to prevent its spread. However, He *et al*., in their study with human H1N1- experimentally infected A549 cells, showed that influenza virus are able to block the mitosis of infected cells, by preventing them from entering S phase and keeping them in G0/G1, in resting mode. Furthermore, this action would be beneficial for the virus, as it would be easier to express viral protein and produce bew virus in G0/G1 than in other phases of the cell cycle (He *et al*., 2010)).

1.10.4 CD3

CD3 is described as a useful cytoplasmatic marker to label T cell populations in immunohistochemistry (Salvadori *et al*., 1994; Vernau and Moore, 1999), although, as a pan marker, it does not distinguish between subpopulations. T lymphocytes play a central role in regulation of the immune response regardless of its origin, upon equine influenza infection, as it is a cell which plays a central role in regulating the immune response to infections, regardless of its nature. In influenza infections, it has been shown that adaptative T cells are crucial for recovery and long-term protection from influenza infection (Nussing *et al*., 2018). Furthermore, the two main T cell populations have specific and highly important functions; whereas cytotoxic (CD8) T cells target infected cells and lyse them via different pathways, such as the production of anti-viral cytokines and direct killing of these (Bender *et al*., 1992; Doherty *et al*., 1996; Topham *et al*., 1996), CD4 T cells initiate the adaptative immune response, produce pro-inflammatory cytokines, coordinate the B cell provision, provide long-lasting memory cells for potential re-infection and directly kill influenza-infected cells

(Brown *et al*., 2012; Hua *et al*., 2013; McKinstry *et al*., 2013). Dynamics of T cells along influenza infection have been studied in depth, and it has been observed that the increase in this cell's numbers is delayed in time, at around 6-8 days after the experimental infection. For example, Myers *et al* reported a coetaneous expansion of CD8 T cells and prominent viral clearance at days 8 and 9 post infection in the lungs of mice infected with a mouse adapted H1N1 virus influenza (Myers *et al*., 2021). Hornick *et al*. also infected mice with a mouse adapted H1N1 influenza virus, and, by using CD49d and CD11a antibodies to track CD4 T cells during influenza infection, observed a peak of these in the lung at day 10 post infection, after an increase in their numbers since days 6-7 post infection (Hornick *et al*., 2019).

1.10.5 PAX5

PAX5 is a B lymphocyte nuclear marker (Fieldman and Dogan, 2007). B lymphocytes are the precursors of plasma cells, which produce specific antibodies to clear infections. They have been reported to have an important role in orchestrating the humoral response. In their review on the role of B lymphocytes in influenza infection, Lam and Baumgarth point to several relevant functions those have upon infection with influenza: provision of natural, pre-existing, and also antigen-induced antibodies to counteract the initial infection, rapid generation of highly specific antibodies and secretion of a wide range of memory B lymphocytes and antibodies in preparation for the next infection with this virus (Lam and Baumgarth, 2019),. Furthermore, in addition to produce antibodies, B cells are described as able to synthesise and release cytokines which they use to modulate the immune response and to behave as antigen-presenting cells to CD8 and CD4 T lymphocytes (Shen and Fillatreau., 2015). In mice experimentally infected with a mouse adapted H1N1 influenza, Kopf *et al*. showed that the absence of B cells resulted in reduced systemic CD4 T cell proliferation and, ultimately, in a diminished viral clearance, suggesting that they might have a decisive role in the outcome and resolution of the infection (Kopf *et al*., 2002). There are a few papers talking about the temporary dynamics of B lymphocytes in different organs of animals experimentally infected with influenza. Wolf *et al*. experimentally infected mice with a mouse-adapted H1N1 influenza and observed a peak of antibody secreting cells (a subpopulation of B cells) at day 15 post infection in the lung, mediastinal lymph node, bone marrow and spleen, although at days 5 and 21pi, moderate numbers of those were already detected (Wolf *et al*., 2011). In a similar experiment, Liang *et al*. experimentally infected mice with HKx31 (H3N2) and saw that the levels of antibody secreting cells in the cervical lymph nodes, bone marrow and NALT increased from 8dpi to 12dpi until between 12dpi

and 42dpi, depending on the tissue. Interestingly, in the lung the levels raised especially markedly between 10dpi and 12dpi, and then at 25dpi and 42dpi, after which high levels could be seen up to 18 months post infection (Liang *et al*., 2001). Tamura *et al*. also infected mice with a mouse adapted H1N1 virus and observed a peak of antibody secreting cells in the cervical lymph nodes, NALT and nasal lymphoid tissue at day 7 post infection, followed by a decrease at 14dpi and further reduction of their numbers at 14dpi (Tamura *et al*., 1998). Finally, Jones and Ada experimentally infected mice with a human H2N2 and determined that levels of antibody secreting cells in the lung dropped markedly at 12dpi after having peaked at 10dpi (Jones and Ada, 1986). No studies on dynamics of B lymphocytes in horses infected with influenza were found.

1.10.6 Surfactant Protein C

Surfactant protein C antibody is a cytoplasmic marker which reacts against surfactant protein C, one of the surfactant proteins found in pulmonary surfactant, known to prevent lung collapse and allow normal respiration. It is produced only by type II pneumocytes (differently from other surfactant proteins, which are also secreted by club cells), which, as explained, are pluripotential, since apart from secreting pulmonary surfactant, they regulate the expression of immunomodulatory proteins and the transepithelial movement of water and ions and act as stem cells for both type I and type II pneumocytes. (Confalonieri *et al*., 2021). Proliferation of type II pneumocyte is a common feature in pneumonias and has been described in experimental infections with different influenza viruses. Narasaraju et al. experimentally infected mice with a mouse adapted H3N2 virus and observed a gradual increase of this cell type's numbers from 24hpi until 72hpi in lung explants obtained from the previously infected animals, interestingly, by staining lung tissues with an anti-Surfactant protein C antibody. Furthermore, on histological observation of H&E-stained lung sections from the same animals, which were euthanised at 4dpi, identified prominent type II pneumocyte proliferation (Narasaraju et al., 2009). Unfortunately, in this experiment all the animals were euthanised at 4dpi. In a similar setting, Major et al. experimentally infected mice with a mouse H3N2 and discovered a gradual increase in Ki67 levels in type II pneumocytes from day 3 post infection until day 10pi, followed by a subtle decrease at 12dpi and a sharp decline at 14dpi (Major et al., 2020). Ogiwara et al. experimentally infected mice with human 2009 pandemic H1N1 and with highly pathogenic avian H5N1 and determined, by double staining type II pneumocytes with SFTPC and proliferation cell nuclear antigen (PCNA), that both induce hyperplasia of type II pneumocytes, although the peak of proliferation differed between H5N1 (6dpi) and H1N1 (9dpi) (Ogiwara *et al*., 2014).

In horses experimentally infected with equine influenza virus, type II pneumocyte proliferation has been described at late stages of the disease (7 and 14 dpi) by Muranaka et al. (Muranaka *et al*., 2012). In addition, Patterson and Kane, working with natural cases of equine influenza during the 2007 outbreak in Australia, identified type II pneumocyte hyperplasia in 9 of the 11 horses analysed (Patterson-Kane *et al.,* 2008). The association between influenza infection and type II pneumocyte hyperplasia in horse, however, is less clear, as, differently from what happened in the aforementioned mice studies, in those working with equine influenza, secondary/opportunistic bacterial infections, which might have accounted for (or at least contributed to) the hyperplasia of type II pneumocytes, were identified in respiratory tissues at the same time these was (Patterson-Kane *et al*., 2008; Muranaka *et al*., 2012).

1.11 Gaps in equine influenza pathology knowledge

As said, existing knowledge on equine influenza pathology in *in vivo* tissues is limited and based on a small number of studies. Several reasons can be highlighted to explain this lack of cognizance. As explained, EI is a relevant disease of the horses due to the economic impact it has more than due to its clinical consequences. For this reason, research is focused on prevention (i.e., vaccines) and diagnostics more than on treatment or clinical/pathological characterization of the disease. Furthermore, due to its low mortality, further decreased thanks to sanitary measures, such as vaccination, cases of horses dying due to or infected with EI are rarely seen, which makes the study of lesions produced after a natural infection with EIV very difficult. As shown above, the 2007 Australian outbreak was a good opportunity to gain some understanding on the pathological landscape originated by equine influenza virus in the respiratory tract of the horses, although it had the bias that only very severe cases, those to lead to death, were studied. Alternatively, other studies have performed experimental infections in biocontainment units. Infecting experimentally is the only option to generate *in vivo* tissues from animals inoculated with EIV, although the price of carrying an assay with infectious agents on alive animals housed in biosecurity facilities is very high and, as a consequence, the sample size of these studies is normally reduced. Both experimental and field studies have mainly focused, first, in describing anatomical (macroscopic) lesions observed in postmortem examination and histological (microscopic) lesions seen in formalin-fixed, paraffin-embedded (FFPE) sections stained with haematoxylin and eosin (H&E), and second, in detecting viral antigen, either in the animal, by isolation or PCR, or in the tissues, by doing IHC. In the case of studies on field cases of EI, they focused on describing histopathological changes, since establishing temporary dynamics of lesions observed in individuals infected with EIV is sometimes especially

difficult, given their variability, in terms of age and immunological status, among others, and the lack of information about when horses became infected. The paper published by Begg *et al*. on horses dying after getting infected with EI in Australia in 2007 is an especially relevant example (Begg *et al*., 2011). On the other hand, experimental studies do allow to determine the presence, severity and extension of pathological changes over time. On this regard, horses studied in this thesis come from a work done by Muranaka *et al*., which is, to the best of my knowledge, the most accurate and in-depth description of EI-induced lesions and cover the lack of understanding on the timeline of lesions induced by EIV. In this study, horses were experimentally infected with EIV and euthanized at different timepoints: 2dpi, 3dpi, 7dpi and 14dpi (Muranaka *et al*., 2012). Lesions observed in the respiratory tissues were described and its severity was assessed by semi quantification. Furthermore, FFPE tissues were immunolabelled with an anti-influenza A antibody to visualize viral antigen in the tissues.

There is lack of studies on the pathology and pathogenesis of EI in the horse, for reasons aforementioned. As a consequence, there is not a standard pathological model for EI, but different papers reporting lesions that sometimes coincide and some others do not. Furthermore, there is a lack of knowledge on the progression and extension of respiratory lesions due to EI over time, since only a few studies have described how the respiratory tract changes, both anatomically and histologically, after EIV infects it, but none have ever purely quantified the extension and severity of these.

On the other hand, the distribution, abundance and temporary dynamics of viral antigen throughout the respiratory tract of the horse have not been studied in depth, although some papers aforementioned have shown them in equine respiratory tissues. Currently there are not published studies that accurately quantified histopathological lesions, virus spread, protein expression and abundance of inflammatory cell populations in respiratory tissues from horses infected with EIV, which is a thing that current imaging technologies would enable.

1.12 Aims

The overall aim of this project was to understand the pathogenesis of equine influenza in the horse, using respiratory sections from EI-infected animals to quantify histological changes, viral spread and expression of proteins with image analysis software.

Specifically, I aimed to:

I. Describe and quantify histological changes and lesions in the equine respiratory tract of horses infected with equine influenza virus.

II. Describe and quantify temporal and anatomical dynamics of EIV within the equine respiratory tract.

III. Describe and quantify temporary and anatomical dynamics of markers of cellular processes and cellular populations.

Chapter 2. Materials and methods

2.1 Study design

Four Thoroughbred horses (17 to 19 months old) were experimentally infected in the Equine Research Institute of the Japan Racing Association by Muranaka *et al*. with A/equine/Ibaraki/1/07 ($10^{8.3}$ 50% egg infectious dose [EID50]/animal) by ultrasonic nebulization and stabled in biosafety level 3 facilities. They were euthanized at days 2 (n=1), 3 (n=2) and 7 (n=1) post infection (Muranaka *et al*., 2012). Three additional Thoroughbred horses were experimentally infected with the same virus by nebulization and housed separately, sharing each horse a stall with a Beagle dog, by Yamanaka *et al*. in the Equine Research Institute of the Japan Racing Association, in order to see interspecies transmission of EI. After 14 days, the three horses were euthanized (Yamanaka *et al*., 2009). Necropsies of the euthanized animals were performed, and tissue samples were collected, fixed in 20% neutral buffered formalin for 48 hours, embedded in paraffin and cut in sections of 6μm of thickness, by Muranaka *et al*. in the Equine Research Institute of the Japan Racing Association. (Muranaka *et al*., 2012).

2.2 Blank sections

Blank sections of FFPE tissues derived from the EIV experimentally infected horses were sent by Dr. Akihiro Ochi, together with blank sections of FFPE tissues derived from uninfected horses. For each horse, 15 serial blank cuts of nasal mucosa (respiratory area), upper trachea, middle trachea, lower trachea, left anterior lung lobe, right anterior lung lobe, left posterior lung lobe, right posterior lung lobe, spleen, submandibular lymph node and intestine were sent.

2.3 Haematoxylin and eosin and PAS

Sections of tissues aforementioned, from EIV-infected and noninfected horses stained with H&E were kindly provided by Dr. Akihiro Ochi. PAS staining of tissues aforementioned was done with a Dako Autostainer by the Histology Laboratory of the University of Glasgow School of Veterinary Medicine.

2.4 Immunohistochemistry

In order to avoid biases as a result of spurious staining I optimized immunostaining (IF and IHC) protocols to minimize background or non-specific staining. In addition, for all my

measurements I included a non-infected control to account for physiological variation in protein expression.

Sections were rehydrated at room temperature with 4x Xylene (10 minutes each) and ascendent alcohol dilutions: Xylene/Isopropyl alcohol 1:1 mix for 5 minutes, 100% Isopropyl alcohol for 10 minutes, 90%, 70% and 50% Isopropyl alcohol for 5 minutes each. After, slides were washed at room temperature for 3 times with purified water. For NP, no unmasking was done, whereas for H3 and Surfactant Protein C antibodies, slides were heated in the microwave 5 times 3 minutes each time in pH 6.0 1x citrate buffer, made of 2.1 grams of citric acid monohydrate per liter of purified water. For slides undergoing MX1, CC3, Ki67, CD3 and PAX5 staining heat-induced epitope retrieval using Menarini Access Retrieval Unit with a Sodium Citrate buffer, pH6, for 1 min 40 sec at 125^0C at full pressure was done. For the stainings done by me (Surfactant protein C and H3), the slides were treated with 3% H_2O_2 in 1x phosphate buffered saline (PBS) for 15 minutes at 4°C, after cooling down for 30 minutes after the unmasking, for endogenous peroxidase blocking, slides were washed three times in 1x pH 7.4 PBS and incubated for half an hour with 10% foetal bovine serum (FBS) in PBS at room temperature for unspecific binding sites blocking. PBS formulation was 160 grams of sodium chloride, 4 grams of potassium chloride, 22.71 grams of anhydrous sodium phosphate dibasic and 5,44 grams of potassium dihydrogen phosphate in purified water per 2L of solution. Sections were incubated overnight at 4°C with the primary antibody, diluted in 10%FBS in PBS as shown in **Table 2-1** and further incubated, for 1 hour and at room temperature, with secondary antibody (for H3, Dako Envision HRP Anti-mouse at 1/1000 was used, whereas for SFTPC, Dako Envision HRP anti-rabbit at 1/1000 was used). Visualization of positive labelling was developed by using a solution of 1 mL of Dako DAB + Substrate buffer + DAB Chromogen in 49mL of 1xPBS, together with 20µL of H_2O_2, on the slides for 1 minute at room temperature. Sections were counterstained by immersion in Mayer's hemalum solution (1:1 in dH_2O) for 40 seconds and dehydrated with decreasing alcohol solutions (same used for rehydration) and xylene and mounted with DPX (Sigma Aldrich 06522 DPX Mountant). Stainings with NP, MX1, CC3, Ki67, CD3 and PAX5 were done by technical staff in the Histology Laboratory of the University of Glasgow School of Veterinary Medicine. For these, and after rehydrating and performing the antigen retrieval, as explained above, the following steps, all at room temperature and done by Dako Autostainer, were performed. Peroxidase blocking was done by using 3% H_2O_2 in PBS for 5 minutes, followed by two washes with Tris tween buffer for 5 minutes each time and incubation with the primary antibody for 30 minutes, at the concentration specified in **Table 2-1** and diluted in 10% FBS in PBS. These were followed by two 5-

minute washes with Tris tween buffer and the incubation with the secondary antibody, for 30 minutes. 10X Tris tween formulation was made of 58.45g of NaCl, 12.1g of Trisma base (Tris (hydroxymethyl) methyl amine), 3.35g of ethylenediaminetetraacetic acid, 5mL of Tween and 1L of dH_2O, at pH 7.5. This was diluted in $dH_2O$to obtain 1x Tris tween buffer. For MX1, Ki67 and PAX5, Dako Envision HRP Anti-mouse at 1/1000 was used, whereas for CC3, NP and CD3, Dako Envision HRP anti-rabbit at 1/1000 was used. Visualization of positive labelling was developed using the same solution of Dako DAB chromogen, but two times for 5 minutes each time, which followed two further washes with Tris tween buffer for 5 minutes each. The slides were washed with purified H_2O two times, and then were manually counterstained, dehydrated and mounted as explained above for SFTPC and H3 stainings.

Procedures described from 2.5 until 2.11 were done by me at the Medical Research Council-University of Glasgow Centre for Virus Research.

Target	Species/Specificity	Brand	Catalog number	Origin	Concentration	Buffer
NP	Influenza A viruses	European Veterinary Labs	Custom made	Rabbit	1:400	10%FBS in PBS
H3	Influenza A viruses	Sigma Aldrich	MAB8254	Mouse	1:1500	10%FBS in PBS
MX1	Human, guinea pig, mouse, rat	Provided by Georg Kochs	Clone M143	Mouse	1:1000	10%FBS in PBS
CC3	Human, rat, mouse, monkey	Cell Signaling	D175	Rabbit	1:1000	10%FBS in PBS
Ki67	Human	Dako	GA626	Mouse	1:200	10%FBS in PBS
CD3	Human	Dako/Agilent	A0452	Rabbit	1:100	10%FBS in PBS
PAX5	Human	Dako/Agilent	GA650	Mouse	1:100	10%FBS in PBS
Surfactant	Human, mouse, rat	Aviva systems biology	OAAJ07121	Rabbit	1:100	10%FBS in PBS

Table 2-1: Specifications of each antibody used in IHC assays.

2.5 Immunofluorescence

After rehydrating, unmasking and blocking endogenous peroxidase and unspecific binding sites the same way done in sections undergoing immunohistochemistry staining, slides were

incubated overnight at 4°C with the primary antibody, anti-H3, diluted 1:1500 in 10%FBS in PBS, and at room temperature for 1 hour with the secondary antibody (Dako Envision HRP Anti-mouse) at 1:1000 in 10%FBS in PBS. Slides were further incubated for an hour at room temperature with Streptavidin Alexa FI 488 (S11223, Thermofisher) in the darkness, overnight at 4°C and in the darkness with the second primary antibody (rabbit polyclonal anti influenza NP (nucleoprotein), European Veterinary Labs) diluted at 1:400 in 10%FBS in PBS and in the darkness for an hour at room temperature with the second secondary antibody (Donkey anti-Rabbit IgG Highly Cross-Adsorbed Secondary Antibody, Alexa Fluor^{TM} 555) at 1:1000 dilution.

Nuclei were stained with DAPI before the mounting of the slides, which was done by applying a mix of Mowiol mounting medium (4.2% glycerol, 0.4% Mowiol 4-88 (Calbiochem, San Diego, CA, USA), 2.1 % 0.2M Tris pH 8.5) with DAPI (1ng/ml).

2.6 RNAscope® In Situ Hybridisation

RNAscope was used for the detection of EIV messenger RNA (mRNA) using NP, M1 and PB2-specific probe sets (Advanced Cell Diagnostics, 322350, 112746-C1, 112747-C1 and 112748-C1). An Equus caballus ubiquitin C (Advanced Cell Diagnostics,Ec-UBC, 512131) probe was used as positive control, whereas DapB - Bacillus subtilis strain SMY methylglyoxal synthase gene (Advanced Cell Diagnostics, 310043) was used as negative control. Blank slides were submerged two times in xylene for 5 minutes at room temperature and in 100% ethanol for 1 minute after the xylene. Sections were dried carefully with paper and were put in the HybEZ oven (provided by Advanced Cell Diagnostics) for 30 minutes at 60°C, for further drying. For endogenous peroxidase blocking, slides were treated with 5 drops per slide of RNAscope Hydrogen Peroxide provided by Advanced Cell Diagnostics for 10 minutes at room temperature. After washing the slides twice to remove the endogenous peroxidase with dH2O, these were submerged in 200mL of boiling target retrieval reagents dilution, made of 20mL of RNAscope 1X Target Retrieval Reagents and 180 mL of dH_2O and provided by the manufacturer, for 30 minutes and washed again in dH_2O for 15 seconds. This was followed by 3 minutes of immersion in 100% ethanol and drying at room temperature, on a paper towel. To delimitate the area to be covered in posterior incubations, two concentric circles were drawn in each tissue slice of each slide with a hydrophobic pen. 5 drops of RNAscope Protease Plus (provided by the manufacturer) were applied on each slice and kept for half an hour at 40°C inside the HybEZ oven, followed by two dH_2O washes. For probe hybridization, 5 drops of the corresponding probe were

applied in each slide and these were incubated for 2 hours at 40°C in the HybEZ oven. After it, slides were washed in 1X wash buffer, provided by the manufacturer and diluted by mixing 60mL of 50X RNAscope Wash Buffer and 2.94L of dH_2O. Signal was amplified with several AMPs (signal amplifiers), provided by the manufacturer, numbered from 1 to 6, interlayered by 1X wash buffer washes, as **Table 2-2** shows. All the incubations were done in a humidity chamber. 120 μL of Fast RED solution, made of 1:60 ratio of Fast RED-B to Fast RED-A (both provided by the manufacturer) were applied to each slide, which were incubated for 10 minutes at room temperature in the humidity chamber and, after it, they were washed 2x with tap water. The kit containing all the reagents (excluding the probes) for the ISH assay was (Advanced Cell Diagnostics, 322350). For counterstain, slides were immersed in Mayer's haemalum (as used for IHC) for 30 seconds at room temperature and washed thoroughly with tap water for another half a minute. For nuclear staining, slides were incubated in Scotts Tap Water Substitute, made of 8.75g of sodium hydrogen carbonate, 50g of magnesium sulphate and 2 crystals of Thymol and diluted in 2.5L of dH_2O, for 2 minutes and washed again in tap water for half a minute. After being dried in the oven for 3 minutes, slides were mounted with the mounting media, EcoMount, provided by the manufacturer.

	Time	Temperature
AMP1	30'	40°C, oven
1X Wash buffer	20''	Room temperature
AMP2	15'	40°C, oven
1X Wash buffer	20''	Room temperature
AMP3	30'	40°C, oven
1X Wash buffer	20''	Room temperature
AMP4	15'	40°C, oven
1X Wash buffer	20''	Room temperature
AMP5	30'	Room temperature
1X Wash buffer	20''	Room temperature
AMP6	15'	Room temperature
1X Wash buffer	20''	Room temperature

Table 2-2*:* AMPs (signal amplifiers) and washes applied to the slides during the amplification process.

2.7 Scanning of slides

Sections stained with H&E and immunohistochemistry and in situ hybridization procedures were scanned with a bright field slide scanner (Leica, Aperio Versa 8) at 40x and with MoticEasyScan Infinity 60 at 80x.

2.8 Collection of IF images

IF-stained slides were visualized and snapshots were taken with Zeiss LSM 880 Confocal Microscope, at 20x and 60x.

2.9 Analysis and quantification of slides

Scanned slides were analyzed and quantified by using the image analyses software Aperio Imagescope®. For the nasal mucosa and trachea, the respiratory epithelium of the entire tissue provided in the slide was selected. For the bronchi, the entire respiratory epithelium of each bronchus of each slide containing lung tissue was selected and studied. For the bronchioles, the respiratory epithelium of 25 bronchioles, randomly picked by using the formula =RANDBETWEEN(1,n) 25 times for each slide, was analyzed in each slide. For the use of the formula, the "n" was replaced by the number of bronchioles present in each slide.

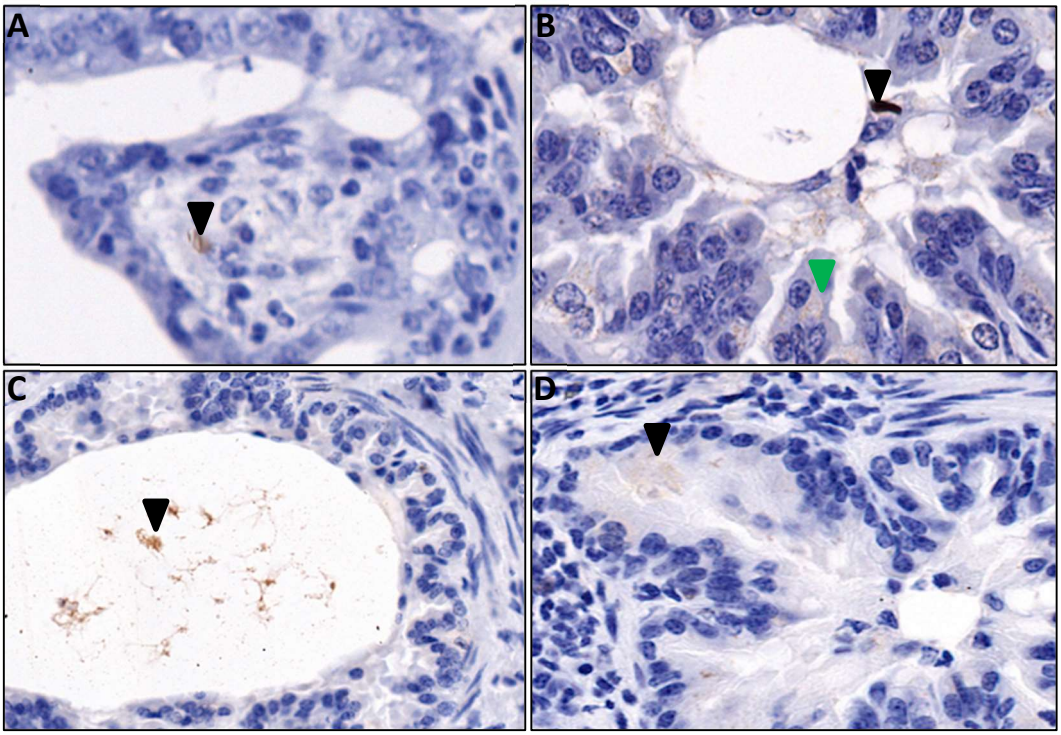

Figure 2-1*:* Examples of unspecific staining in IHC assay. (**A**) Positive NP signal (black arrowhead) in the submucosa of a bronchiole from a non-infected horse. 30x. (**B**) Hyperchromatic fragment in the lumen of a bronchiole from a NP-infected horse (black arrowhead) and characteristic NP granular staining of the epithelial cells of the respiratory epithelium (green arrowhead). 40x. (**C**) Ki67-positive acellular fragments (black arrowhead) in the lumen of a bronchiole of an infected horse. 20x. (**D**) Cytoplasmic Ki67 positive staining in the respiratory epithelium of a bronchiole from a non-infected horse 30x.

For alveoli, 5 alveoli squares (measuring 5 by 2,5 millimetres each) randomly chosen as per the bronchioles, were quantified. Areas of these alveoli squares not containing alveoli (e.g.:

blood vessels, airways, septa) were manually removed and not analysed. In total, for each antibody in which quantification was done, excluding Surfactant Protein C, 1 nasal mucosa, 3 tracheas, a variable number of bronchi, 100 bronchioles and 20 alveoli squares were quantified for each horse. For Surfactant Protein C, only the alveoli were analyzed (20 alveoli squares per horse). Stained sections were scanned for background and nonspecific staining (such as haemosiderin, shown in Figure 4-23). In the slides that had undergone immunohistochemistry, unspecific staining was carefully removed and not analysed. Figure 2-1 illustrates several examples of unspecific binding. Furthermore, artifacts, such as folding of the tissue, were removed manually for all sections examined.

2.10 Statistical analysis

RStudio version 4.0.2. was used for statistical analysis on all data points per sample condition. Statistically significant differences were accepted at $p < 0.05$. Initially, the possibility of using parametric statistics was explored, as these are considered more powerful and accurate than their nonparametric equivalents, but the fact that my data were not normally distributed (as indicated by Shapiro-Wilk test) dismissed this possibility. Among non-parametric statistical test to compare quantitative data among groups, Wilcoxon rank-sum test was chosen. This test is designed for comparison of two (pairwise) independent samples (e.g., the values of %NP staining in the trachea of two different horses), and it is known to cope well with ties in the data, which were quite abundant in my data, and with unequal sample sizes, also frequent among my data. Furthermore, it has the advantage that it works with ranks instead of raw data, which makes it less affected by outliers or extreme values, which, as shown in the following chapters, are common among my data. Finally, it is described as a more powerful and specific tool to make two-group comparisons, compared to tests that assess differences between multiple groups (Conover, W.K., 1999). On the other hand, the main limitation of pairwise tests is that, as they compare only two values at a time, can lack of a completely comprehensive understanding of the data set, as the interactions between multiple items are not fully explored. As a consequence, the richness of the insights obtained from the data analysed with pairwise tests is reduced and there is a risk of oversimplification of complex relationships between items. An alternative statistical approach considered was the usage of Kruskal-Wallis test, which is a nonparametric test designed to make comparisons among 3 or more independent groups of quantitative data. The advantage of having used this test would have been a better and more holistic understanding of the relationship between groups and, therefore, the obtention of stronger conclusions, which were lost by using Wilcoxon rank-sum test; however, these conclusions

might have been skewed by the presence of factors, such as unequal sample sizes and presence of ties, that are known to be detrimental for the power of Kruskal-Wallis test (Whitley *et al*., 2002; Hollander *et al*., 2013; Neuhäuser M., 2011).

2.11 Data plotting

Data were visualized and plotted with GraphPad Prism Version 9.5.0.

Chapter 3. Characterization and quantification of histological lesions in respiratory tissues of horses infected with equine influenza virus

3.1 Introduction

Equine influenza virus is a highly contagious respiratory infectious agent of horses that replicates in the respiratory epithelial cells of the upper and lower respiratory tract (Donis, 2017). It causes equine influenza, which shows high morbidity and low mortality and is normally self-limiting, since animals generally recover within two weeks and after developing a mild disease. Most common symptoms include pyrexia, nasal discharge, cough, depression and anorexia (Timoney, 1996; van Maanen and Cullinane, 2002). In rare cases, when horses are immunologically depleted, bacteria that are part of the normal flora of the upper respiratory tract, such as *Streptococcus zooepidemicus or Staphylococcus aureus*, can act as opportunistic agents and establish a bacterial pneumonia that is potentially lethal (Daly M. *et al*., 2004; López, 2001; Perglione *et al*., 2016; Timoney, 1996).

There are few studies describing the histopathology of EI. It is known that EI causes destruction of the respiratory epithelium of the airways by killing mainly ciliated and goblet cells, which leads to the partial or complete suppression of the mucociliary clearing system (López, 2001; Willoughby *et al*., 1992). These changes lead to the inflammation of the airways and the lung, which clinically translate into pyrexia, cough, nasal discharge (that rapidly becomes purulent), depression and anorexia. Pathological changes in the respiratory tract include loss of goblet cells and cilia, epithelial degeneration, necrosis and hyperplasia, epithelial and submucosa inflammation and pulmonary hyperaemia and oedema (Begg *et al*., 2011; Muranaka *et al*., 2012; Patterson-Kane *et al*., 2008).

Another consequence of the suppression of the mucociliary system, is that in some cases, especially in young or immunologically naïve or incompetent horses, severe secondary bacterial pneumonia can be developed (Willoughby *et al*., 1992). This could be caused by mucus and particles not being cleared and, as a consequence, resident bacteria overgrowing and establishing an active infection. At this stage, lesions such as pulmonary oedema and haemorrhage and inflammation, type II pneumocyte proliferation, bronchial and bronchiolar respiratory epithelial degeneration, necrosis, inflammation and desquamation are frequently described (Muranaka *et al*., 2012; Peek *et al*., 2004).
To better understand the mechanisms of EI pathogenesis and to deepen into the limited knowledge about the histopathology of the respiratory tract in uncomplicated cases of EI, I characterised the lesions and pathological changes observed in respiratory tissues of horses experimentally infected with EIV in previous studies (Muranaka *et al*., 2012; Yamanaka *et al*., 2009).

Ibaraki 07/DPI	0	1	**2**	**3**	4	5	6	**7**	8	9	10	11	12	13	**14**
Horse 5															
Pyrexia	38.1	37.9	38.9	38.1	38	38.2	38.6	38.6	39.8	39.3	38.9	38.6	38.1	38.2	37.9
Nasal discharge	-	-	-	+	+	+	+++	++	+++	+++	++	++	++	++	+
Cough	-	-	-	+	-	+	++	+	++	+	+	+	+	+	+
Horse 6															
Pyrexia	37.8	38	38.7	38.8	38.4	38.2	38.7	38.7	39.3	39.1	38.9	38.2	38.4	38	38
Nasal discharge	-	-	+	+	+	++	+	++	+++	++	-	++	-	++	+
Cough	-	-	-	+	+	+	++	-	++	+	+	+	+	-	+
Horse 7															
Pyrexia	38	38.3	39.3	38.5	38.4	38.6	38.6	39.3	39.3	39.2	38.6	38.4	38	38	38.3
Nasal discharge	-	-	+	+	+++	+++	++	++	++	++	++	-	+	-	-
Cough	-	-	-	+	+	+	+	+	-	+	+	+	+	+	-

Table 4-2*:* Pyrexia, nasal discharge and cough scores during the infection of the three horses euthanized at day 14 post infection. - = absent, + = mild, ++ = moderate, +++ = severe. Data provided by Dr. Akihiro Ochi.

This chapter focuses on the identification and quantification of lesions in the respiratory tract. This was achieved by observing haematoxylin and eosin-stained slides of the nasal mucosa, trachea, bronchi, bronchioles and alveoli of two uninfected horses, and seven horses that had been infected and euthanised at various days post infection (pi): one horse was euthanized at 2dpi, two horses were euthanised at 3dpi, one horse was euthanised at 7dpi and three horses were euthanised at 14dpi. Samples from horses euthanised at 2, 3 and 7 dpi were generated in a study by (Muranaka *et al*., 2012), whereas samples from horses euthanised at 14dpi were obtained from a different study, carried out by the same group and using the same EIV strain (Yamanaka *et al*., 2009). The only difference between the two studies is that in the second one each horse was kept for the entire experiment in a separate stall with a dog to study interspecies transmission.

As reported by Muranaka *et al*. and Yamanaka *et al*., horses shed virus until days 6 and 7 pi. The peak of symptoms (nasal discharge, cough and fever) was observed between the 5th and 10th day after infection (**Table 3-1**).

The quantification of lesion was done by using image analyses. To this end, histological sections were scanned using a slide scanner and scanned images were analysed using Aperio Imagescope® software.

3.2 Results

3.2.1 Quantification of histological changes.

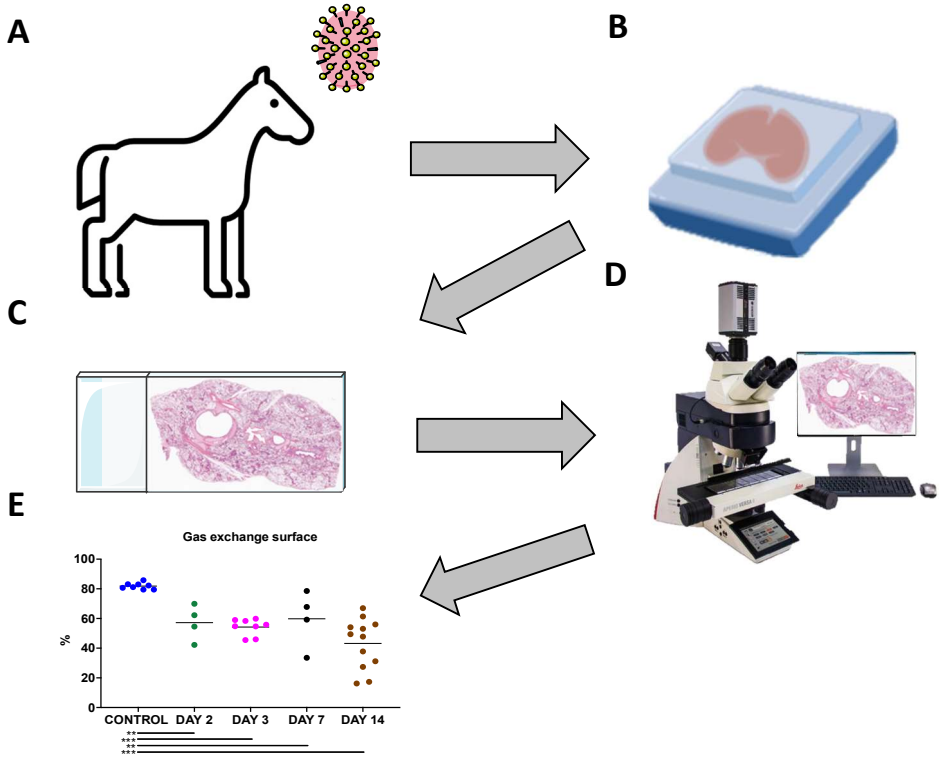

Figure 3-1*:* Schematic representation of the workflow. (**A**) Horses were experimentally infected with EIV A/equine/Ibaraki/1/2007 and euthanized at different timepoints. (**B**) Formalin-fixed and paraffin-embedded respiratory tissues were obtained in post-mortem examination. (**C**) Blank slides of respiratory tissues underwent H&E or PAS staining. (**D**) H&E and PAS sections were scanned with Leica Aperio Versa 8® and analysed with Aperio Imagescope®. (**E**) Data were plotted with GraphPad Prism 9.

To better understand the pathological processes triggered by EIV infection, I quantified histological changes associated with some of the lesions explained above. I used images of H&E-stained sections for all the parameters with the only exception of the quantification of goblet cells, for which images subject to PAS staining were used. These slides were scanned with Leica Aperio Versa 8® and the quantification of histological changes was done by using Aperio Imagescope® software (**Fig.3-1**)

Three different strategies were followed to quantify changes in the respiratory tissues: nuclear count, pixel count and distance and area measurement.

Nuclear count. To determine changes in the number of nuclei in respiratory tissues as result of death or tissues regeneration, I counted nuclei by using a modification of the default nuclei

count algorithm of Aperio Imagescope®. I used this algorithm to quantify goblet cell numbers and size and nuclei numbers, size and density. **Figure 3-2** shows how it works.

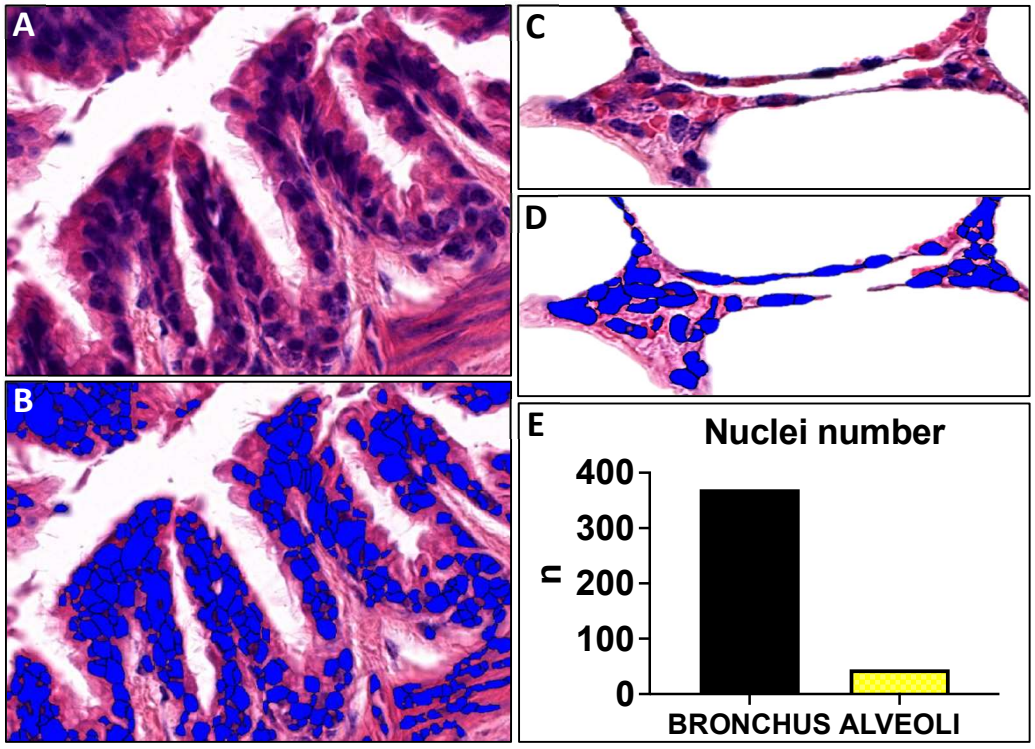

Figure 3-2*:* Snapshots of lung section stained with H&E. (**A**) Detail of a bronchial respiratory epithelium. (**B**) The same area, after being analysed by the nuclei count algorithm of Aperio Imagescope® software. (**C**) Detail of alveoli. (**D**) The same alveoli, after being analysed by the nuclei count algorithm of Aperio Imagescope® software. Blue objects are nuclei identified by the software. 30x. (**E**) Bar plot showing nuclei number in bronchus and alveoli.

Pixel count. To determine the surface of images occupied by tissue and by air, I utilised a modification of the positive pixel count algorithm of Aperio Imagescope®. I quantified the percentage of airway blockage and the percentage of gas exchange surface with this method. **Figure 3-3** shows how the positive pixel count algorithm works on respiratory tissues.

Distance and area measurements. To make measurements of length and area in respiratory tissues, the Pen tool of Aperio Imagescope® was used. Percentage of epithelial surface covered by cilia, percentage of lung fibrosis/granulation tissue and thickness of respiratory epithelia was quantified by using it, as **Figure 3-4** shows.

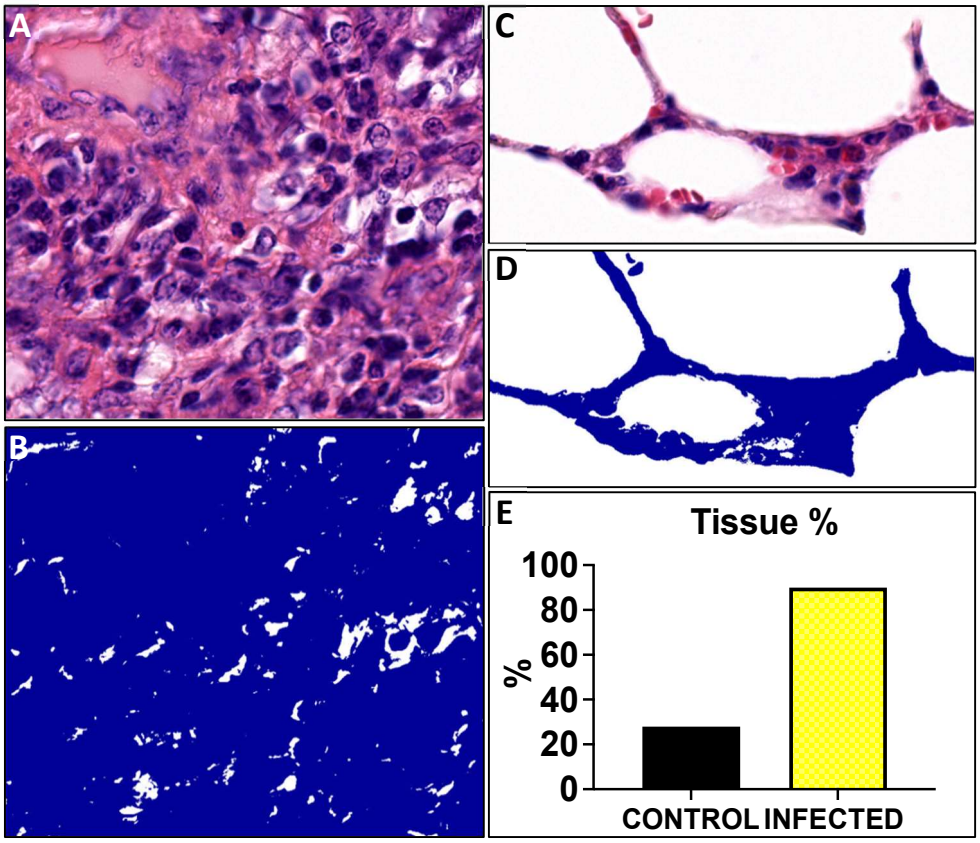

Figure 3-3*:* Snapshots of alveoli stained with H&E. (**A**) Detail of alveoli from a 14dpi infected horse. (**B**) The same area, after being analysed by the pixel count algorithm of Aperio Imagescope® software. (**C**) Detail of alveoli from a noninfected horse. (**D**) The same area, after being analysed by the positive count algorithm of Aperio Imagescope® software. Blue objects are pixels identified by the software. 30x. (**E**) Bar plot percentage of tissue in the alveoli.

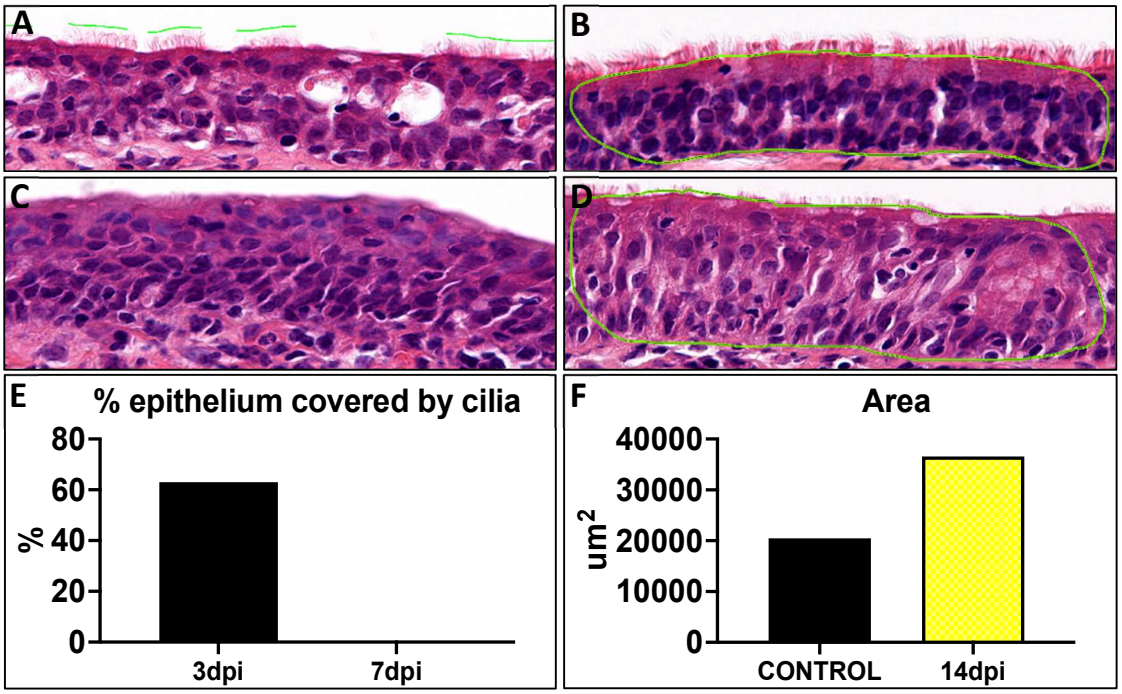

Figure 3-4*:* Snapshots of tracheas stained with H&E. (**A**) Tracheal respiratory epithelium from a horse infected and euthanized at 3dpi, showing some areas covered by cilia and outlined (in green) with Aperio Imagescope® Pen tool. (**B**) Tracheal respiratory epithelium from an uninfected horse outlined (in green) with Aperio Imagescope® Pen tool for its area to be measured. (**C**) Tracheal respiratory epithelium from the horse infected and euthanized at 7dpi, showing no areas covered by cilia (**D**) Tracheal respiratory epithelium from a horse infected and euthanized at 14dpi outlined (in green) with Aperio Imagescope® Pen tool for its area to be measured. 25x. **(E)** Barplot showing percentage of tracheal respiratory epithelium covered by cilia. (**F**) Bar plot showing area of tracheal respiratory epithelium.

3.2.1.1 Loss of cilia

To quantify the loss of cilia during EIV infection, I manually quantified the percentage of respiratory epithelium covered by cilia in each section of nasal mucosa and trachea and in the biggest bronchus of each slide by measuring the total length of the epithelia and, within it, the length covered by cilia, as **Figure 3-4a**, **c** and **e** show.

In the nasal mucosa, after a small increase in % of epithelium covered by cilia between controls and 2dpi (from 85 to 98%), the percentage stayed at 98 at 3dpi and decreased to 13 by 7dpi. At 14dpi, the percentage raised to 96% (**Figure 3-5**). Note that only one of the three nasal mucosa sections from horses euthanized at 14dpi exhibited respiratory epithelium, which means this value, together with any values showing quantification in nasal mucosa at 14dpi, are based on measurements collected from a single section.

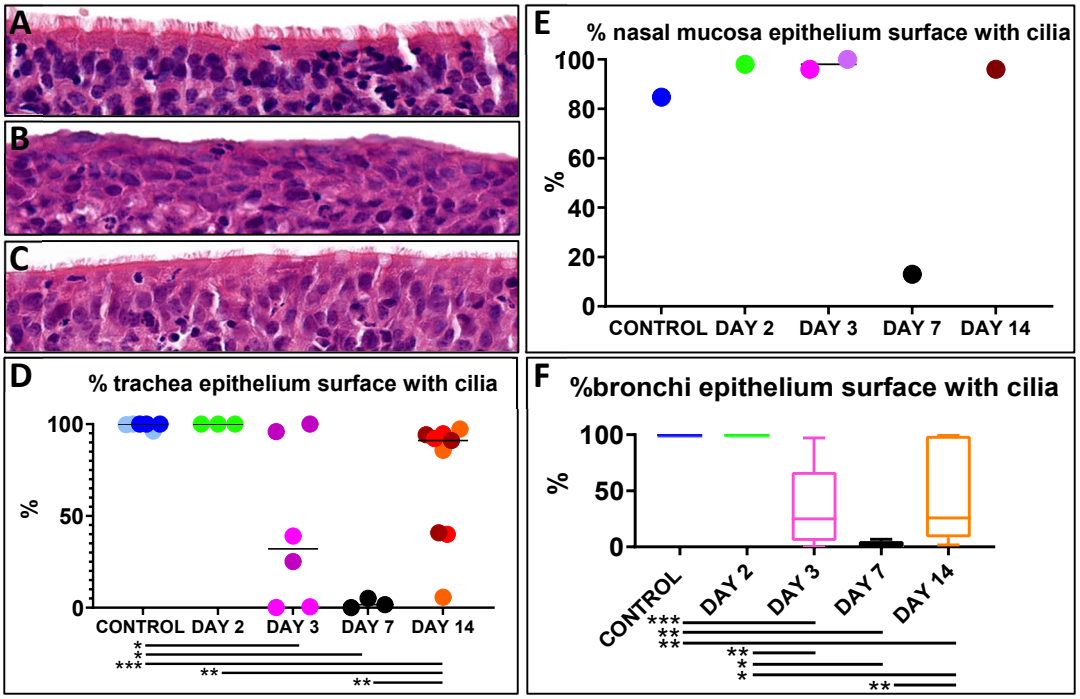

Figure 3-5: Representative images of trachea sections stained with H&E from 2dpi (**A**) 3dpi (**B**) and 14dpi (**C**) horses showing respiratory epithelia of the trachea. Dot/box plots showing % of nasal mucosa (**D**), trachea (**E**) and bronchial (**F**) respiratory epithelial surface covered by cilia. Loss of some cilia can be observed at 3dpi, whereas at 7dpi no cilia can be seen. At 14dpi cilia can be observed again. 15x. Light blue = control 2, dark blue = control 4, pink = horse 2, purple = horse 3, orange = horse 5, red = horse 6, brown = horse 7 Statistical significances were assessed using a Wilcoxon rank sum test, *=p<0.05, **=p<0.01, ***=p<0.001. Each data point represents a tissue section or a bronchus. Bar shows the median. Whiskers show the highest and lowest values.

In the trachea, 99% of the epithelium length was covered by cilia in the controls and 100% at 2dpi. The percentage decreased to 43% at 3dpi and further decreased to 2% by 7dpi. As

seen in the nose, at 14dpi the percentage increased, although in a lower degree (71%) (**Fig.3-5**).

Similar dynamics were observed in the bronchi. In the controls and in the 2dpi horse the coverage was 100% and there was a loss of cilia at 3dpi (35% of coverage). The loss was bigger at 7dpi (2%).

Like the other tissues, the bronchi had recovered part of the cilia coverage of the epithelia (47%) by 14dpi (**Fig.3-5)**.

These results show a decrease of cilia at 3dpi, a maximum loss at day 7pi in all tissues and a recovery at day 14pi. Furthermore, it can be seen a gradient of loss and recovery of cilia from the nasal mucosa, where this loss is the smallest in all timepoints, until the bronchi, where the percentage of epithelium covered by cilia is the lowest among the three tissues analysed, during the entire course of the infection. These data suggest that the nasal mucosa is the least affected tissue with regards to loss of cilia.

To assess differences of cilia dynamics depending on the location, the data of the trachea was divided into 3 locations (upper, middle and lower) and the data of the bronchi was divided into two in the craniocaudal axis (anterior and posterior) and in the laterolateral axis (left and right).

Regarding tracheal locations, the values of % of epithelial surface covered by cilia in the upper, middle and lower regions did not show differences in the controls, in the horse euthanized at 2dpi and in the horse euthanized at 7dpi. At days 3pi and 14pi, a gradient of loss of cilia was observed from the upper part, which had the highest % of surface covered by cilia (70% 3dpi, 93% 14dpi), to the middle part (48% 3dpi, 65% 14dpi) and the lower part (13% 3dpi, 56% 14dpi), which had the lowest. However, no statistical differences were revealed in any of the comparisons (**Fig.3-6**).

These results suggest that the gradient of cilia loss observed between the nasal mucosa and the bronchi is reproduced at a lower scale within the trachea.

In the bronchi, at 3dpi I observed that anterior lobes (50%) had a higher % of surface covered by cilia compared to the posterior lobes (21%). On the other hand, at 7dpi (3%) and 14dpi (86%) posterior lobes had higher % of epithelium covered by cilia than anterior lobes (0% and 24%). Noninfected controls and the 2dpi horse did not show any differences when

comparing between anterior and posterior lobes. Statistical comparisons were performed, and no differences were seen in any of the comparisons (**Fig.3-6**).

Regarding laterolateral differences, the right bronchi had higher % of cilia coverage at 3dpi (31% vs 40%), 7dpi (0% vs 3%) and 14dpi (43% vs 51%) than left ones, although none of

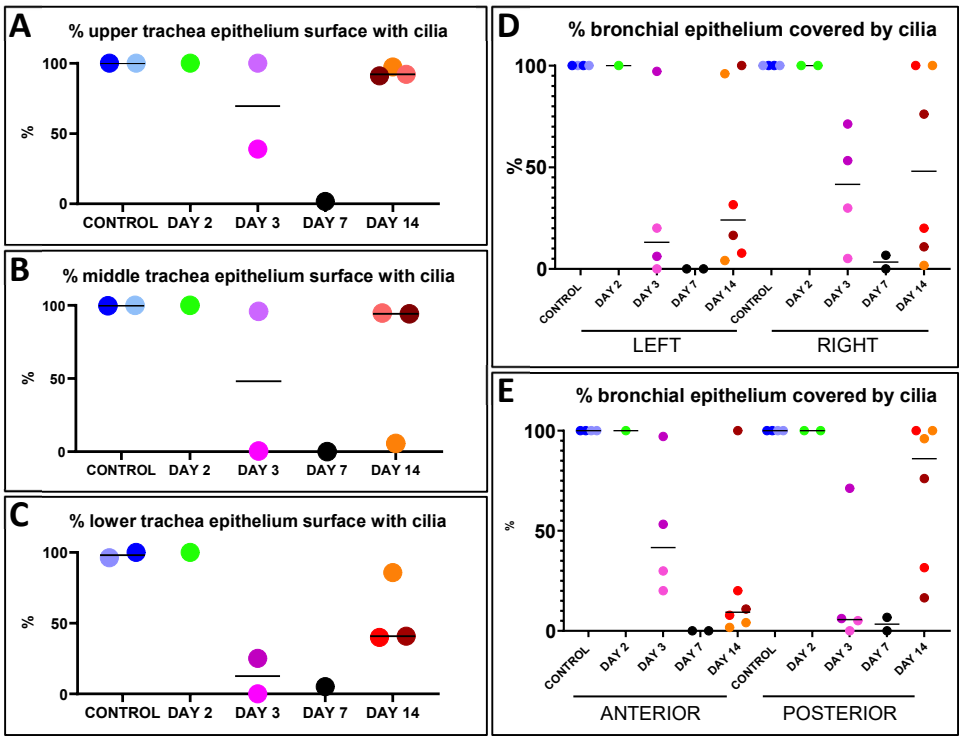

Figure 3-6: Dot plots showing % of respiratory epithelial surface covered by cilia in the upper (**A**), middle (**B**) and lower trachea (**C**) and in the bronchi (**D** and **E**). Light blue = control 2, dark blue = control 4, pink = horse 2, purple = horse 3, orange = horse 5, red = horse 6, brown = horse 7. Each data point represents a tissue section or a bronchus. Bar shows the median.

These results suggest that respiratory epithelia of the bronchi from anterior and left lobes are more affected at late timepoints.

To highlight interindividual differences between the two horses euthanized at 3dpi and among the three horses euthanized at 14dpi, I stratified the data of loss of cilia at this two timepoints by horse. At 3dpi, differences were seen between horse 2 and horse 3 in the % of epithelium covered by cilia in the trachea (13% horse #2, 74% horse #3) and in the bronchi (13% horse #2, 57% horse #3). At 14dpi, horse 5 had lower % of epithelium covered by cilia compared to horses 6 and 7 (62 vs 75 and 75%) in the trachea, and in the bronchi, horse 6 had lower % than horse 5 and 7 (40 vs 58 and 59%).

These results suggest that, in the lower respiratory tract, horse 2 was more affected by EIV than horse 3. Also, horse 7 would be the least affected horse of its group (n=3). However, no statistical differences were observed.

3.2.1.2 Loss of goblet cells

To determine the degree of loss of goblet cells throughout EIV infection, I calculated the density of goblet cells per epithelium millimetre in the respiratory epithelia of each nasal mucosa and trachea and in the biggest bronchus of each slide. Goblet cells were counted with the nuclei count algorithm by using PAS-stained slides and their numbers were divided by the length of the epithelium, which was determined by using the Pen tool.

In the respiratory epithelium of the nasal mucosa, a small decrease in goblet cell density was observed from noninfected controls (10 gc/mm) to 2dpi (8.7 gc/mm). A further decrease in goblet cell density was seen at 3dpi (6.7 gc/mm), whereas at 7dpi no goblet cells were seen (0 gc/mm). Finally, at 14dpi goblet cells were identified again, although in a lower density than in the early infection timepoints (4.5 gc/mm) (**Fig. 3-7**).

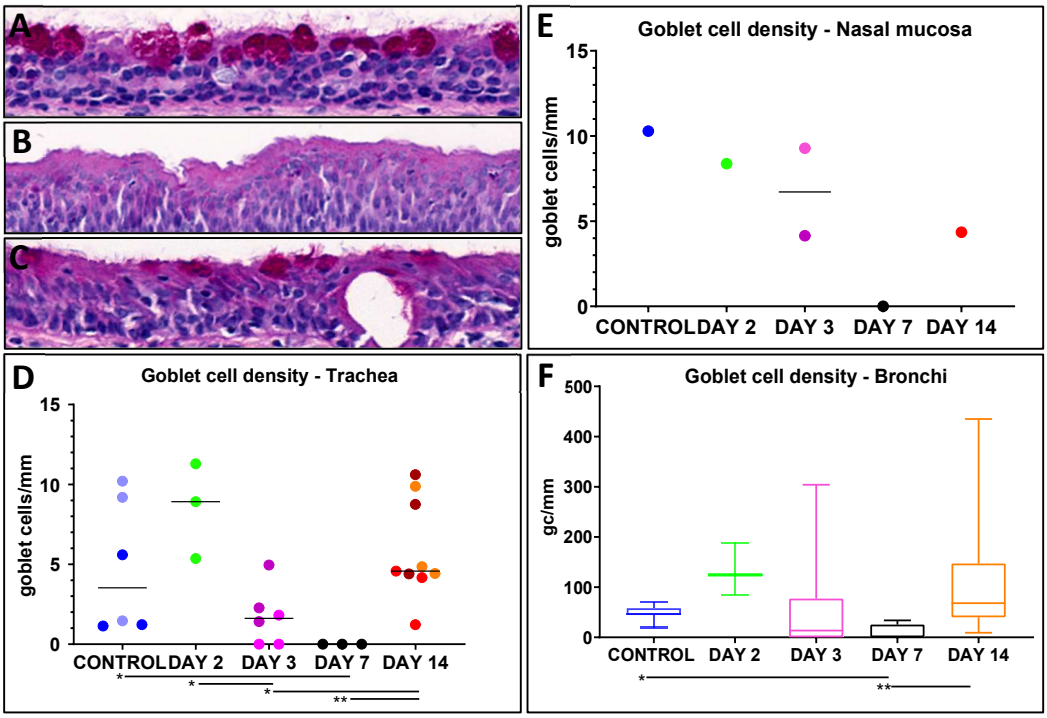

Figure 3-7: Representative images of nasal mucosa sections stained with PAS from control (**A**), 7dpi (**B**) and 14dpi (**C**) horses showing loss and recovery of goblet cells. Dot /box plots showing density of goblet cells per millimetre of respiratory epithelia in the trachea (**D**) nasal mucosa (**E**) and bronchi (**F**). A marked decrease of goblet cell density can be seen at 7dpi. 15x. Each data point represents a tissue section or a bronchus. Light blue = control 2, dark blue = control 4, pink = horse 2, purple = horse 3, orange = horse 5, red = horse 6, brown = horse 7. Statistical significances were assessed using a Wilcoxon rank sum test, *=p<0.05, **=p<0.01. Bar shows the median. Whiskers show the highest and lowest values. Note that, among nasal mucosa sections from horses euthanized at day 14pi, only one exhibited respiratory epithelium.

In the tracheal respiratory epithelium, from controls to 2pi the density of goblet cells almost doubled (4.8 to 8.5 gc/mm.), whereas it decreased to a third at 3dpi (1.7 gc/mm). Similar to

what happened in the nasal mucosa, at 7dpi no goblet cells were seen (0 gc/mm). By 14dpi goblet cells were present in the epithelium again (5.8 gc/mm) (**Fig. 3-7**).

Finally, in the bronchi, the loss of goblet cells followed a pattern similar to the one revealed in the trachea, although in a superior scale. The peak of goblet cell density was at 2dpi (130 gc/mm), which triplicated the density seen in the controls (5 gc/mm). Goblet cell density decreased to levels seen in controls at 3dpi (57 gc/mm), whereas by day 7, three of the four bronchi analysed did not have any goblet cells, and the mean density of the four airways was 8 goblet cells per millimetre of respiratory epithelium. At 14dpi, as seen in the other tissues, the density of goblet cells increased (106 gc/mm) (**Fig.3-7**).

Overall, these results show that goblet cells completely disappear from respiratory epithelia at 7dpi and can be seen again at 14dpi, which is compatible with descriptions made by Muranaka *et al*. (Muranaka *et al.*, 2012). There is a density increase by 2dpi, which could belong to a goblet cell hyperplasia, described as a histological change in several viral infections, such as respiratory syncytial virus (Cortez and Schultz-Cherry, 2021; Curran and Cohn, 2010).

As done with the cilia data, to evaluate goblet cell density differences depending on the anatomical location, the data from the trachea were divided into three groups (upper, middle and lower) and the data of the bronchi was divided in two in the craniocaudal axis (anterior and posterior) and in the laterolateral axis (left and right).
In the upper trachea, from controls to 2dpi the density increased from 5.7 gc/mm to 8.9 gc/mm. At 3dpi it decreased to 2 gc/mm and at 7dpi no goblet cells were detected (0.0 gc/mm) The density increased to 5.7 gc/mm at 14dpi.
The middle part of the trachea had a similar dynamic, although in a lower magnitude. Controls had a density of 3.5 gc/mm and at 2dpi it was 5.3 gc/mm. By 3dpi it had decreased to 2.5 gc/mm and at 7dpi there were no goblet cells (0.0 gc/mm) in the epithelium. At 14dpi the density increased to 6.7 gc/mm.
The lower trachea repeated the dynamics seen in the other two parts of the trachea. From the controls (5.2 gc/mm) to 2dpi (11.2 gc/mm) the density of goblet cells in the epithelium doubled. At 3dpi goblet cells had reduced drastically (0. 7 gc/mm) and at 7dpi had disappeared (0.0 gc/mm). By 14dpi goblet cells were seen again in the epithelium (5.2 gc/um), in similar levels seen in the controls. The sample size of these comparisons was too small to do statistical tests (**Fig.3-8**).

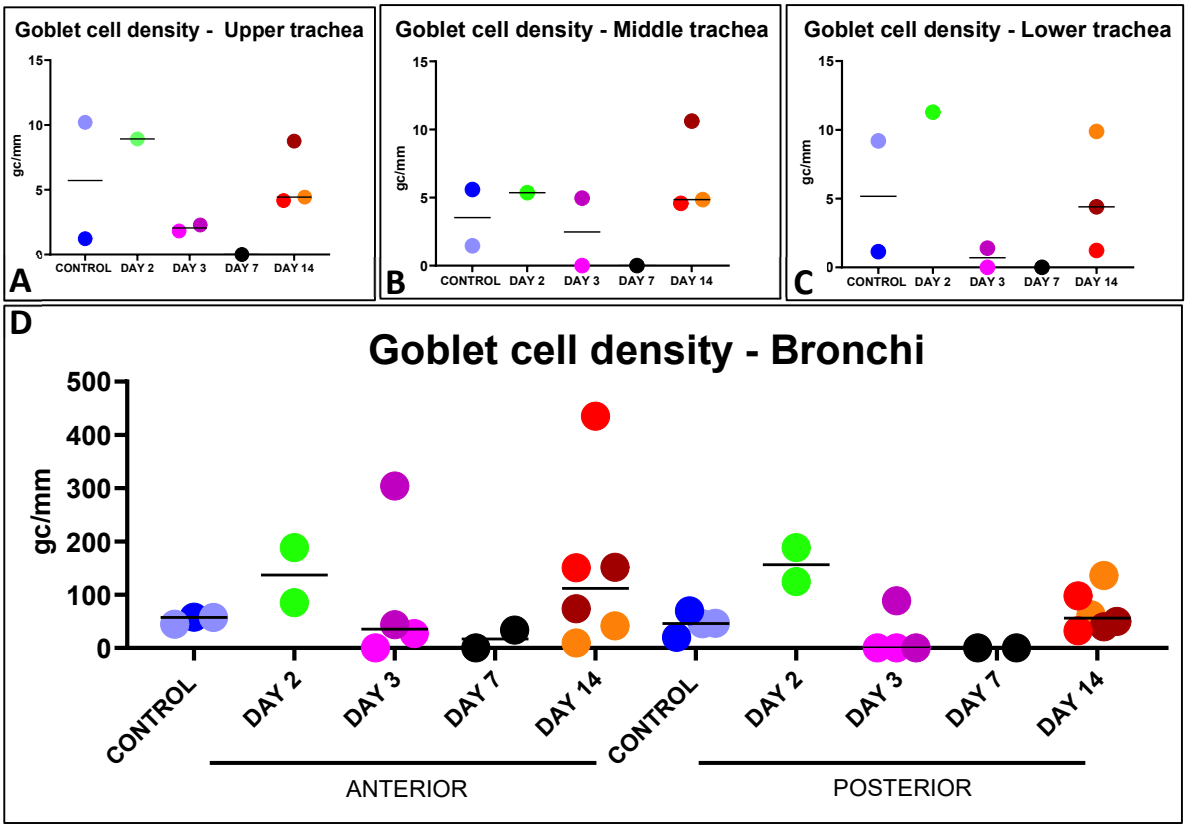

Figure 3-8: Dot plots showing goblet cell density in the respiratory epithelia of the upper (**A**), middle (**B**) and lower trachea (**C**) and the bronchi (**D**). Each data point represents a section or a bronchus. Light blue = control 2, dark blue = control 4, pink = horse 2, purple = horse 3, orange = horse 5, red = horse 6, brown = horse 7 Bar shows the median.

Overall, these results show an increase in goblet cell density after two days of infection, and a decrease afterwards, until the complete disappearance of goblet cells by 7dpi.

Regarding the bronchi, anterior lobes had a higher goblet cell density at 3dpi (90 gc/mm), 7dpi (16 gc/mm) and 14dpi (150 gc/mm) than posterior lobes (20, 0 and 70 gc/mm) and a lower density at 2dpi (90 vs. 16 gc/mm). Also, left lobes had more goblet cells per squared micrometre than right lobes in all timepoints: 2dpi (190 vs. 100 gc/mm), 3dpi (80 vs. 40 gc/mm), 7dpi (16 vs 0 gc/mm) and 14dpi (130 vs 80 gc/mm). Given the small size sample, I could not perform some statistical comparisons, whereas the ones I could run did not show any statistical differences.

Overall, these results suggest that anterior lobes lose less goblet cells per epithelial surface than posterior lobes during EIV infection (**Fig.3-8**).

Regarding interindividual differences, at 3dpi horse 2 had less goblet cells/um in the trachea (0.6 gc/mm) and the bronchi (6 gc/mm) than horse 3 (2 and 110 gc/mm), whereas in the nasal mucosa, horse 3 had less density of goblet cells (4 gc/mm) than horse 2 (9 gc/mm). At 14dpi, in the trachea horse 5 had 6 gc/mm, horse 6 had 3 gc/mm and horse 7 had 8 gc/mm. In the bronchi, goblet cell density of horse 5 was 60 gc/mm, horse 6 had 180 gc/mm and

horse 7 78 gc/mm. Only one of the three nasal mucosa sections from 14dpi horses had respiratory epithelium. None of the comparisons made between horses was statistically significant. These data show that horse 2 lost a higher amount of goblet cells in the lower respiratory tract and a smaller amount in the upper respiratory tract, compared to horse 3. Furthermore, horse 6 had less goblet cells per millimetre of epithelium in the trachea compared to horse 5 and 7, whereas it had more than them in the bronchi (**Fig.3-9**).

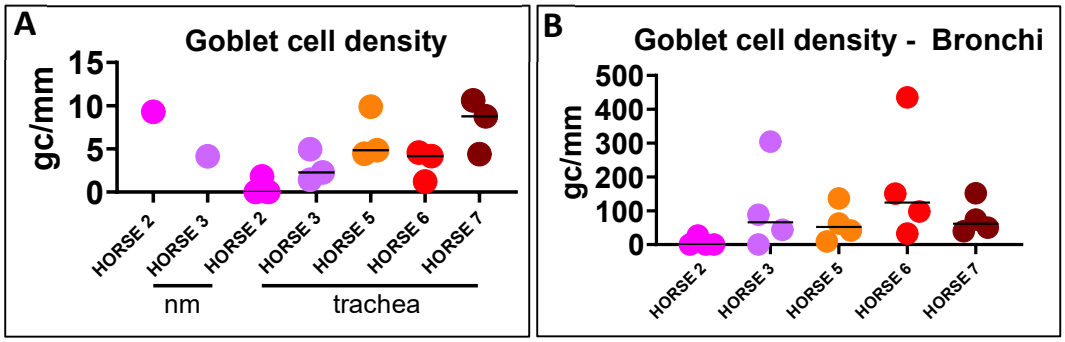

Figure 3-9 Dot plots showing density of goblet cells per millimetre of respiratory epithelia in the nasal mucosa and trachea (**A**) and bronchi (**B**). Each data point represents a nasal mucosa section, tracheal section or bronchus. Bar shows the median.

3.2.1.3 Goblet cell size

Regardless of the density of goblet cells and the region of the respiratory tract examined and the tissue, when examining PAS-stained sections, I observed that the size of the PAS-positive area of the goblet cells (in other words, the area occupied by mucin) seemed bigger in early timepoints, especially at day 2 post infection, compared to late timepoints. This could be explained by goblet cells hypersecreting mucins.

To test this hypothesis, I quantified the average surface positive to PAS staining within this cell type as a proxy for goblet cell size, by using the nuclei count algorithm in the nasal mucosa, trachea and bronchi. PAS-stained slides were used for this purpose. Some tissues, especially those coming from the horse euthanized at 7dpi, did not have any goblet cell to count. Also, as explained above, only one of the three nasal mucosa sections from horses euthanized at 14dpi displayed respiratory epithelium. Goblet cell size was quantified in the respiratory epithelia of all nasal mucosa, tracheas and in the biggest bronchus of each lung lobe.

In the nasal mucosa, the size of goblet cells increased markedly from noninfected horses (24 um^2) to 3dpi (57 um^2), before disappearing completely at 7dpi. At 14dpi the size was 77 um^2 (**Fig.3-10**).

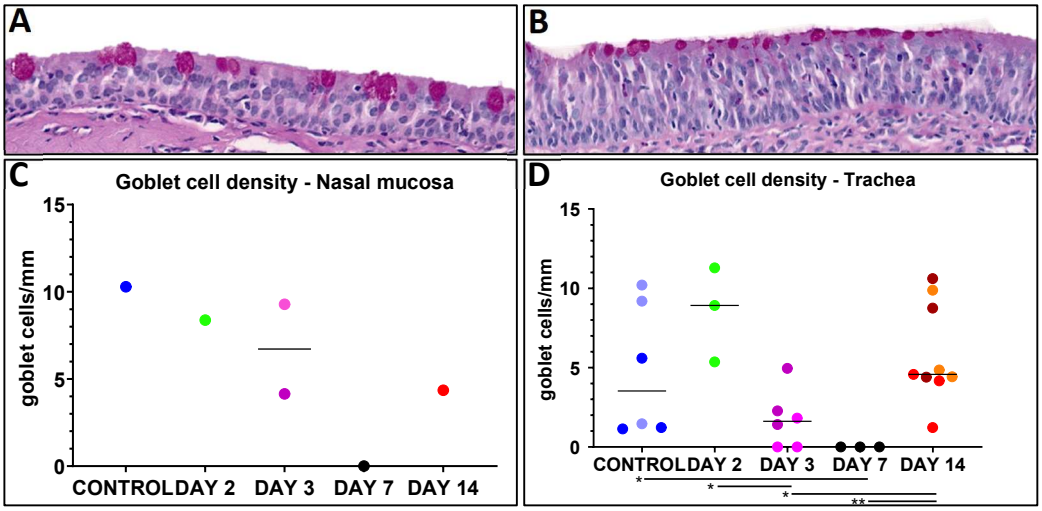

Figure 3-10: Representative images of nasal mucosa sections stained with PAS from horses experimentally infected and euthanised at 2dpi (**A**) and 14dpi (**B**) showing respiratory epithelia of the trachea. Dot plots showing goblet cell density in the respiratory epithelia of the nasal mucosa (**C**) and trachea (**D**). Note that horse 6 and horse 7 did not have respiratory epithelium in the sections of nasal mucosa. 15x. Light blue = control 2, dark blue = control 4, pink = horse 2, purple = horse 3, orange = horse 5, red = horse 6, brown = horse 7. Statistical differences were assessed using a Wilcoxon rank sum test, *=p<0.05. Each data point represents a tissue section. Bar shows the median.

In the trachea, goblet cell's area increased in size between the noninfected controls and the horse infected and euthanized at 2dpi, going from 26 to 45 um^2. There was a decrease at 3dpi (19 um^2,) and a small increase (23 um^2) at 14dpi. No goblet cells were identified at 7dpi (**Fig. 3-10**).

In the bronchi, goblet cells size stayed stable during the first 2 days of infection (23 um^2) and increased at 3dpi (25 um^2). At 7dpi only one of the four lobes had goblet cells, which were the smallest (14 um^2), whereas at 14dpi there size was 22 um^2. No statistically significant differences were seen.

When I stratified the trachea into its three anatomical locations, no statistical differences were seen, since the sample size was either very reduced or too small to run statistical comparisons. Nevertheless, some specific characteristics were observed depending on the region. In the upper trachea, the mean goblet cell area increased from 26 um^2 to 58 um^2 from controls to 2dpi. At 3dpi the size had dropped to 20 um^2, whereas at 14dpi it had increased again, to 28um^2.

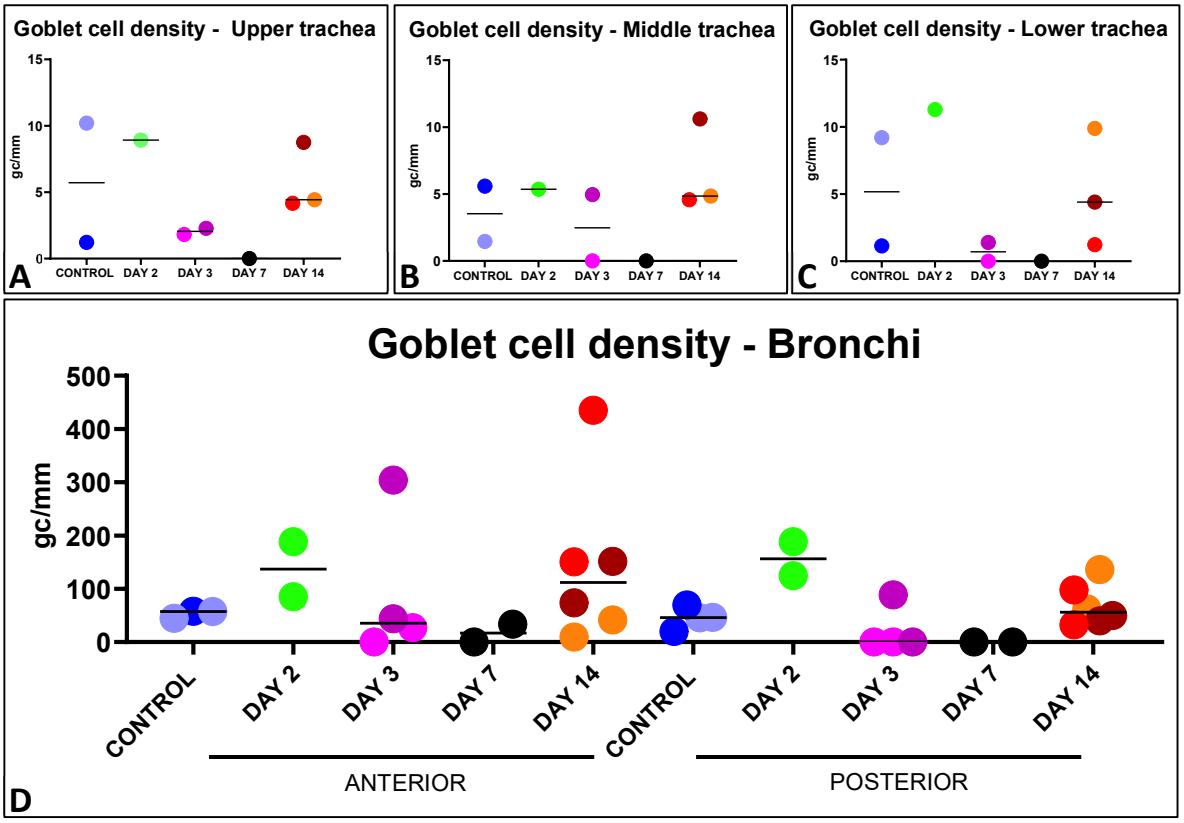

Figure 3-11: Dot plots showing goblet cell size in the upper (**A**), middle (**B**) and lower trachea (**C**) and in the bronchi (**D**). No goblet cells were seen at 7dpi, except in the anterior bronchi. Light blue = control 2, dark blue = control 4, pink = horse 2, purple = horse 3, orange = horse 5, red = horse 6, brown = horse 7. Each data point represents a tissue section or bronchus. Bar shows the median.

The middle trachea revealed a similar dynamic, with the goblet cell area being especially high at 2dpi (55 um^2) and lower in the controls (27 um^2) and at 3dpi (23 um^2) and 14dpi (22 um^2). In the lower trachea, a different dynamic was observed. The goblet cell size was already high in the controls (24.5 um^2) and increased at 2dpi (26 um^2), dropping posteriorly to 14 um^2 at 3dpi and increasing slightly at 14dpi (17 um^2). Furthermore, as shown, the peak of goblet cell size in the lower trachea (2dpi) was half of the peak of goblet cell size in the upper and middle trachea (also 2dpi) (**Fig.3-11**).

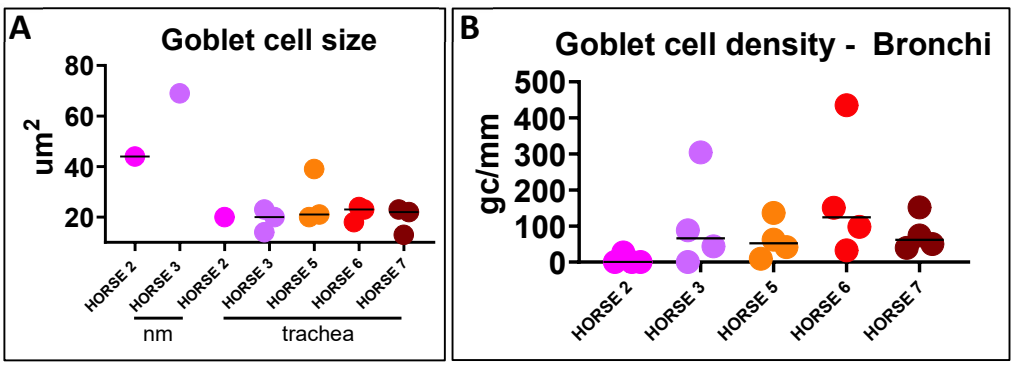

Figure 3-12: Dot plots showing goblet cell size in the nasal mucosa and trachea (**A**) and bronchi (**B**). 15x. Each data point represents a tissue section or a bronchus. Bar shows the median.

In the bronchi, anterior lobes had bigger goblet cells at 3dpi (26 um^2) than posterior lobes (23 um^2), whereas in the controls, 2dpi and 14dpi the situation was reverse (22 vs. 24 um^2 controls, 20 vs 26 um^2 2dpi, 19 vs. 25 um^2 14dpi). Also, goblet cells from right lobes were bigger than left lobes in controls (25 vs. 22 um^2), 3dpi (22 vs. 28 um^2) and 14dpi (22 vs. 23 um^2) and the same size at 2dpi (24 vs. 24 um^2). None of these differences were significant (**Fig.3-11**).

Regarding interindividual differences, horse 2 showed more goblet cell area than horse 3 in the trachea (20 vs 19 um^2), whereas in the nasal mucosa (44 vs 69 um^2) and the bronchi (22 vs. 26 um^2) it showed less. In the horses euthanized at 14dpi, a gradient of goblet cell area was seen in the trachea and bronchi, from horse 5 (27 and 27 um^2) and horse 6 (22 and 21 um^2) to horse 7 (19 and 19 um^2) (**Fig.3-12**).

Overall, there are two things to highlight with these data. First, these results indicate that, in the nasal mucosa and the trachea, goblet cells area increases at early infection timepoints in the equine respiratory epithelia of the airways, before disappearing by 7dpi, which suggests that, in response to EIV infection, in a first stage there is a mucus hypersecretion coming from goblet cells. Mucus hypersecretion has been described in mice infected with H1N1 influenza virus (Li and Tang, 2021).

Also, the decrease in goblet cell numbers (described in the previous section) and size by 3dpi and onwards might explain, at least partially, the worsening of the lesions in the airways and the lung at these timepoints. As explained in the introduction, goblet cells are known to have a protective role against viral infections, including influenza. At 14dpi goblet cells could be seen again in the nasal mucosa and trachea and their size was the same or higher than they were before the infection, suggesting that their population was recovering, if had not recovered already. Regarding the bronchi, there are two features that distinguish them from the nasal mucosa and the trachea: first, size of areas occupied by mucin changed in a very small scale among controls, 2dpi, 3dpi and 14dpi, and second, some goblet cells were still detectable at 7dpi. Second, data suggest different dynamics in size change depending on the location. A gradient could be seen from the nasal mucosa to the bronchi, according to the degree of size change that areas occupied by mucin show; in the nasal mucosa these seemed to be more flexible in size. Their size at 14dpi was almost four times the size than in uninfected controls, whereas in the trachea the difference between the highest value (2dpi, 46 um^2) and the lowest (3dpi, 19 um^2) was much smaller, and in the bronchi, as explained,

sizes barely changed. The fact that goblet cells in the nasal mucosa were bigger than those in the trachea and bronchi at 14dpi, suggests that the recovery of goblet cells' population in this tissue is faster than in the trachea and bronchi. However, the small sample size makes essential to do further analysis on this regard.

3.2.1.4 Change in thickness of the respiratory epithelia

To quantify the respiratory epithelial thickness, and specifically to determine the presence of epithelial hyperplasia, I used the pen tool to measure epithelial area and length in the nasal mucosa and the trachea, and, by dividing the earlier by the latter, I obtained the respiratory epithelial thickness. This parameter was quantified in all the sections of nasal mucosa and trachea. Due to their size variability, which would have resulted in highly variable results, bronchi and bronchioles were not analysed.

In the nasal mucosa, a peak at 2dpi was seen (127 um). At 3dpi, a decrease to 70 um was followed by an increase at 7dpi (108 um) and 14dpi (121um) (**Fig.3-13**).

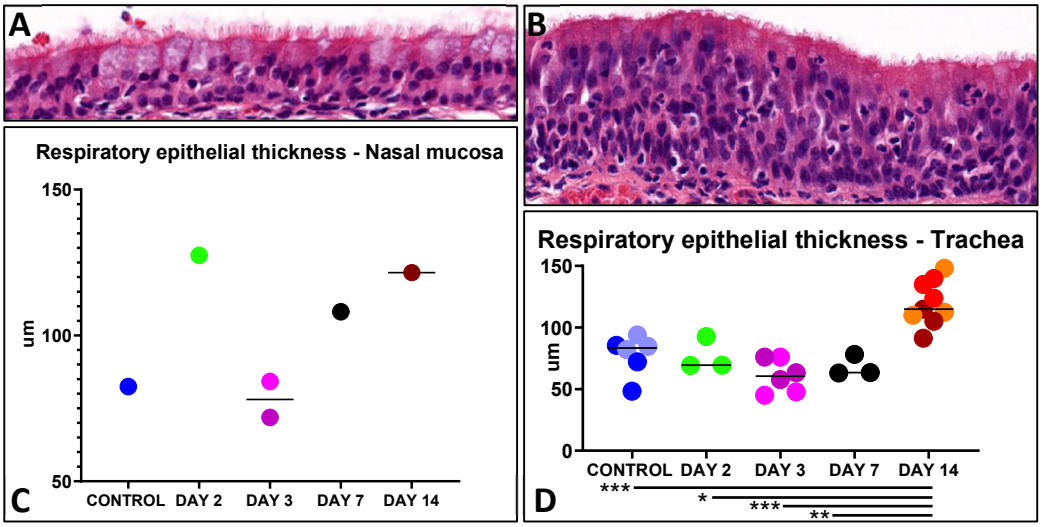

Figure 3-13: Representative images of trachea sections stained with H&E from horses experimentally infected and euthanised at 3dpi (**A**) and 14dpi (**B**), showing respiratory epithelia. Dot plots showing thickness of the respiratory of the nasal mucosa (**C**) and trachea (**D**). 15x. Each data point represents a tissue section. Note that no respiratory epithelium was displayed in sections of nasal mucosa from horses 5 and 7. Light blue = control 2, dark blue = control 4, pink = horse 2, purple = horse 3, orange = horse 5, red = horse 6, brown = horse 7. Statistical significances were assessed using a Wilcoxon rank sum test, *=p<0.05, **=p<0.01, ***=p<0.001 Bar shows the median.

A different pattern was seen in the trachea, with a big peak at 14dpi (120 um), whereas the values of controls (78 um), 2dpi (77 um), 3dpi (61) and 7dpi (68) were lower (**Fig. 3-13**).

Minor differences were seen among the upper, middle, and lower part of the trachea. In all three regions, a peak was observed at 14dpi, being the smallest thickness at 3dpi in the middle and lower trachea, and at 7dpi in the upper trachea. In the upper trachea, epithelial thickness decreased at 3dpi (75 um) after being stable in the controls (89 um) and the 2dpi horse (93 um). It decreased again at 7dpi (63 um) and increased markedly at 14dpi (134 um). The middle trachea showed similar dynamics, with stable values between the controls (66 um) and 2dpi (69 um). A small decrease in thickness at 3dpi (55 um) was followed by a subtle increase at 7dpi (63 um) and a big one at 14dpi (112). Finally, in the lower trachea, the thickness decreased from the controls (77 um) to 2dpi (69 um) and 3dpi (51 um). It increased at 7dpi (78 um) and further at 14dpi (113 um). No statistical changes were revealed in the very few comparisons where the sample size was big enough to allow statistical analysis. Overall, these data show that epithelial hyperplasia at 14dpi can be observed in the three tracheal sections.

Regarding interindividual differences, horse 2 had higher epithelial thickness than horse 3 in the nasal mucosa (84 vs. 72 um) and lower in the trachea (56 vs. 66 um)
No comparisons were able to be done among horse euthanized at 14dpi in the nasal mucosa, since only one of the three sections exhibited respiratory epithelia in the FFPE section. In the trachea, horse 6 showed the biggest epithelial thickness (133 um) and horse 7 the lowest (104 um), whereas horse 5 had 123 micrometres of epithelial thickness. Interindividual differences were not seen.

Overall, these results show a clear pattern of decrease in epithelial thickness at the beginning of the infection and a big increase at the end of it, in the trachea, regardless of its location. Nasal mucosa also shows a similar pattern, although it is less prominent, and it is based in a small sample size. As **Fig. 3-13** shows, epithelia at day 14 post infection were undergoing hyperplasia. These findings suggest that at late timepoints the epithelium was regenerating (and maybe over-regenerating), after it had lost some of its cells due to the action of EIV.

3.2.1.5 Airway blockage

To better understand the pathology caused by EIV infection in the intrapulmonary airways, I measured the degree of blockage of bronchi and bronchioles, by estimating the total lumen area and, within it, the surface covered by cells and debris. Airway blockage was quantified in all bronchi and 25 bronchioles of each lung lobe. Sample size of n=25 was established in

order to have a powerful enough number to do statistical comparisons. Airway blockage after influenza infection has been described in horses (Begg *et al*., 2011), dogs (Crawford, *et al*., 2005), ferrets (Zitzow *et al*., 2002) and pigs (Rajao *et al*., 2014).

In the bronchi, a decrease from uninfected controls (90% of free airway) to the horse euthanized at 2dpi (70%) was revealed. A further decrease was seen at 7dpi (53%) after a 3dpi in which there was not change compared to the previous timepoint (69%). At 14dpi, the percentage of the lumen occupied by air had increased to 75% (**Fig.3-14**).

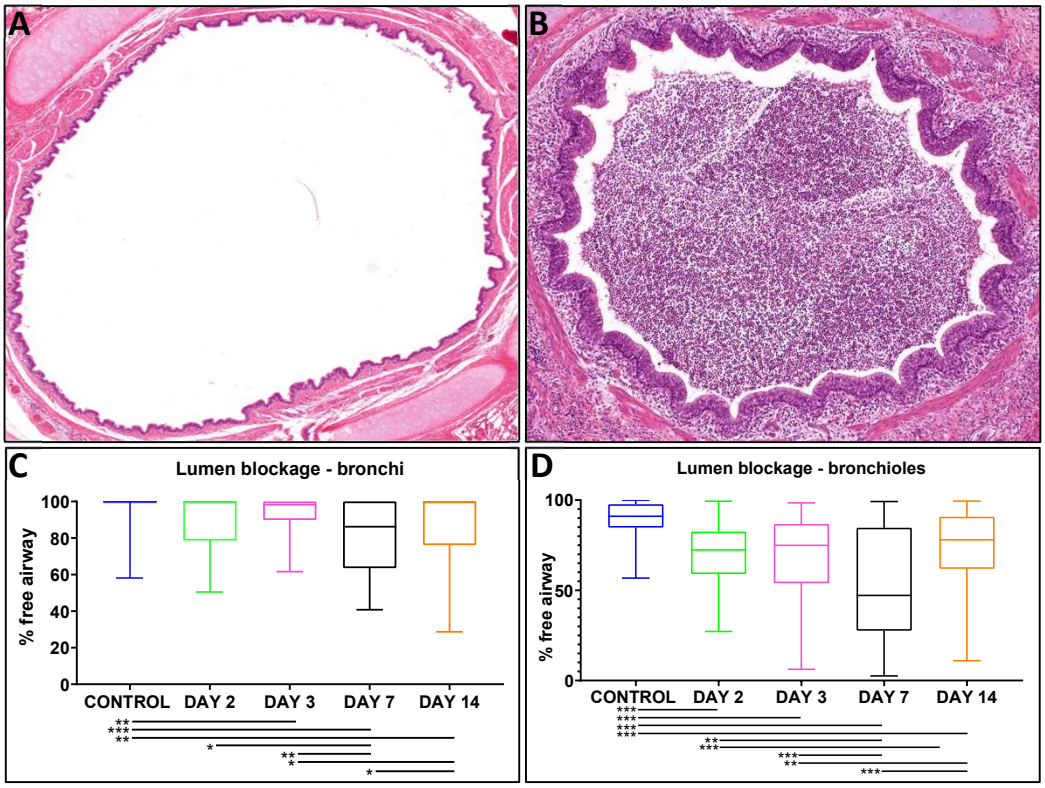

Figure 3-14: Representative images of lung sections stained with H&E from uninfected controls (**A**) and a horse experimentally infected and euthanized at 7dpi (**B**). Box plot showing the percentage of free airway in each bronchus (**C**) and bronchiole (**D**). A decrease of % of free airway can be seen in different timepoints, being especially high at 7dpi.. Statistical significances were assessed using a Wilcoxon rank sum test, *=p<0.05, **=p<0.01, ***=p<0.001. 15x. Each data point represents a bronchus/bronchiole. Bar shows the median. Whiskers show the highest and lowest values.

Similar dynamics were seen in the bronchioles, with the controls having the highest % of free airway (91%) and the 7dpi the lowest (53%). Days 2, 3 and 14 post infection had values around 70-75% of free airway (**Fig. 3-14**).

These results showed a peak of airway blockage at 7dpi, suggesting that at this timepoint was when detachment of cells in the respiratory epithelia was the highest.

After the stratification between anterior and posterior lobes, I observed additional differences in the bronchi. The anterior lobes had more % of free airway at 2dpi (99.7%) and 3dpi (96%) compared to the posteriors (83% 2pi*, 91% 3pdi**), whereas at 14dpi had less (76% vs. 97%***).

The stratification following the latero-lateral axis showed similar dynamics between left and right lobes, although at 2dpi (96% vs. 82%) and 14dpi (92% vs. 83%*), the percentage of free airway was higher in right lobes.

In the bronchioles, the situation was similar. The dynamics of airway blockage were similar to bronchi. Anterior lobes had less % of free airway (65%) at 14dpi compared to posterior lobes (84%***). Also, left lobes had less bronchioles blockage compared to right lobes at 2dpi.
Regarding interindividual differences, I observed that horse 2 had less airway lumen free (91%) compared to horse 3 (97%*) in the bronchi, whereas at day 14 horse 5 had more % free airway (93%) than horse 6 (84%) and horse 7 (81%*). In the bronchioles, horse 3 (71%) had more % of free airway than horse 2 (68%), and horse 6 (69%) had less % of free airway than horse 5 (80%***) and horse 7 (74%**).

Overall, these results suggest a higher degree of bronchiole pathology in horse 2 compared to horse 3, whereas at day 14 post infection horse 5 would have less histopathological changes in the bronchioles than horse 6 and 7.

3.2.1.6 Gas exchange surface

To determine the amount of gas exchange surface, I measured, within the alveoli, the area not detected by the pixel count algorithm, belonging to air space, and the area detected by it, occupied by cells and liquid. Gas exchange surface was measured in the entire lung parenchyma area of each lung lobe.

The loss of gas exchange surface exhibited a stepwise reduction over time. The first decrease was between the controls (81% of the parenchyma area) and 2dpi (57%). The amount of free air space stayed stable until 7dpi (60%), and it decreased again at 14dpi (43%) (**Fig. 3-15**).

At the same time, as **Fig. 3-15** shows, there were two histological patterns of loss of gas exchange surface, that did not correspond to the two phases of gas exchange surface reduction aforementioned. At days 2 and 3 post infection, this loss was due to a thickening of the alveoli, due to the higher presence of liquid, erythrocytes and inflammatory cells in their blood vessels and interstitial space. On the other hand, at days 7 and 14dpi the alveoli were still thicker than normal, but inflammatory and blood cells and extracellular fluid were also observed outside the interstitium, in the alveolar spaces.

These results suggest that EIV disrupts the lung homeostasis, by triggering an inflammatory response that, in an initial stage is restricted to the interstitial space but expands to the air space at later phases.

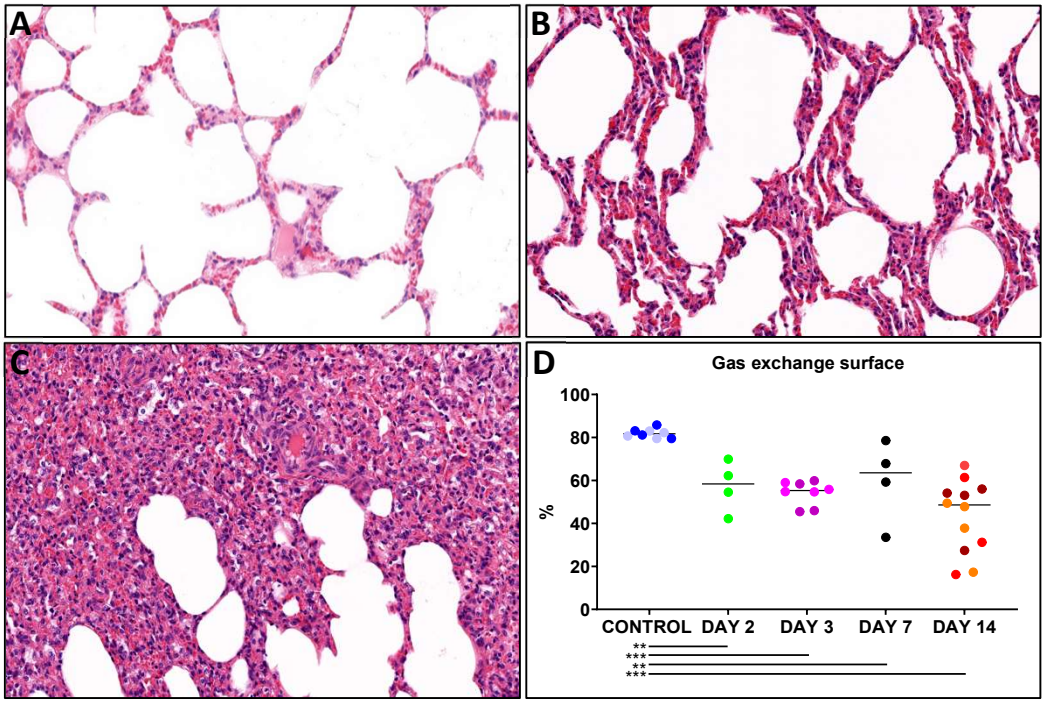

Figure 3-15*:* Representative images of lung sections stained with H&E from uninfected controls (**A**) and horses infected and euthanized at 2dpi (**B**) and 14dpi (**C**), showing alveoli with different degree of loss of gas exchange surface. (**D**) Dot plot showing the percentage of gas exchange surface in each lobe and timepoint. A decrease of gas exchange surface can be seen at 2dpi and 14dpi. 15x. Statistical significances were assessed using a Wilcoxon rank sum test, **=p<0.01, ***=p<0.001. Each data points represents a lung lobe. Light blue = control 2, dark blue = control 4, pink = horse 2, purple = horse 3, orange = horse 5, red = horse 6, brown = horse 7. Bar shows the median.

Although they were not significant, some differences between anterior and posterior lobes were revealed. At 2dpi (58%) and 3dpi (58%), anterior lobes had more % of gas exchange surface than posterior lobes (56% 2dpi, 50% 3dpi). At 7dpi (73%) and 14dpi (51%) posterior lobes had more gas exchange surface % than anterior lobes (46% 7dpi, 36% 14dpi).

The same happened when I compared the left and right lobes. No statistical differences were seen, although left lobes had a higher % gas exchange surface at 3dpi (56%) and 14dpi (48%) than right lobes (52% 3dpi, 39% 14dpi), and lower % at 2dpi (48% vs. 66%) and 7dpi (51% vs. 69%).
Interindividual differences were seen among the horses euthanized at 14dpi. Horse 5 had a 38% of gas exchange surface, whereas horse 6 had a 44% and horse 7 a 48%. No statistical significance was detected.

3.3 Discussion

In this chapter I aimed to describe and quantify lesions produced by EIV within the equine respiratory tract by staining respiratory FFPE sections from experimentally EIV-infected horses with H&E and PAS.

There are two points to consider from when discussing these results, and these also apply to following chapters. First, the small sample size I worked with (n=7). As a result, my conclusions on histopathological changes observed at, for example, 2dpi and 7dpi, are based on a single horse. Furthermore, statistical tests were impossible to perform in some comparisons, whereas in others their power was not ideal. And second, the timepoints when horses were euthanized. These were 2dpi, 3dpi, 7dpi and 14dpi, described as key moments during EIV infection (Muranaka *et al*., 2012), which means I was not able to get any data based on tissue analysis in sections from days 1, 4, 5, 6, 8, 9, 10, 11, 12, and 13 post infection. These two limitations conditioned the interpretation of results.

I observed pathological changes in the respiratory tissues of the horses I studied that were consistent with those observed in other studies of EIV-infected horses (A/equine/Sydney/2007 H3N8) (Begg *et al*., 2011; Patterson-Kane *et al*., 2008), such as loss of cilia and goblet cells, epithelial hyperplasia and squamous metaplasia of the respiratory epithelia of the airways, airway lumina blockage due to the presence of necrotic epithelial and inflammatory cells, bronchopneumonia and alveolar haemorrhage. It seems that, regardless of the viral strain (and potentially the dose), these lesions are always present in EI-infected horses. Furthermore, these are lesions that have also been described in other mammals infected with influenza, like the ferret (Zitzow *et al*, 2002; Govorkova *et al*., 2005; Tumpey *et al*., 2007; Huang *et al*., 2011; Tsuda *et al*., 2017; Lee *et al*., 2018), the dog (Song *et al*., 2008; Jung *et al*., 2010; Castleman *et al*., 2010; Kang *et al*., 2013; Tangwangvivat *et*

al., 2022), the Cynomolgus macaque (Rimmelzwaan *et al*., 2003), the mouse (Semkow *et al*., 1979), the cotton rat (Ottolini *et al*., 2005) and the pig (Brockmeier *et al*., 2002; Grau-Roma and Segalés, 2007; Khatri *et al*., 2010; Gauger *et al*., 2001; Janke B.H., 2013a; Lyoo *et al*., 2014; Montoya *et al*., 2017).

Overall, there seems to be different dynamics in the development and resolution of lesions and histopathological changes between the airways and the alveoli (**Fig. 3-16**).

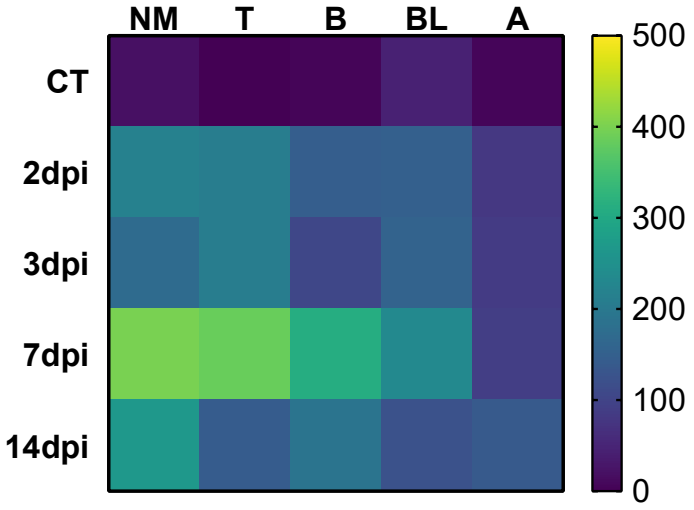

Figure 3-16*:* Heatmap showing degree of histopathological changes in different tissues and timepoints. Each parameter quantified earlier in the chapter was given a score from 0 to 100, according to its proximity to the normal value. Each square of the heatmap shows the sum of each parameter quantified, normalised to 500, in the corresponding tissue and timepoint. **NM** = nasal mucosa, **T** = trachea, **B** = bronchi, **BL** = bronchioles, **A** = alveoli. **CT** = control.

The airways are histologically similar, and similar is also the way the virus affects their microscopic architecture. I saw that at 2dpi the histology of nasal mucosa (respiratory portion), trachea and bronchi is almost normal, since the biggest histological change seen was an increase in goblet cell density and size. At 3dpi I started to see loss of some cilia, which was more severe in the lower airways compared to the upper, and loss of some goblet cells, apart from the presence of inflammatory infiltration, mainly in the submucosa, and of desquamated epithelial and inflammatory cells in the airways lumina. It seems that, on this regard, equine influenza has a similar pathogenesis to influenza in other species, such as the pig, the dog and the ferret as, as explained in chapter 1, loss of cilia and goblet cells and necrosis of the respiratory epithelium are reported in these species from 3dpi onwards. By 7dpi the cilia and goblet cells had completely disappeared, and the degeneration of the respiratory epithelium was evident, with frequent dead cells and others that had undergone squamous metaplasia. As seen in Chapter 1, according to literature, squamous metaplasia is

a lesion that develops mostly in intermediate and late stages of influenza disease in species such as the pig.

As a consequence of the aforementioned histopathological changes, lumina of intrapulmonary airways were filled by sloughed epithelial and inflammatory cells. The fact that the main inflammatory cells in the airways by that time were neutrophils reinforces the idea of a bacterial pneumonia developing at late timepoints, secondary to the histopathological changes caused by EIV. Two weeks after the infection, some cilia and goblet cells were seen again, although they had not repopulated the epithelium entirely, and the normal architecture of the epithelium was starting to restore. However, a marked epithelial hyperplasia, which is a consequence of the proliferation of epithelial basal cells, was present in the trachea and nose, as well as a small degree of blockage in the lumen of intrapulmonary airways.

As a conclusion, I can state that by 14dpi the respiratory epithelia of the airways have not recovered their normal histological architecture, however, clear signs of recovery can be seen.

On the other hand, the alveoli display a different dynamic. To summarize it can be stated that histopathological changes and lesions are delayed in time, compared to those seen in the airways, and are not showing any sign of recovery two weeks after animals have been infected.

During the first timepoints, small changes that were not quantified, such as mild alveolar inflammation and oedema, can be observed. There was also a reduction of about the 25% of the gas exchange surface between the uninfected controls and the horse infected and euthanized at 2dpi. One week after the infection, the lung looked completely reactive, with lots of inflammatory infiltrate, oedema and haemorrhage. Furthermore, some areas of the lung, especially in the anterior lobes, were completely collapsed by the accumulation of liquid, inflammatory cells, fibrin and blood. At day fourteen post infection, the gas exchange surface had reduced a further 30% compared to the previous timepoint.

All these findings, isolated from other observations, indicate that the horses were not being able to control the agent that is causing the pathology in the lung by 14dpi, either if it was secondary bacteria, host reaction or a mix of both. The severity of pathological changes in the alveoli increased compared to the previous timepoints, and this fact most likely contributed to a worsening of the physical condition and the symptomatology and a delay in

the recovery. However, considering the information shown in **Table 3-1,** the situation seems to be different. According to it, between 8dpi and 10dpi is when horses were showing the most severe symptomatology, which matches with the second febrile response, described in the literature as a worsening of the clinical outcome between 7dpi and 10dpi due to the action of opportunistic bacteria in the lung (Muranaka *et al*., 2012; Sarasola *et al*., 1992; van Maanen and Cullinane, 2002), whereas at 14dpi, the corporal temperature was back to normal and the nasal discharge and cough were either mild or absent. Therefore, these data suggest that the most severe lesions in the airways and in the lung would also be between 8dpi and 10dpi. My data indicates that 7dpi is the timepoint in which the histopathology of the airways was the gravest along the infection, although I did not have respiratory tissues from EIV-infected horses euthanized at 8-10dpi to see whether at these days it had increased its severity. On the other hand, at 7dpi lungs also had severe lesions, although these were milder than at 14dpi. There is no consensus in the literature about the time at which the histopathological lesions and clinical signs are the most severe, and, from that point onwards, the respiratory architecture begins to be restored and the outcome improves. Although, as explained in this thesis, data on the clinical and pathological progression of equine influenza in horses is considerably limited, most works on other species, such as the dog and the ferret, establish the peak of severity of the clinical signs (normally body temperature and body weight, although some studies include further observations, such as cough, depression, ocular and nasal discharge, appetite, labored breathing, neurological symptoms, sneezing, diarrhea and hair aspect) and histopathological changes in the first 5-6 days post infection, during or shortly after the period of highest viral shedding, after which these clinical signs and lesions disappear gradually. Differently to what happened with the horses I studied for the writing of this thesis, the dogs and ferrets participating in these studies (Govorkova *et al*., 2005; Song *et al*., 2008; Huang *et al*., 2011; Kang *et al*., 2013; Tangwangvivat *et al*., 2022) were not reported to have secondary bacterial infections following the virus inoculation, and this is considered the explanation why there was no worsening of the clinical signs and histopathological changes in the respiratory tract later in the experimental viral challenge.

As a conclusion, as stated above, I would expect to observe the most severe pathological changes in both the airways and the lung between 8dpi and 13dpi, which would mean that the normal histological architecture of the airways and lung would be starting to recover by 14dpi. Further investigation is needed to determine the degree of airway and lung pathology in timepoints between 7dpi and 14dpi.

I analysed the differences between three different locations in the trachea (upper, middle and lower part) and also between four lung lobes. Although some patterns were identified, the sample size was a problem to obtain statistically significant differences.

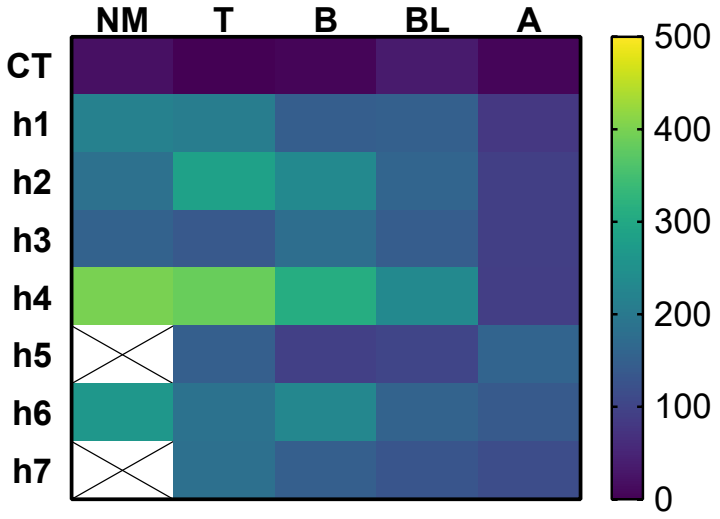

Figure 3-17*:* Heatmap showing degree of histopathological changes in different tissues and horses. Each parameter quantified earlier in the chapter was given a score from 0 to 100, according to its proximity to the normal value. Each square of the heatmap shows the sum of each parameter quantified, in the corresponding tissue and timepoint, normalised to 500. **NM** = nasal mucosa, **T** = trachea, **B** = bronchi, **BL** = bronchioles, **A** = alveoli. **Ct** = control, **h2** = horse 2, **h3** = horse 3, **h5** = horse 5, **h6** = horse 6, **h7** = horse 7. No respiratory epithelia in the nasal mucosa were displayed in sections from horse 5 and 7.

In the airways, dynamics of loss of goblet cells, goblet cell size and epithelial thickness were similar in the three different tracheal regions. Although no significative differences were obtained, a gradient of increasing loss of cilia and goblet cells between the upper trachea and the lower trachea was observed. This reproduced within the trachea what had been observed between the nasal mucosa and the bronchi.

Regarding interindividual differences, this were small, considering that comparisons between horses 2 and 3 (3dpi) and among horses 5, 6 and 7 (14dpi) were made and very few statistically significances were obtained. A pattern, however, was seen at 3dpi, since horse 2 showed less % of cilia coverage and less goblet cell density in the trachea and bronchi, less epithelial thickness in the trachea and more intrapulmonary airway blockage compared horse 3. Based on this data, it seems that the degree of degeneration of the respiratory epithelia in horse 2 was higher than in horse 3 (**Figure 3-17**), although, according to (Muranaka *et al*., 2012), it did not correlate with a higher fever or viral load. Concerning horses euthanized at 14dpi, as **Figure 3-17** shows, data say that, in the airways, horse 6 had the biggest pathological changes, whereas horse 5 had the mildest ones. On the other hand, in the lung, horse 5 was seen to have the most severe histological alterations. The comparison of these

data to the symptoms displayed in **Table 3-1** show how horse 7 was the individual that had less lung histopathology and, at the same time, the only one that did not show any cough and nasal discharge at 14dpi, suggesting that, by this time, these two symptoms would be related to the lung status over the status of the airways. Although some literature on different species experimentally infected with influenza shows differences between individuals, in terms of clinical signs, viral load and gross/histopathological changes, belonging to the same experimental group was found, data on clinical, viral and pathological scores of each individual were not provided and, therefore, comparison with the data seen in the horses I studied could not be performed.

In the lung, I compared between anterior and posterior lobes and between left and right lobes, and these did not shed much light, since no statistical differences were obtained. Nonetheless, at the end of the infection a different pattern between anterior and posterior lobes can be highlighted, since anterior lobes had more % of bronchial epithelium not covered by cilia and less % gas exchange surface than posterior lobes at days 7 and 14 post infection. These findings suggest that anterior lobes develop more severe lesions compared to posterior lobes, at late infection timepoints, as **figure 3-18** shows. As reported in (Muranaka *et al*., 2012), after the sixth day of infection no EIV antigen was detected in respiratory tissues from the infected horses I studied and, at the same time, genetic material of *Streptococcus zooepidemicus,* one of the most common bacteria developing pneumonia after EIV infection, was seen by PCR in formalin-fixed, paraffin-embedded lungs from the same horses, euthanized at days seven and fourteen post infection.

These observations are highly suggestive of a bacterial process, secondary to the primary viral infection, developing at late stages of the infection, and increasing the severity and range of lesions in the respiratory tract. Furthermore, my observations provide two additional evidences of a bacterial pneumonia being developed at late timepoints. First, as explained, at 7dpi and 14dpi, the lesions were more severe in the cranial lobes, which is consistent with the common distribution of bacterial pneumonias (Oikawa *et al*., 1994). Second, as shown in **Figures 1-10D** and **1-11**, the inflammatory component seen in the airways at late timepoints was mainly neutrophilic, which is a cell type associated with bacterial infections. In their works, Begg *et al*. and Patterson and Kane *et al*., working with naturally EIV-infected horses, described similar changes and identified bacteria in the lungs of these, although no temporary dynamics could be established as the day of infection of these horses was not known (Patterson-Kane *et al*., 2008; Begg *et al*., 2011).

There is extensive literature about the relationship between influenza viruses and secondary bacterial infections in different species, although data on horses was not found. Kalhoro *et al*. showed increased bacterial loads in different organs and blood, increased clinical signs and increased severity of lesions in mice coinfected with canine H3N2 and *Staphylococcus intermedius* (72 hours later) compared with those only inoculated with *Staphylococcus intermedius* (Kalhoro *et al*., 2016). Mueller Brown *et al*., in a similar experiment with ferrets, inoculated individuals with 2009 pandemic H1N1, *Streptococcus pneumoniae* or the former followed by the latter 48 hours later, resulting in a higher bacterial load and more severe clinical signs in animals coinfected (Mueller Brown *et al*., 2022). Zhou *et al* studied three cases of H3N2 canine influenza virus (CIV)-*Enterococcus faecalis* naturally coinfected dogs and hypothesized that the bacteria increased the severity of the disease, as these animals died and infections with CIV H3N2 normally have low mortality (Zhou *et al*., 2019). On this regard, it is well known, and my data support it, that the virus disrupts the respiratory epithelium at early timepoints, by killing its goblet and ciliated cells, which leads to the impairment or complete suppression of the mucociliary clearance in the nasal mucosa, trachea and bronchi. In addition, the destruction of the epithelial barrier and the depletion of the immune response are facilitating factors for the internalization and spread of bacteria and, in later stages, the development of a bacterial pneumonia and potentially sepsis, aggravated by the host cytokine storm (Okahashi *et al*., 2022). The mechanisms by which influenza viruses induce defects in the immunologic response of the host and, as a consequence, facilitate secondary bacterial infections, are extensively reviewed in (Robinson *et al*., 2015) and in (Metersky *et al*., 2012) and include alterations in phagocyte's numbers and function, suppression of the production of antimicrobial peptides, increased bacterial adherence, upregulated expression of genes coding for toxins and attenuation of natural killer cell responses.

As a consequence of these, the bacteria are unlikely to be efficiently eliminated from the respiratory tract and a secondary bacterial pneumonia is likely to develop. Therefore, lesions observed after the sixth day might be, thus, caused by either the opportunistic bacteria that populate the lung, by the inflammatory host response or by a combination of both, but not by EIV.

In summary, in this chapter I characterised and quantified the main lesions induced by equine influenza in its natural host, the horse, throughout its respiratory tract and during a period of two weeks, with a focus on the first (2 and 3dpi) and second febrile response (7dpi) and also on the defervescence or resolution period (14dpi).

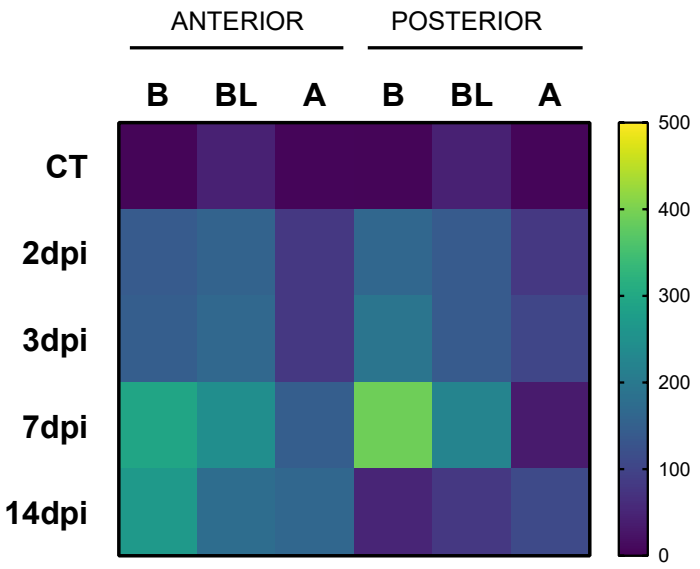

Figure 3-18*:* Heatmap showing degree of histopathological changes in different lung tissues and horses, stratified in anterior and posterior lobes. Each parameter quantified earlier in the chapter was given a score from 0 to 100, according to its proximity to the normal value. Each square of the heatmap shows the sum of each parameter quantified, in the corresponding tissue and timepoint, normalised to 500. **B** = bronchi, **BL** = bronchioles, **A** = alveoli. **CT** = control.

Chapter 4. Characterisation and quantification of equine influenza antigens in respiratory tissues of horses infected with equine influenza virus

4.1 Introduction

In the previous chapter I described and quantified lesions caused by EIV during the course of the infection. The aim of this chapter is to characterize the spread and distribution of EIV throughout the respiratory tract during the course of infection.

EIV spreads fast and infects animals through aerosols and fomites (Murphy *et al*., 1999). It initially penetrates the ciliated cells of the respiratory epithelia of the upper and lower respiratory tract, where it replicates (López, 2007). Replication leads to viral spread by infecting nearby cells, having as a result the necrosis of the respiratory epithelium (Sack *et al*., 2019). As explained previously, degeneration of the respiratory epithelium leads to a deterioration of the mucociliary clearing system and, therefore, particles and foreign agents that get into the airways are not eliminated. This can lead to secondary bacterial infections (López, 2007; Willoughby *et al*., 1992).

The incubation period of EIV lasts for up to three days (Radostits *et al*., 2003), and during this time horses are already shedding virus (Donis, 2017). Animals can be infectious for a period between 5 and 10 days after getting infected (Daly M. *et al*., 2004; Donis, 2017; Paillot *et al*., 2013; Radostits *et al*., 2003; Wattrang *et al*., 2003; Yamanaka *et al*., 2009), although it has been reported that EIV RNA was detected in nasal swabs by PCR two weeks after infection and, in an intermittent fashion, for up to 35 days (Read *et al*., 2011). In other species, such as pigs, mice, ferrets and dogs, viral shedding lasts for up to 8-10 days (Easterday and Van Reeth, 1999; Lloyd *et al*., 2011; Marriott *et al*., 2014; Reuman *et al*., 1983; Rosas *et al*., 2008; Schorr and Hinshaw, 1994; Su *et al*., 2015).

To visualize viral antigens, I combined immunohistochemistry and immunofluorescence using antibodies against the nucleoprotein and haemagglutinin. To detect EIV nucleic acids I performed in-situ hybridization. Specifically, I used probes that hybridize with messenger RNA of three EIV genes: M1, NP and PB2. Sections of respiratory tissues obtained from experimentally infected and noninfected horses were subject to the aforementioned techniques.

Immunostaining and ISH signal were visualized and quantified using image analysis software (Aperio Imagescope®) and confocal microscopy.

4.2 Results

4.2.1 Identification of viral protein in respiratory tissues

4.2.1.1 Immunohistochemistry

To validate the specificity of the anti-NP antibodies against A/equine/Ibaraki/07 I performed IHC on different respiratory tissues. An EIV-infected equine tracheal explant used in (Amat *et al*., 2021) was used as a positive control, whereas the negative control was a section of the trachea from an uninfected horse. **Figure 4-1A and B** show an EIV-infected tracheal explant, displaying positive staining, and a noninfected tracheal explant, which is completely negative. These observations in NP staining in tracheal explants are consistent with what has been observed in other works (Amat *et al*., 2021; Feng *et al*., 2015; Gonzalez *et al*., 2014).

To determine the distribution of EIV within the respiratory tract of infected horses, I performed an immunohistochemistry assay against influenza NP, as explained in Materials and methods, on nasal mucosa, trachea and lung sections from horses used in (Muranaka *et al*., 2012) and (Yamanaka *et al*., 2009).

Tracheal sections from EIV-infected and uninfected horses were used as positive and negative controls respectively (**Figure 4-1C** and **D**), before performing the staining in slides from all respiratory tissues of all horses. In addition, sections of splenic lymph node and spleen and of respiratory tissues from infected horses (used as a negative control, with no primary antibody added during the staining procedure) also underwent NP staining.

As **figures 4-2, 3, 4** and **5** prove, NP was detected in several respiratory tissues of EIV infected horses, showing mainly nuclear staining, although signal in the cytoplasm was also observed.

In the nasal mucosa, areas of positivity were seen in the respiratory epithelium, the main target of the virus, but also in the submucosa, the submucosal glands, the MALT and the muscular wall of arteries. Signal was especially strong in sections from horses euthanized at day 3 post infection. **Figure 4-2** shows details of different tissues positive to NP at 2dpi: epithelial cells of the respiratory epithelium, myocytes in the arterial muscular wall, lymphocytes within a Nose-associated lymphoid tissue patch and epithelial cells of submucosal glands. In the trachea, the respiratory epithelium and the submucosa (including its glands) showed NP-positive regions.

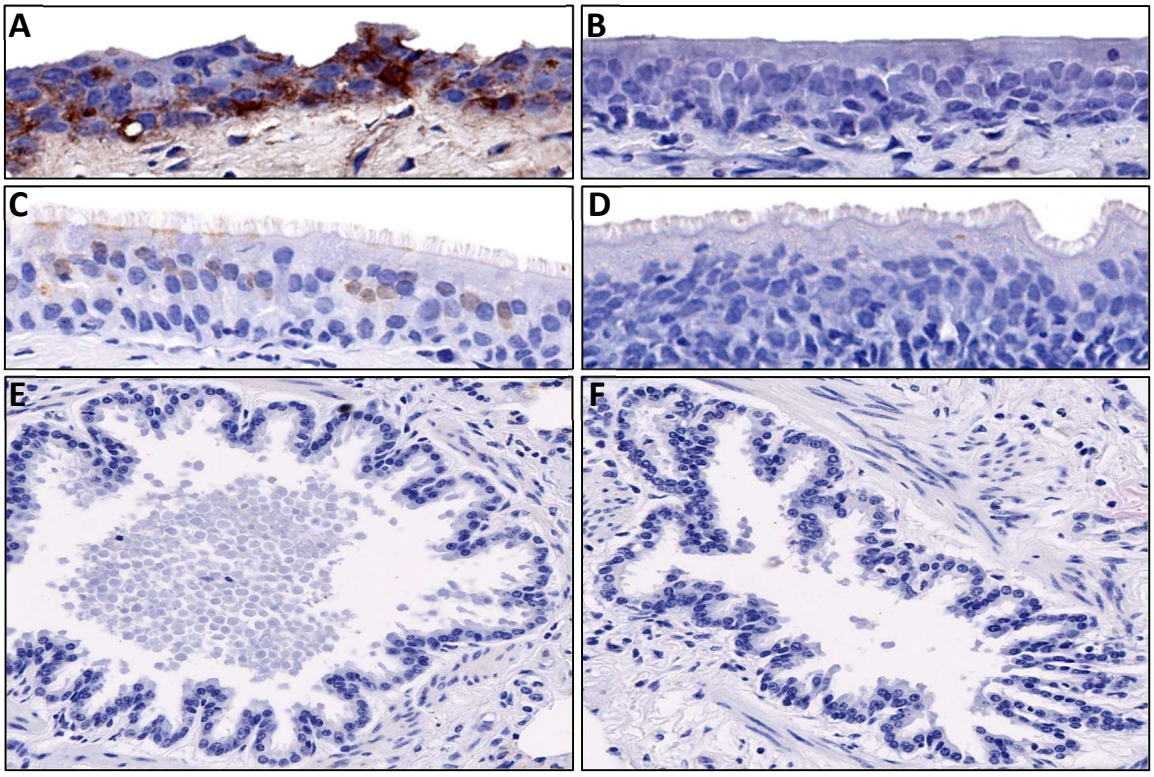

Figure 4-1*:* Representative images of tracheal sections stained with an anti-NP antibody under an IHC procedure and haematoxylin counterstain. (**A**) EIV-infected equine tracheal explant. (**B**) Uninfected tracheal explant. (**C**) Tracheal section from an EIV-infected horse. (**D**) Tracheal section from a noninfected horse. 40x. Sections of lung of a noninfected control (E) and an infected animal but with no primary antibody addition during the IHC staining (F). 30x.

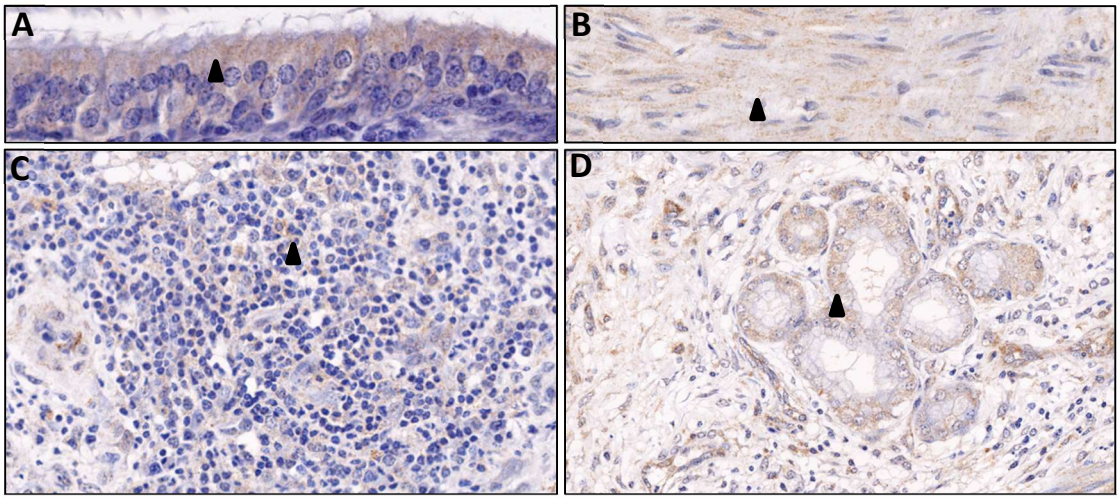

Figure 4-2*:* Representative images of nasal mucosa sections from the horse euthanized at 2dpi stained with an anti-NP antibody under an IHC procedure and haematoxylin counterstain. (**A**) Respiratory epithelium (40x). (**B**) Muscular wall of an artery (40x). (**C**) NALT (25x). (**D**) Submucosal glands (20x). Arrowheads show positivity in the different tissues.

Figure 4-3 shows representative areas of IHC staining against NP in tracheal epithelium and submucosa (**A**) and tracheal submucosal glands (**B**), in sections from a horse euthanized at 3dpi. Positive areas were also seen in muscular wall of arteries. As in the nasal mucosa, NP positive signal seemed to be stronger in tissues from horses euthanized at 3dpi.

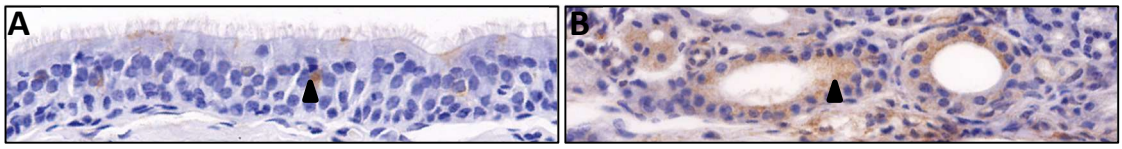

Figure 4-3*:* Representative images of tracheal sections from a horse euthanized at 3dpi stained with an anti-NP antibody under an IHC procedure. and haematoxylin counterstain. (**A**) Respiratory epithelium (25x). (**B**) Submucosal glands (18x). Arrowheads show positivity in the different tissues.

The respiratory epithelium, the submucosa, and the submucosal glands of the bronchi displayed NP-positive areas (**Figure 4-4A, B** and **D**). Viral protein was also detected in the lumina of the airways, among sloughed cells and debris, in the blood vessels walls and in inflammatory cells within BALT patches (**Figure 4-4C**). Also, there was positive signal in myocytes of the bronchial smooth muscle and chondrocytes of the bronchial hyaline cartilage (**Figure 4-4A**), findings that, to best of my knowledge, had never been described before. IHC staining was strong at day 14 post infection, especially in the epithelia and the smooth muscle. In the bronchioles, I observed NP-positive regions in the respiratory epithelium, the submucosa and its glands and in detached epithelial cells in the lumina. As seen in the bronchi, cells in the bronchiolar smooth muscle stained positive, which I consider a novel finding. Positivity seemed to be more intense at 14dpi.

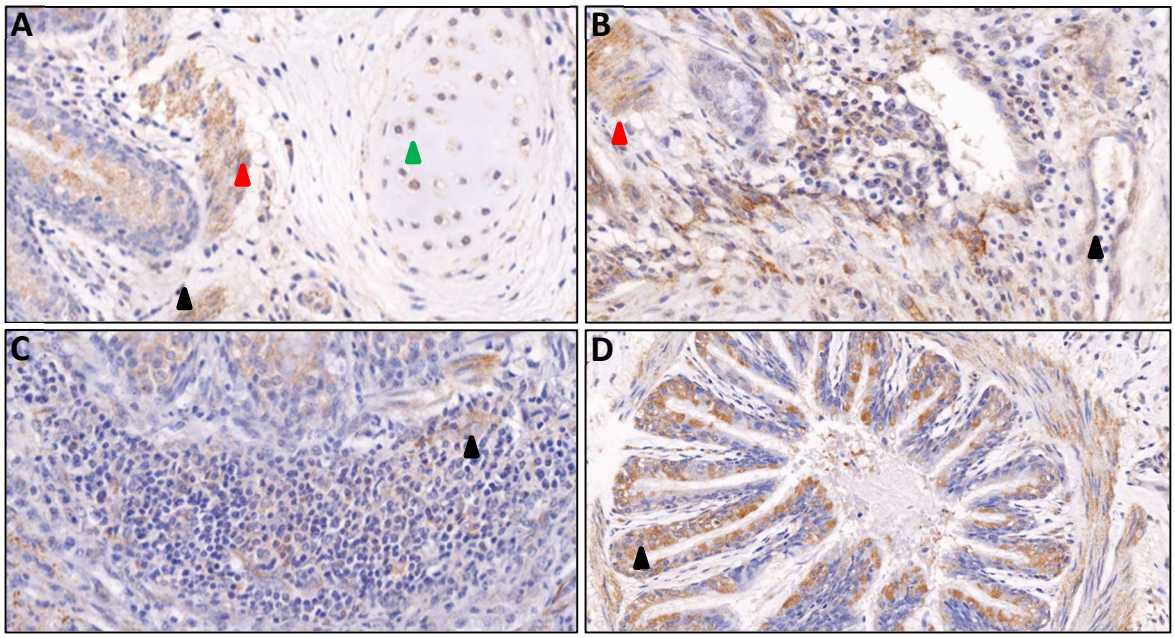

Figure 4-4*:* Representative images of lung sections derived from a horse infected with EIV and euthanized at 14dpi. Images show anti-NP staining and haematoxylin counterstain in bronchial areas. (**A**) Smooth muscle, submucosa and cartilage (20x). (**B**) Submucosal glands and endothelia of a blood vessel (20x). (**C**) BALT (20x). (**D**) Respiratory epithelium (15x). Arrowheads show positivity in the different tissues: (**A**) red = smooth muscle, green = hyaline cartilage, black = submucosa, (**B**) red = submucosal glands, black = blood vessel wall.

Figure 4-5 shows representative areas of tissues stained positive to NP in bronchioles, at day 14 post infection. In the alveoli, the alveolar epithelium and the capillaries showed positivity to NP, as well as endothelia and blood vessels. NP-positive signal was also seen in the fibrous tissue of the lung and the muscular wall of lung arteries (**Fig. 4-4B** and **Fig. 4-5C**) As it happened in the intrapulmonary airways, the NP signal in the lung parenchyma and blood vessels seemed more intense at 14dpi.

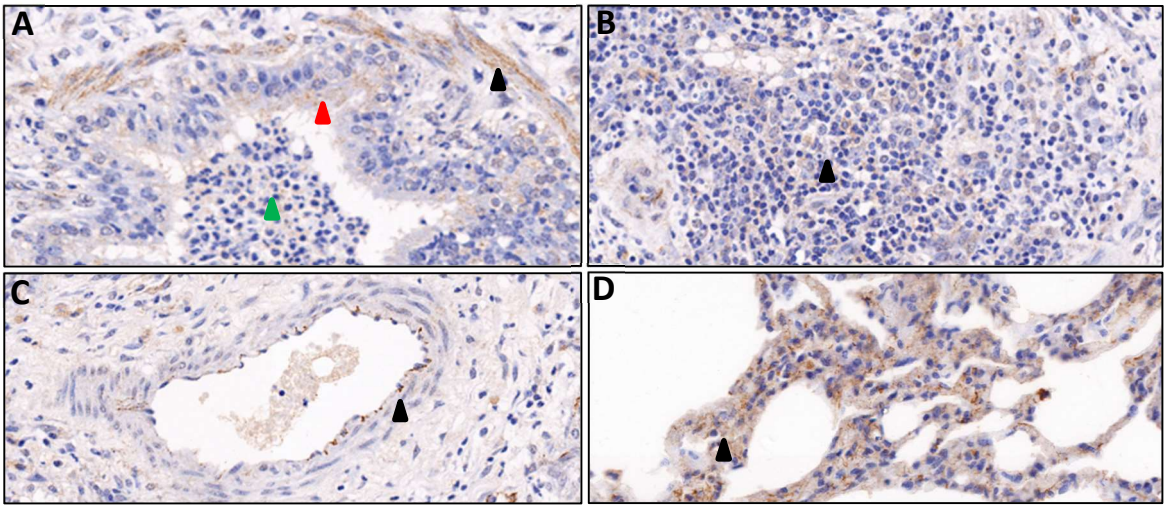

Figure 4-5: Representative images of lung sections from a horse euthanized at 14dpi stained with an anti-NP antibody under an IHC procedure and haematoxylin counterstain showing bronchioles and alveoli. (**A**) Smooth muscle and respiratory epithelium of a bronchiole (25x). (**B**) BALT (25x). (**C**) Arterial wall (25x). (**D**) Alveoli (20x). Arrowheads show positivity in the different tissues: (**A**) red = respiratory epithelium, green = intraluminal debris, black = smooth muscle.

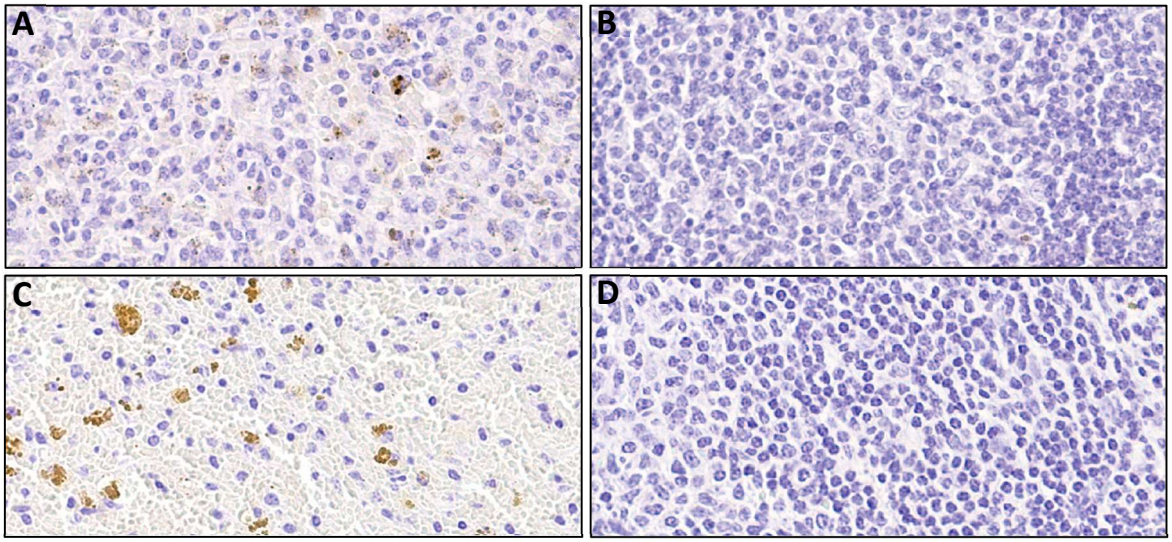

Figure 4-6*:* Representative images of spleen (**A**) and splenic lymph node (**B**) of an experimentally EIV-infected horse and of spleen (**C**) and splenic lymph node (**D**) of an uninfected control, stained with an anti-NP antibody under an IHC procedure and haematoxylin counterstain. 30x. Brown areas in the spleen are deposits of haemosiderin inside the macrophages.

As expected, no positive signal was seen in the splenic lymph node or the spleen at any timepoint, suggesting that there was not viremia nor infection of organs outside the respiratory tract during the course of infection (**Figure 4-6**). Influenza virus viremia has been

described in mice (Mori *et al*., 1995b), ferrets (Likos *et al*., 2007), and humans (Naficy, 1963), although the latter is a rare event (Likos *et al*., 2007). IAV viremia has not been reported in horses.

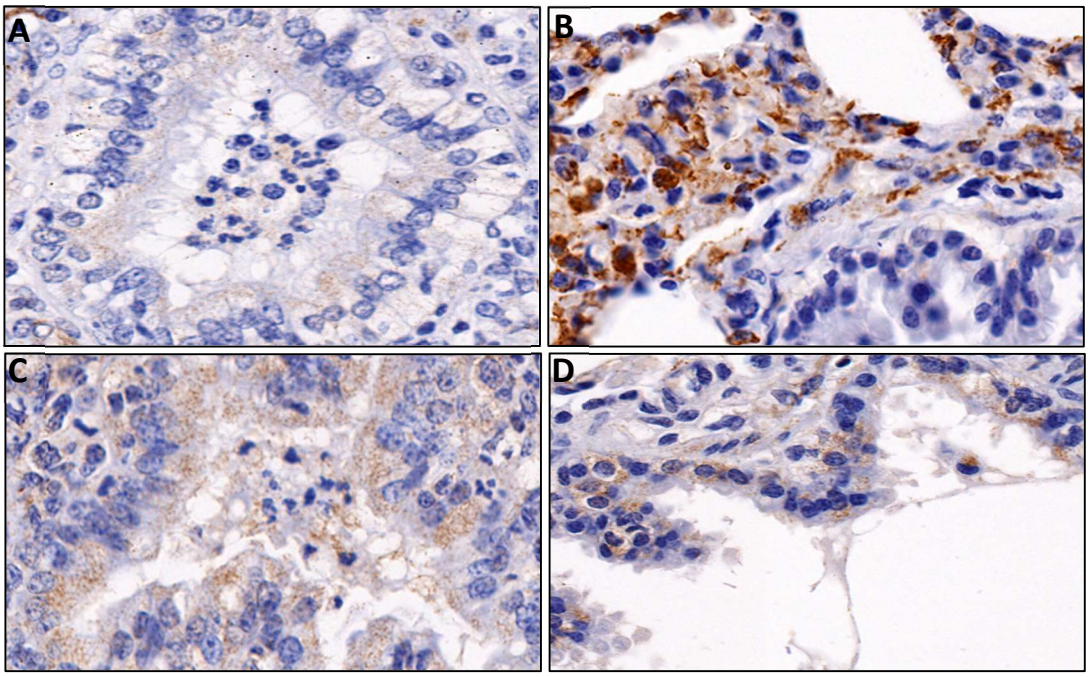

Figure 4-7*:* Representative images of respiratory sections stained with an anti-NP antibody under an IHC procedure and haematoxylin counterstain. (**A**) Day 2 post infection. (**B**) Day 3 post infection. (**C**) Day 7 post infection. (**D**) Day 14 post infection. 45x.

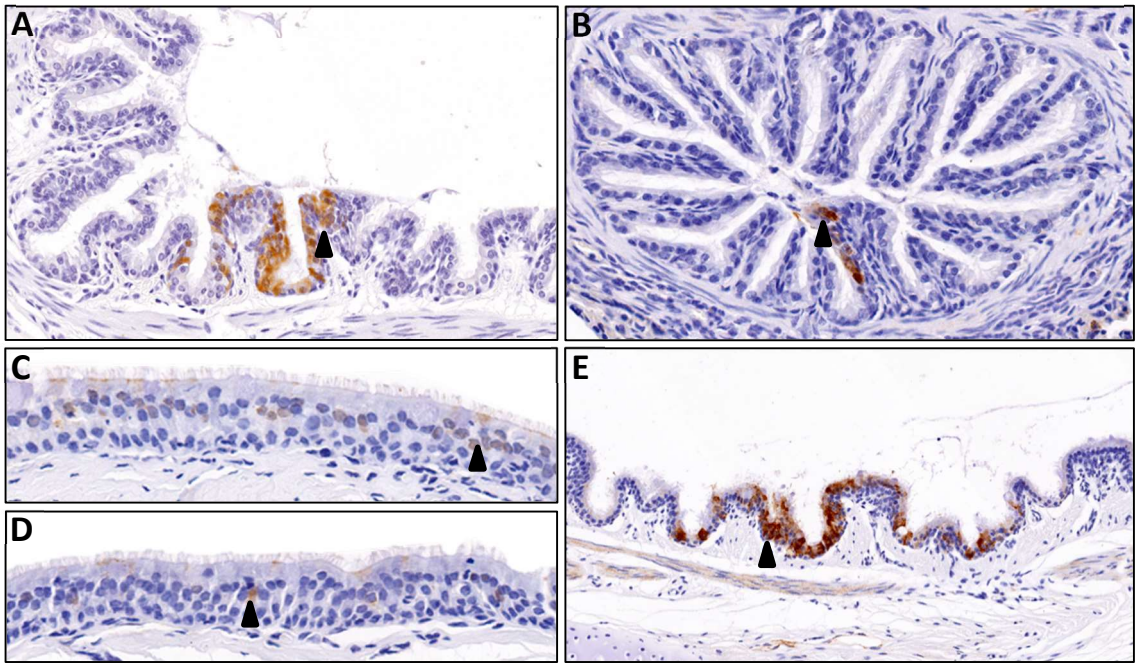

Figure 4-8*:* Representative images of respiratory sections from the horse euthanized at day 2 post infection stained with an anti-NP antibody under an IHC procedure and haematoxylin counterstain. (**A**) Bronchial respiratory epithelium (15x). (**B**) Bronchiolar respiratory epithelium (20x). (**C**) and (**D**) Tracheal respiratory epithelium (25x). (**E**) Bronchial respiratory epithelium (10x). Arrowheads show positivity.

I focused on EIV NP from the nasal mucosa to the alveoli because the respiratory epithelia of the airways, mainly of the upper respiratory tract, are the main target of EIV. As showed in **Figure 4-7**, positive areas to NP were seen in the respiratory epithelia from the 2dpi until 14dpi, whereas no positive staining was seen in the uninfected controls.

Interestingly, NP positive area seemed to increase after 2dpi, and changed its pattern over the infection course, moving from the apical surface at the beginning of the infection to the basal membrane of the respiratory epithelium at late timepoints. Furthermore, the distribution of positive areas in respiratory epithelia of nasal mucosa, trachea, bronchi and bronchioles moved from focal/multifocal at day 2 post infection to diffuse at day 3 post infection and onwards. **Figure 4-8** shows the pattern of positive staining in the horse euthanized at 2dpi, whereas **Figure 4-9** shows it in horses euthanized at 3dpi.

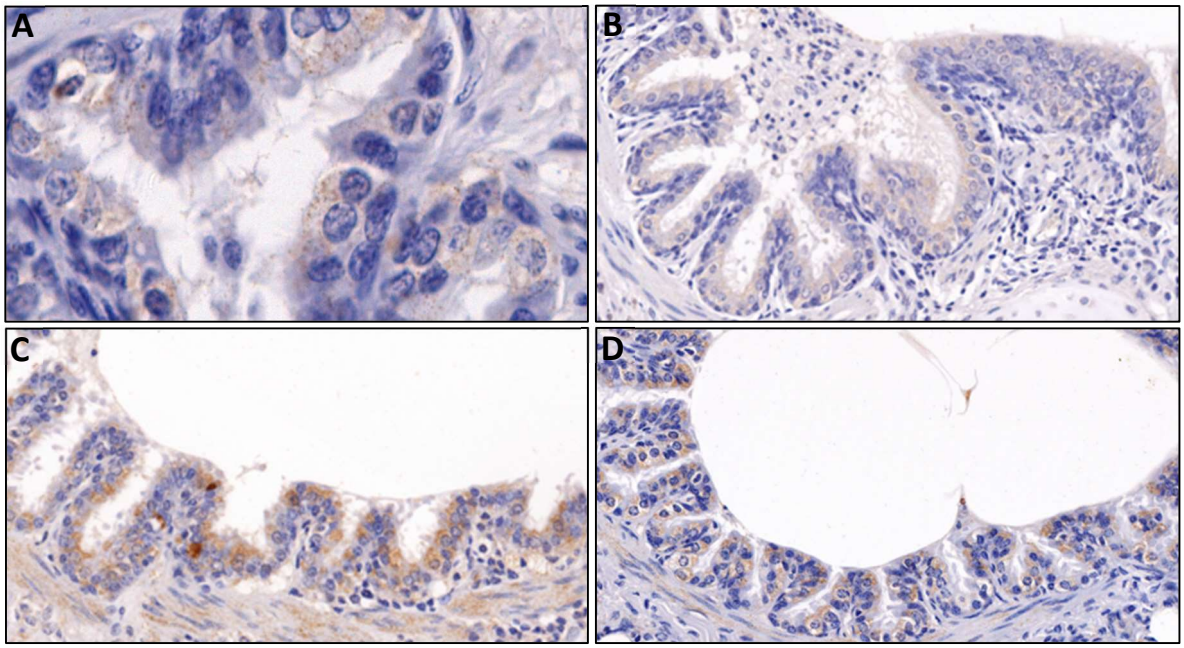

Figure 4-9*:* Representative images of respiratory sections from horses euthanized at day 3 post infection stained with an anti-NP antibody under an IHC procedure and haematoxylin counterstain. (**A**) Bronchial respiratory epithelium (45x). (**B**), (**C**) and (**D**) Bronchial respiratory epithelium (25x).

Serial sections of the same tissues stained with anti-NP antibodies were subject to IHC using an anti-HA antibody. As done with NP, an EIV-infected equine tracheal explant was used as a positive control, whereas lung sections from uninfected horses were used as negative controls. As **Figure 4-10** shows, specific positive staining was found in the epithelium and sloughed epithelial cells of the positive control (**A**), whereas in the negative control no signal was revealed (**B**). Positive areas were seen at early timepoints, days 2 and 3 post infection, in the respiratory epithelia of the bronchi.

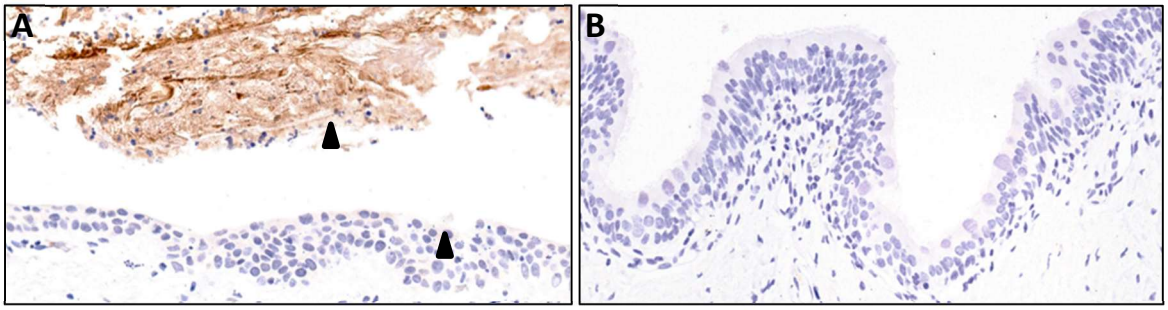

Figure 4-10*:* Representative images of sections from an EIV-infected tracheal explant (**A**, 20x) and a bronchial respiratory epithelium from an uninfected control (**B**, 18x) stained with an anti-HA antibody under an IHC procedure and haematoxylin counterstain. Arrowheads show positivity.

Staining was focal, as **figure 4-11** shows, and HA antibody labelled principally the apical membrane and the cytoplasm of the first layer of cells in the respiratory epithelia of the airways. Positive staining was also seen within the debris in intrapulmonary airways' lumina. **Figure 4-11** also shows side by side comparison of HA and NP staining for serial sections, displaying how these regions identified as positive to HA were also positive in serial cuts that underwent NP staining, although the intensity of the staining was very different; whereas NP-positive tissues showed a strong brown coloration, HA-positive ones were stained in light brown or orange. In lungs from horses euthanized at days 7 and 14 post infection no HA-positive areas were observed.

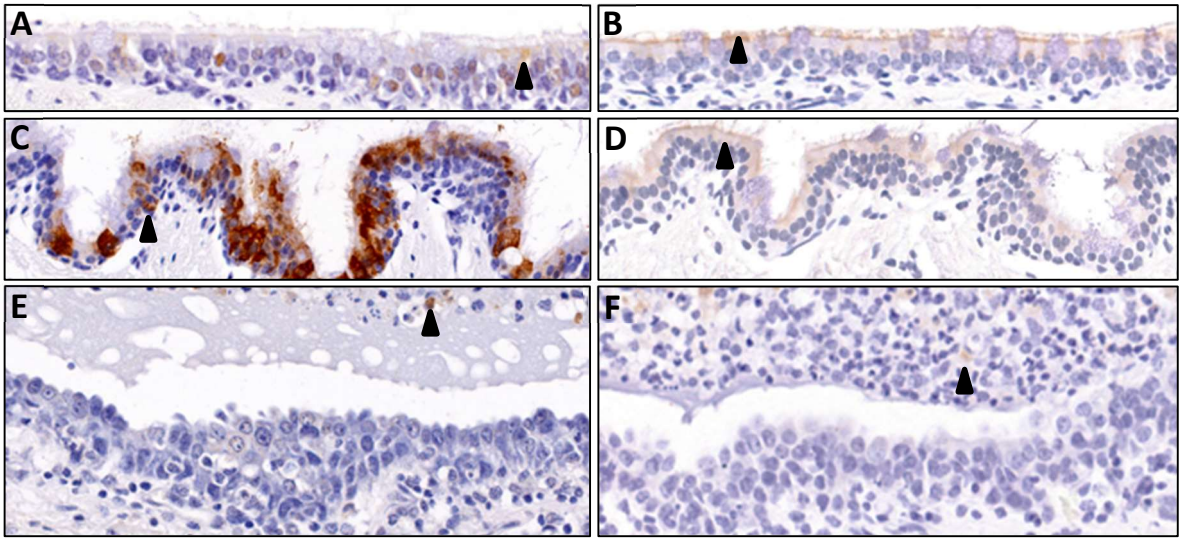

Figure 4-11*:* Representative images of sections from EIV-infected horses stained with viral protein antibodies under an IHC procedure and haematoxylin counterstain. (**A**) Tracheal respiratory epithelium from the horse euthanized at day 2 post infection stained with NP (25x). (**B**) Tracheal respiratory epithelium from the horse euthanized at day 2 post infection stained with HA (25x). (**C**) Bronchial respiratory epithelium from the horse euthanized at day 2 post infection stained with NP (25x). (**D**) Bronchial respiratory epithelium from the horse euthanized at day 2 post infection stained with HA (25x). (**E**) Bronchial respiratory epithelium from horses euthanized at day 3 post infection stained with NP (40x). (**F**) Bronchial respiratory epithelium from horses euthanized at day 3 post infection stained with HA (40x). Arrowheads show positivity.

At this point, it is interesting to highlight that HA was optimized by me in the lab and the best signal I could obtain was the one I am showing in this thesis. The fact that its intensity

was far lower than that observed in NP-stained slides shows that either this antibody was not very sensitive, or HA was expressed at lower levels than NP, or both.

Overall, these results evidence the presence of a second viral protein in the respiratory tract of the horse at days 2 and 3pi, whereas shows that no HA is found in the same tissues after 7 and 14 days of the infection. However, given the fact that HA signal proved not to be as strong as NP signal, might be that HA is still in the tissues at late timepoints but is too weak to be detected.

4.2.1.2 Immunofluorescence

To assess the distribution of NP and HA positive areas within the same sections, I performed an immunofluorescence co-staining with the same antibodies I used for the IHC assays. Serial cuts of the equine tracheal explants used as controls in IHC were utilized to optimize the IF protocol and as controls for the technique. A green dye, Goat anti-Mouse Alexa Fluor™ 488, was applied to stain HA-positive areas, whereas for NP, Donkey anti-Rabbit Alexa Fluor™ 555, a red colorant, was utilized. **Figure 4-12** shows the positive control, in which positive areas to NP (red) and HA (green) in sloughed epithelial cells can be seen, and the negative control, which does not show any positive cell. Lung sections from uninfected controls and horses euthanized at days 2, 3, 7 and 14 post infection were used to this purpose. Protocol followed is explained in Materials and methods.

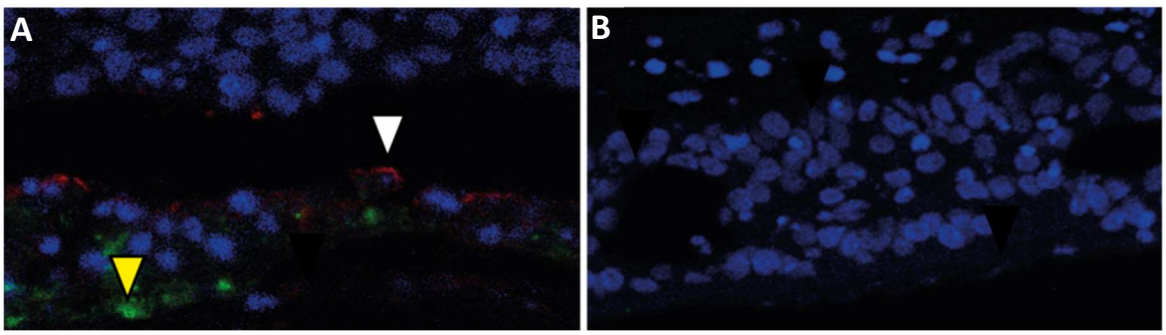

Figure 4-12*:* Representative images of sections from an EIV-infected tracheal explant (**A**) and a trachea from an uninfected control (**B**) co-stained with an anti-HA (green) and an anti-NP antibody (red) under an IF procedure. Yellow arrowhead shows positivity to HA, white arrowhead shows positivity to NP. 30x.

Positive signal to HA (green) and NP (red) was seen co-localized in bronchial respiratory epithelium at 2dpi (**Figure 4-13**).

HA signal was not detected in later timepoints nor in other tissues. Regarding NP, it was seen at days 7 and 14 post infection in the respiratory epithelia of the bronchi, although the signal was very weak (**Figure 4-14**).

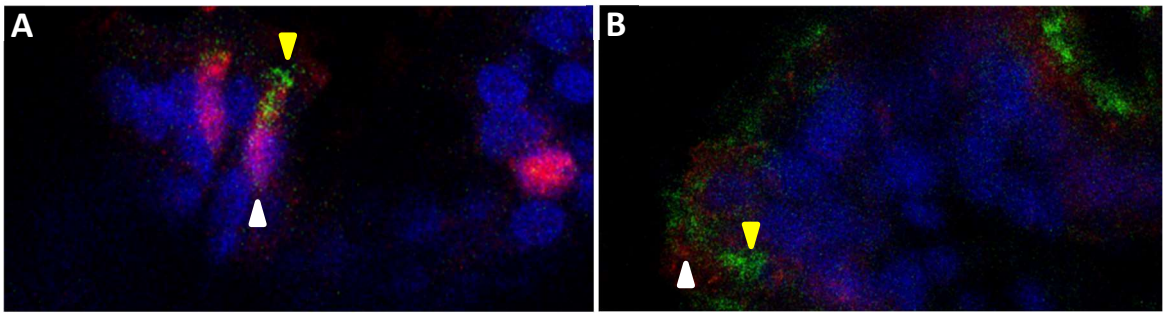

Figure 4-13*:* Representative images of sections of tracheas from the horse euthanized at day 2 post infection co-stained with an anti-HA (green) and an anti-NP antibody (red) under an IF procedure. Yellow arrowhead shows positivity to HA, white arrowhead shows positivity to NP. 63x.

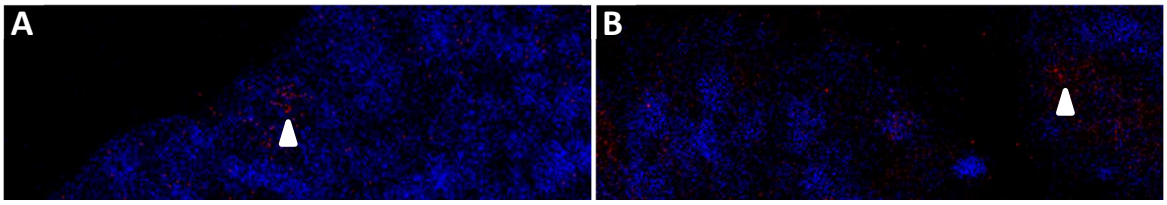

Figure 4-14*:* Representative images of sections of tracheas from a horse euthanized at day 7 (**A**) and 14 post infection (**B**) co-stained with an anti-HA (green) and an anti-NP antibody (red) under an IF procedure. Arrowheads show positivity to NP. 40x.

In summary, IF results were not optimal. Positive controls showed clear positivity for both antibodies, whereas infected tissues were only positive at 2dpi for HA, and until 14dpi for NP, although the level and the intensity of staining, as shown, was extremely weak compared to the IHC NP-stained slides. Therefore, with immunofluorescence I was not able to achieve my initial goals, which were, first, to show co-localization at 2dpi and 3dpi, which is what the IHC, with NP and HA stainings being applied in separated slides suggested, and second, to show colocalization at 14dpi, to have a stronger evidence of EIV presence in the respiratory tract of infected horses at this timepoint. As explained above, the lack of specificity of the HA antibody used might be the explanation of these results.

4.2.1.3 In-Situ Hybridisation

To detect viral mRNA in respiratory tissues of EIV infected horses, I performed a RNAscope® In-Situ Hybridisation 2.5 High Definition (HD)—Red Assay technique on lung sections from uninfected and infected animals. Specific probes to detect M1, NP and PB2 mRNA by labelling them with a pink-red dye, as explained in Materials and methods, were used. A probe to detect equine ubiquitin was used as a positive control, whereas for the negative control, a probe to label DapB, a gene from the soil bacterium *Bacillus subtilis*, was utilized. All the slides were counterstained with haematoxylin.

Abundant positive signal to Equine Ubiquitin was detected in different cell types of the respiratory tract stained with Equine Ubiquitin. Negative control slides did not show any positivity (**Figure 4-15**).

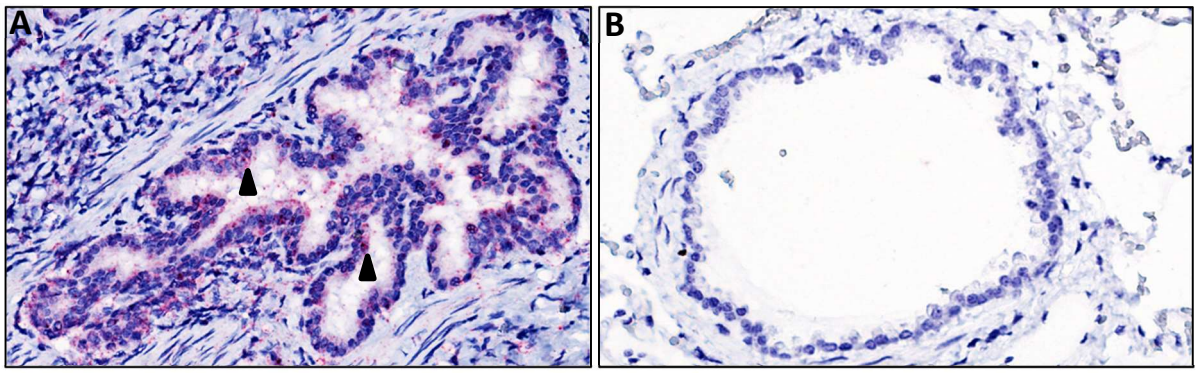

Figure 4-15*:* Representative images of bronchioles in lung sections from uninfected horses stained with an Equine Ubiquitin probe (**A**) and a DapB probe (**B**) under an ISH procedure. Arrowheads show positivity to NP. 25x.

ISH-positive staining was detected in cells of the bronchial respiratory epithelia of lung sections from horses euthanized at days 2 and 3 post infection. Furthermore, at day 3 post infection viral mRNA was also seen in cells occupying the bronchi lumen. Positive areas to M1, NP and PB2 were seen in the same locations in serial cuts, although the patterns of staining were specific to each protein; M1 hybridized in the cytoplasm, NP in the cytoplasm and the nuclei and PB2 only in the nuclei. These areas were also positive to NP and HA in immunohistochemistry (**Fig.4-16**).

These results show that viral mRNA can be found in the lung of infected horses at days 2 and 3 days after infection but not at days 7 and 14 post infection. Muranaka *et al*. and Yamanaka *et al*. reported detection of infectious virus by egg culture of nasal swabs until day 6 post-infection in the horse euthanized at day 7 and in 2 of the 3 horses that were euthanized at day 14 after infection, whereas the third horse euthanized at day 14 post infection shed virus until day 7 post infection, although in very small quantities (1.5 log10 EID50/200 µl) (Muranaka *et al*., 2012; Yamanaka *et al*., 2009). My findings match, therefore, what they described, since every time viral shedding was detected, I detected positive signal in ISH, and every time the shedding was negative, ISH was also negative, as **Table 4-1** shows.

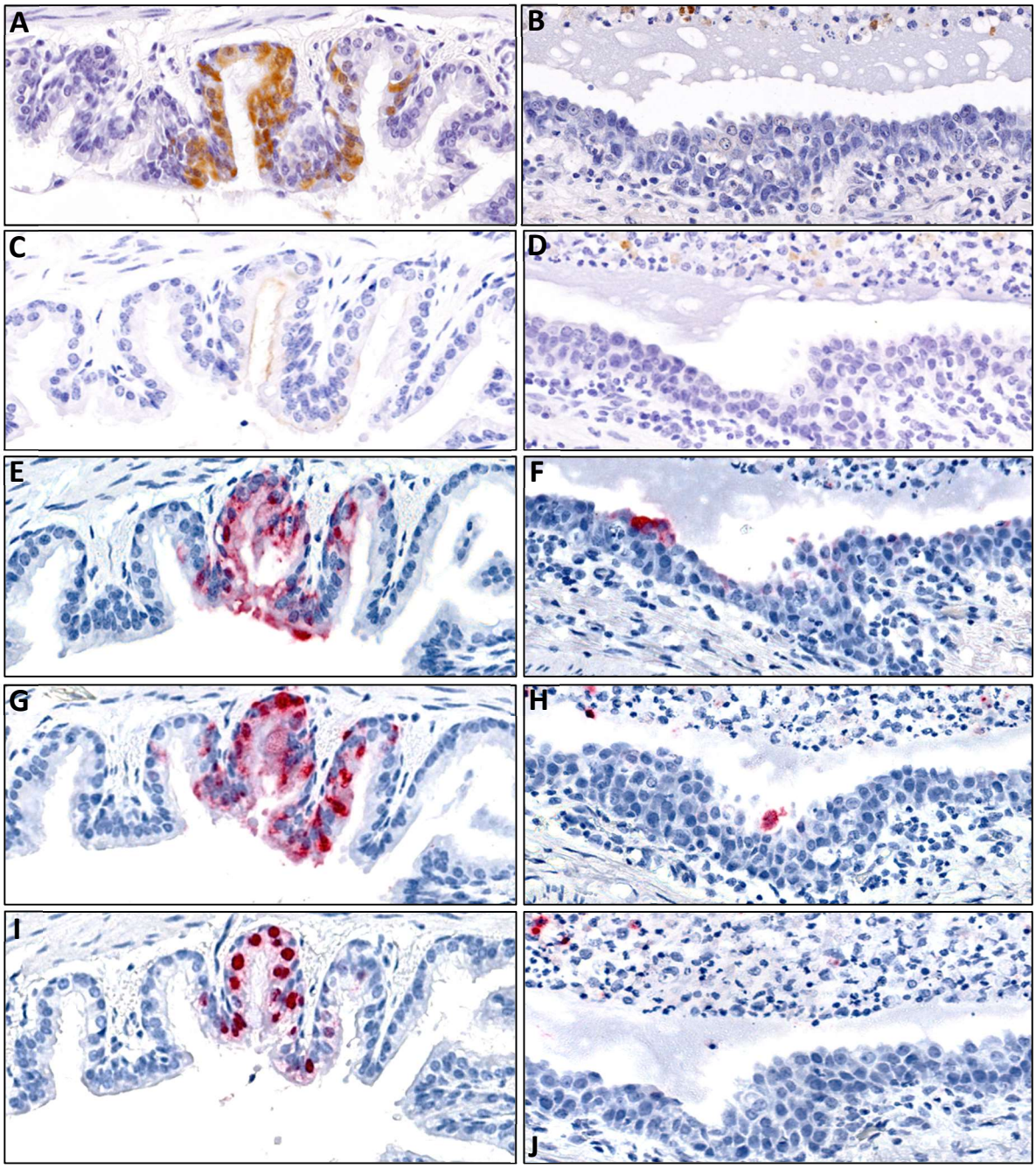

Figure 4-16*:* Representative images of sections from EIV-infected horses stained with different techniques against viral antigens. All the images of IHC are counterstained with haematoxylin (**A**) Bronchial respiratory epithelium from the horse euthanized at day 2 post infection stained with an anti NP antibody (IHC). (**B**) Bronchial respiratory epithelium from a horse euthanized at day 3 post infection stained an anti NP antibody (IHC). (**C**) Bronchial respiratory epithelium from the euthanized at day 2 post infection stained with an anti HA antibody (IHC). (**D**) Bronchial respiratory epithelium from a horse euthanized at day 3 post infection stained with an anti HA antibody (IHC). (**E**) Bronchial respiratory epithelium from the horse euthanized at day 2 post infection stained with a M1 probe. (**F**) Bronchial respiratory epithelium from a horse euthanized at day 3 post infection stained with a M1 probe. (**G**) Bronchial respiratory epithelium from the horse euthanized at day 2 post infection stained with a NP probe. (**H**) Bronchial respiratory epithelium from a horse euthanized at day 3 post infection stained with a NP probe. (**I**) Bronchial respiratory epithelium from the horse euthanized at day 2 post infection stained with a PB2 probe. (**J**) Bronchial respiratory epithelium from a horse euthanized at day 3 post infection stained with a PB2 probe. 25x.

	H1 - Day 2	H2 - Day 3	H3 - Day 3	H4 - Day 7	H5 - Day 14	H6 - Day 14	H7 - Day 14
Viral detection	+	+	+	-	-	-	-
ISH (M1, NP, PB2)	+	+	+	-	-	-	-

Table 4-1*:* Viral detection by egg culture of nasal swabs (done by Muranaka *et al.*, 2012 and Yamanaka *et al.*, 2009) and ISH for viral protein mRNA results in the seven horses experimentally infected with EIV.

Furthermore, my observations are consistent with previous reports, where equine influenza shedding was monitored over time and ranged between 5 and 10 days (Daly M. *et al.*, 2004; Donis, 2017; Murcia *et al.*, 2010; Radostits *et al.*, 2003; Wattrang *et al.*, 2003).

Overall, these results suggest, first, that virus can be found in the bronchial epithelia until day 3 post infection, since I have seen positive signal to five different viral antigens (three viral mRNAs and two viral proteins) in the same region, and second, that the patterns of detection of viral proteins and mRNA are different during the course of the infection, being most consistent at days 2 and 3pi, during the peak of infection and shedding. Furthermore, my data show that M1, NP and PB2 ISH are potentially useful tools to infer whether horses were shedding virus or not at the moment of the euthanasia.

4.2.2 Quantification of NP signal

To better understand the temporary and anatomical dynamics of EIV, I quantified EIV antigen signal in the respiratory tissues over time. I used the slides stained for visualization of NP (shown above), which was the antibody that proved to have the highest sensitivity against viral antigen and did not show any background at the same time, to count positive and negative pixels to viral antigen. I worked with the positive pixel count algorithm of Aperio Imagescope®, as **Figure 4-17** shows. I quantified the respiratory epithelium of all the nasal mucosa, tracheas and bronchi, and of 25 bronchioles and five randomly selected areas of pulmonary tissue, consisting of alveoli, of 5 by 2,5 millimeters (alveoli squares) in each slide. Presence of background or nonspecific staining was assessed subjectively, on the basis of the pattern of staining, as explained in **Figure 4-23.** Very scarce nonspecific NP positive signal was found, concretely in a bronchiole which was infiltrated by macrophages containing haemosiderin, which stains in brown but has a globular pattern, instead of the granular pattern shown by true NP staining

In the nasal mucosa the peak of NP positive area was at 3dpi, with 13% of positive pixels. After a decrease to 5% at 7dpi, a smaller peak was seen at 14dpi (8%) (**Fig.4-18).** Given the small sample size, running statistical comparisons was not possible.

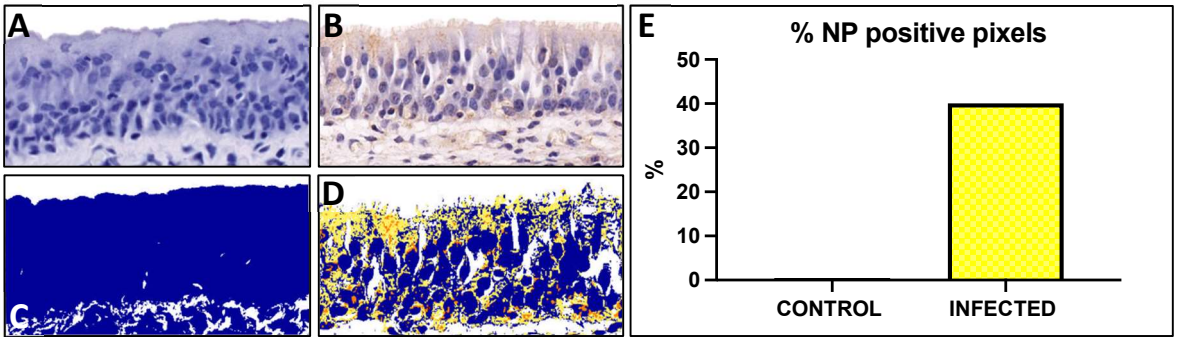

Figure 4-17: Quantification with Aperio Imagescope®. Respiratory epithelia of the nasal mucosa from an uninfected horse (**A**) and a horse euthanized at day 3 post infection (**B**). (**C**) and (**D**) Same epithelia after Aperio Imagescope® analyzed their pixels. Blue shows negative areas, yellow to red show positive areas. 20x. (**E**) Bar plot showing % of positivity of the epithelia analysed.

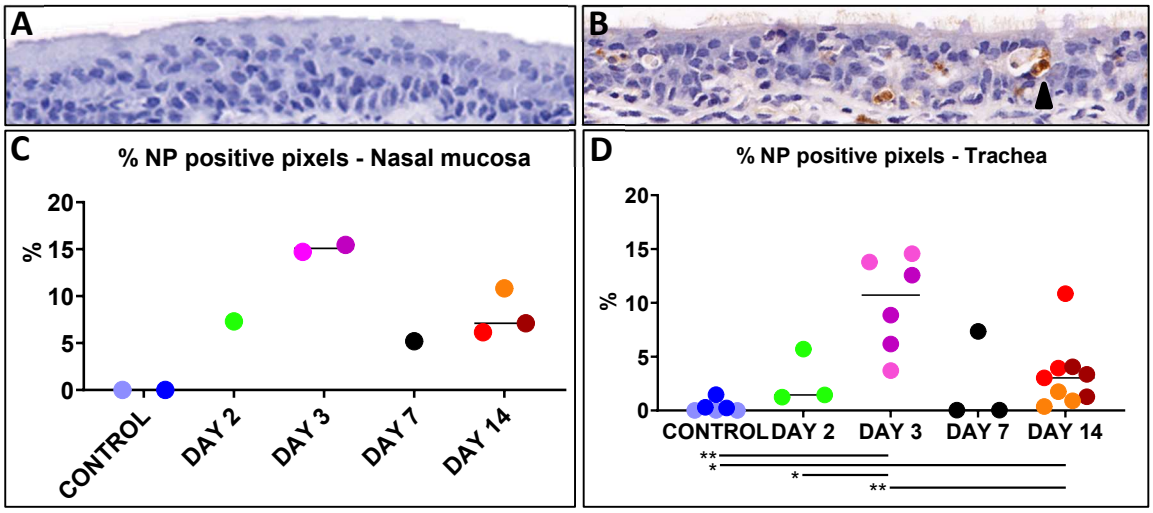

Figure 4-18*:* Representative images of tracheal respiratory epithelia from uninfected controls (**A**) and horses euthanized at day 2 (**A**) and 3 (**B**) stained with NP and counterstained with haematoxylin. 25x. Arrowheads show positive areas. Dot plot showing % of NP positive pixels in the respiratory epithelium of the nasal mucosa (**C**) and trachea (**D**). Light blue = control 2, dark blue = control 4, pink = horse 2, purple = horse 3, orange = horse 5, red = horse 6, brown = horse 7. Each dot represents a tracheal or nasal mucosa section. Bars show the median.

Same dynamics were seen in the trachea, with 10% of positive pixels at 3dpi and 3% at 14dpi (**Fig.4-18**).

In the bronchi, the situation was reverse. At day 2 positivity was low (3% of positive pixels) and it increased by day 3 (9%), although the biggest peak was at day 14, with 12% of the area being positive to NP (**Fig. 4-19**). Regarding the bronchioles, the positivity peaked at 14dpi (12%). A subpeak of 6% of positive pixels was seen at 3dpi (**Fig.4-19**). Finally, the positive signal in the alveoli increased over time, peaking at 14dpi (33%) (**Fig.4-20**).

These results suggest that there are three different dynamics of NP expression in the respiratory tract of the horse: nasal mucosa and trachea, with a peak at day 3pi and a subpeak at day 14pi, bronchi and bronchioles, with a small peak at day 3pi and a peak at day 14, and alveoli, with increasing NP signal over time. Furthermore, results show that NP remains in the tissues for some time after the animal has stopped shedding virus, which, as said, in the horses I studied was at days 6 and 7 post infection.

To see differences in NP dynamics depending on the anatomic location, I stratified the trachea into its three areas, upper, middle and lower, and saw different dynamics. In the upper trachea, the peak was at 2dpi, with 6% of positive pixels.
Positivity decreased to 5% at 3dpi and further, to 0%, at 7dpi. At 14dpi it increased to 3%. In the middle trachea, an increase from 1 to 11% of positive pixels was seen between 2dpi and 3pdi, when it peaked. Signal decreased at 7dpi (7%) and 14dpi (2%). Finally, the lower trachea had its NP peak at 3dpi, in which 14% of the area was positive to NP. % of positivity was almost 0 at 7dpi (0.026%), whereas at 14dpi it had increased to 5% (**Fig. 4-21**). Given the small sample size, running statistical comparisons was not possible.

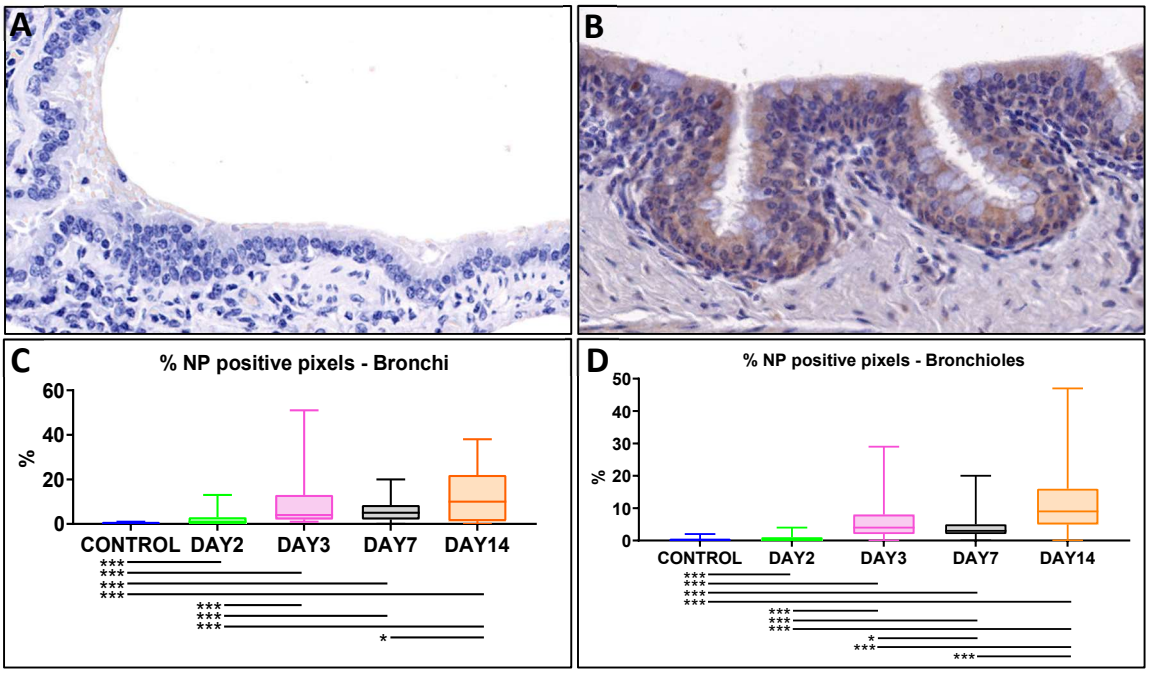

Figure 4-19*:* Representative images of bronchial respiratory epithelia from uninfected controls (**A**) and horses euthanized at day 3 (**B**) stained with NP and counterstained with haematoxyilin. 20x. Box plots showing % of NP positive pixels in the bronchial (**C**) and bronchiolar (**D**) respiratory epithelia. Statistical significances were assessed using a Wilcoxon rank sum test, *=p<0.05, ***=p<0.001. Bar shows the median. Whiskers show the highest and lowest values.

I stratified the bronchi, bronchioles and alveoli in the four lobes of the lung. I first analyzed the data of the three tissues of the lung (bronchi, bronchioles and alveoli) together. Anterior lobes showed higher positivity at days 2 and 3pi (3% and 12%) compared to the posterior lobes (0.33% and 5%). Furthermore, right lobes had more %NP positive pixels at days 2, 3 and 7pi (3%, 10% and 8%) than left lobes (0.63%, 5% and 15%) (**Fig.4-22**).

To see differences at tissue level in the lung, I divided the data into the three main pulmonary compartments: bronchi, bronchioles and alveoli. In the bronchi, at days 2 and 3 post infection anterior lobes had higher % of NP positive pixels (4% and 16% respectively) compared to posterior lobes (0.2 and 3%). Also, at these timepoints, % of positive pixels in the right lobes was bigger than in left lobes (1 and 7% vs 4 and 10%).

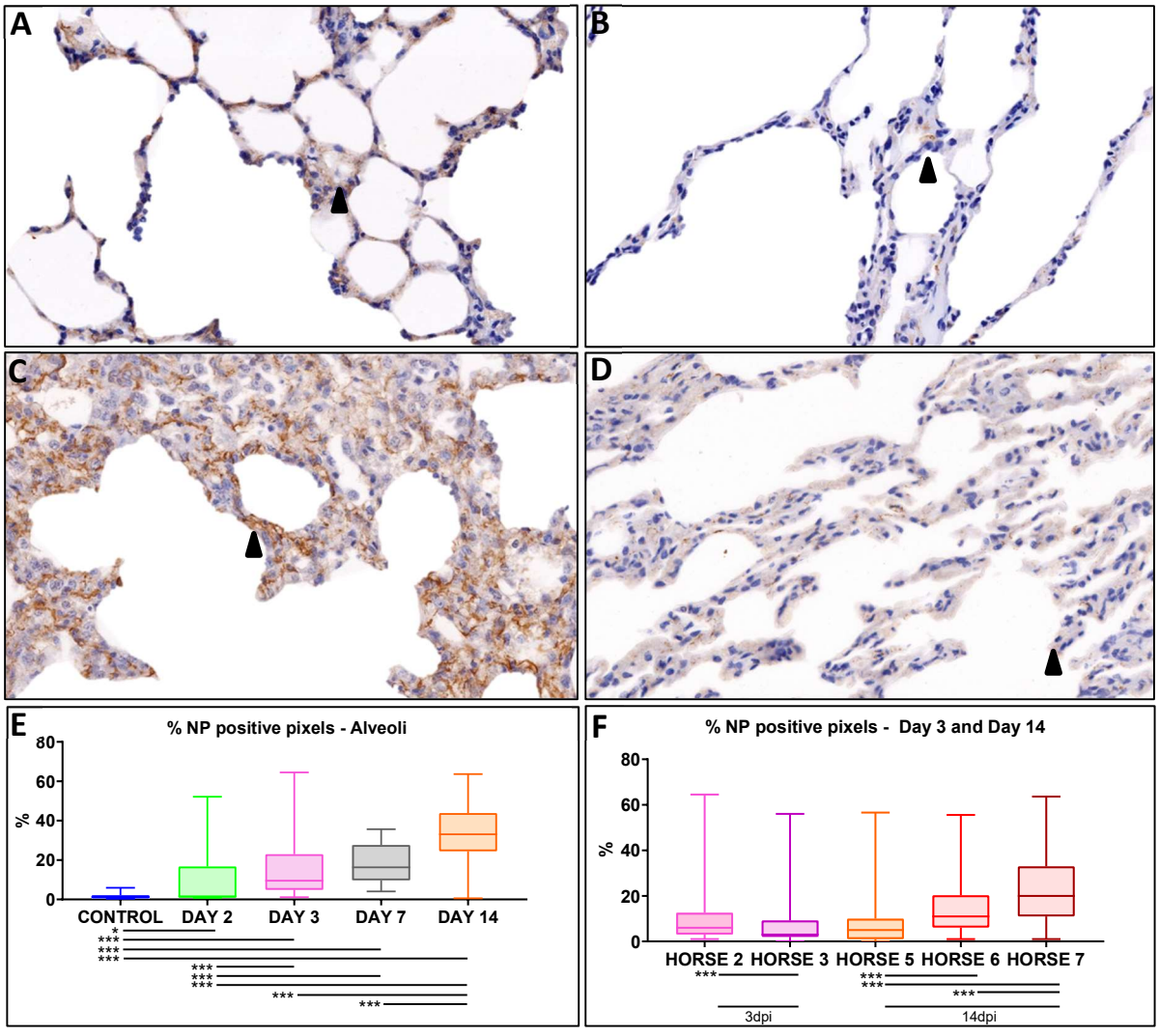

Figure 4-20*:* Representative images of alveoli from horses euthanized at day 2 (**A**), 3 (**B**), 7 (**C**) and 14 (**D**) stained with NP and counterstained with haematoxyilin. 20x. Arrowheads show positive areas. (**E**) Box plot showing % of NP positive pixels in the alveoli. (**F**) Box plot showing % of NP positive pixels in the tissues. Statistical significances were assessed using a Wilcoxon rank sum test, *=p<0.05, ***=p<0.001. Bar shows the median. Whiskers show the highest and lowest values.

Regarding the bronchioles, similarly to the bronchi, anterior lobes had more % of positive pixels to NP at days 2 and 3 post infection than the posterior lobes. Anterior lobes had 1 and 8% of positive pixels at days 2 and 3pi respectively, whereas posterior lobes had 0.14% and 4 %. On the other hand, at day 7 post infection more % of NP positive pixels were seen in the posterior lobes (5%) than in the anterior lobes (3%). Furthermore, NP signal was lower in the left lobes at days 3, 7 and 14, compared to right lobes (4, 3 and 12% vs 8, 5 and 13%)).

In the alveoli, anterior lobes had higher %NP positive pixels than posterior lobes at days 2 and 3 (16 and 24% vs. 10 and 20%). Also, right lobes had more % NP positive pixels at days 3 and 7 (9 and 14% vs 25 and 22%).

These results show that anterior lobes have a bigger amount of NP at early timepoints, compared to the posterior, suggesting that larger amounts of virus infected them at the beginning of the infection. Also, at intermediate timepoints (days 3 and 7) right lobes have more % NP positive pixels than left lobes.

To investigate interindividual differences, I stratified the data into 9 groups, corresponding to the 9 horses analyzed.
I first studied differences of NP expression among individuals. I saw that horse 2 exhibited more %NP positive pixels than horse 3 in all tissues examined. In addition, horse 5 exhibited less %NP positive area than horses 6 and 7 and horse 6 exhibited less %NP positive area than horse 7 (**Fig.4-20f**).

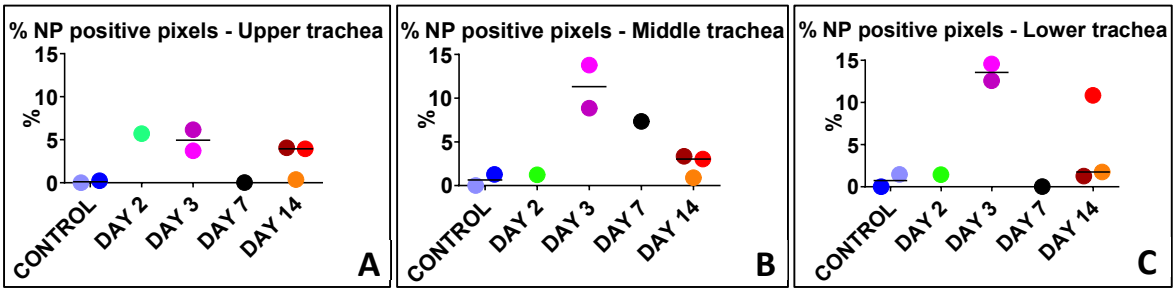

Figure 4-21*:* Dot plots showing percentage of NP positive pixels in the upper trachea (**A**), middle trachea (**B**) and lower trachea (**C**). Each dot represents a tracheal section. Bar shows the median. Light blue = control 2, dark blue = control 4, pink = horse 2, purple = horse 3, orange = horse 5, red = horse 6, brown = horse 7.

To learn interindividual differences at tissue level, I stratified the data of each horse into 5 groups, corresponding to the 5 respiratory tissues studied: nasal mucosa, trachea, bronchi, bronchioles and alveoli.

Between the controls, differences were seen in the bronchioles and alveoli, where control 1 displayed higher %NP than control 2.

At 3dpi, horse 2 exhibited higher %NP positive pixels than horse 3 in bronchi and bronchioles, whereas in the alveoli no statistical differences were seen.

At 14dpi, horse 5 continued to display less %NP than horse 6 and horse 7 in the bronchi, bronchioles and alveoli, whereas horse 6 exhibited less %NP in the bronchioles and alveoli.

No differences were seen among horses in the trachea, whereas in the nasal mucosa the sample size was too small to run statistical tests.

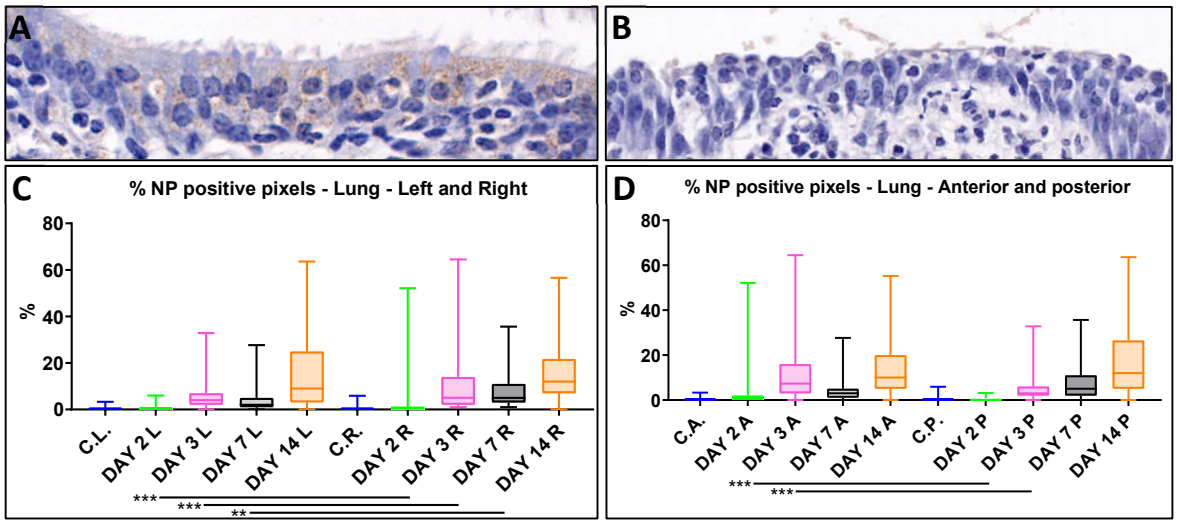

Figure 4-22*:* Representative images of bronchial respiratory epithelium of the right anterior lobe from horse euthanized at day 2 (**A**) and 3 post infection (**B**). (**C**) and (**D**) Box plots showing % of NP positive pixels in the lung. Statistical significances were assessed using a Wilcoxon rank sum test, **=p<0.01, ***=p<0.001. Bar shows the median. Whiskers show the highest and lowest values.

These results show clear interindividual differences in NP levels 3 days after the infection, and also 14 days after the infection, when the viral shedding is assumed to have been resolved. At the same time, data indicate the presence of NP positive areas in each tissue analyzed of each of the three horses euthanized at 14dpi, which strengthens the hypothesis that viral antigen stays throughout the respiratory tract for some time after the infective virus is cleared.

Interindividual differences between controls can be explained by the difference in the amount of haemosiderin in the tissue (specifically in the macrophages), which has a brown color, as **Figure 4-23** shows.

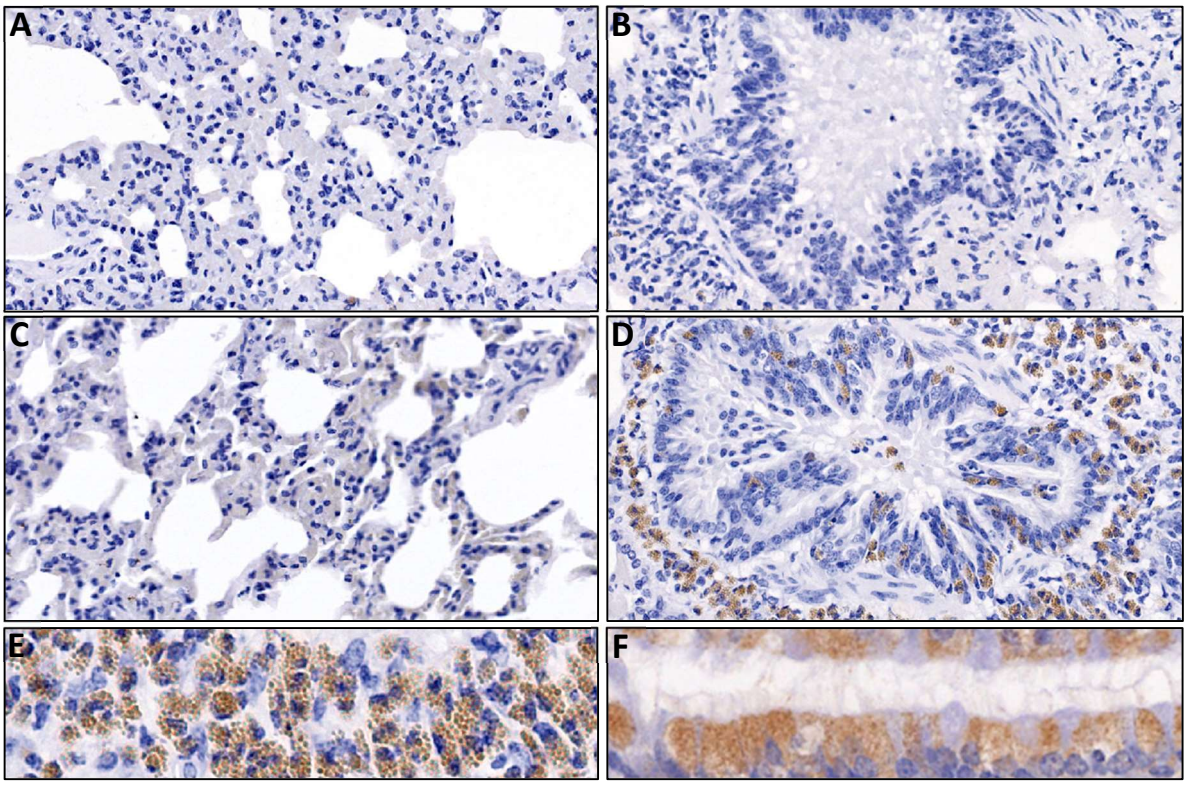

Figure 4-23*:* Images of alveoli and bronchioles stained with NP in an IHC procedure and haematoxylin counterstain from uninfected horses. (**A**) Alveoli from control 2. (**B**) Bronchiole from control 2. (**C**) Alveoli from control 1. (**D**) Bronchiole from control 1, showing macrophages containing haemosyderin infiltrating the respiratory epithelium. 20x. (**E**) Magnification of Figure **4-27d**, showing the globular pattern of the haemosyderin within the macrophages. (**F**) Magnification of a bronchiolar respiratory epithelium from an EIV-infected horse, showing granular, real positive NP-staining. 40x.

4.3 Discussion

Major objectives of this research were (1) to set a staining protocol to detect EIV in tissues, and (2) to determine virus spread by performing IHC, IF and ISH assays and software-based quantification on respiratory tissues from experimentally EIV-infected horses.

As explained in Chapter 3, there are two things to consider from the beginning of this discussion. First, the small sample size I worked with, 7 horses. This presented as usual things that I was only seeing in one, two or three individuals. Furthermore, as said, statistical tests were impossible to perform in some comparisons, whereas in others their power was not ideal. And second, the timepoints when horses were euthanized. These were 2dpi, 3dpi, 7dpi and 14dpi, described as key moments during EIV infection (Muranaka *et al.*, 2012), which means I was not able to get any data based on tissue analysis in sections from days 1, 4, 5, 6, 8, 9, 10, 11, 12, and 13 post infection. These two limitations conditioned the interpretation of results.

Regarding the first objective, NP in IHC proved to be the most sensitive technique to stain EIV antigens in FFPE sections. As shown in **figures 4-12, 14, 15** and **17**, other antibodies, such as HA, and techniques, such as IF and ISH, showed less effectivity in successfully labelling EIV genetic material. With NP in IHC I was able to detect positive immunostaining up to 14 days post infection, which is a thing I could only repeat with NP in IF, although in a far smaller scale. ISH proved to be a good technique to highlight viral mRNA at days 2 and 3 post infection, but not further, whereas HA showed a very limited proficiency on EIV-infected equine FFPE tissues.

As a summary, data showed that experimental inoculation with A/equine/Ibaraki/1/07 was followed by the viral colonization of respiratory epithelia of the airways and the alveoli at day 2 post infection, in a focal to multifocal fashion. EIV spread by 3dpi, reaching most epithelial cells and also other tissues, which had not been described to have viral antigen before, like the hyaline cartilage and the smooth muscle. It stayed at day 7, in lower amounts, and until day 14 post infection, although in different levels depending on the tissue and on the individual horse. Nasal mucosa and trachea showed a peak of NP in the respiratory epithelia at 3dpi and a subpeak at 14dpi, bronchi and bronchioles had the peak at 14dpi after a subpeak at 3dpi, and in the alveoli NP signal increased over time (**Figs**. **4-18**, **19**, **20** and **24**).

These findings partially match with observations made previously in horses and other species. Working with horses, Muranaka *et al*. described the presence of viral antigen in the tracheal respiratory epithelium at days 7 and 14 post infection (Muranaka *et al*., 2012), in the respiratory epithelium of the airways (7dpi) and in macrophages in the lamina propria (14dpi). As explained, in addition to these observations I was able to detect viral antigen (NP) at day 14 post infection in the respiratory epithelium of the nasal mucosa, trachea, intrapulmonary airways and alveoli and in the smooth muscle, cartilage and submucosal glands (**Figs. 4-4, 4-5, 4-18, 4-19** and 4-**20** show it). Long term influenza antigen detection was also made by Sutton *et al*., who reported it in "alveolar macrophage-like cells" in bronchoalveolar lavage from H3N8 EIV-experimentally infected ponies at 21 days post infection (Sutton *et al*., 1997), and by Read *et al*., in an intermittent fashion, for up to 35 days after infection in H3N8 EIV-naturally infected horses (Read *et al*., 2011), as commented above. As explained, in other species the viral shedding and immunopositive labelling of viral proteins has been studied and been shown to be especially intense in the first days post infection. Su *et al*, working with canine H3N2-experimentally infected dogs,

detected viral shedding until day 5pi, with a peak at 4dpi and rapid decline afterwards, and immunopositive stain to NP in the lung at some point during the infection (not specified in the paper) (Su *et al*., 2015). Rosas *et al*. infected dogs with canine H3N8 and observed viral shedding up to 8 days after the experimental infection, with a peak at 4dpi (Rosas *et al*., 2008). Lloyd *et al*. experimentally infected pigs with swine H1N1 and obtained the highest values of shedding between 3 and 4dpi, depending on the individual, after which the viral load decreased sharply (Lloyd *et al.,* 2011). Similar results were obtained by Marriott *et al.* in an experimental challenge of human 2009 pandemic H1N1 on ferrets, as they saw the peak of viral loads between 2 and 4dpi, depending on the those received by the animals, followed by a marked decline (Marriott *et al*., 2014). In a model of viral transmission, Sun *et al*. infected ferrets with different human and avian influenza viruses, and saw a peak of viral shedding between 2 and 6dpi, depending on the virus these had received, together with strong NP signal in the lungs at 4dpi (the staining in other timepoints was not shown) (Sun *et al.,* 2023). Siegers *et al*. experimentally challenged ferrets with highly pathogenic H5N1 avian influenza and detected similar amounts of positive signal to NP in animals euthanized 3dpi and 6dpi in nasal turbinates (Siegers *et al*., 2023). Finally, Vidaña *et al*. worked on 2009 pandemic human H1N1 experimentally infected ferrets and observed a peak of virus at 1 or 2dpi, with elevated virus up to 6dpi and strong NP staining at days 3 and 5dpi in the airways (Vidaña *et al*., 2021). Other examples are mentioned in the first chapter. Overall, in terms of viral shedding, it seems that experimental infections of horses with EI behave similarly to experimental infections with other influenza strains in their natural hosts, as explained above, with the highest loads of virus between 2 and 6dpi followed by a variably quick decline. Importantly, experimental infections of animals, mainly ferrets and mice, with human and avian influenza strains also showed a pattern of peak of shedding during 2 to 6dpi, preceded by the first 1-2 days post infection, in which no virus was detected, and followed by a decrease in viral loads from 7dpi (Groves *et al*., 2018; Vidaña *et al*., 2009; Marriott *et al*., 2014; Siegers et a., 2023), suggesting that the pattern of shedding of influenza viral particles in natural hosts might be similar to that one shown by animals infected with influenza strains belonging to other species.

Regarding immunostaining against viral antigens, as seen, the information on other species is limited, especially concerning the temporary dynamics and abundance of this immunolabelling, however, positive signal is consistently and generally found in the days 1-2 to 5-6 post infection, with some species, like the dog, displaying presence of viral antigen until 9dpi, and this is something that I observed in respiratory tissues from EI-infected horses.

NP values I found in horse tissues did not show correspondence with severity of lesions, which were explained in the previous chapter. In the nasal mucosa and trachea, the biggest loss of respiratory epithelia normal architecture was seen at day 7 post infection, which is when both tissues had the smallest amounts of NP. Same situation was found in the bronchi and bronchioles, which showed severe histopathological changes at day 7 but not high values of NP. The only exception is the alveoli, which displayed the highest degree of histological alteration and of % NP-positive area at day 14 post infection. Results of histological changes and NP signal at 7dpi suggest that the virus itself might not be the main cause of the pathology in the airways. It is a possibility, as explained in several publications, that the innate immune system and the inflammatory response triggered by it, explain the pathological manifestations of influenza (Biondo *et al*., 2019; Brandes *et al*., 2013; Lee *et al*., 2011; Tavares *et al*., 2017). Alternatively, it is possible that the changes observed at 7dpi were caused by the virus the previous days and the normal architecture of the respiratory epithelium of the airways had not started recovering yet. On this respect, Muranaka *et al*., reported successful isolation of EIV until day 6pi in the horse euthanized at 7dpi. Regarding the alveoli, even if the NP signal peaked at 14dpi, the lesions found at this timepoint are believed not to be caused by EIV, as virus was isolated up to days 6/7pi in the horses euthanized at 14dpi. Furthermore, as said, Muranaka *et al*. described positive identification of *S. zooepidemicus*' antigenic material at day 14 post infection in lung sections (Muranaka *et al*., 2012), pointing to the existence of a secondary bacterial pneumonia. The specific characteristics and cell types present in the alveoli might have also accounted for the different pattern and dynamics of the histological changes and immunomarkers, as shown in Chapter 3 and Chapter 5.

I identified positive staining to NP in the bronchial/bronchiolar smooth muscle and bronchial hyaline cartilage of the equine respiratory tract, which indicates that, at some point, these tissues were infected, although it is unknown whether this infection was productive or abortive. To the best of my knowledge had not been described before. Although it is not a common finding, partly because it is not tested on regular basis, a small number of references showing presence of influenza antigen, or even virus, in the muscular tissue of different species is available. Tang and Chong experimentally infected Guinea pigs with human H1N1 and H3N2 influenza viruses and showed very mild staining of influenza antigens in the bronchiolar smooth muscle at days 1 and 3 post infection (Tang and Chong, 2009). Zhu *et al*. infected human aortic smooth muscle cells with influenza A and B viruses and observed production of both viruses in these cells. (Zhu *et al*., 2019). In their work with human skeletal muscle cells experimentally infected with human seasonal and pandemic H1N1, Desdouits

et al. showed positive immunofluorescent staining against NP in this cell type, from 4 hours post infection onwards (Desdouits *et al.,* 2013). Kessler *et al*. isolated human H3N2 from a muscle biopsy specimen from a patient that presented with muscle weakness during an outbreak of H3N2 A/Texas/1/77 influenza (Kessler *et al.,* 1980). Similarly, Gamboa *et al*. reported isolation of A influenza from muscle in a human patient with myoglobinuria and polymyositis (Gamboa *et al*., 1979). Finally, Partin *et al*. isolated human H3N2 in muscle tissue from a human patient affected by respiratory symptoms (Partin *et al*., 2016). Overall, these reports support that influenza can infect the smooth muscle of the intrapulmonary airways, and this is consistent with my findings. On the other hand, it is unknown whether the infection affected the function of smooth muscle. Some reports have described a deleterious effect of influenza A viruses on the smooth muscle of the airways. Cheah *et al*. pointed to the influenza A-induced disruption of the respiratory epithelia of the airways as the responsible for the attenuation of smooth muscle relaxation response, in their work on mouse isolated tracheal smooth muscle infected with mouse-adapted H1N1 (Cheah *et al*., 2015). Other work, such as (Szarek *et al*., 1995) and (Bodelsson and Caverius, 1999), have demonstrated a dependency on an uninjured epithelium of smooth muscle relaxation responses, by using different myorelaxants in rat airways. Desdouits *et al.* established that H1N1 influenza infection on experimentally infected muscle cells led to their lysis, although they used skeletal myoblasts (Desdouits *et al*., 2013). As shown in the previous chapter, respiratory epithelia of the airways of horses were severely injured by EIV, which suggests smooth muscle's function could be deteriorated, although this is only a hypothesis and further investigation on this regard is needed. Regarding the detection of NP staining in cartilage, no literature related to this finding was found. The fact that in both tissues no viral mRNA or HA expression was detected points to the need of further investigation on this regard, in order to find a lab technique that undoubtedly establishes whether these two tissues were infected by EIV or not.

I discovered interindividual differences between horses euthanized at the same time. Horse 2 consistently showed more NP positive staining than horse 3 in the bronchi, bronchioles and alveoli. In the previous chapter I showed how some pathological changes in the respiratory epithelium, such as loss of cilia and goblet cells and loss of epithelial thickness were more severe in horse 2 compared to horse 3. These observations would support the widely proven tropism of A influenza viruses for the respiratory epithelia of the airways. Also, interestingly, horse 2 did not have higher fever or viral load than horse 3 (reported in (Muranaka *et al*., 2012). Regarding horses euthanized at day 14 post infection, I saw a

gradient of %NP positive area from horse 5 (the lowest) to horse 7 (the highest) in respiratory tissues, although, as shown in the previous chapter, it did not correspond to a gradient of severity of the pathology in the tissues.

Interestingly, horse 7 seemed to develop and terminate the clinical disease a day earlier than horse 5 and 6. As **Table 4-2** shows, horses 5 and 6 had the fever peak one day after horse 7 had it and at the day of euthanasia they still had a cough and nasal discharge. Horse 5 also started having nasal discharge a day later than horse 6 and 7. Again, these findings lead me to think that NP presence does not determine the severity of the lesions nor the clinical outcome. As said, some works, highlighted above, point to the host response following influenza as the main determinator of the both the tissular pathology and the symptoms that animals display.

Ibaraki 07/DPI	0	1	2	3	4	5	6	7	8	9	10	11	12	13	14
Horse 5	38.1	37.9	38.9	38.1	38	38.2	38.6	38.6	39.8	39.3	38.9	38.6	38.1	38.2	37.9
Nasal discharge	-	-	-	+	+	+	+++	++	+++	+++	++	++	++	++	+
Cough	-	-	-	+	-	+	++	+	++	+	+	+	+	+	+
Horse 6	37.8	38	38.7	38.8	38.4	38.2	38.7	38.7	39.3	39.1	38.9	38.2	38.4	38	38
Nasal discharge	-	-	+	+	+	++	+	++	+++	++	-	++	-	++	+
Cough	-	-	-	+	+	+	++	-	++	+	+	+	+	-	+
Horse 7	38	38.3	39.3	38.5	38.4	38.6	38.6	39.3	39.3	39.2	38.6	38.4	38	38	38.3
Nasal discharge	-	-	+	+	+++	+++	++	++	++	++	++	-	+	-	-
Cough	-	-	-	+	+	+	+	+	-	+	+	+	+	+	-

Table 4-2*:* Pyrexia, nasal discharge and cough scores during the infection of the three horses euthanized at day 14 post infection. - = absent, + = mild, ++ = moderate, +++ = severe. Data provided by Dr. Akihiro Ochi.

Regarding anatomical location, the lower trachea showed higher levels of virus than the middle and the anterior thirds at 3dpi, and this is what presumably lead to the more severe disruption of its respiratory epithelia at this timepoint, as shown in Chapter 3. Furthermore, the anterior lung lobes had more NP at early timepoints than posterior lobes. The fact that the distance between the bifurcation of the trachea and the lung parenchyma of the anterior lobes is smaller than of the posterior lobes is a potential explanation, since the virus would access the intrapulmonary airways and the alveoli faster in the anterior lobes than in the posterior lobes. Also, at days 2, 3 and 7 post infection, right lobes had higher NP positivity than left lobes, which matches with the fact that the right primary bronchus is bigger in diameter than the left primary bronchus and, thus, it transports more air and more particles contained in it. These findings, however, did not correspond to a higher pathological severity. As explained in the previous paragraph, this is in line with what some literature has

described. No literature related to air flow and pathogen distribution within the respiratory tract was found.

I saw positive signal to HA in IHC and IF in bronchial respiratory epithelia at days 2 and 3 post infection, although the intensity and the amount of signal detected was very reduced, compared to NP, as shown in **Figure 4-11** and **16**. These findings, together with the data of NP, indicate the presence and co-localization of two viral proteins (HA and NP) at these timepoints in the bronchial respiratory epithelium. At days 7 and 14 post infection, however, no HA positive signal was detected, contrasting with the big amounts of positivity that the staining with NP revealed at late timepoints, especially at day 14 post infection. Furthermore, no positive signal to HA was detected at any time in bronchial and bronchiolar smooth muscle and hyaline cartilage. As stated, it is important to highlight that the HA antibody I used was a limitation, since its specificity against the haemagglutinin of A/equine/Ibaraki/1/07 proved not to be optimal (**Figure 4-11** shows it**).** To do further optimization of the HA staining protocols or to work with an anti-HA antibody which is more specific to the virus used in the horses I studied would have improved the quality of the staining and might have shed light on whether HA can be found in other tissues and later timepoints in the respiratory tract of EIV-infected horses.

Finally, with RNAscope® ISH I was able to determine whether the positivity seen in lung slides that underwent immunostaining procedures belonged to viral mRNA and to confirm IHC results for days 2 and 3 post infection. Detection of positivity to three different viral protein mRNAs (M1, NP and PB2) in an ISH procedure in the same areas where IHC and IF positive signal was seen simultaneously validated the three assays as reliable techniques to label EIV antigens in FFPE sections and gave robust evidence of the presence of EIV in those locations. However, as it happened with HA, slides that underwent ISH did not show any positivity with any of the three probes (including NP) applied to them at late times post infection (7dpi and 14dpi). On top of that, no positive ISH labelling was seen in any timepoints in the smooth muscle of the airways or the cartilage. Nevertheless, it is impossible to establish whether horses were shedding when they were euthanized by performing IHC, IF or ISH assays on FFPE tissues. Having said that, as explained above, Muranaka *et al*. and Yamanaka *et al*. determined shedding periods of 6 or 7 days after infection in the horses I have been studying. My data, although are limited, show that ISH is a tool that is potentially useful to estimate whether horses were shedding at the moment they were euthanized or not (**Table 4-1**), given the fact that every time virus shedding was detected by nasal swab and

egg culture in the papers aforementioned, positive ISH-signal against viral mRNA was found by me in respiratory tissues of the horses used in those works.

Respiratory epithelial cells of the respiratory tract contained viral antigen (NP) in large quantities at 14dpi. The means used for the development of this thesis do not allow to determine whether the signal detected at 14dpi means that there was viable virus or viral shedding at that timepoint, however, several facts lead to the hypothesis that this is very unlikely. As shown, there are multiple evidences of the veracity of the positive signal seen at days 2 and 3dpi: Muranaka *et al*. reported viral detection in nasal swabs and positive immunostaining in respiratory tissues at these timepoints and different staining techniques performed by me consistently revealed positive signal in the same tissues. **Figures 4-11**, **4-12**, **4-13** and **4-16** are illustrative of this. At 7dpi, no virus was detected on nasal swabbing, however, IHC staining against human influenza A (H1, H2, H3) performed by Muranaka *et al*. and IHC and IF against NP performed by me showed consistent positive signal in respiratory tissues (**Figure 4-7** shows it). Furthermore, horses are known to excrete virus until up to 10dpi; on this regard, one of the three horses euthanized at 14dpi studied in this thesis excreted virus until 7dpi, as reported by Yamanaka *et al*. (Yamanaka *et al*., 2009). Whereas the horse euthanized at 7dpi was reported to shed up to 6dpi, it might have had viral antigen in its respiratory tract for longer. The fact that Muranaka *et al*. were not able to isolate virus at 7dpi but did find positive staining against EIV antigens in the tissues at this timepoint (in the same animal) is consistent with this and highly relevant for the discussion about the veracity of the NP signal seen at 14dpi by me. On the other hand, at 14dpi there was only signal in IHC and IF using NP; in IHC the positive staining was strong and detected not only in the airways and the alveoli, but also in the cartilage and the smooth muscle surrounding them (**Figures 4-1**, **4-3**, **4-4**, **4-5** and **4-23**), and in IF it was very weak (**Figure 4-14**). Given the fact that, as explained in the introduction of this chapter, evidences of virus at 14dpi in the respiratory tract of horses are scarce and not robust, the possibility of all the signal seen at this timepoint not belonging to viable virus, but to viral antigen, is considered the most likely one.

The core of the discussion of this chapter is the justification for the positive signal to NP seen in respiratory tissues of horses infected and euthanized at 14dpi. A consideration prior to answering this is that there is no literature on the study of expression of NP in tissues of horses infected with EI, therefore, the finding I report, if true, is novel and does not contradict

findings made by other researchers. This also applies to the findings of NP positive signal in the smooth muscle and hyaline cartilage of the intrapulmonary airways.

To dismiss the possibility of the NP-positive signal detected at 14dpi being background, several negative controls (tissues from non-infected animals undergoing the same NP staining protocol as those from infected animals and tissues from infected animals undergoing the same protocol but skipping the incubation with the primary antibody) were ran and counterstained parallelly to the infected tissues, with no positive staining present (**Figure 4-1**) other than a single bronchiole being strongly positive due to pigment deposition (shown in **Figure 4-23**). Furthermore, in slides from tissues of infected horses, within the same slide (**Figures 4-3A, 4-4, 4-5** and **4-8** are good examples) some areas were strongly positive whereas the immediately adjacent ones were negative. Other explanations for the staining seen at 14dpi being not related to the presence of viral antigen were considered. As the horses euthanized at 14dpi came from an experiment done 3 years earlier than the other 4 horses, it might be possible that an increased storage time artificially increased the positivity of those tissues to immunoassays. No evidence of this was found in the literature, whereas several papers reported loss of antigenicity in long-term stored FFPE tissues (Jacobs *et al*., 1996; DiVito *et al*., 2004) and more recent research found no difference between tissues stored for different time lengths (Karlsson and Karlsson, 2011). Furthermore, as said, in their work, Muranaka *et al*. found very small signal for EIV antigen in tissues from horses euthanized at 14dpi compared to previous timepoints, and I stained these same tissues with HA in IHC and did not find any positivity. In summary, there is no reason for this positive staining to be background.

The finding of viral antigen in tissues of *in vivo*, influenza infected horses, after they have finished shedding virus has been reported before. As explained, Muranaka *et a*l. reported viral shedding until 6dpi and observed positive IHC signal to viral antigen at 7 and 14dpi. Furthermore, the presence of viral genetic material at 14dpi or beyond in experimental infections with influenza virus has been documented in several species. Mori *et al*. infected mice with a mice-adapted H1N1 influenza and detected viral nucleoprotein (NP) by PCR in the lungs of animals euthanized at 14dpi (Mori *et al*., 1995b). Bissel *et al*. infected ferrets with human 2009 pandemic H1N1 and, by performing ISH, detected influenza matrix protein mRNA at 14dpi in the lamina propria of the small intestine of four animals. In the same experiment, Bissel *et al*. also challenged ferrets with human 2009 pandemic H1N1 and reinfected them, 90 days after the first inoculation, with highly pathogenic avian H5N1, finding ISH positive signal to influenza matrix protein at 18dpi in the lamina propria of the small intestine, in the liver and in the red and white pulp of the spleen (Bissel *et al*., 2014).

Abou-Donia experimentally inoculated mice with human H0N1 and isolated virus from the lungs of animals euthanized at 14dpi (Abou-Donia *et al*., 1981). Finally, Aronsson *et al*. infected mice in utero with human H1N1 and detected RNA encoding for M or NP viral proteins at days 20, 35, 60 and 90 post infection in the brain (Aronsson *et al*., 2002). Works *in vitro* with cell/tissue cultures by Gavrlilov *et al*. and Reed also demonstrated that influenza virus antigen can remain in infected tissues in the long term (Reed, 1969; Gavrilov *et al*., 1972). Although it has not been demonstrated before, it is feasible to think, based on the results presented here and the findings by others described above, that viral antigen remains in the tissues of EI-infected horses for longer than previously perceived, regardless of whether the signal observed at 14dpi in the lungs of EI-infected horses means that there is residual viral protein, viable virus (as shown by Abou-Donia in mice) or even viral shedding. On the other hand and related to the finding of NP at 14dpi in horse lungs, according to the literature mentioned above it seems that NP is one of the viral structural elements most commonly found in long-term influenza-infected animals. A plausible hypothesis is that the positive staining seen at 14dpi in the respiratory tract of the horses might be NP protein produced by the virus earlier in the infection and not degraded by the cells. On this regard, although for the influenza protein polymerase acidic-X (PA-X), half-life has been estimated to be inferior to 24 hours (Levene *et al*., 2021), no data was found regarding NP. A reinfection of the horses was initially also considered, as the three individuals euthanized at 14dpi were housed each, during these 14 days, with a dog that had not been infected, in order to study interspecies transmission. In their work with pigs infected with different swine influenza viruses, Lyoo *et al*. observed positive antigen to H1N1 in the lungs at 14dpi, hypothesizing that the pigs might have been reinfected among themselves (Lyoo *et al*., 2014). In the case of the horses, this might have been possible in two of the three animals, as the dogs housed with them shed virus until day 8 and 9 respectively, although at low levels; however, the third dog never shed virus during the challenge (Yamanaka *et al*., 2009) and thus could not reinfect the horse housed with it. Furthermore, if horses had been reinfected, they would have possibly shed virus again at 14dpi, and this was not reported. It is uncertain whether it is possible that a reinfection led to a production of NP without detectable shedding, although it is considered unlikely given that there is no scientific literature that supports such theory.

Regarding the effect that NP might have on the cells containing it, only speculations can be highlighted. Papers studying the presence of residual SARS-CoV-2 spike protein in tissues have suggested different effects, such as contribution to neurological symptoms in the long

term due to persistent accumulation in the nervous tissue (Rong *et al*., 2023) and induction of expression of inflammatory mediators in epithelial cells (Khan *et al*., 2021). No literature has been found about the effect that NP might have on epithelial cells of the respiratory tract, however, these might not be relevant, given the fact that, as shown in Chapter 4 (**Table 4-2**), symptoms shown by horses at 14dpi, the timepoint when the most NP is detected in the lung, had become milder since day 10 post infection.

Same as discussed for the respiratory tissues applies for the staining found in the cartilage and smooth muscle at 14dpi: the negative controls did not show positivity in these tissues, whereas there was an apparent increase in the amount and intensity of the signal towards the end of the challenge. Only a reference showing positive staining of influenza antigen in the smooth muscle was found (Tang and Chong, 2009), however, it is uncertain if this finding has been made before, as none of the publications where IHC for influenza antigen is performed on respiratory tissues from animals infected with influenza reported that the smooth muscle of the intrapulmonary airways was negative to viral antigen. Whereas the probability of this being unspecific background is considered low, as said, the possibility of this positive signal reflecting the presence of viable virus is unlikely, however impossible to rule out by the means used. The nature of this positive signal and, in case of being real NP protein, whether it had any effect on the myocytes and chondrocytes it was contained, requires further research.

Regarding RNAscope, it has been described as a technique to detect antigens in FFPE tissues with similar sensitivity and suitability than IHC. On this regard, it is especially relevant the work done by Gaide *et al*. on validating RNAscope assay for the detection of avian A influenza virus (Gaide *et al*., 2023). The reason for the mismatch between RNAscope results and IHC results is believed to be due to the different target that these techniques have (IHC detects proteins, whereas RNAscope detects mRNA). Greenbaum *et al*. reviewed the possible reasons explaining the absence of correlation between mRNA levels and protein levels, highlighting the existence of several not well understood mechanisms involved in turning mRNA into protein, the lack of knowledge on the *in vivo* half-lives of proteins and the notable amount of noise and errors in experiments for the detection of mRNA and proteins (Greenbaum *et al*., 2003). On this regard, as said, it is possible that at day 7 and 14dpi the viral mRNA had been eliminated (or remained at undetectable levels) and the protein was still present in the tissues.

In summary, my results demonstrated the existence of EIV antigens in the respiratory tract of the horse from the beginning of the infection until 14 days post infection, which had never been described before, in the respiratory tissues and also in the smooth muscle and hyaline cartilage of the airways, which was something never described before too. Furthermore, NP in IHC proved to be an optimal tool to label EIV antigens, giving good staining and minimal background, whereas HA in IF and IHC, and ISH demonstrated a limited ability to highlight these antigens. My work provided new insights on spatial and temporary dynamics of EIV, a key aspect of the pathogenesis of equine influenza, and highlighted the need for further research on the field, to establish, first, why at day 14 post infection big amounts of NP can be found in the respiratory epithelia, smooth muscle and cartilage, given the fact that horses are not infective anymore, and second, whether smooth muscle and cartilage cells get infected by EIV.

Chapter 5. Characterization and quantification of cell populations and cellular processes in respiratory tissues of horses infected with equine influenza virus

5.1 Introduction

Chapter 3 focused on EIV-induced lesions, showing pathological changes in the respiratory tissues of EI-infected horses, whereas chapter 4 focused on showing virus distribution across tissues and over time. This chapter will focus on the host response to infection. To this end, I validated different antibodies as reliable markers for cellular processes such as apoptosis, innate immune activation and mitosis, and as markers of cell types, such as Paired box gene 5 (PAX5) and Cluster of Differentiation 3 (CD3), and examined their expression in EIV-infected horse tissues. To this purpose, I used formalin-fixed, paraffin-embedded sections of respiratory tissues from the same horses described in previous chapters (7 infected, 2 noninfected controls) and immunohistochemical approaches to identify and quantify different cellular markers.

Finally, to describe and quantify type II pneumocyte proliferation, a change described by (Muranaka *et al*., 2012) in EIV-infected horses, I stained respiratory tissues from the animals utilized in that experiment with a Surfactant Protein C antibody, which specifically stains this cell type in the lung (Zhang *et al*., 2015).

5.2 Results

5.2.1 Quantification of protein expression in equine tissues

To better understand the dynamics of the processes and cell populations stained with the antibodies shown above, I used an image analyses software, Aperio Imagescope®, to quantify positive signal to markers described above in FFPE sections from respiratory tissues of EIV experimentally infected and euthanized horses.

As done in the first two chapters of this thesis, IHC-stained slides were scanned with Leica Aperio Versa 8®. Positive signal was measured using two algorithms. For MX1, CC3 and CD3 antibodies, a modification of the positive pixel count algorithm was utilized. **Figure 4-21** in **Chapter 4** explains how it works. For Ki67, PAX5 and Surfactant protein C, I used a positive nucleus count algorithm. **Figure 5-1** shows how it works.

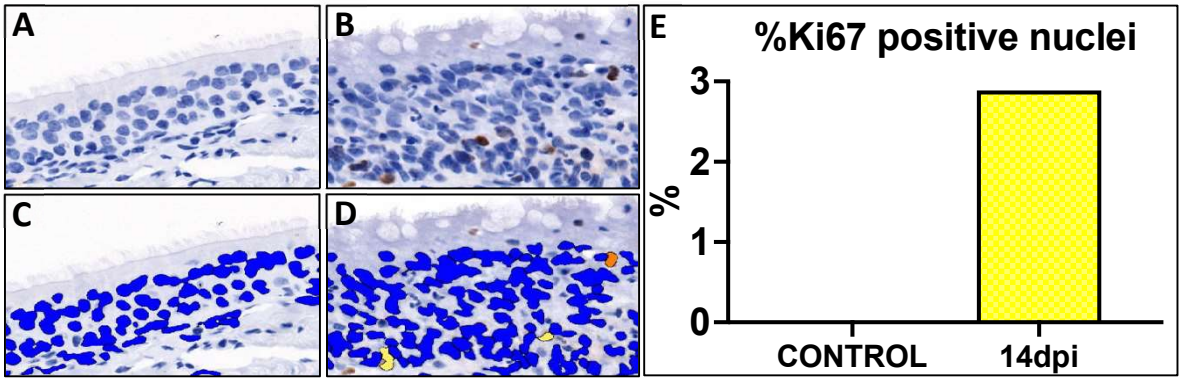

Figure 5-1: Quantification of nuclei in equine respiratory tissues using Aperio Imagescope®. Respiratory epithelia of the trachea from an uninfected horse (**A**) and a horse euthanized at day 14 post infection (**B**). (**C**) and (**D**) Same epithelia after Aperio Imagescope® has analyzed their pixels. Blue shows negative areas, yellow to red show positive areas. 20x. (**E**) Bar plot showing % of positivity of the epithelia analysed.

To identify cells developing an IFN mediated response I used an anti-MX1 antibody. Sections from nasal mucosa, trachea and lung of EIV infected and noninfected horses underwent an IHC procedure, and their respiratory epithelia were quantified with the Aperio Imagescope® Positive pixel count algorithm. Each nasal mucosa, trachea and bronchus were quantified, together with 25 bronchioles and 5 alveoli squares in each lung slide.

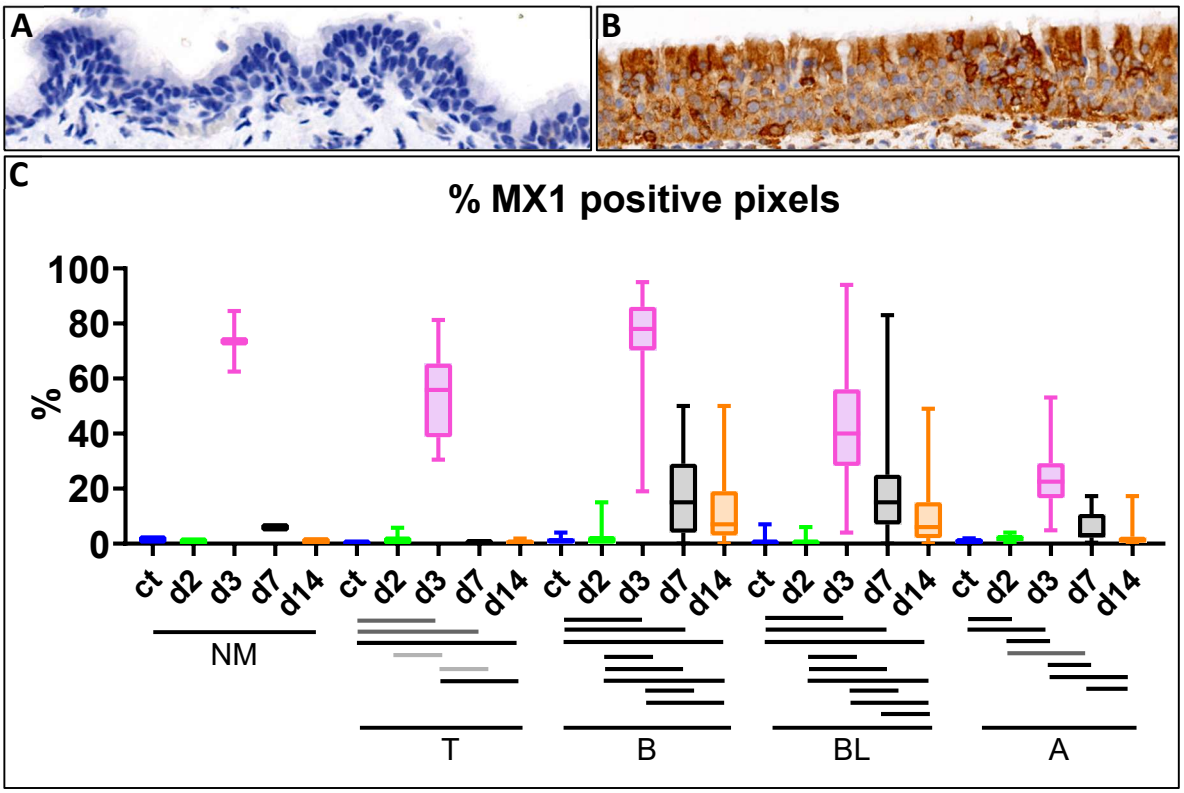

Figure 5-2: Representative images of bronchial respiratory epithelia from EIV-infected horses stained with an anti-MX1 antibody under an IHC procedure and haematoxylin counterstain. (**A**) Noninfected control. (**B**) Day 3 post infection. (**C**) Box plot showing % of MX1 positive pixels in each tissue and timepoint. NM = nasal mucosa, T = trachea, B = bronchi, BL = bronchioles, A = alveoli. 20x. Statistical significances were assessed using a Wilcoxon rank sum test, light grey=$p<0.05$, dark grey=$p<0.01$, black=$p<0.001$. Bar shows the median. Whiskers show the highest and lowest values.

MX1 was vastly expressed at 3dpi, regardless of the organ, after showing low values at 2dpi. Percentages of positivity were especially high in the nasal mucosa (73) and the bronchi (75)

and low in the alveoli (24). At 7dpi MX1-positive area decreased in all tissues, but in a higher degree in the nasal mucosa (6%), trachea (1%) and alveoli (6%), since bronchi (17%) and bronchioles (19%) still had considerable amounts of positive area, whereas at 14dpi a further decrease in all tissues was seen (**Fig. 5-2**).

These results suggest a transient and fast activation of the innate immunity at 3dpi in the entire respiratory tract, regardless of the fact that the virus signal is at its peak (as it happens in the nasal mucosa and trachea) or not.

This finding, together with **Figure 5-3C** and **5-16C**, suggests that not all the cells that express MX1 are infected with the virus. In their study with equine tracheal explants infected with EIV/2003, Amat *et al*. found similar results. They described a pattern of significant increase of MX1 signal between day 2, when almost no MX1 positivity was observed, and day 4 post infection, resulting in a four-fold increase (Amat, 2022).

5.2.1.2 Quantification of apoptosis

Respiratory tissues of EI-infected horses were stained with CC3 and their respiratory epithelia were quantified with Aperio Imagescope® Positive pixel count. Each nasal mucosa, trachea and bronchus were counted, together with 25 bronchioles and 5 alveoli squares in each lung slide.

CC3 showed low tissue staining percentages in respiratory tissues, although the staining proved to be very specific. In the nasal mucosa and trachea, the peak of cells undergoing apoptosis was at 3dpi, matching with the peak of NP. This is compatible with an early inhibition of apoptosis by the virus, to facilitate viral replication, followed by a later promotion of it, as explained in the first chapter. In the bronchi the peak of CC3 was also at 3dpi, although there was a smaller peak at 14dpi.

Regarding the bronchioles the peak of apoptosis was at 7dpi, although the values of positivity were generally low. In the alveoli the peak was at 7dpi too, but values were higher, especially in the two controls, which showed almost three times more tissue positive to CC3 than 7dpi. Knowing that apoptosis is a pathway that cells can take as a response to different stimuli, and not only EIV infection, is normal to see CC3-positive cells in uninfected tissues, although it was not expected that these had higher values than EIV-infected ones. It is possible that the processing of control tissues was done in a different way than the infected

ones and it caused damage to cells (**Fig. 5-3**).

Overall, these results show that nasal mucosa, trachea and bronchi have the most cells undergoing apoptosis at 3 days post infection, when virus presence and innate immunity expression are peaking. This is compatible with an early inhibition of apoptosis by the virus, to facilitate viral replication, followed by a later promotion of it, as explained in the first chapter. The link between MX1 expression and apoptosis by endoplasmic reticulum stress (ERS), in cells infected with influenza has been suggested in some studies (Numajiri Haruki *et al*., 2011; Pavlovic *et al*., 1990), and might be the explanation of my observation. On the other hand, in the bronchioles and alveoli, the peak of CC3 and MX1 happened at different timepoints. A possible explanation is that, in these tissues, the activation of MX1 at 3dpi, considerably lower in % of tissue stained compared to the nasal mucosa, trachea and bronchi, is not strong enough to induce apoptosis in as many cells as it is induced in these tissues. On the other hand, given that it has been suggested, as explained above, that EIV eventually induces apoptosis, it is possible that the lack of increase of apoptosis levels at 3dpi is because the amount of virus present in bronchioles and alveoli at 3dpi was substantially lower than in other tissues, such as the nasal mucosa and trachea.

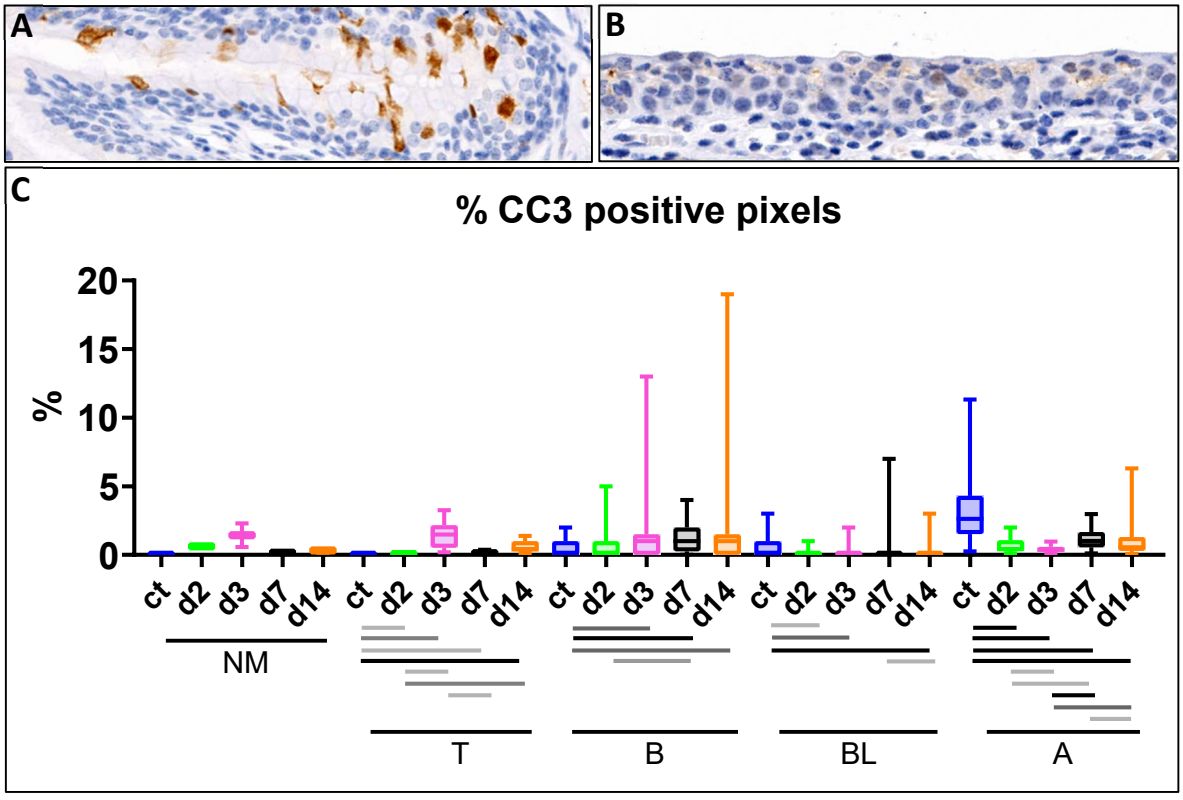

Figure 5-3: Representative images of respiratory tissues from EIV-infected horses stained with an anti-CC3 antibody under an IHC procedure and haematoxylin counterstain. (**A**) Bronchus. Day 3 post infection. (**B**) Bronchus. Day 14 post infection. (**C**) Box plot showing % of MX1 positive pixels in each tissue and timepoint. NM = nasal mucosa, T = trachea, B = bronchi, BL = bronchioles, A = alveoli. 20x. Statistical significances were assessed using a Wilcoxon rank sum test, light grey=$p<0.05$, dark grey=$p<0.01$, black=$p<0.001$. Bar shows the median. Whiskers show the highest and lowest values.

Alternatively, the fact that bronchioles and alveoli have very specialized cell populations, such as club cells and pneumocytes, in which apoptosis might be a less common response to the activation of the innate immunity, might explain these differences in apoptosis values. The ability of these cells to undergo apoptosis has been reported (Barbas-Filho *et al*., 2001; Nakamura *et al*., 2004; Sagiv *et al*., 2018; Sutherland *et al*., 2001), although, to the best of my knowledge, no estimations of how frequent it is compared to other cell types have been published.

Furthermore, the fact that positivity to CC3 is far lower than NP or MX1 ones suggests that not all the cells that are infected by EIV nor show innate immunity activation undergo apoptosis. **Figure 5-4** shows an example.

Some previous studies suggest that influenza induces different programmed cell death pathways, such as necrosis, necroptosis and pyroptosis, in addition to apoptosis (Atkin-Smith *et al*., 2018; Fujikura and Miyazaki, 2018). On the other hand, as explained above, it is believed that apoptosis is initially blocked by the virus, to be triggered by it at later stages. On this regard, according to what I observed in the sections studied, seems clear that, although some cells with features compatible with cell death are positive to apoptosis labelling, not all of them undergo apoptosis.

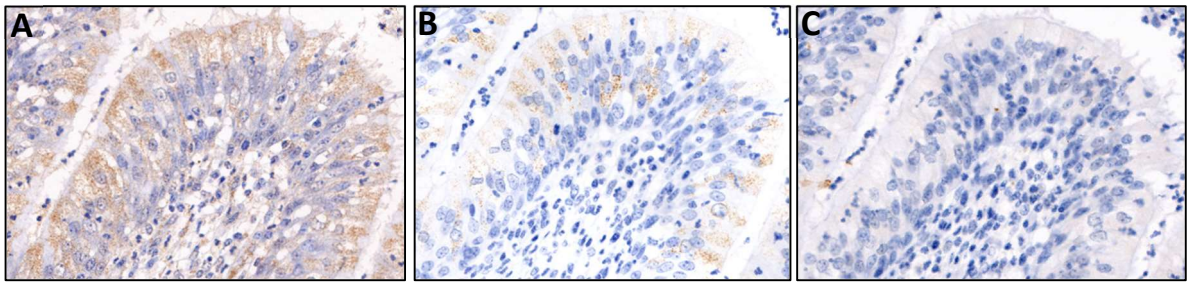

Figure 5-4: Images of a bronchial respiratory epithelium area stained with NP (**A**), MX1 (**B**) and CC3 (**C**) and counterstained with haematoxylin. 15x.

5.2.1.3 Quantification of mitosis

Mitosis was quantified in the respiratory epithelia of the airways and lung with Aperio Imagescope® Positive nuclei count. Each nasal mucosa, trachea and bronchus were counted, together with 25 bronchioles and 5 alveoli squares in each lung slide.

In the nasal mucosa and trachea, the peak of Ki67 positive pixels was at day 3 post infection, with 6 and 4% of the epithelial nuclei undergoing mitosis respectively. In the bronchi and bronchioles, the peak was at 7dpi, although values were lower (2 and 0.8%). Finally, in the

alveoli, the peak was at day 14pi (4%), although it had increased already at 7dpi (2.8%) (**Fig. 5-5**).

In the case of the nasal mucosa and trachea, as explained above, at 3dpi happens the peak of expression of viral protein, innate immunity activation, apoptosis and mitosis. This suggests that at the same time virus levels are the highest, innate immunity is activated at high levels and, maybe as a consequence of it, the levels of cells undergoing apoptosis are the highest. In response to this loss of cells, basal cells in the respiratory epithelia exit the interphase and enter the active phases of cell cycle.

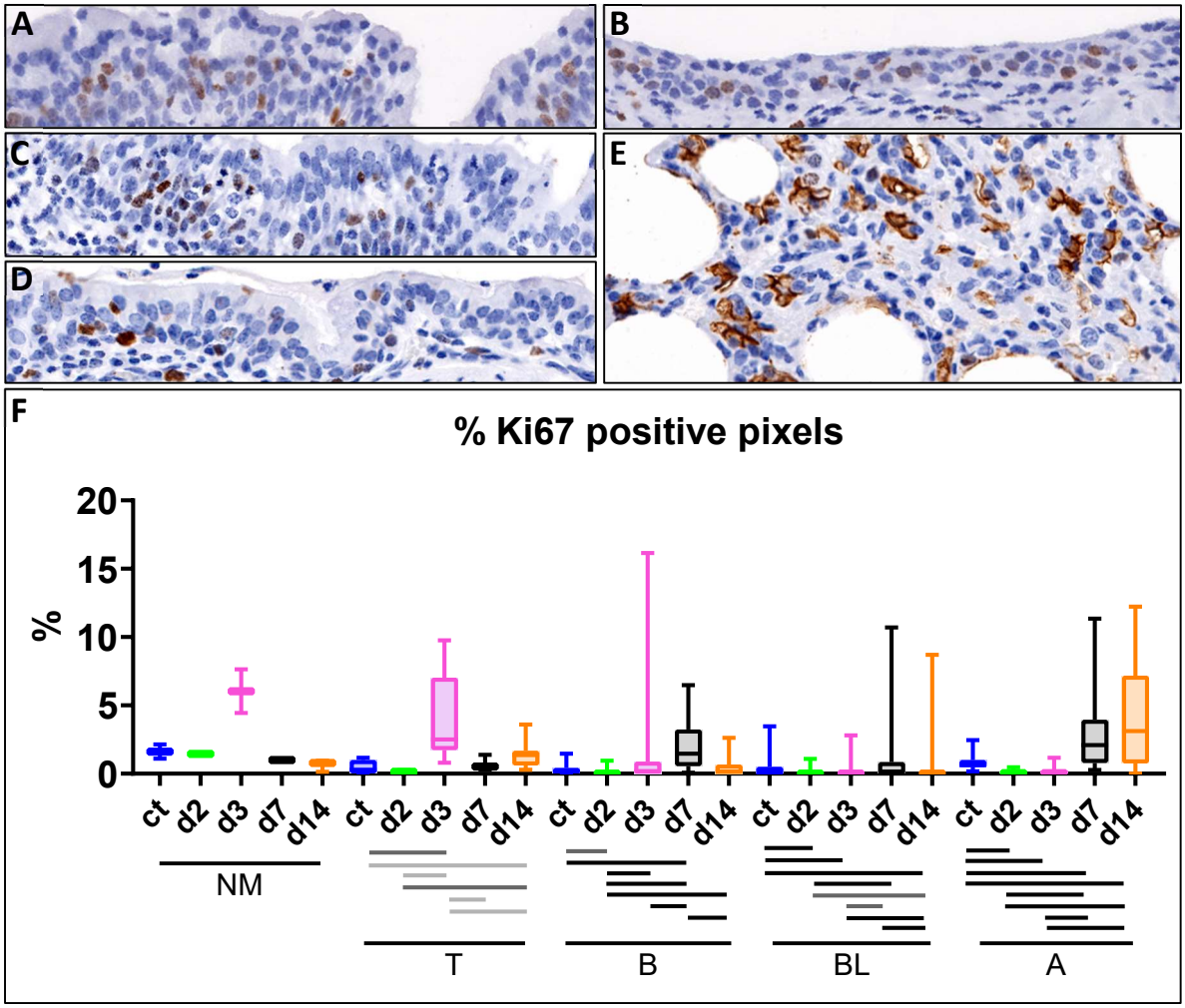

Figure 5-5: Representative images of respiratory tissues from EIV-infected horses stained with an anti-Ki67 antibody under an IHC procedure and haematoxylin counterstain. (**A**) Nasal mucosa. Day 3 post infection (**B**) Trachea. Day 3 post infection. (**C**) Bronchus. Day 7 post infection. (**D**) Bronchioles. Day 7 post infection. (**E**) Alveoli. Day 14 post infection. 15x. (**F**) Box plot showing % of MX1 positive pixels in each tissue and timepoint. NM = nasal mucosa, T = trachea, B = bronchi, BL = bronchioles, A = alveoli. Statistical significances were assessed using a Wilcoxon rank sum test, light grey=$p<0.05$, dark grey=$p<0.01$, black=$p<0.001$. Bar shows the median. Whiskers show the highest and lowest values.

Regarding the bronchi and bronchioles, the peak of cell division was at day 7 post infection, whereas the peak of virus was at 14dpi and the peak of apoptosis and innate immune

expression was at day 3 post infection. These data suggest that at day 7 post infection is when the tissue is more in need to regenerate, which means is when the cell population is lowest. The fact that apoptosis is not peaking at this timepoint indicates that, as explained above, epithelial cells infected by EIV might not be undergoing this programmed cell death pathway, but others, such as necrosis, necroptosis and pyroptosis.
Finally, in the alveoli the peak of cells dividing was at 14dpi, matching with the highest values of viral protein.

As stated before, these data indicate that infected tissues need to regenerate, which means cell populations have decreased in size, suggesting that, during EI, an abnormally high number of cells of the respiratory tract die. However, as seen in the airways, not all these cells would be undergoing apoptosis, given that CC3 values are low at 14dpi. On the other hand, it was also notable the slight change in staining pattern seen in the alveoli, in which positive cells had brown areas not only in their nuclei, but also in the perinuclear region (**Fig. 5-16**).

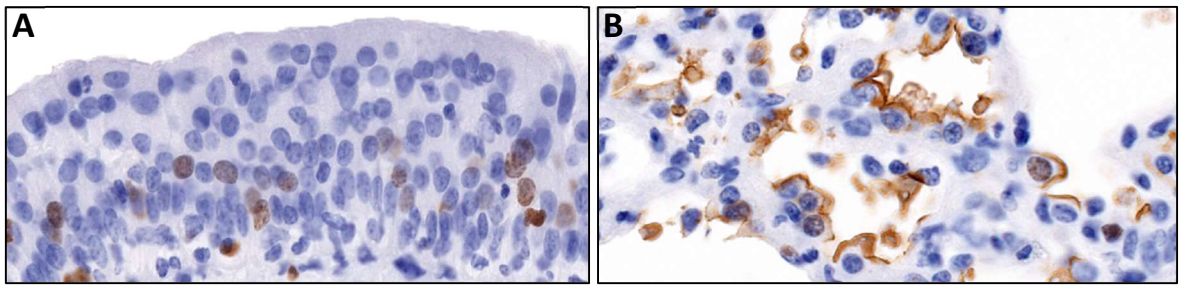

Figure 5-6: Images of tracheal (**A**) and alveolar (**B**) respiratory epithelium from a horse infected with EIV and euthanised at 3dpi stained with Ki67 and counterstained with haematoxylin, showing the difference in the pattern of immunostaining. 30x.

Overall, Ki67 data show that mitosis is a phenomenon that happens in healthy tissues and also in infected tissues. Furthermore, it suggests that, due to the presence of the virus or the host response to it, tissues lose cells, and they try to restore them by triggering a regenerative response, although not in all tissues the peak of virus matches with the peak of cell division. The fact that both apoptosis and mitosis show similarly low values throughout the respiratory tract and along time (**Figures 5-3** and **5-5**) further supports the idea that these are related phenomena, as cell loss is followed by cell proliferation in order to compensate it. As a consequence, it seems that mitosis is delayed in time in the lung and intrapulmonary airways compared to the nasal mucosa and trachea. On the other hand, there is an alternative explanation to the aforementioned observations. By following data shown in (Amat, 2022), which shows that Ki67 response is delayed in time compared to the peak of NP and CC3, it could be hypothesized that the real peak of Ki67 was at timepoints where no horses were

euthanized, for example, at days 4-5 post infection in the nasal mucosa and the trachea and after day 14 post infection in the intrapulmonary airways and the alveoli.

5.2.1.4 Quantification of type II pneumocytes

To study the proliferation of type II pneumocytes in the lung, which are known to be the stem cells for both type I and II alveolar cells (Confalonieri *et al*., 2021), I stained FFPE respiratory tissues from uninfected controls and EIV-infected horses with an anti-Surfactant protein C antibody. Five alveoli squares were quantified in each lung slide.

Surfactant protein C signal increased over time in each timepoint of the infection, from day 2 (4.3% positive nuclei) until day 14 post infection (10.4% positive nuclei), including days 3 (6.5%) and 7 (6.9%). Controls also showed signal (6.4% positive nuclei), which was predictable considering that the lung, as all the other tissues, is constantly renewing their cell populations (**Fig. 5-7**). Type II pneumocyte proliferation was also reported by Muranaka *et al*., in the same horses I studied, at 14dpi (Muranaka *et al*., 2012).

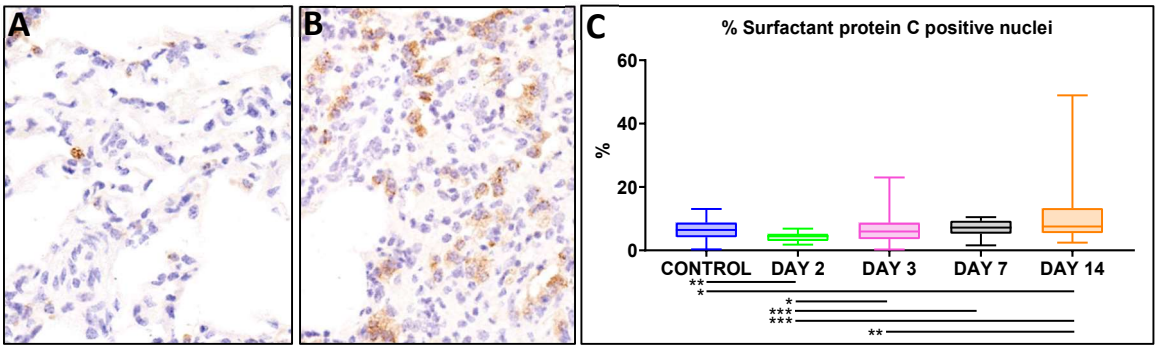

Figure 5-7: Representative images of alveoli from EIV-infected horses stained with an anti-surfactant protein C antibody under an IHC procedure and haematoxylin counterstain. (**A**) Noninfected control. (**B**) Day 14 post infection. (**C**) Box plot showing % of Surfactant protein C positive nuclei. 12x. Statistical significances were assessed using a Wilcoxon rank sum test, *=p<0.05, **=p<0.01, ***=p<0.001. Bar shows the median. Whiskers show the highest and lowest values.

As expected, Surfactant Protein C dynamics mimicked Ki67, since alveolar regeneration is done by Type II pneumocytes. However, as **Figure 5-2** shows, values of Ki67 were at least two times smaller than Surfactant protein C ones, indicating that less than half of the type II pneumocytes would be undergoing mitosis during the different timepoints of the infection.

Furthermore, notably, type II pneumocytes peaked at the timepoint where, as described in Chapter 1, the pathology in the alveoli was the highest and its architecture, most damaged (14dpi). This finding is in accordance with the description, made in some studies (Evans *et al*., 1978; Honda *et al*., 2003), of type II pneumocyte proliferation as a good indicator for alveolar damage.

5.2.1.5 Quantification of T lymphocytes

To study the dynamics of T lymphocytes during equine influenza, I stained respiratory tissues from uninfected controls and EIV-infected horses with an anti-CD3 antibody under an IHC procedure. All nasal mucosa, tracheas and bronchi were quantified, together with 25 bronchioles and 5 alveoli squares in each slide (**Fig. 5-8**).

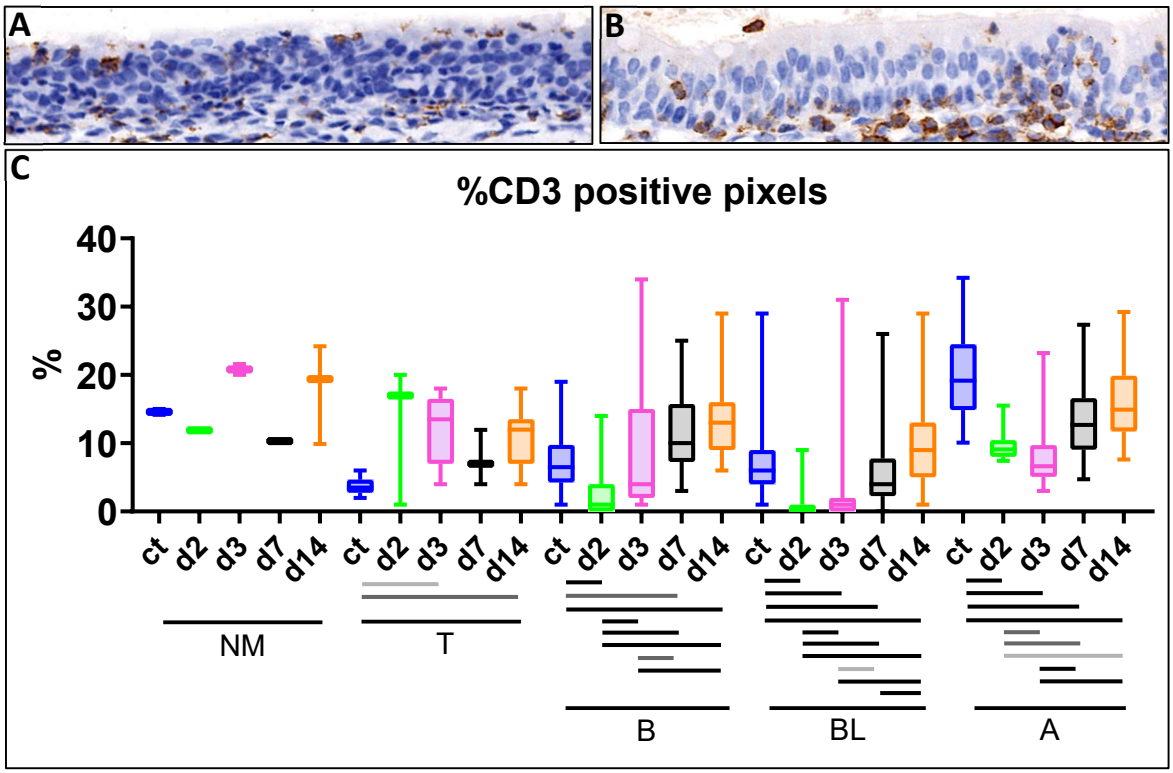

Figure 5-8: Representative images of respiratory tissues from EIV-infected horses stained with an anti-CD3 antibody under an IHQ procedure. (**A**) Bronchus. Noninfected control. (B) Bronchus. Day 14 post infection. 20x. (**C**) Box plot showing % of CD3 positive pixels in each tissue and timepoint. NM = nasal mucosa, T = trachea, B = bronchi, BL = bronchioles, A = alveoli. Statistical significances were assessed using a Wilcoxon rank sum test, light grey=p<0.05, dark grey=p<0.01, black=p<0.001. Bars show the median. Whiskers show the highest and lowest values.

In the nasal mucosa, two peaks of CD3 were seen at 3 and 14dpi, matching with the two timepoints in which viral NP was the highest. On top of that, as explained, at 3dpi the innate immunity also peaked. Similar dynamics were seen in the trachea, although a previous peak, at 2dpi, was revealed. Regarding the bronchi, bronchioles and alveoli, CD3 signal increased over time during the infection, after decreasing between the noninfected controls and 2dpi.

Overall, these results show an increase in T lymphocytes numbers in the lung at late timepoints, whereas in the extrapulmonary airways the trend is less clear. A first thing to consider is the fact that CD3 is a pan T lymphocyte marker, in other words, it stains all T lymphocytes regardless of their characteristics. As a consequence, it is impossible to make

any distinction between CD3+ positive cells in the tissues. T cells are an immune cell type normally divided into two main groups: innate T cells (or innate-like T cells) and adaptive T cells, with each group having different subpopulations within it.

T lymphocytes are known to play a crucial role in the adaptive immune response against influenza infections, especially two of their subpopulations: CD4+ T cells and CD8+ T cells. The former are responsible for expressing antiviral cytokines, such as interleukin 2 (IL-2), TNF (Tumor necrosis factor) and IFNγ (gamma interferon) (Szabo *et al*., 2000) and for activating B cells (Swain *et al*., 2012) and alveolar macrophages (Liu *et al*., 2012), among other functions, whereas the latter differentiate into cytotoxic T lymphocytes, which kill cells that are infected and restrict viral replication by producing cytokines and effector molecules (Chen *et al*., 2018). The function that T lymphocytes develop within the innate immune response is less clear, although it is known that they are functionally diverse (Wencker *et al*., 2014) and the principal contributing factor to the total IFNγ response (Kastenmüller *et al*., 2012).

Further research is needed to determine, first, the dynamics of each T cell subpopulation/s during EIV infection, being a good way to begin to differentiate between CD4+ and CD8+ T cells, two main subpopulations of the adaptive immune response, and second the relationship between T lymphocytes, innate immunity and virus levels.

5.2.1.6 Quantification of B lymphocytes

To know the dynamics of B lymphocytes in the respiratory tract of horses infected with equine influenza, I stained with an anti-PAX5 antibody FFPE respiratory tissues from uninfected and experimentally infected individuals. All nasal mucosas, tracheas and bronchi were quantified, together with 25 bronchioles and 5 alveoli squares in each slide.

PAX5 showed generally very low values, with most percentages of positive nuclei below 1. As **Figure 5-9** shows, MALT patches in the submucosa had abundant B lymphocytes, and the epithelial areas above these lymphoid tissues had very scarce numbers of this cell type. In the nasal mucosa, the peak of B lymphocytes was at 2dpi, with 0.14% of positive nuclei to PAX5. Positivity decreased at days 3 (0.03%) and 7 (0.02%) post infection, whereas at 14dpi it increased slightly (0.05%).

Regarding the trachea, % of positive nuclei to PAX5 increased from controls (0.02%) to

days 2 (0.04%) and 3 (0.06%) post infection, whereas decreased at 7dpi (0.03%). The peak of signal was at 14dpi (0.07%).

In the bronchi, the peak of B lymphocytes was at day 14 post infection (0.064%), with a subpeak at 3dpi (0.057%) and a small decrease at 7dpi (0.047%). Positivity was 0.032% at 2dpi and 0.005% in the controls. Bronchioles showed their PAX5 signal peak at day 7 post infection (0.048%) and a decrease at 14dpi (0.014%), after showing no B lymphocytes at 2dpi (0.0%) and very little at 3dpi (0.0029%). Finally, in the alveoli, PAX5 positivity was notably higher than in the other respiratory organs. The signal was 0.26% in the controls and decreased at 2dpi (0.23%) and 3dpi (0.16%). At 7dpi it increased to 0.25% and at 14dpi was the peak of positivity, with 0.35% of cell nuclei positive to PAX5 (**Fig. 5-9**).

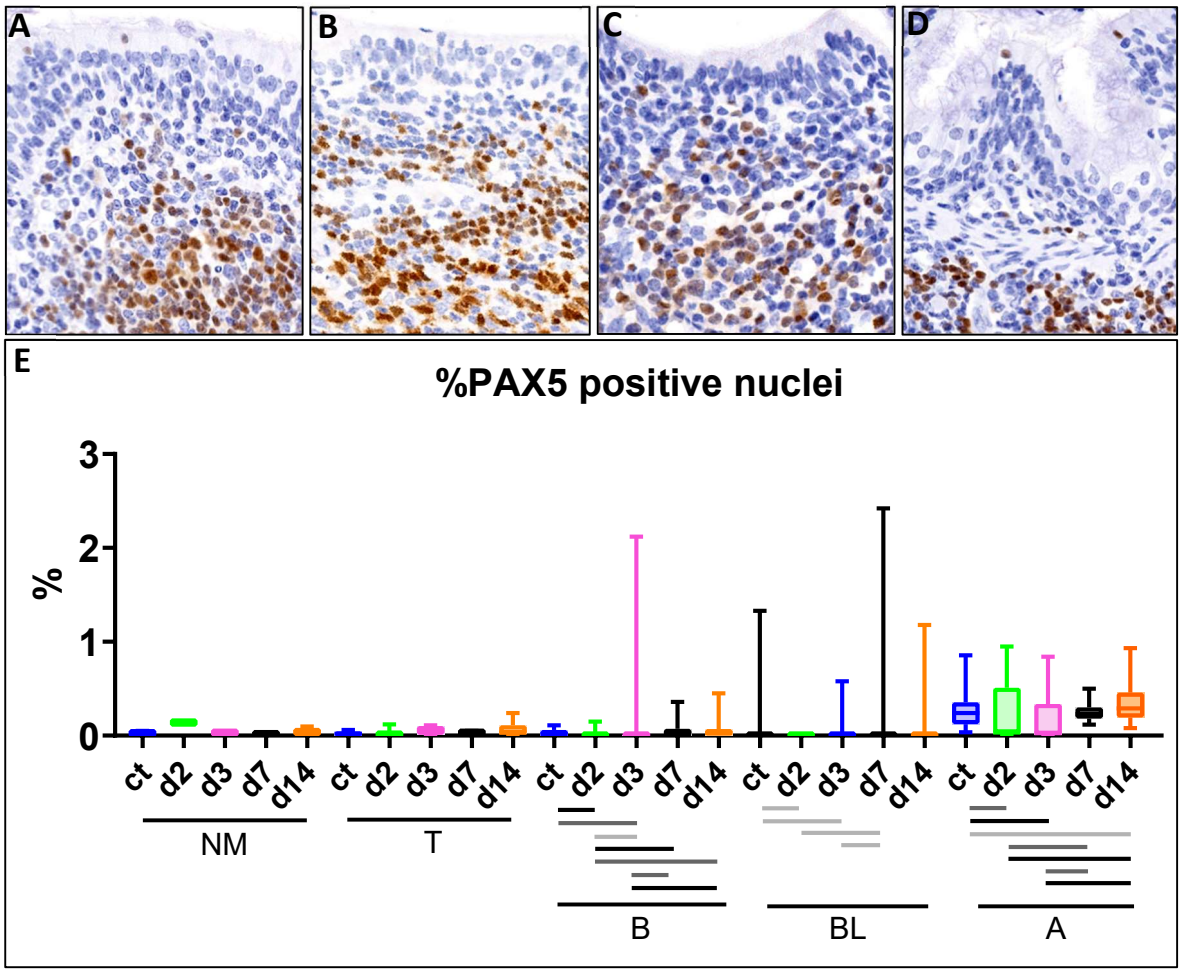

Figure 5-9: Representative images of respiratory tissues from EIV-infected horses stained with an anti-PAX5 antibody under an IHC procedure and haematoxylin counterstain. (**A**) Bronchus. Day 2 post infection. (**B**) Bronchus. Day 3 post infection. (**C**) Bronchus. Day 7 post infection. (**D**) Bronchus. Day 14 post infection. 18x. (**E**) Box plot showing % of CD3 positive pixels in each tissue and timepoint. NM = nasal mucosa, T = trachea, B = bronchi, BL = bronchioles, A = alveoli. Statistical significances were assessed using a Wilcoxon rank sum test, light grey=p<0.05, dark grey=p<0.01, black=p<0.001. Bar shows the median. Whiskers show the highest and lowest values.

Overall, PAX 5 results showed that B lymphocytes proliferate in the lung at late timepoints

(7 and especially 14dpi), similarly to what was seen with other markers, such as CD3, CC3, Ki67 and Surfactant protein C, and also to what has been previously reported (Angeletti *et al*., 2017; Lam and Baumgarth, 2019). On the other hand, especially in the nasal mucosa, but also in the trachea, higher values of PAX5 positive nuclei could be seen at the beginning of the infection, when other stainings also showed their peak.

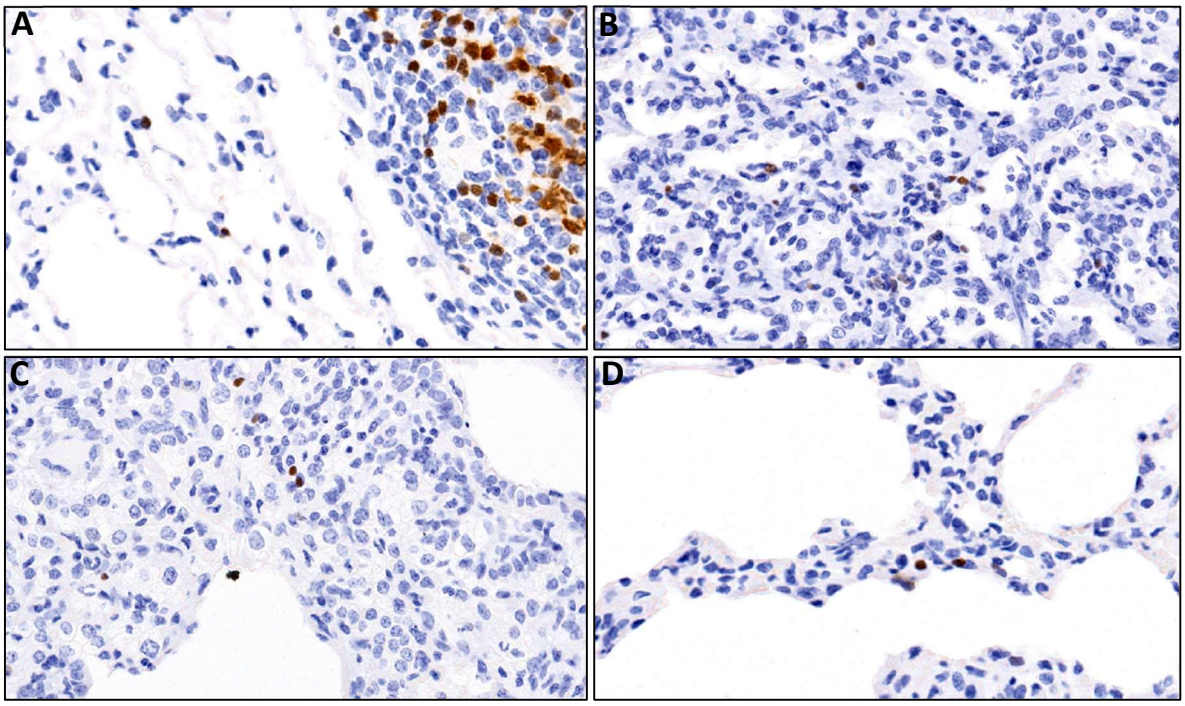

Figure 5-24: Images of alveoli from a horse infected with EIV and euthanised at 3dpi stained with an anti-PAX5 antibody under an IHC procedure and haematoxylin counterstain showing B lymphocytes stained in brown. (**A**) Alveoli and BALT. (**B**), (**C**) and (**D**) Alveoli. 18x.

These data also showed that the presence of B lymphocytes in the respiratory tract of EIV-infected horses was very limited. As explained, more PAX5 positive nuclei could be seen in the alveoli, although the highest mean % of positive nuclei in this tissue was only 0.35. Furthermore, as shown in **Figure 5**-9, the very infrequent B lymphocytes found in the airways were visualized, in most cases, near MALT patches, suggesting that they might have infiltrated the respiratory epithelia from these lymphoid aggregates.

In the alveoli, as **Figure 5-10** shows, some B lymphocytes were close to BALT, but some others were not, suggesting that they might had come from the blood vessels.

No data or estimation of the proportion of B and T cells within the lymphoid population in the lung of the horse was found, however, a paper established 82-18 as the ratio of % of T and B lymphocytes in peripheral blood of young horses (McFarlane, Sellon and Gibbs, 2001). Furthermore, MALT patches in the nasal mucosa, trachea and lung slides of the horses I studied showed, in most cases, a majority of T lymphocytes (**Fig. 5-11**).

Although these observations are not necessarily comparable to the data I obtained with CD3 and PAX5 stainings, they give more insight on the idea that T lymphocytes are generally more abundant than B lymphocytes.

As it happened with CD3 and T lymphocytes, PAX5 stains all B lymphocytes, regardless of their characteristics. No distinction between B cell types is possible with this marker, thus.

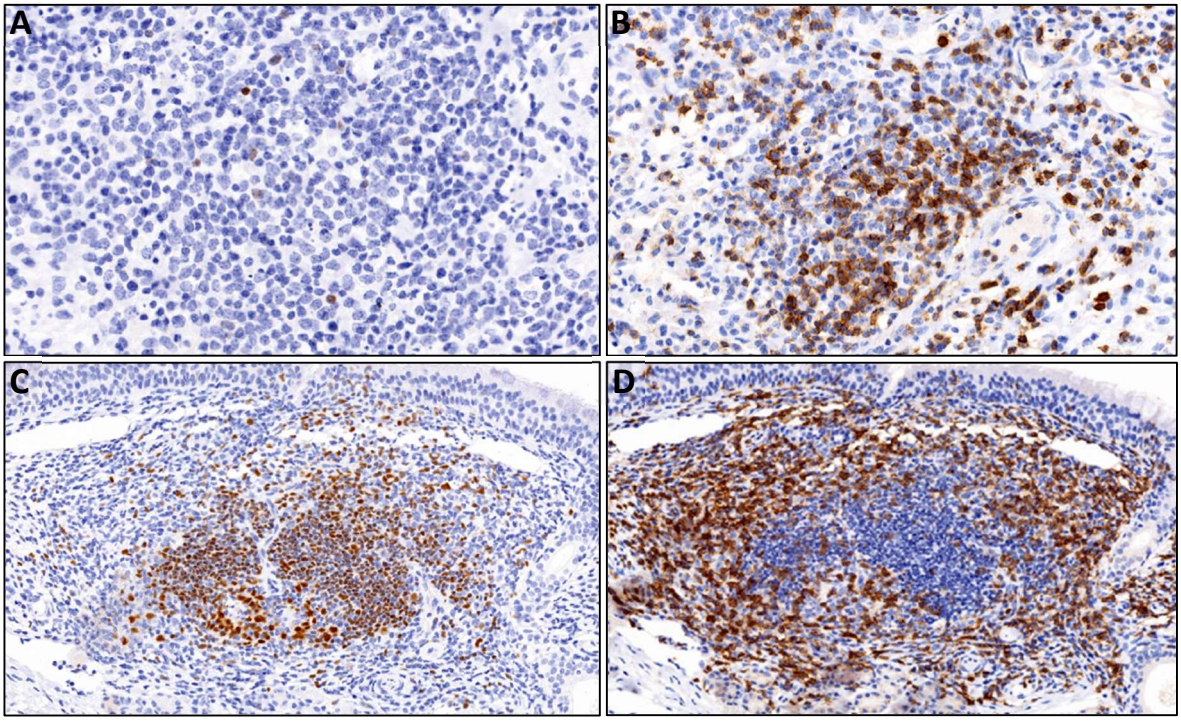

Figure 5-11: Images of MALT from EIV-infected horses at different timepoints (**A** and **C**, 3dpi, **B** and **D**, 14dpi) stained with anti-PAX5 (**A**, 15x and **C**, 7x) and anti CD3 antibody (**B**, 15x and **D**, 7x) and haematoxylin counterstain.

However, as stated with T lymphocytes, in the first timepoints is feasible to think that PAX5-positive cells would belong to the innate immune response. These would be B-1 cells, a B lymphocyte subset frequently found in peripheral sites and known to secrete antibodies in the early stage of some infections, including influenza (Choi and Baumgarth, 2008). On the other hand, at late timepoints (7 and 14dpi), PAX5 positive cells would be those belonging to the adaptive immunity.

An important thing to consider is the fact that PAX5 is a marker for B lymphocytes and not for plasma cells (Krenacs *et al*., 1998), which are one of the descendants of that cell type. Plasma cells are antibody-producing immune cells and were identified in the respiratory tissues of EIV-infected horses, as **Figure 5-12** shows, according to their main features, defined by the Hungarian pathologist Tamas Marschalko: blocked chromatin, ovoid/spherical shape, eccentrical nucleus and perinuclear pallor (Bortnick and Murre,

2016). Although the abundancy of plasma cells was not estimated, research on their presence in response to EIV would be interesting, for example, by using cluster of differentiation 38 (CD38) or 138 (CD138) antibodies, which have proved to be effective labelling this cell type (Bataille *et al*., 2006).

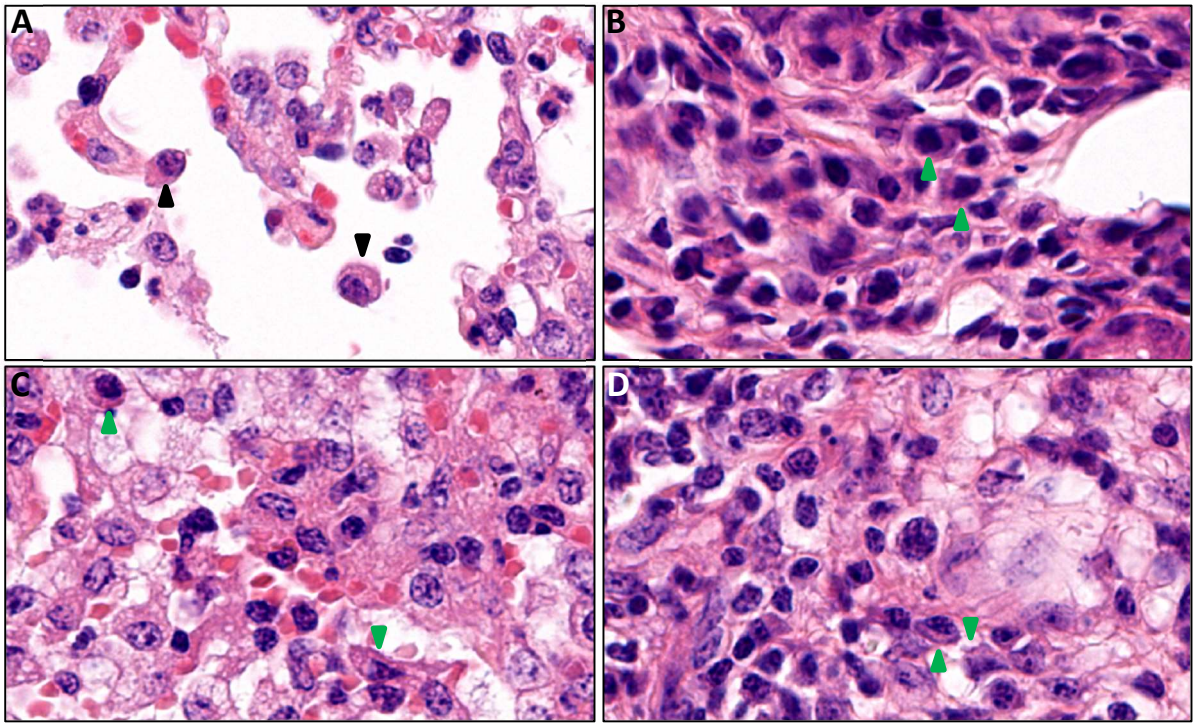

Figure 5-12: Images of respiratory tissues from EIV-infected horses at different timepoints stained with H&E showing cells with features compatible with plasma cells. (**A**) Alveoli. 14 days post infection. (**B**) Nasal mucosa submucosa. 7 days post infection. (**C**) Alveoli. 7 days post infection. (**D**) Bronchial submucosa. 14 days post infection. 30x. Arrowheads show cells identified as plasma cells.

5.3 Discussion

Results shown in this chapter highlight several conclusions, that have to be taken carefully, considering the horse sample size and the limited amount of timepoints in which horses were euthanized. Innate immunity activation was widespread and at its maximum at day 3pi, as illustrated by the quantification of MX1, and declined after it, suggesting that it spreads from the upper respiratory tract, where the peak of virus spread is at this timepoint, to the lung, in which no relation between its levels and viral levels were seen. Furthermore, it is clear that the levels of expression of MX1 at 3dpi were triggered by EIV colonization of the respiratory tract and, furthermore, likely restricted EIV spread, given the fact that, in the next timepoint, 7dpi, viral values had decreased in all tissues except the alveoli. The fact that Muranaka *et al*. and Yamanaka *et al*. showed in their respective works that the peak of viral shedding was at 2dpi (horse 5) or 3dpi (horses 2, 3, 4, 6 and 7), is consistent with an IFN response, triggered by MX1, being activated at 3dpi and successfully reducing the viral spread. The MX1 positivity was the lowest by far in the alveoli, which suggested that the amount of MX1

expression might be relevant in the restriction of the viral spread. This finding is consistent with the literature. As an example, Verhelst *et al.* found that the inhibition of influenza virus (measured as inhibition of the interaction between NP and PB2) by MX1 was dependent on its dose (Verhelst *et al*., 2012). No data on signal in IHC staining was found.

As said, according to my data, MX1 activation would be initially triggered by EIV and its expression would decrease as viral levels decrease, which at day 14 post infection were undetectable. Furthermore, as a well-known mechanism of the antiviral response, the fact that there was a bacterial infection at late timepoints did not translate into an increase MX1 levels in the tissues. As explained, the effect that MX1 might have on apoptosis is not clear, although apoptosis by ERS driven by MX1 has been suggested in several publications (Numajiri Haruki *et al*., 2011; Pavlovic *et al*., 1990). Consistent with this, in the horses I studied, tissues where the MX1 signal was the highest at 3dpi was also where CC3 levels increased the most at this day. Nonetheless, apoptosis is known to be a complex process depending on many different signaling stimuli and able to being activated by different pathways; therefore, these might be different depending on the tissue and/or the timepoint and that is why the dynamics of MX1 and CC3 are not always parallel. Studies on within-host evolution of EIV have shown a biphasic curve of viral shedding (Murcia *et al*., 2013, 2010) that could be explained by an IFN response similar to the one reported in this thesis by quantification of MX1 positive signal quantification. Regarding CC3, its low values, together with observations such as **Figure 5-4,** where areas with features compatible with cell death, such as vacuolization of cells and presence of anuclear eosinophilic fragments (Shubin *et al*., 2016), are shown to be negative to apoptosis, suggest that apoptosis is not the only cell death pathway that EIV-infected cells follow. As discussed earlier in this chapter, investigation on the abundance of cells positive to markers for other programmed cell death pathways is needed to shed light on this regard.

Furthermore, as shown in **Figure 5-4**, not all the infected cells or cells expressing MX1 undergo apoptosis. As explained by Wang *et al*., apoptosis might be a cell death pathway not beneficial for the host, in terms of viral spread (Wang *et al*., 2014), and might be managed by the virus, promoting it in late stages of the infection but restricting it at the beginning, to allow viral spread (seen earlier in this chapter). On the other hand, as they are unlikely to be due to the viral action, the increased values of apoptosis seen in the alveoli at 7 and 14dpi are presumed to be consequence of the action of opportunistic bacteria and/or the inflammatory response secondary to these. On this regard, although the role of apoptosis in secondary bacterial infections is controversial (Häcker *et al*., 2006). *Streptococcus equi subs*. *zooepidemicus* has been found to be able to promote a self-beneficial macrophage

apoptosis. Xie *et al*. infected macrophages with wild-type and mutant *Streptococcus equi subs*. *zooepidemicus* and found increased levels of apoptosis and higher bacterial load in the population of macrophages infected with the mutant bacteria (Xie *et al*., 2024). It is possible, therefore, that the increase of apoptosis positive signal in the alveoli at late timepoints is due to the action of *Streptococcus* on the macrophagic population, which, according to Muranaka *et al*., had mildly increased numbers at 7dpi and 14dpi. On the other hand, apoptosis of tissue cells and inflammatory cells at the inflammation site is a well described phenomenon, although, as said, the literature is controversial on whether it is beneficial or detrimental for the host. However, apoptosis of host cells mediated by inflammatory cells is well known. As reviewed by Haanen and Vermes (Haanen and Vermes, 1995), secretion of cytokines such as IL-2, IL-4 and TNF-α by macrophages, monocytes, neutrophils and T lymphocytes promotes apoptosis. Although further analysis would be necessary to determine whether these cytokines were secreted in the lungs of EI-infected horses, this mechanism might account, at least partially, for the increased apoptotic levels in the late infection, given that, as shown, the inflammation is prominent at late timepoints.

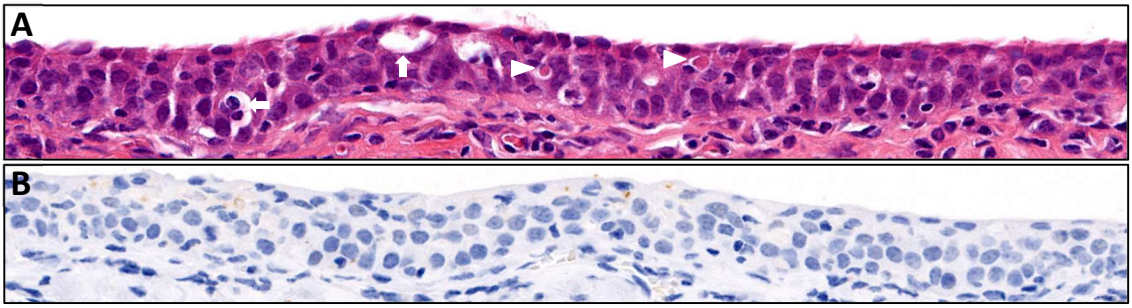

Figure 5-13: Images of tracheas of EIV-infected horses at 3dpi stained with H&E (**A**) and CC3 + haematoxylin counterstain (**B**). (**A**) Areas with features compatible with cell death (vacuolisation, presence of cytoplasmic fragments) are shown by arrows and arrowheads respectively. (**B**) Serial cut of **A**, showing that some areas where features compatible with cell death were highlighted are not positive to CC3. 15x.

With Ki67 I showed cell proliferation and tissue regeneration, and it is fair to understand that the timepoint when the biggest loss of cells has happened has to be followed by a period where the percentage of Ki67 positive nuclei is increased, to compensate this loss. In the nasal mucosa, trachea and alveoli, the peak of apoptosis, mitosis and virus matched, whereas in the bronchi and bronchioles did not. As speculated above, might be that the real mitosis peak is delayed in time compared to the virus (as shown by Amat *et al*.) and I have not detected it, given the intermediate points in which no horses were euthanized, or another option is the opposite, in other words, that the peak of virus (and of Ki67) in the bronchi and bronchioles was not one of the timepoints in which horses were euthanized. Altogether, is important to note that, as shown in chapter 3, at 14dpi there is a clear epithelial hyperplasia of the respiratory epithelia, suggesting that, earlier or later, at some point a prominent

epithelial regeneration occurs. Concerning Surfactant Protein C, it showed, as expected, similar dynamics to Ki67 in the lung. This fact, together with the other antibodies data and the lesions observed and described in the first chapter establish day 14 post infection as the timepoint where the lung disruption is the biggest. As explained in Chapter 1, proliferation of type II pneumocytes is a well described chronic lesion in different species infected with influenza A viruses, in response to loss of both type I and type II pneumocytes. Work by van der Brand *et al*. on ferrets (van der Brand *et al*., 2010), Tangwangvivat *et al.* on dogs (Tangwangvivat *et al*., 2022), Baskin *et al*. in cynomolgus macaques (Baskin *et al*., 2009), van Riel *et al.* in cats (van Riel *et al*., 2010) and Brockmeier *et al.* and Grau-Roma and Segalés in pigs (Brockmeier *et al*., 2002, Grau-Roma and Segalés, 2007) are good examples of this. However, in the horses I studied, given that viral shedding was detected until day 7pi, the loss of alveolar epithelial cells and consequential type II pneumocyte proliferation is presumed to be secondary to the action of opportunistic bacteria. Type II pneumocyte proliferation secondary to bacterial pneumonia in EIV-infected horses was described by Begg *et al*. (Begg *et al*., 2011).

Finally, markers for inflammatory cells provided an indication of the role of T and B lymphocytes in the respiratory tract of EIV-infected horses. Overall, it showed a vague increase in T lymphocytes' abundancy along the infection course, whereas it proved B lymphocytes' numbers were extremely reduced. However, given the broadness of spectrum that the antibodies I used had, it was not possible to make statements regarding cell populations and subsets. As explained, T cells already showed high levels in the first timepoints, and this might be the explanation why along the infection they were always more numerous. As a consequence, T cell immunity would start earlier during the infection, whereas the B cell immunity would be delayed, considering that with PAX5 only B cells, and not plasma cells, are stained. On the other hand, considering that adaptive immunity response takes effect between 4 and 7 days after infection (Janeway *et al*., 2001), and although it is impossible to prove, seems fair to say that, in the early infection, CD3 positive cells will mainly be innate-like T cells. Increases of CD3 positivity at days 7 and 14 post infection would be, thus, due to the infiltration of T lymphocytes belonging to the adaptive immunity.

As explained, further research on T and B cell subpopulations would shed light on all the questions that, after my research, remain open. Furthermore, whereas data showed that a prominent innate immune response at 3dpi is followed by an increase in numbers of T

lymphocytes and, in later stages and in a much reduced scale, by B lymphocytes, other immune cell populations known to have an important role against influenza infections, such as neutrophils (George *et al*., 2021) and alveolar macrophages (Somerville *et al*., 2020), both increased at late timepoints (7dpi and 14dpi) according to Muranaka *et al*. (Muranaka *et al*., 2012).

In summary, my results showed the existence of a strong and fast innate immunity activation at 3dpi, which resulted in a reduction of viral levels in the airways, where increased numbers of cells dying and dividing were seen. Alveoli showed reduced activation of the innate immunity, and a delay in the increase of apoptosis and mitosis of type II pneumocytes. As explained, although a trend of increasing numbers of T and B cells throughout the infection was seen, further research is needed to gain understanding on lymphocytes dynamics during equine influenza.

Chapter 6: Discussion

The aim of this thesis was to shed light on the pathogenesis of equine influenza in its natural host to better understand the mechanisms triggered by EIV and the host response at respiratory tissue level. Very few studies describing histological lesions in EI-infected horses have been performed, and, as a consequence, the knowledge on this field is limited. In this thesis, by expanding the broadness of the analysis performed by Muranaka *et al*. (Muranaka *et al*., 2012), I characterized and quantified the viral spread throughout the respiratory tissues and I also illustrated how the microscopic architecture of the equine respiratory tract changes along the infection. Finally, I expanded the experiments carried by Amat *et al*. (Amat *et al*., 2021), with immunomarkers on EI-infected tracheal explants, by using the same antibodies, and additional ones, on respiratory tissues from EI-infected horses, to better understand cellular and inflammatory mechanisms. Working on animal samples already generated and used in previous studies aligned this work with the 3Rs principles of ethical use of animals in scientific research, which were first described by Russell and Burch in 1959 (Russell and Burch, 1959): Replacement, which refers to avoiding or replacing the use of animals, Reduction, in the sense of using a smaller number of animals, and Refinement, meaning the improvement of experimental procedures in order to reduce pain and distress on animals used in research. On this regard, materials generated in previous studies done on different species, and even with different viruses, could be reused in the same way it was done in this thesis, allowing new insights on virus pathogenesis without doing any new experimental infections on animals.

As explained in previous chapters, all the knowledge generated in my PhD project and displayed in this thesis was based on data that had two main limitations: small sample size and limited timepoints. Regarding the sample size, two of the four timepoints were based on a single horse, whereas the other two had either two or three individuals. A n=3 in each timepoint would have been the minimum number of animals to run basic statistical analysis and obtain robust conclusions. The lack of intermediate timepoints impeded a comprehensive characterization of the histopathological changes that occur during the entire infection period. Although in an ideal situation each day of infection would be a timepoint, a sensible compromise between scientific rigor and 3Rs principles would have been to add an intermediate timepoint between days 2 and 7pi (e.g., day 5pi) and two more between days 7 and 14pi (e.g., days 9/10 and 11/12pi). Obviously, working with 18 horses (six timepoints with three horses in each) instead of seven would have drastically increased the cost of the experiment and the need for biocontainment stalls.

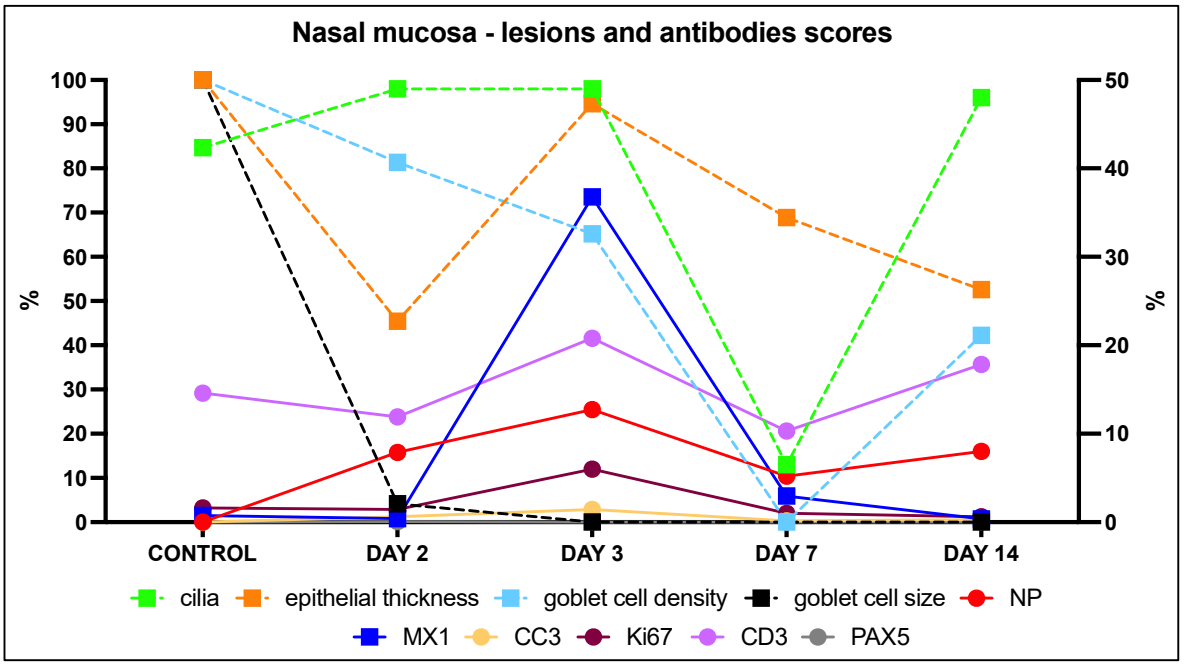

Figure 6-1: Line chart showing the percentage of degree of histopathological changes (discontinuous lines) and of antibody expression (continuous lines) in the nasal mucosa. Each histopathological change quantified in chapter 3 was given a score from 0 to 100, according to its proximity to the value shown by the noninfected controls. A second Y axis (right) was applied for better visualization of small values. Squares show values linked to left axis and circles show values linked to right axis.

Horses were infected by nebulization and after two days virus was detected along the epithelia of respiratory tract, their site of replication, showing a focal to multifocal pattern (**Fig. 4-10**). At this point, the only changes observed were an increase in airway blockage, produced by epithelial and inflammatory cells detached (**Fig. 3-14**), and a reduction of the gas exchange surface in the alveoli, mainly due to the increased amount of red blood cells and extracellular fluid in the interstitial space of the lung (**Fig. 3-15**). As explained, these changes were consistent with those seen in other species at early timepoints.

At day 3 post infection, the number of infected cells increased substantially, and NP-positive signal was seen in most respiratory epithelial cells of the nasal mucosa, trachea and lung, showing a diffuse pattern of staining (**Figures 4-10** and **4-11**). Simultaneously, the vast majority of cells, either positive or not to viral staining, of the epithelia of the respiratory tract, showed strong positive staining to MX1, a marker for innate immunity activation, although in the alveoli and bronchioles this signal was notably lower (**Figure 5-2**). Alveolar epithelial cells are known to be able to mount a significant innate immune response in influenza-infected tissues (Wang *et al*., 2011), although according to lung sections stained with MX1, in the alveoli this protein's expression was less intense than in the airways, as **Figure 5-2** shows, despite the fact that most cells expressed it. MX1 revealed itself as the

key marker along the infection, since the peak at 3dpi and posterior decrease of the innate immunity expression likely reduced viral spread and therefore attenuated the lesions. As explained in Chapter 5, this is consistent with the literature, which describes MX1 as an important antiviral protein. Throughout the airways the normal histological architecture was notably disrupted, with a partial loss of cilia and goblet cells in the respiratory epithelia (**Figures 6-1**, **6-2** and **6-3).** Although these continued to be low, increased values of apoptosis were detected, meaning that, due to the virus, or to stop its spread, as discussed in chapter 5, cells were undergoing programmed death. The potential contribution that MX1 had to the increased apoptosis levels was also discussed in Chapter 5. As explained there, some bibliography has attributed MXA (the name for human MX1) the capability to accelerate apoptosis in influenza-infected cells (Numajiri *et al*., 2006; Numajiri Haruki *et al*., 2011). This theory would explain why in those tissues where the MX1 activation is less intense (bronchioles and alveoli), apoptosis levels did not increase compared to 2dpi. Generalised low values of apoptosis were also seen in other studies working with EI-infected tissues, such as (Amat *et al*., 2021), with CC3 positive signal peaking at day 2pi. As explained in Chapter 5, these findings suggest that apoptosis might not be the main/only cell death pathway that EIV-infected cells undergo. On this regard, in their review on programmed cell death in the pathogenesis of influenza, Fujikura and Miyazaki, mentioned apoptosis, necroptosis and pyroptosis as cell death pathways present in tissues infected with influenza virus (Fujikura and Miyazaki, 2018). Further determination of the role of each of these programmed cell death pathways is necessary to better understand the pathogenesis of influenza viruses.

At day 3 post infection, mitotic cells (Ki67 positive) were also increased, in order to compensate the cell loss (**Figure 5-5**). On the other hand, the presence of T lymphocytes infiltrating the epithelia also increased in the airways, except in the trachea, whereas in the alveoli the number of T cells reduced (**Figure 5-8**). Although the effect of type I interferon on T cells' dynamics can be inhibitory depending on the timing and the context of presence of other signaling factors, in other cases is reported as stimulatory of their populations (Crouse *et al*., 2015). Again, the fact that the tissue with the lowest MX1 expression, the alveoli, was the only that from 2dpi to 3dpi did not increase their T cell presence, would support this statement.

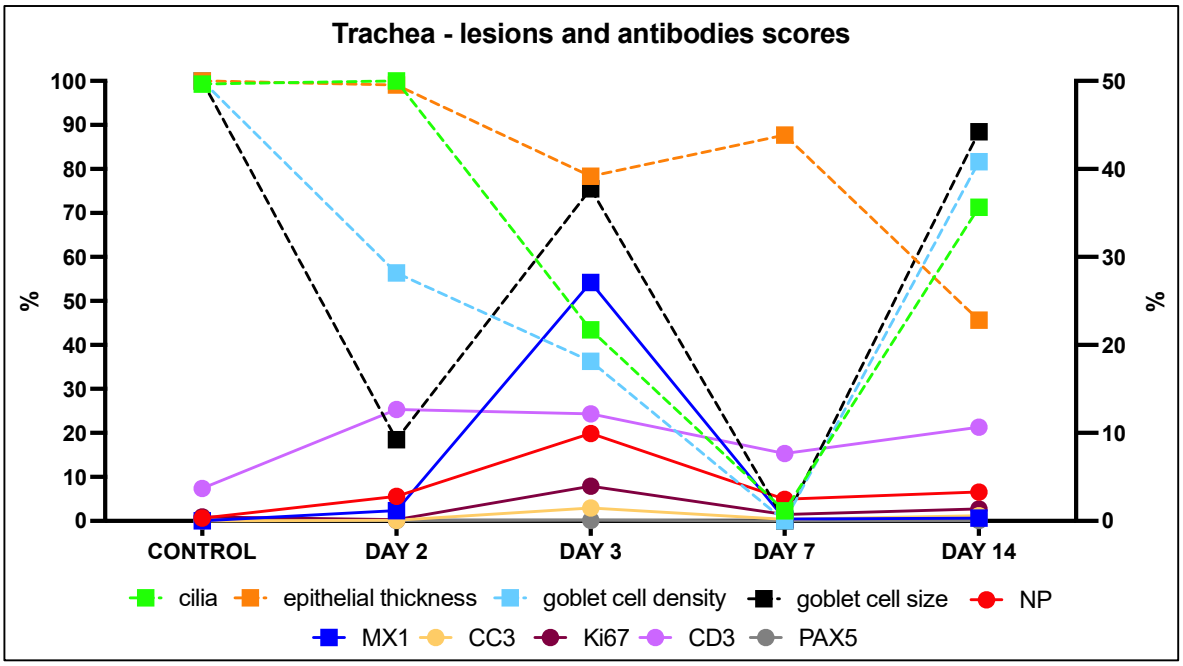

Figure 6-2: Line chart showing the percentage of degree of histopathological changes (discontinuous lines) and of antibody expression (continuous lines) in the trachea. Each histopathological change quantified in chapter 3 was given a score from 0 to 100, according to its proximity to the value shown by the noninfected controls. A second Y axis (right) was applied for better visualization of small values. Squares show values linked to left axis and circles show values linked to right axis.

Although it was not a consistent finding across tissues and timepoints, a variably severe goblet cell hyperplasia (measured as increase in goblet cell size in PAS-stained tissues) was seen in the first timepoints in the nasal mucosa and trachea. This is believed to be a compensatory response to the loss of goblet cells in the respiratory epithelium, and, to the best of my knowledge, it is a novel finding in equine influenza. As said in Chapter 3, there is literature describing goblet cell hyperplasia in response to influenza infection in mice (Li and Tang., 2021).

The histological architecture of the alveoli at 3dpi continued to be mildly disrupted, whereas the viral levels increased slightly, although not as much as the airways ones. The markers of innate immunity, apoptosis, mitosis, lymphocytes and type II pneumocytes did not show any relevant changes. Only MX1 increased to around 25% of positive pixels (**Figure 5-2**). As said, the fact that the activation of this interferon-stimulated gene was small compared to the other tissues might explain the lack of increase of other markers, such as apoptosis and T lymphocytes. A hypothesis for this minimized activation of the innate immunity is the need to prevent any disruptions that a prominent activation of the innate immunity would trigger, in the lung, where, given its function, any minimal alteration would have serious consequences.

According to the data shown in chapter 3, where I examined lesions in respiratory tissues from EI-infected horses, day 7 post infection was, out of the four timepoints of the experiment, the day in which the lesions in the airways were the most severe. Cilia and goblet cells were barely seen in the respiratory epithelia, which displayed frequent dead cells and others that had undergone squamous metaplasia, in response to the removal of the ciliated and goblet cells from the surface of the epithelia. All these lesions are believed to be direct consequence of the action of the virus, as they are very similar to those seen in other species experimentally infected with influenza virus and no reported secondary bacterial infection, as explained in Chapter 3, even if the virus, in the horse euthanized at 7dpi, was detectable only until 6dpi. On the other hand, in the intrapulmonary airways, epithelial detached cells and neutrophils were frequently observed in the lumina, narrowing the airflow space (**Figures 3-14, 6-3** and **6-4**). Given the neutrophilic component of the inflammation and blockage of the airways and the reported positive detection of bacterial antigen in the lungs at 7dpi, secondary opportunistic bacteria are thought to account for these changes. Overall, the changes seen in the horse euthanized at 7dpi are consistent with the literature on the pathology observed in horses infected with EIV (Patterson-Kane *et al*., 2008; Begg *et al*., 2011). As a summary, **Figures 6-1**, **6-2**, **6-3** and **6-4** show how values representing the degree of histological changes decrease notably at this timepoint. Day 7 also showed a drastic decrease in innate immune expression, which was simultaneous to the decrease in virus levels, except in the alveoli. This suggests that the innate immunity successfully attenuates EIV spread. As said, consistent with this, in Muranaka *et al*.'s and Yamanaka *et al*.'s works, the peak of virus shedding was seen at 2 or 3dpi, depending on the horse, followed by a decline until fully disappearing at days 6 or 7pi. In other species, such as mice, guinea pig, pig and ferret, a notable decline of viral antigens in the airways at 3dpi was described (Guarner and Falcón-Escobedo, 2009). As explained, the lack of intermediate timepoints does not allow a full understanding of viral antigens' dynamics between 3dpi and 7dpi. Dismissing this detail, the fact that the biggest lesions in the airways are observed when viral levels are low would suggest that EIV induces the first pathological changes, but its presence is not essential to develop all the histologic lesions observed in later timepoints. In fact, as reviewed in (Mina and Klugman, 2014), many IAV-mediated mechanisms, such as reduced mucociliary clearance, aberrant immune defenses and excess immunopathological and tissue damage, even a regular activation of antiviral mechanisms (van der Sluijs *et al*., 2010), are described as facilitators for secondary bacterial colonization of the lung and development of bacterial pneumonia. On this regard, the robust activation of the innate antiviral immunity at 3dpi might facilitate the proliferation of the bacteria in the lung. This

is consistent with the observation of lesions compatible with bacterial pneumonia, such as hepatization of the lung parenchyma, necrosis of the respiratory epithelia, neutrophilic infiltration and exudation in the airways and the alveoli and alveolar oedema and haemorrhage, in the lung from 7dpi, which is the first timepoint in which no virus was isolated from the horses, and with the fact that antigenic material of *Streptococcus zooepidemicus* was only detected in horses 4 (euthanized at 7dpi) 5, 6 and 7 (euthanized at 14dpi) in (Muranaka *et al*., 2012).

Whereas the lesions were severe at 7dpi, the amounts of CC3 positive signal decreased in the airways. The aforementioned MX-1 driven apoptosis might account for the decrease of the apoptosis levels following a drastic decrease of the expression of MX1. On the other hand, in the bronchi and bronchioles, the levels of mitosis peaked. This is consistent with an epithelial regeneration secondary to the loss of cells (seen as increased CC3 levels in the previous timepoints) due to the action of the virus. On the other hand, in the nasal mucosa and trachea, mitosis levels were lower than at 3dpi. According to the data shown in Chapter 3, at 7dpi, the respiratory epithelium of the nasal mucosa and trachea had recovered its normal thickness, if not increased it, and might not be in need of further regeneration (measured as Ki67 expression).

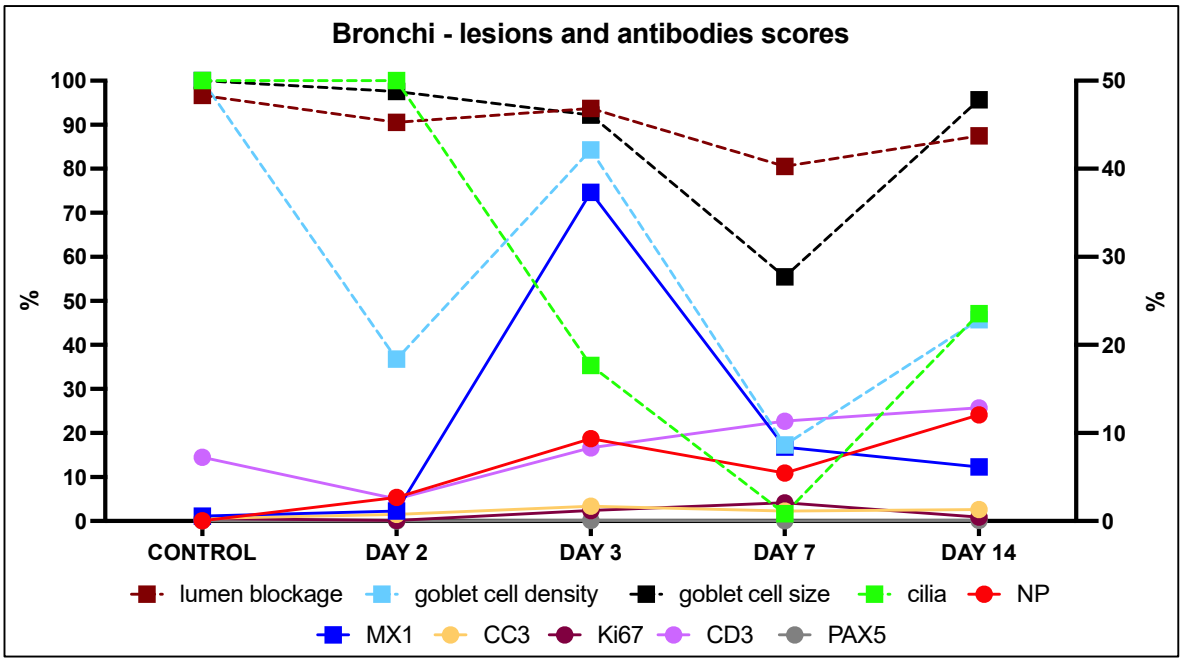

Figure 6-3: Line chart showing the percentage of degree of histopathological changes (discontinuous lines) and of antibody expression (continuous lines) in the bronchi. Each histopathological change quantified in chapter 3 was given a score from 0 to 100, according to its proximity to the value shown by the noninfected controls. A second Y axis (right) was applied for better visualization of small values. Squares show values linked to left axis and circles show values linked to right axis.

increased in extension and severity. On this regard, as hypothesized in chapter 5, either the

low values of innate immunity expression seen in the alveoli at 3dpi compared to the other tissues, or the smaller susceptibility of pneumocytes to MX1-induced apoptosis, or a combination of both factors, would explain why, instead of decreasing, at 7dpi the abundance of viral antigens increased in the alveoli. As suggested above, this would mean that, in the areas where a strong innate immune response is mounted, the virus is likely controlled, whereas in the areas where this response is milder, the virus can continue proliferating. Overall, the fact that the gas-exchange surface in the lung further decreased from 7dpi to 14dpi gives additional evidence on the horse incapacity to restrict the detrimental action of the offending agent, whether it is EIV or opportunistic bacteria, in this organ. As hypothesized, the primary reason why the alveoli develop these lesions would be the impairment of the mucociliary system in the airways. On this regard, although this information is not available, the virtually complete destruction of cilia and goblet cells in the respiratory airways, described at 7dpi, would be observable earlier, probably around 4dpi, because the reduction of cilia and goblet cells from 2dpi to 3dpi was, depending on the tissue, between 30 and 70%.

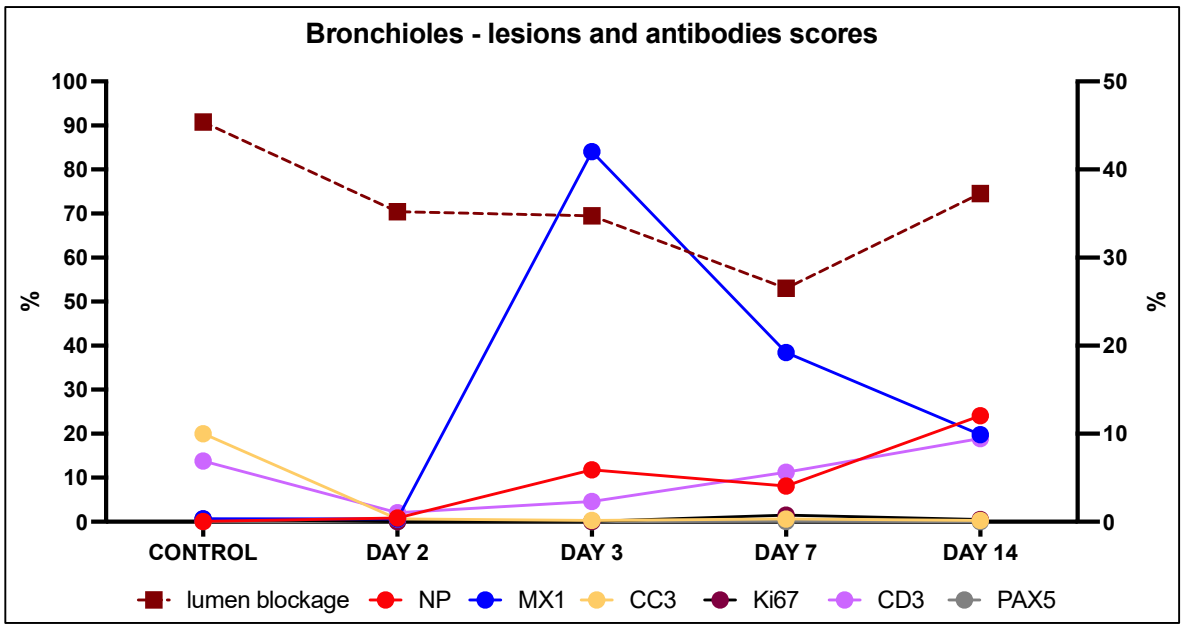

Figure 6-4: Line chart showing the percentage of degree of histopathological changes (discontinuous lines) and of antibody expression (continuous lines) in the bronchioles. Each histopathological change quantified in chapter 3 was given a score from 0 to 100, according to its proximity to the value shown by the noninfected controls. A second Y axis (right) was applied for better visualization of small values. Squares show values linked to left axis and circles show values linked to right axis.

Finally, at day 14 post infection airways showed signs of recovery, since goblet cells and cilia could be observed again, as **figures 6-1**, **6-2**, **6-3** and **6-4** show. Although the degree of restoration of the respiratory epithelia varied depending on the tissue, all the parameters

quantified to characterize the integrity of the epithelia improved, except epithelial thickness. In this case, as shown, in response to the loss of cells, the epithelia had undergone hyperplasia (**Fig 3-13**). Consequences of epithelial hyperplasia of the nose and the trachea are two; first, in the short term, the air flow space is reduced, and in the long term, it can progress to neoplasia (Herbert *et al*., 2018). Apoptosis and mitosis levels were low, which was consistent with the observation that the destruction of the epithelia had finished and the regeneration of the epithelium, which was now hyperplastic, was also terminating.

One of the main findings at this timepoint was the presence of viral antigen (NP) in high quantities in the respiratory tract of the horse, when the animals were not shedding virus anymore. To the best of my knowledge, this had never been described before, and its relevance is unclear. As thoroughly discussed in Chapter 4, further characterization of the positive signal to NP seen at 14dpi is needed, given that it is highly unlikely that this positive signal belongs to viable virus. As seen in Chapters 3 and 5, the high levels of NP signal seen at 14dpi did not correspond with an increased severity of the histopathological lesions nor a raised positive signal to the immune markers used, except in the lungs. On this regard, as shown in Chapter 3, lesions observed in the lungs of horses euthanized at 14dpi are in line with the common features of bacterial bronchopneumonia (consolidation of the parenchyma, necrosis of the respiratory epithelia, suppurative infiltration of the alveoli, alveolar oedema and hemorrhage), a fact that is further consolidated by the negative viral detection and the positive bacterial identification in the lungs of horses euthanized at days 7 and 14pi. Nonetheless, the possibility of viable virus still infecting the lungs 14 days after being inoculated is not fully dismissed, considering that animals were sampled by nasal swabbing. As shown in Chapter 4, during my project I tried to obtain further evidence of viral antigen being present in the equine respiratory tract for longer than reported in the bibliography by combining different lab techniques, such as IHC, IF and ISH, and antigenic targets, such as NP, HA, M1 and PB2, but those efforts were unsuccessful. Whereas at days 2 and 3 post infection all the tests had a positive result, at days 7 and 14 post infection only the NP labelling in immunohistochemistry and immunofluorescence showed positivity. These findings might suggest that, as all the bibliography says, by day 14pi no viable virus can be found in the respiratory tract of the horses, although the way to confirm this would be to try to isolate the virus from fresh lung samples, which nowadays is impossible to do with the horses I studied. On the other hand, given the fact that the positive staining observed at 14dpi is real, having ruled out the possibility of it being artifact/background, as shown in Chapter 4, the alternative explanation to its presence is the possibility that either residual viral antigen stays in the tissues for longer than the viable virus or viral levels are too low to be detected.

Another issue regarding NP is the presence of positive signal in the smooth muscle and hyaline cartilage of the intrapulmonary airways (**Figure 4-4**). As it was observed in infected animals, being especially strong in 14dpi animals, and not in uninfected controls, the possibility of it being unspecific background is estimated minimal. As shown in Chapter 4, availability of literature on immunolabelling of influenza antigens in these tissues is minimal, however, in skeletal muscle influenza NP has been successfully stained and even influenza virus has been isolated (Gamboa *et al*., 1979; Kessler *et al*., 1980; Desdouits *et al*., 2013; Partin *et al*., 2016). On the other hand, as shown in Chapter 4, very limited references on possible pathological or clinical consequences of it were found (Szarek *et al*., 1995; Bodelsson and Caverius, 1999; Desdouits *et al*., 2013; Cheah *et al*., 2015). However, as shown in chapter 5, both smooth muscle and hyaline cartilage were especially negative to different markers showing cellular responses (especially MX1, but also CC3 and Ki67), although they are tissues that are known to be able to develop an innate immune response and undergo apoptosis and mitosis (Bi *et al*., 2021; Bradley *et al*., 1996; Himes *et al*., 2015; Orlowsky and Kraus, 2015; Rossios *et al*., 2017), and no infiltration of inflammatory cells was found, suggesting that the presence of NP in these tissues might not induce substantial changes. Potential deleterious effects of influenza A viruses on bronchial smooth muscle and hyaline cartilage cells were discussed in Chapter 4.

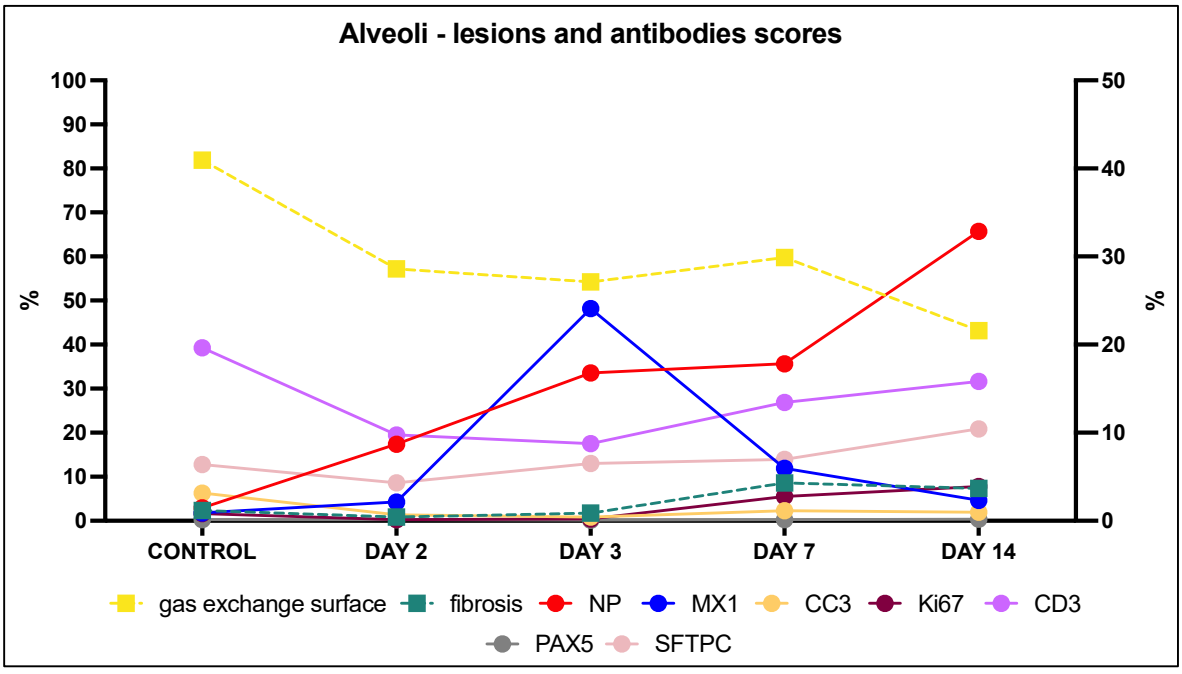

Figure 6-5: Line chart showing the percentage of degree of histopathological changes (discontinuous lines) and of antibody expression (continuous lines) in the alveoli. Each histopathological change quantified in chapter 3 was given a score from 0 to 100, according to its proximity to the value shown by the noninfected controls. A second Y axis (right) was applied for better visualization of small values. Squares show values linked to left axis and circles show values linked to right axis.

The extension of lesions in the alveoli increased at 14dpi (**Figure 6-5**). Data on loss of gas exchange surface and proliferation of type II pneumocytes are illustrative of this. Furthermore, as explained, levels of NP also peaked at 14dpi, together with all the other markers used. Representative images of the lung architecture after 14 days of the virus inoculation are shown in chapter 3 and in **Figure 6-6** and illustrate the degree of disruption of the normal alveolar tissue. As it can be seen, no alveoli can be identified anymore, and the space formerly occupied by air is filled by liquid, erythrocytes, fibrin and inflammatory cells. This combination of histological features, often referred as hepatization because of the liver-like macroscopical aspect the lung acquires, might explain some data obtained: due to the presence of bacteria, reported by (Muranaka *et al*., 2012) but not examined in this thesis, cellularity in the lung increases, mainly because of the extravasation of erythrocytes and inflammatory cells which, as shown in **figure 6-6**, fill the space occupied by air in physiologic conditions. Under these circumstances, with a lack of oxygen perfusion into the alveoli and the effect of toxins secreted by bacteria and the inflammatory cells, some alveolar cells die and some others, mainly type II pneumocytes, proliferate to repopulate the lung parenchyma. The finding of increased numbers of type II pneumocytes (measured as % nuclei positive to SFTPC staining) at day 14pi is consistent with this and the stem cell role these cells are known to have.

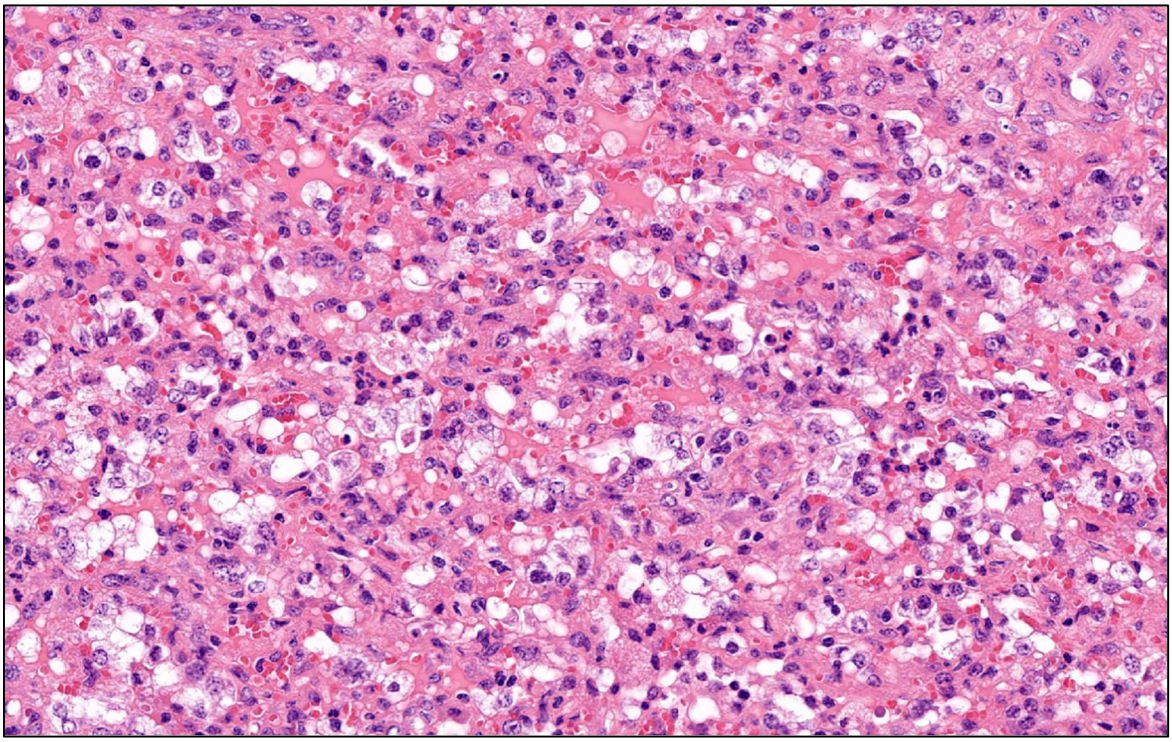

Figure 6-6: Representative landscape image of lung parenchyma of an EI-infected horse, euthanized at 14dpi, stained with H&E. Alveoli cannot be recognized anymore, as the air space has been filled by liquid, fibrin, inflammatory cells and erythrocytes. 18x.

By using image analysis software, I developed a platform to reliably and consistently quantify histological changes and protein expression in FFPE equine respiratory tissues, although its usefulness could be expanded to other species and other tissues and organs. Given its purely quantitative nature, this scoring system might have potential further purposes, such as determination of virulence of different infectious agents. Viral evolution studies, like the one developed in (Amat *et al*., 2021), would be a good example of it.

Future work on data generated in this thesis necessarily refers to pitfalls during the research that has allowed its writing. As commented, it is especially important to determine whether the NP signal observed at day 14pi really belongs to viable virus or not. On this regard, finding new antibodies against influenza A antigens that successfully work on FFPE tissues would be an interesting thing to do. The case of HA antibody and its low sensitivity on equine FFPE sections, explained in the fourth chapter, illustrates why. Furthermore, deeper insights on techniques that have been used for limited and specific reasons during my project, such as IF and ISH, are other potential future steps to take. Whereas ISH revealed as a consistent assay to label EIV antigens, the aforementioned lack of specificity of the antibodies made IF a tool with poor performance. On the other hand, as commented above, in future experimentation with horses inoculated with EIV, fresh lungs samples should be taken in order to attempt the isolation of the virus at late timepoints, to clarify whether viable virus stays in the equine respiratory tract for longer than reported in the literature or not.

It is highly relevant to fully understand the role of the different inflammatory cells in the pathogenesis and resolution of EI. A broad quantification of T and B lymphocytes was made by using an antibody for each of these cell types, however, no clear dynamics other than an overall increase in T-cell numbers were seen, and this is believed to have happened because of a too superficial approach to the characterization of these two immune cell populations. In the case of T lymphocytes, as explained, a pan-T lymphocyte marker was used, and this did not allow to distinguish between populations within the cell type. As a highly complex and versatile immune cell, next steps on the quantitative characterization of EIV pathogenesis should focus on T lymphocytes. Regarding B cells, my work showed that their numbers are extremely reduced in respiratory tissues from EIV-infected horses outside the submucosal lymphoid aggregates, where they are meant to be numerous. As explained in Chapter 5, quantifying plasma cells might shed light on the role of these and B cells on the pathogenesis of EI.

On the other hand, as said, to better characterize the inflammatory response some other cell types that play a role in the resolution of the infection, such as macrophages and neutrophils,

could be labelled and quantified. Ionized calcium-binding adapter molecule 1 (Iba-1) (Komohara *et al*., 2017) and cluster of differentiation 68 (CD68) (Heusinkveld and van der Burg, 2011) for macrophages and cluster of differentiation 66b (CD66b) (Kargl *et al*., 2017) and neutrophil elastase (NE) (Amanzada *et al*., 2011) for neutrophils would be notable suggestions.

In addition, markers of proteins that show how cells respond to the infection would also help to get a broader view on EI pathogenesis. Whereas mitosis, innate immunity activation and apoptosis have been studied in this project, deeper insights in cell death pathways other than apoptosis, such as necrosis, necroptosis and pyroptosis, are necessary to clarify the relationship between EIV and cell death, given the fact that, as explained, the literature is abundant and often contradictory. Finally, although the presence of opportunistic bacteria in EI-infected horses has been reported in numerous studies, it is necessary to gain deeper knowledge on their anatomical and temporary distribution as well as their pathogenic effect on EI-infected equine respiratory tissues, to better understand the original mechanism of the lesions seen in the lung at late timepoints post infection.

As commented at the beginning of this chapter, an increase on the sample size in the work done by Muranaka *et al*. would have been beneficial to minimize the effect that the interindiviual variation had on the results and given robustness to the conclusions of this thesis. Again, an intermediate point between the scientific ideal situation and the full alignment with the 3Rs principles might have been working with 6 timepoints (dpi 3, 5, 7, 9/10, 11/12 and 14) and an n=3 in each of these. Having said this, according to the statistical analysis, the interindividual differences among horses within the same experimental group were mild, although the small number of measurements within individuals contributed to a decreased statistical power and an increased likelihood of not finding statistical significances. Nonetheless, as seen in Chapters 3 and 4, it seemed that horse 2 had a more severe degree of disruption of the respiratory tract than horse 3, as several measurements for integrity of the architecture of the respiratory system were more markedly altered. Again, at the same time this horse had higher values of NP positive staining, and this is consistent with the reported tropism that EIV has for the epithelial cells of the respiratory epithelium of the airways and the pathologic effect it has on them. On the other hand, at 14dpi, horse 5 was the individual within the group with the least virus but the most severe lesions, whereas the situation was the opposite in horse 7. These findings suggest first, that the NP positive signal at 14dpi might not belong to viable virus and second, that the second opportunistic bacteria likely account for the pathology in the respiratory tract, and more precisely, the lung, at late stages of the disease. Furthermore, it is possible that horse 5 had a stronger immunologic

response against EIV, resulting in less viral loads, but this had as a consequence an impaired immunologic capability against the bacteria. Similarly, the fact that horse 7 did not stop the viral spread as much as the other two horses euthanized at 14dpi might mean that its immunity was in a better preservation status to neutralize the bacteria. On this regard, although raw data was generated, the interindividual differences among horses on the amount of positive signal to the immunomarkers other than NP used were not analyzed. This might have allowed further insights in both the pathogenesis of EI and the individual component of the host response to EI. As explained, no data on interindividual differences in animals undergoing experimental influenza infection were found

From data obtained, my interpretation of the pathogenesis of EI in the respiratory tract of the horse can be briefly explained as it follows. Upon infection, EIV colonizes the entire respiratory tract as soon as 2dpi, mainly infecting epithelial cells of the respiratory epithelia. It induces histological changes that can be seen at 3dpi in the airways (mainly loss of cilia and goblet cells) and triggers a strong and brief activation of the innate immunity that results in a reduction of the viral levels, except in the alveoli, where innate immune activation is much lower. Furthermore, in the airways, due to the effect of the virus or to prevent its spread, some cells undergo apoptosis and others mitosis, to balance the cell loss. From day 4 to day 6pi only hypothesis can be formulated, although it is clear that cilia and goblet cells at some point completely disappear, leading to an accumulation of mucus and debris in the airways that enable opportunistic bacteria to grow and establish a pneumonia. As the effect of innate immunity declines, so does the amount of virus. The lack of cilia and goblet cells at 7dpi is followed by a regeneration of the respiratory epithelia, which between day 8 and 13dpi start displaying some of these, whereas in the alveoli the secondary bacterial infection progresses and the areas of consolidation gain extension, leading the immune system to mount and adaptative response, mainly lead by T lymphocytes.

The prognosis that horses studied in this thesis would have depended on their ability to stop the progress of the bronchopneumonia and to clear the bacteria producing it, given the fact that the airways were on the way to going back to its normal architecture. On this regard, as said, at 14dpi there were acute (haemorrhage, oedema, neutrophilic infiltration) and chronic (lymphocytic infiltration) signs in the lung, whereas no signs of recovery were seen, other than the proliferation of type II pneumocytes. Given the degree of histological alteration of the lungs at 14dpi (shown in **Figure 6-6**), it exists the possibility of (some of) this lung parenchyma to be replaced by granulation tissue and, in the long term, fibrosis. By definition, granulation tissue leads to fibrosis and it is developed when repair mechanisms fail

(Wansleeben *et al*., 2013), which means this pulmonary space formerly occupied by alveoli will not be regenerated and remain as a scar (fibrous tissue) forever. Extrapolating my data to the entire lung, horses euthanized at 14dpi might lose up to 50% of the lung parenchyma (on average), in case all the consolidated areas were replaced by fibrous tissue. Although these animals might have survived, it is hard to imagine that they would have been able to perform as high as they were able before the experimental infection. Nevertheless, as explained, in uncomplicated cases, horses have to strictly rest for as many weeks as days of fever they have had, which, depending on the case, were between 6 and 7 (**Table 3-1**). Considering that these cases were not uncomplicated, and although no estimations on recovery timings for horses infected with EI and concomitant secondary bacterial infections have been found, seems fair assuming that these might have been much longer.

To summarize, this thesis provides a more comprehensive understanding of the pathogenesis of equine influenza in the respiratory tract of the horse, its natural host, by describing temporary and anatomical dynamics of histological changes, cell populations and expression of proteins. Additionally, it provides observations not made previously and it points to critical aspects of the knowledge on the disease that remain controversial.

References

Abente, E.J., Kitikoon, P., Lager, K.M., Gauger, P.C., Anderson, T.K., Vincent, A.L., 2017. A highly pathogenic avian-derived influenza virus H5N1 with 2009 pandemic H1N1 internal genes demonstrates increased replication and transmission in pigs. Journal of General Virology 98, 18–30. https://doi.org/10.1099/jgv.0.000678

Abou-Donia H, Jennings R, Potter CW. 1981. The spread and persistence of influenza viruses in normal and cyclophosphamide-treated mice. J Med Virol. 7(4):251-62. doi: 10.1002/jmv.1890070402. PMID: 7334358.

Ali, M.Y., 1965. Histology of the human nasopharyngeal mucosa. J Anat 99, 657–72.

Amanzada, A., Malik, I.A., Nischwitz, M., Sultan, S., Naz, N., Ramadori, G., 2011. Myeloperoxidase and elastase are only expressed by neutrophils in normal and in inflammed liver. Histochem Cell Biol 135, 305–315. https://doi.org/10.1007/s00418-011-0787-1

Amat, J.A.R., 2022. Adaptation of avian-origin influenza virus to the horse.

Amat, J.A.R., Patton, V., Chauché, C., Goldfarb, D., Crispell, J., Gu, Q., Coburn, A.M., Gonzalez, G., Mair, D., Tong, L., Martinez-Sobrido, L., Marshall, J.F., Marchesi, F., Murcia, P.R., 2021. Long-term adaptation following influenza A virus host shifts results in increased within-host viral fitness due to higher replication rates, broader dissemination within the respiratory epithelium and reduced tissue damage. PLoS Pathog 17, 1–25. https://doi.org/10.1371/journal.ppat.1010174

American Association of Equine Practitioners, 2017. Risk-based vaccination guidelines: equine influenza. [WWW Document].

Angeletti, D., Gibbs, J.S., Angel, M., Kosik, I., Hickman, H.D., Frank, G.M., Das, S.R., Wheatley, A.K., Prabhakaran, M., Leggat, D.J., McDermott, A.B., Yewdell, J.W., 2017. Defining B cell immunodominance to viruses. Nat Immunol 18, 456–463. https://doi.org/10.1038/ni.3680

Aronsson F, Lannebo C, Paucar M, Brask J, Kristensson K, Karlsson H. 2002. Persistence of viral RNA in the brain of offspring to mice infected with influenza A/WSN/33 virus during pregnancy. J Neurovirol. 8(4):353-7. doi: 10.1080/13550280290100480. PMID: 12161820.

Aster, Jon.C., Abbas, A. k, Kumar, V., 2015a. Cellular responses to stress and toxic insults: adaptation, injury and death, in: Robbins and Cotran Pathologic Basis of Disease. Elsevier, Philadelphia, Pennsylvania, pp. 35–38.

Aster, Jon.C., Abbas, A. k, Kumar, V., 2015b. Chapter 2, in: Robbins and Cotran Pathologic Basis of Disease. Elsevier, Philadelphia, Pennsylvania, pp. 40–45.

Atkin-Smith, G.K., Duan, M., Chen, W., Poon, I.K.H., 2018. The induction and consequences of Influenza A virus-induced cell death. Cell Death Dis 9. https://doi.org/10.1038/s41419-018-1035-6

Barbas-Filho, J. V, Ferreira, M.A., Sesso, A., Kairalla, R.A., Carvalho, C.R.R., Capelozzi, V.L., 2001. Evidence of type II pneumocyte apoptosis in the pathogenesis of idiopathic pulmonary fibrosis (IFP)/usual interstitial pneumonia (UIP), J Clin Pathol.

Baskerville A, Thomas G, Wood M, Harris WJ. 1974. Histology and ultrastructure of metaplasia of alveolar epithelium following infection of mice and hamsters with influenza virus. Br J Exp Pathol. 55(2):130-7. PMID: 4835801; PMCID: PMC2072526.

Baskin CR, Bielefeldt-Ohmann H, Tumpey TM, Sabourin PJ, Long JP, García-Sastre A, Tolnay AE, Albrecht R, Pyles JA, Olson PH, Aicher LD, Rosenzweig ER, Murali-Krishna K, Clark EA, Kotur MS, Fornek JL, Proll S, Palermo RE, Sabourin CL, Katze MG. Early and sustained innate immune response defines pathology and death in nonhuman primates infected by highly pathogenic influenza virus. Proc Natl Acad

Sci U S A. 2009 Mar 3;106(9):3455-60. doi: 10.1073/pnas.0813234106. Epub 2009 Feb 13. PMID: 19218453; PMCID: PMC2642661.

Bataille, R., Jégo, G., Robillard, N., Barillé-Nion, S., Harousseau, J.-L., Moreau, P., Amiot, M., Pellat-Deceunynck, C., 2006. The phenotype of normal, reactive and malignant plasma cells. Identification of "many and multiple myelomas" and of new targets for myeloma therapy. Haematologica 91, 1234–1240.

Begg, A.P., Reece, R.L., Hum, S., Townsend, W., Gordon, A., Carrick, J., 2011. Pathological changes in horses dying with equine influenza in Australia, 2007. Aust Vet J 89, 19–22. https://doi.org/10.1111/j.1751-0813.2011.00731.x

Belser, J.A., Eckert, A.M., Huynh, T., Gary, J.M., Ritter, J.M., Tumpey, T.M., Maines, T.R., 2020. A Guide for the Use of the Ferret Model for Influenza Virus Infection. American Journal of Pathology. https://doi.org/10.1016/j.ajpath.2019.09.017

Bender BS, Croghan T, Zhang L, Small PAJ Jr. 1992. Transgenic mice lacking class I major histocompatibility complex-restricted T cells have delayed viral clearance and increased mortality after influenza virus challenge. J Exp Med 175(4): 1143–1145

Berche, P., 2022. The Spanish flu. Presse Medicale 51. https://doi.org/10.1016/j.lpm.2022.104127

Best, S. M., Bloom. M. E., 2004. Caspase activation during virus infection: more than just the kiss of death? Virology 320, 191-194.

Bi, X., Du, C., Wang, X., Wang, X.Y., Han, W., Wang, Y., Qiao, Y., Zhu, Y., Ran, L., Liu, Y., Xiong, J., Huang, Y., Liu, M., Liu, C., Zeng, C., Wang, J., Yang, K., Zhao, J., 2021. Mitochondrial Damage-Induced Innate Immune Activation in Vascular Smooth Muscle Cells Promotes Chronic Kidney Disease-Associated Plaque Vulnerability. Advanced Science 8. https://doi.org/10.1002/advs.202002738

Biondo, C., Lentini, G., Beninati, C., Teti, G., 2019. The dual role of innate immunity during influenza. Biomed J 42, 8–18. https://doi.org/10.1016/j.bj.2018.12.009

Bissel SJ, Wang G, Carter DM, Crevar CJ, Ross TM, Wiley CA. 2014. H1N1, but not H3N2, influenza A virus infection protects ferrets from H5N1 encephalitis. J Virol. 88(6):3077-91. doi: 10.1128/JVI.01840-13. Epub 2013 Dec 26. PMID: 24371072; PMCID: PMC3957958.

Bodelsson, M., Caverius, K., 1999. Smooth Muscle via Epithelial Prostanoid 355–359.

Boltz, D.A., Rehg, J.E., McClaren, J., Webster, R.G., Govorkova, E.A., 2008. Oseltamivir prophylactic regimens prevent H5N1 influenza morbidity and mortality in a ferret model. Journal of Infectious Diseases 197, 1315–1323. https://doi.org/10.1086/586711

Bortnick, A., Murre, C., 2016. Cellular and Chromatin Dynamics of Antibody-Secreting Plasma Cells. Wiley Interdiscip Rev Dev Biol. 5, 136–149. https://doi.org/10.1002/wdev.213.Cellular

Bradley, K., North, J., Saunders, D., Schwaeble, W., Jeziorska, M., Woolley, D.E., Whaley, K., 1996. Synthesis of classical pathway complement components by chondrocytes, Immunology.

Brandes, M., Klauschen, F., Kuchen, S., Germain, R.N., 2013. XA systems analysis identifies a feedforward inflammatory circuit leading to lethal influenza infection. Cell 154, 197. https://doi.org/10.1016/j.cell.2013.06.013

Bressenot A, Marchal S, Bezdetnaya L, Garrier J, Guillemin F, Plénat F. 2009. Assessment of apoptosis by immunohistochemistry to active caspase-3, active caspase-7, or cleaved PARP in monolayer cells and spheroid and subcutaneous xenografts of human carcinoma. J Histochem Cytochem. 57(4):289-300.

Brockmeier, Susan L., Halbur, Patrick G., Thacker Eileen L., 2002. Chapter 13. Porcine Respiratory Disease Complex., in: Brogden K.A., Guthmiller J.M. (Eds.), Polymicrobial Diseases. ASM Press.

Brown DM, Roman E, Swain SL. 2004. CD4 T cell responses to influenza infection. Semin Immunol. 16:171–7. doi: 10.1016/j.smim.2004.02.004

Budras, K.-D., Sack, W.O., Röck, S., 2011. Chapter 7: Thoracic cavity, in: Anatomy of the Horse. schlütersche, Hannover, Germany, pp. 60–61.

Carstens, A., Kirberger, R.M., Grimbeek, R.J., Donnellan, C.M.B., Saulez, M.N., 2009. Radiographic quantification of tracheal dimensions of the normal Thoroughbred horse. Vet Radiol Ultrasound 50, 492–501. https://doi.org/10.1111/j.1740-8261.2009.01570.x

Castleman, W.L., Powe, J.R., Crawford, P.C., Gibbs, E.P.J., Dubovi, E.J., Donis, R.O., Hanshaw, D., 2010. Canine H3N8 influenza virus infection in dogs and mice. Vet Pathol 47, 507–517. https://doi.org/10.1177/0300985810363718

Caswell, J.L., Williams, K.J., 2007. Equine influenza, in: Jubb, Kennedy and Palmer's Pathology of Domestic Animals. Fifth Edition. Volume 2. Saunders Elsevier, Philadelphia, Pennsylvania, pp. 628–689.

CDC, C. for D.C. and P., 2019. Types of Influenza Viruses | CDC. Cdc.Gov.

Cheah, E.Y., Mann, T.S., Burcham, P.C., Henry, P.J., 2015. Influenza A infection attenuates relaxation responses of mouse tracheal smooth muscle evoked by acrolein. Biochem Pharmacol 93, 519–526. https://doi.org/10.1016/j.bcp.2014.12.015

Chen, X., Liu, S., Goraya, M.U., Maarouf, M., Huang, S., Chen, J.L., 2018. Host immune response to influenza A virus infection. Front Immunol 9, 1–13. https://doi.org/10.3389/fimmu.2018.00320

Choi, Y.S., Baumgarth, N., 2008. Dual role for B-1a cells in immunity to influenza virus infection. Journal of Experimental Medicine 205, 3053–3064. https://doi.org/10.1084/jem.20080979

Chung HK, Lee JH, Kim SH, Chae C., 2004 Expression of interferon-alpha and MX1 protein in pigs acutely infected with porcine reproductive and respiratory syndrome virus (PRRSV). J Comp Pathol. 130(4), 299-305. doi: 10.1016/j.jcpa.2003.12.006. PMID: 15053933.

Collins, M., 1995. Potential role of apoptosis in viral pathogenesis. Am. J. Respir. Crit. Care Med 152, S20–S24.

Conenello, G.M., Palese, P., 2007. Influenza A Virus PB1-F2: A Small Protein with a Big Punch. Cell Host Microbe 2, 207–209. https://doi.org/10.1016/j.chom.2007.09.010

Confalonieri, M., Salton, F., Ruaro, B., Confalonieri, P., Volpe, M.C., 2021. Alveolar Epithelial Type II Cells, Second Edi. ed, Encyclopedia of Respiratory Medicine, Second Edition. Elsevier. https://doi.org/10.1016/B978-0-08-102723-3.00157-8

Conover, W. J. 1999. *Practical Nonparametric Statistics* (3rd ed.). Wiley

Corrin, B., Nicholson, A.G., 2011. The structure of the normal lungs, Pathology of the Lungs. https://doi.org/10.1016/b978-0-7020-3369-8.00001-x

Cortez, V., Schultz-Cherry, S., 2021. The role of goblet cells in viral pathogenesis. FEBS Journal 288, 7060–7072. https://doi.org/10.1111/febs.15731

Cowled, B., Ward, M.P., Hamilton, S., Garner, G., 2009. The equine influenza epidemic in Australia: Spatial and temporal descriptive analyses of a large propagating epidemic. Prev Vet Med 92, 60–70. https://doi.org/10.1016/j.prevetmed.2009.08.006

Crawford, P.C., Dubovi, E.J., Castleman, W.L., Stephenson, I., Gibbs, E.P.J., Chen, L., Smith, C., Hill, R.C., Ferro, P., Donis, R.O., 2005a. Transmission of Equine Influenza Virus to Dogs. Science (1979) 310, 482–485.

Crawford, P.C., Dubovi, E.J., Castleman, W.L., Stephenson, I., Gibbs, E.P.J., Chen, L., Smith, C., Hill, R.C., Ferro, P., Pompey, J., Bright, R.A., Medina, M.-J., Johnson, C.M., Olsen, C.W., Cox, N.J., Klimov, A.I., Katx, J.M., Donis, R.O., 2005b. Transmission of Equine Influenza to Dogs. Science (1979) 310, 482–485.

Crouse, J., Kalinke, U., Oxenius, A., 2015. Regulation of antiviral T cell responses by type i interferons. Nat Rev Immunol. https://doi.org/10.1038/nri3806

Curran, D.R., Cohn, L., 2010. Advances in mucous cell metaplasia: A plug for mucus as a therapeutic focus in chronic airway disease. Am J Respir Cell Mol Biol 42, 268–275. https://doi.org/10.1165/rcmb.2009-0151TR

Daly, J.M., Whitwell, K.E., Miller, J., Dowd, G., Cardwell, J.M., Smith, K.C., 2006. Investigation of Equine Influenza Cases Exhibiting Neurological Disease: Coincidence or Association? J Comp Pathol 134, 231–235. https://doi.org/10.1016/j.jcpa.2005.09.001

Daly M., J., Newton, J.R., Mumford, J.A., 2004. Current perspectives on control of equine influenza. Vet. Res. 35, 411–423. https://doi.org/10.1051/vetres

Davis, M.S., Lockard, A.J., Marlin, D.J., Freed, A.N., 2002. Airway cooling and mucosal injury during cold weather exercise. Equine Vet J Suppl 34, 413–416. https://doi.org/10.1111/j.2042-3306.2002.tb05458.x

Davis, M.S., Royer, C.M., Mckenzie, E.C., Williamson, K.K., Payton, M., Marlin, D., 2006. Cold air-induced late-phase bronchoconstriction in horses. Equine Vet J 38, 535–539. https://doi.org/10.1111/j.2042-3306.2006.tb05600.x

De Vleeschauwer A, Atanasova K, Van Borm S, van den Berg T, Rasmussen TB, *et al*. 2009. Comparative Pathogenesis of an Avian H5N2 and a Swine H1N1 Influenza Virus in Pigs. PLOS ONE 4(8): e6662. https://doi.org/10.1371/journal.pone.0006662

De Wit, E., Siegers, J.Y., Cronin, J.M., Weatherman, S., Van Den Brand, J.M., Leijten, L.M., Van Run, P., Begeman, L., Van Den Ham, H.J., Andeweg, A.C., Bushmaker, T., Scott, D.P., Saturday, G., Munster, V.J., Feldmann, H., Van Riel, D., 2018. 1918 H1N1 Influenza Virus Replicates and Induces Proinflammatory Cytokine Responses in Extrarespiratory Tissues of Ferrets. Journal of Infectious Diseases 217, 1237–1246. https://doi.org/10.1093/infdis/jiy003

Desdouits M, Munier S, Prevost MC, Jeannin P, Butler-Browne G, Ozden S, Gessain A, Van Der Werf S, Naffakh N, Ceccaldi PE. 2013. Productive infection of human skeletal muscle cells by pandemic and seasonal influenza A(H1N1) viruses. PLoS One. 8(11):e79628. doi: 10.1371/journal.pone.0079628. PMID: 24223983; PMCID: PMC3818236.

DiVito KA, Charette LA, Rimm DL, Camp RL. Long-term preservation of antigenicity on tissue microarrays. 2004. Lab Invest.84(8):1071-8

Dionísio, L., Medeiros, F., Pequito, M., Faustino-Rocha, A.I., 2021. Equine influenza: A comprehensive review from etiology to treatment. Anim Health Res Rev. https://doi.org/10.1017/S1466252321000050

Doherty PC, Topham DJ, Tripp RA. 1996. Establishment and persistence of virus-specific CD4+ and CD8+ T cell memory. Immunol Rev.150(1): 23–44

Donis, R.O., 2017. Orthomyxoviridae, in: Fenner's Veterinary Virology. Elsevier, London, pp. 398–401. https://doi.org/10.1016/B978-0-12-800946-8.00021-0

Driskell, E., 2014. Influenza in Animals, in: Pathobiology of Human Disease: A Dynamic Encyclopedia of Disease Mechanisms. Elsevier Inc., pp. 1071–1082. https://doi.org/10.1016/B978-0-12-386456-7.03408-0

Easterday, B., Van Reeth, K., 1999. Swine Influenza, in: Straw, B.E., D'Allaire, S., Mengeling, W.L., Taylor, D.J. (Eds.), Disease of Swine. Iowa State University Press, Ames, USA, pp. 277–290.

Easterday, B.C., Trainer, D.O., Tůmová, B., Pereira, H.G., 1968. Evidence of infection with influenza viruses in migratory waterfowl. Nature 219, 523–524. https://doi.org/10.1038/219523a0

Equiflunet, 2022. Veterinary information [WWW Document]. URL https://equinesurveillance.org/equiflunet/

Evans, M.J., Dekker, N.P., Cabral-Anderson, L.J., Freeman, G., 1978. Quantitation of Damage to the Alveolar Epithelium by Means of Type 2 Cell Proliferation. American Review of Respiratory Disease 118.

Fatima, U., Zhang, Z., Zhang, H., Wang, X.F., Xu, L., Chu, X., Ji, S., Wang, X., 2019. Equine MX1 restricts influenza a virus replication by targeting at distinct site of its nucleoprotein. Viruses 11, 1–19. https://doi.org/10.3390/v11121114

Feldman, A.L., Dogan, A., 2007. Diagnostic uses of Pax5 immunohistochemistry. Adv Anat Pathol 14, 323–334. https://doi.org/10.1097/PAP.0b013e3180ca8a49

Feng, K.H., Gonzalez, G., Deng, L., Yu, H., Tse, V.L., Huang, L., Huang, K., Wasik, B.R., Zhou, B., Wentworth, D.E., Holmes, E.C., Chen, X., Varki, A., Murcia, P.R., Parrish, C.R., 2015. Equine and Canine Influenza H3N8 Viruses Show Minimal Biological Differences Despite Phylogenetic Divergence. J Virol 89, 6860–6873. https://doi.org/10.1128/jvi.00521-15

Fleming, G., 1891. Influenza in Horses. The Journal of comparative medicine and veterinary archives 12, 129–137.

Flieder, D.B., 2018. Normal Anatomy, Tissue Artifacts, and Incidental Structures, Second Edi. ed, Pulmonary Pathology: A Volume in the Series: Foundations in Diagnostic Pathology. Elsevier Inc. https://doi.org/10.1016/B978-0-323-39308-9.00001-7

Fu Y, Dürrwald R, Meng F, Tong J, Wu NH, Su A, Yin X, Haas L, Schmidtke M, Zell R, Krumbholz A, Herrler G. 2019. Infection Studies in Pigs and Porcine Airway Epithelial Cells Reveal an Evolution of A(H1N1)pdm09 Influenza A Viruses Toward Lower Virulence. J Infect Dis. (10):1596-1604. doi: 10.1093/infdis/jiy719. PMID: 30776304; PMCID: PMC7107423.

Fujikura, D., Miyazaki, T., 2018. Programmed cell death in the pathogenesis of influenza. Int J Mol Sci 19, 1–14. https://doi.org/10.3390/ijms19072065

Gaide N, Crispo M, Jbenyeni A, Bleuart C, Delverdier M, Vergne T, Le Loc'h G, Guérin JL. 2023. Validation of an RNAscope assay for the detection of avian influenza A virus. J Vet Diagn Invest. 35(5):500-506.

Gamboa ET, Eastwood AB, Hays AP, Maxwell J, Penn AS. 1979. Isolation of influenza virus from muscle in myoglobinuric polymyositis. Neurology. (10):1323-35. doi: 10.1212/wnl.29.10.1323. PMID: 384294.

Gauger PC, Vincent AL, Loving CL, Lager KM, Janke BH, Kehrli ME Jr, Roth JA., 2011. Enhanced pneumonia and disease in pigs vaccinated with an inactivated human-like (δ-cluster) H1N2 vaccine and challenged with pandemic 2009 H1N1 influenza virus. Vaccine. 29(15):2712-9. doi: 10.1016/j.vaccine.2011.01.082

Gavrilov VI, Asher DM, Vyalushkina SD, Ratushkina LS, Zmieva RG, Tumyan BG. 1972Persistent infection of continuous line of pig kidney cells with a variant of the WSN strain of influenza A 0 virus. Proc Soc Exp Biol Med. 140(1):109-17. doi: 10.3181/00379727-140-36405. PMID: 5033080.

George, S.T., Lai, J., Ma, J., Stacey, H.D., Miller, M.S., Mullarkey, C.E., 2021. Neutrophils and Influenza: A Thin Line between Helpful and Harmful. https://doi.org/10.3390/vaccines

Gerber, H., 1970. Clinical features, sequelae and epidemiology of equine influenza. Clinical features, sequelae and epidemiology of equine influenza," in Proceedings of the 2nd International Conference on Equine Infectious Diseases, Paris.

Gonzalez, G., Marshall, J.F., Morrell, J., Robb, D., McCauley, J.W., Perez, D.R., Parrish, C.R., Murcia, P.R., 2014. Infection and Pathogenesis of Canine, Equine, and Human Influenza Viruses in Canine Tracheas. J Virol 88, 9208–9219. https://doi.org/10.1128/jvi.00887-14

Govorkova, E.A., Rehg, J.E., Krauss, S., Yen, H.-L., Guan, Y., Peiris, M., Nguyen, T.D., Hanh, T.H., Puthavathana, P., Long, H.T., Buranathai, C., Lim, W., Webster, R.G., Hoffmann, E., 2005. Lethality to Ferrets of H5N1 Influenza Viruses Isolated from Humans and Poultry in 2004. J Virol 79, 2191–2198. https://doi.org/10.1128/jvi.79.4.2191-2198.2005

Gown, A.M., Willingham, M.C., 2002. Improved detection of apoptotic cells in archival paraffin sections: Immunohistochemistry using antibodies to cleaved caspase 3. Journal of Histochemistry and Cytochemistry 50, 449–454. https://doi.org/10.1177/002215540205000401

Grau-Roma L, Segalés J. Detection of porcine reproductive and respiratory syndrome virus, porcine circovirus type 2, swine influenza virus and Aujeszky's disease virus in cases of porcine proliferative and necrotizing pneumonia (PNP) in Spain. Vet Microbiol. 2007. 31;119(2-4):144-51. doi: 10.1016/j.vetmic.2006.09.009.

Greenbaum D, Colangelo C, Williams K, Gerstein M. 2003. Comparing protein abundance and mRNA expression levels on a genomic scale. Genome Biol. 4(9):117

Groves HT, McDonald JU, Langat P, Kinnear E, Kellam P, McCauley J, Ellis J, Thompson C, Elderfield R, Parker L, Barclay W, Tregoning JS. 2018. Mouse Models of Influenza Infection with Circulating Strains to Test Seasonal Vaccine Efficacy. Front Immunol.9:126. doi: 10.3389/fimmu.2018.00126. PMID: 29445377; PMCID: PMC5797846.

Guarner, J., Falcón-Escobedo, R., 2009. Comparison of the pathology caused by H1N1, H5N1, and H3N2 influenza viruses. Arch Med Res. https://doi.org/10.1016/j.arcmed.2009.10.001

Guo, Y., Wang, M., Kawaoka, Y., Gorman, O., Ito, T., Saito, T., Webster+', R.G., 1992. Characterization of a New Avian-like influenza A Virus from Horses in China, VIROLOGY.

Haanen C, Vermes I. 1995. Apoptosis and inflammation. Mediators Inflamm. 4(1):5-15. doi: 10.1155/S0962935195000020.

Häcker, G., Kirschnek, S. & Fischer, S.F. 2006. Apoptosis in infectious disease: how bacteria interfere with the apoptotic apparatus. Med Microbiol Immunol 195, 11–19 https://doi.org/10.1007/s00430-005-0239-4

Halfmann PJ, Nakajima N, Sato Y, Takahashi K, Accola M, Chiba S, Fan S, Neumann G, Rehrauer W, Suzuki T, Kawaoka Y. SARS-CoV-2. 2022. Interference of Influenza Virus Replication in Syrian Hamsters. J Infect Dis. 225(2):282-286. doi: 10.1093/infdis/jiab587. PMID: 34875072; PMCID: PMC8689717.

Haller, O., Arnheiter, H., Lindenmann, J., Gresser, I., 1980. Host gene influences sensitivity to inferferon action selectively for influenza virus. Nature 283.

He Y, Xu K, Keiner B, Zhou J, Czudai V, Li T, Chen Z, Liu J, Klenk HD, Shu YL, Sun B, 2010. Influenza A virus replication induces cell cycle arrest in G0/G1 phase. J Virol. 84(24):12832-40.

Herbert, R.A., Janardhan, K.S., Pandiri, A.R., Cesta, M.F., Miller, R.A., 2018. Nose, Larynx, and Trachea, in: Boorman's Pathology of the Rat. Elsevier, pp. 391–435. https://doi.org/10.1016/b978-0-12-391448-4.00022-8

Heusinkveld, M., van der Burg, S.H., 2011. Identification and manipulation of tumor associated macrophages in human cancers. J Transl Med. https://doi.org/10.1186/1479-5876-9-216

Himes, B.E., Koziol-White, C., Johnson, M., Nikolos, C., Jester, W., Klanderman, B., Litonjua, A.A., Tantisira, K.G., Truskowski, K., MacDonald, K., Panettieri, R.A., Weiss, S.T., 2015. Vitamin D modulates expression of the airway smooth muscle transcriptome in fatal asthma. PLoS One 10. https://doi.org/10.1371/journal.pone.0134057

Hinshaw, V.S., Olsen, C.W., Dybdahl-Sissoko, N., Evans, D., 1994. Apoptosis: a mechanism of cell killing by influenza A and B viruses. J Virol 68, 3667–3673. https://doi.org/10.1128/jvi.68.6.3667-3673.1994

Hinshaw, V.S., Webster, R.G., Turner, B., 1980. The perpetuation of orthomyxoviruses and paramyxoviruses in Canadian waterfowl. Can J Microbiol 26, 622–629. https://doi.org/10.1139/m80-108

Holcombe, S.J., Derksen, F.J., Robinson, N.E., 2007. Electromyographic activity of the palatinus and palatopharyngeus muscles in exercising horses. Equine Vet J 39, 451–455. https://doi.org/10.2746/042516407X197752

Hollander, M., Wolfe, D. A., & Chicken, E. 2013. *Nonparametric Statistical Methods* (3rd ed.). John Wiley & Sons

Honda, T., Ota, H., Yamazaki, Y., Yoshizawa, A., Fujimoto, K., Sone, S., 2003. Proliferation of type II pneumocytes in the lung biopsy specimens reflecting alveolar damage. Respir Med 97, 80–85. https://doi.org/10.1053/rmed.2002.1408

Hornick, Emma E., Zacharias, Zeb R., Legge, Kevin L, 2019. Kinetics and Phenotype of the CD4 T cell response to Influenza Virus infection. Front. Immunol., Sec. Viral Immunology 10. https?//doi.org/10.3389/fim-mu.219.02351

Hua L, Yao S, Pham D, Jiang L, Wright J, Sawant D, et al. 2013. Cytokine-dependent induction of CD4+ T cells with cytotoxic potential during influenza virus infection. J Virol. 87:11884–93. doi: 10.1128/JVI.01461-13

Huang, S.S.H., Banner, D., Fang, Y., Ng, D.C.K., Kanagasabai, T., Kelvin, D.J., Kelvin, A.A., 2011. Comparative analyses of pandemic H1N1 and seasonal H1N1, H3N2, and influenza B infections depict distinct clinical pictures in ferrets. PLoS One 6. https://doi.org/10.1371/journal.pone.0027512

Hufford, M.M., Kim, T.S., Sun, J., Braciale, T.J., 2015. The effector T cell response to Influenza infection. Curr Top Microbiol Immunol 386, 423–455. https://doi.org/10.1007/82

ICTV, 2021. Virus Taxonomy: 2021 Release [WWW Document].

ICTV, 2020. Orthomyxoviridae ICTV.

Iverson, A.R., Boyd, K.L., McAuley, J.L., Plano, L.R., Hart, M.E., McCullers, J.A., 2011. Influenza virus primes mice for pneumonia from Staphylococcus aureus. Journal of Infectious Diseases 203, 880–888. https://doi.org/10.1093/infdis/jiq113

Jacobs TW, Prioleau JE, Stillman IE, Schnitt SJ. 1996. Loss of tumor marker-immunostaining intensity on stored paraffin slides of breast cancer. J Natl Cancer Inst 88(15):1054-9

Janeway, C.J., Travers, P., Walport, M., 2001. Immunobiology: The Immune System in Health and Disease, 5th ed. Garland Science, New York.

Janke, B.H., 2013. Influenza A Virus Infections in Swine: Pathogenesis and Diagnosis. Vet Pathol 51, 410–426. https://doi.org/10.1177/0300985813513043

Janke, B.H. 2013. Clinicopathological Features of Swine Influenza. In: Richt, J., Webby, R. (eds) Swine Influenza. Current Topics in Microbiology and Immunology, vol 370. Springer, Berlin, Heidelberg. https://doi.org/10.1007/82_2013_308

Jones PD, Ada GL. Influenza virus-specific antibody-secreting cells in the murine lung during primary influenza virus infection. J Virol. 1986 Nov;60(2):614-9. doi: 10.1128/JVI.60.2.614-619.1986. PMID: 3773053; PMCID: PMC288933

Jones, L.D., Nuttall, P.A., 1989. Non-viraemic transmission of Thogoto virus: influence of time and distance. Trans R Soc Trop Med Hyg 83, 712–714. https://doi.org/10.1016/0035-9203(89)90405-7

Jung, K., Lee, C.S., Kang, B.K., Park, B.K., Oh, J.S., Song, D.S., 2010. Pathology in dogs with experimental canine H3N2 influenza virus infection. Res Vet Sci 88, 523–527. https://doi.org/10.1016/j.rvsc.2009.11.007

Kai McKinstry, K., Dutton, R.W., Swain, S.L. *et al*., 2013. Memory CD4 T Cell-Mediated Immunity against Influenza A Virus: More than a Little Helpful. Arch. Immunol. Ther. Exp. 61, 341–353. https://doi.org/10.1007/s00005-013-0236-z

Kalhoro, D.H., Gao, S., Xie, X. *et al*. 2016. Canine influenza virus coinfection with Staphylococcus pseudintermedius enhances bacterial colonization, virus load and clinical presentation in mice. BMC Vet Res 12, 87. https://doi.org/10.1186/s12917-016-0708-6

Kang, Y.M., Kim, H.M., Ku, K.B., Park, E.H., Yum, J., Seo, S.H., 2013. H3N2 canine influenza virus causes severe morbidity in dogs with induction of genes related to inflammation and apoptosis. Vet Res 44, 1–12. https://doi.org/10.1186/1297-9716-44-92

Kargl, J., Busch, S.E., Yang, G.H.Y., Kim, K.H., Hanke, M.L., Metz, H.E., Hubbard, J.J., Lee, S.M., Madtes, D.K., McIntosh, M.W., McGarry Houghton, A.M., 2017.

Neutrophils dominate the immune cell composition in non-small cell lung cancer. Nat Commun 8. https://doi.org/10.1038/ncomms14381

Karlsson C, Karlsson MG. 2011 Effects of long-term storage on the detection of proteins, DNA, and mRNA in tissue microarray slides. J Histochem Cytochem. 59(12):1113-21

Kastenmüller, W., Torabi-Parizi, P., Subramanian, N., Lämmermann, T., Germain, R.N., 2012. A spatially-organized multicellular innate immune response in lymph nodes limits systemic pathogen spread. Cell 150, 1235–1248. https://doi.org/10.1016/j.cell.2012.07.021

Kessler HA, Trenholme GM, Harris AA, Levin S. Acute myopathy associated with influenza A/Texas/1/77 infection. Isolation of virus from a muscle biopsy specimen. 1980. JAMA. 243(5):461-2. PMID: 7351766.

Khan, S., Shafiei, M.S., Longoria, C., Schoggins, J.W., Savani, R.C., Zaki, H., 2021. SARS-CoV-2 spike protein induces inflammation via TLR2-dependent activation of the NF-κB pathway. Elife 10. https://doi.org/10.7554/eLife.68563

Khan, Y.S., Lynch, D.T., 2019. Histology, Lung - StatPearls - NCBI Bookshelf.

Khatri M, Dwivedi V, Krakowka S, Manickam C, Ali A, Wang L, Qin Z, Renukaradhya GJ, Lee CW., 2010. Swine influenza H1N1 virus induces acute inflammatory immune responses in pig lungs: a potential animal model for human H1N1 influenza virus. J Virol. 84(21):11210-8. doi: 10.1128/JVI.01211-10.

Kim, S., Kim, M.J., Park, D.Y., Chung, H.J., Kim, C.H., Yoon, J.H., Kim, H.J., 2015. Mitochondrial reactive oxygen species modulate innate immune response to influenza A virus in human nasal epithelium. Antiviral Res 119, 78–83. https://doi.org/10.1016/j.antiviral.2015.04.011

Klivleyeva, N.G., Glebova, T.I., Shamenova, M.G., Saktaganov, N.T., 2022a. Influenza A viruses circulating in dogs: A review of the scientific literature. Open Vet J 12, 676–687. https://doi.org/10.5455/OVJ.2022.v12.i5.12

Klivleyeva, N.G., Glebova, T.I., Shamenova, M.G., Saktaganov, N.T., 2022b. Influenza A viruses circulating in dogs: A review of the scientific literature. Open Vet J. https://doi.org/10.5455/OVJ.2022.v12.i5.12

Komohara, Y., Nakagawa, T., Ohnishi, K., Kosaki, Y., Saito, Y., Horlad, H., Fujiwara, Y., Takeya, M., 2017. Optimum immunohistochemical procedures for analysis of macrophages in human and mouse formalin fixed paraffin-embedded tissue samples, Journal of clinical and experimental hematopathology.

König, H.E., Liebich, H.G., 2008. Capítulo 8: Aparato respiratorio, in: Anatomía de Los Animales Domésticos. Tomo 2. Órganos, Sistema Circulatorio y Sistema Nervioso. Editorial Médica Panamericana, Madrid, pp. 81–100.

Kopf M, Brombacher F, Bachmann MF. Role of IgM antibodies versus B cells in influenza virus-specific immunity. Eur J Immunol. 2002 Aug;32(8):2229-36.

Kosai, K, Seki, M, Tanaka, A, Morinaga, Y, Imamura, Y, Izumikawa, K, Kakeya, H, Yamamoto, Y, Yanagihara, K, Tomono, K, Kohno, S. 2011. Increase of Apoptosis in a Murine Model for Severe Pneumococcal Pneumonia during Influenza A Virus Infection. Japanese journal of infectious diseases. 64. 451-7. 10.7883/yoken.64.451.

Krenacs, L., Himmelmann, A.W., Quintanilla-Martinez, L., Fest, T., Riva, A., Wellmann, A., Bagdi, E., Kehrl, J.H., Jaffe, E.S., Raffeld, M., 1998. Transcription factor B-cell-specific activator protein (BSAP) is differentially expressed in B cells and in subsets of B-cell lymphomas. Blood 92, 1308–1316. https://doi.org/10.1182/blood.v92.4.1308

Kuiken, T., van den Brand, J., van Riel, D., Pantin-Jackwood, M., Swayne, D.E., 2010. Comparative pathology of select agent influenza a virus infections. Vet Pathol 47, 893–914. https://doi.org/10.1177/0300985810378651

Kumar, V., Abbas, A. k, Aster, Jon.C., 2015a. Chapter 3, in: Pathologic Basis of Veterinary Disease. Fifth Edition. Elsevier, Philadelphia, Pennsylvania, p. 115.

Kumar, V., Abbas, A. k, Aster, Jon.C., 2015b. Chapter 5, in: Robbins and Cotran Pathologic Basis of Disease. Fifth Edition. Elsevier, Philadelphia, Pennsylvania, pp. 105–110.

Lam, J.H., Baumgarth, N., 2019. The Multifaceted B Cell Response to Influenza Virus. J. Immunol 202, 351–359. https://doi.org/10.4049/jimmunol.1801208.The

Lam, W.Y., Tang, J.W., Yeung, A.C.M., Chiu, L.C.M., Sung, J.J.Y., Chan, P.K.S., 2008. Avian Influenza Virus A/HK/483/97(H5N1) NS1 Protein Induces Apoptosis in Human Airway Epithelial Cells. J Virol 82, 2741–2751. https://doi.org/10.1128/jvi.01712-07

Lang, G., Gagnon, A., Geraci, J.R., 1981. Isolation of an Influenza A Virus from Seals. Arch Virol 68, 189–195.

Lee, I.W., Kim, Y. Il, Lim, G.J., Kwon, H. Il, Si, Y.J., Park, S.J., Kim, E.H., Kim, S.M., Nguyen, H.D., Song, M.S., Choi, Y.K., 2018. Comparison of the virulence and transmissibility of canine H3N2 influenza viruses and characterization of their canine adaptation factors article. Emerg Microbes Infect 7. https://doi.org/10.1038/s41426-017-0013-x

Lee, N., Chan, P.K.S., Wong, C.K., Wong, K.T., Choi, K.W., Joynt, G.M., Lam, P., Chan, M.C.W., Wong, B.C.K., Lui, G.C.Y., Sin, W.W.Y., Wong, R.Y.K., Lam, W.Y., Yeung, A.C.M., Leung, T.F., So, H.Y., Yu, A.W.Y., Sung, J.J.Y., Hui, D.S.C., 2011. Viral clearance and inflammatory response patterns in adults hospitalized for pandemic 2009 influenza A(H1N1) virus pneumonia. Antivir Ther 16, 237–247. https://doi.org/10.3851/IMP1722

Lekeux, P., Art, T., Hodgson, D.R., 2014. The respiratory system: Anatomy, physiology, and adaptations to exercise and training. The Athletic Horse: Principles and Practice of Equine Sports Medicine: Second Edition 125–154. https://doi.org/10.1016/B978-0-7216-0075-8.00018-6

Levene, R.E., Shrestha, S.D., Gaglia, M.M., 2021. The Influenza A Virus Host Shutoff Factor PA-X Is Rapidly Turned Over in a Strain-Specific Manner. J Virol 95. https://doi.org/10.1128/jvi.02312-20

Lewis, N.S., Daly, J.M., Russell, C.A., Horton, D.L., Skepner, E., Bryant, N.A., Burke, D.F., Rash, A.S., Wood, J.L.N., Chambers, T.M., Fouchier, R.A.M., Mumford, J.A., Elton, D.M., Smith, D.J., 2011. Antigenic and Genetic Evolution of Equine Influenza A (H3N8) Virus from 1968 to 2007. J Virol 85, 12742–12749. https://doi.org/10.1128/jvi.05319-11

Li, Y., Tang, X.X., 2021. Abnormal Airway Mucus Secretion Induced by Virus Infection. Front Immunol 12, 1–11. https://doi.org/10.3389/fimmu.2021.701443

Liang B, Hyland L, Hou S. Nasal-associated lymphoid tissue is a site of long-term virus-specific antibody production following respiratory virus infection of mice. J Virol. 2001 Jun;75(11):5416-20. doi: 10.1128/JVI.75.11.5416-5420.2001. PMID: 11333927; PMCID: PMC114951

Likos, A.M., Kelvin, D.J., Cameron, C.M., Rowe, T., Kuehnert, M.J., Norris, P.J., 2007. Influenza viremia and the potential for blood-borne transmission. Transfusion (Paris) 47, 1080–1088. https://doi.org/10.1111/j.1537-2995.2007.01264.x

Liu, H., Golebiewski, L., Dow, E.C., Krug, R.M., Javier, R.T., Rice, A.P., 2010. The ESEV PDZ-Binding Motif of the Avian Influenza A Virus NS1 Protein Protects Infected Cells from Apoptosis by Directly Targeting Scribble. J Virol 84, 11164–11174. https://doi.org/10.1128/jvi.01278-10

Liu, S.Y., Sanchez, D.J., Aliyari, R., Lu, S., Cheng, G., 2012. Systematic identification of type I and type II interferon-induced antiviral factors. Proc Natl Acad Sci U S A 109, 4239–4244. https://doi.org/10.1073/pnas.1114981109

Lloyd, L.E., Jonczyk, M., Jervis, C.M., Flack, D.J., Lyall, J., Foote, A., Mumford, J.A., Brown, I.H., Wood, J.L., Elton, D.M., 2011. Experimental transmission of avian-like swine H1N1 influenza virus between immunologically naïve and vaccinated pigs.

Influenza Other Respir Viruses 5, 357–364. https://doi.org/10.1111/j.1750-2659.2011.00233.x

López, A., 2007. Chapter 9. Respiratory System, Mediastinum and Pleurae., in: McGavin, M.D., Zachary, J.F. (Eds.), Pathologic Basis of Veterinary Disease. Fifth Edition. Mosby Elsevier, St Louis, Missouri, pp. 511–518.

López, A., 2001. Chapter 3. Respiratory System, Thoracic Cavity, and Pleura., in: McGavin, M.D., Carlton, W.W., Zachary, J.F. (Eds.), Thomson's Special Veterinary Pathology. Third Edition. Mosby Elsevier, St Louis, Missouri, pp. 170–171.

López, A., Martinson, S.A., 2017. Respiratory System, Mediastinum, and Pleurae. Pathologic Basis of Veterinary Disease Expert Consult 471-560.e1. https://doi.org/10.1016/B978-0-323-35775-3.00009-6

Lyoo KS, Kim JK, Jung K, Kang BK, Song D., 2014. Comparative pathology of pigs infected with Korean H1N1, H1N2, or H3N2 swine influenza A viruses. Virol J.:170. doi: 10.1186/1743-422X-11-170.

MacLachlan, N.J., Dubovi, E.J. (Eds.), 2011. Chapter 21 - Orthomyxoviridae, in: Fenner's Veterinary Virology (Fourth Edition). Academic Press, pp. 353–370.

Maines, T.R., Lu, X.H., Erb, S.M., Edwards, L., Guarner, J., Greer, P.W., Nguyen, D.C., Szretter, K.J., Chen, L.M., Thawatsupha, P., Chittaganpitch, M., Waicharoen, S., Nguyen, D.T., Nguyen, T., Nguyen, H.H., Kim, J.H., Hoang, L.T., Kang, C., Phuong, L.S., Lim, W., Zaki, S., Donis, R.O., Cox, N.J., Katz, J.M., Tumpey, T.M., 2005. Avian influenza (H5N1) viruses isolated from humans in Asia in 2004 exhibit increased virulence in mammals. J Virol 11788–11800.

Mair, T.S., Battern, E.H., Stokes, C.R., Bourne, F.J., 1987. The histological features of the immune system of the equine respiratory tract. J Comp Pathol 97.

Majno, G., Joris, I., 2004. Cells, tissues and disease. Principles of general pathology, 2nd ed. Oxford University Press, New York.

Major J, Crotta S, Llorian M, McCabe TM, Gad HH, Priestnall SL, Hartmann R, Wack A. Type I and III interferons disrupt lung epithelial repair during recovery from viral infection. Science. 2020 Aug 7;369(6504):712-717. doi: 10.1126/science.abc2061. Epub 2020 Jun 11. PMID: 32527928; PMCID: PMC7292500.

Marriott, A.C., Dove, B.K., Whittaker, C.J., Bruce, C., Ryan, K.A., Bean, T.J., Rayner, E., Pearson, G., Taylor, I., Dowall, S., Plank, J., Newman, E., Barclay, W.S., Dimmock, N.J., Easton, A.J., Hallis, B., Silman, N.J., Carroll, M.W., 2014. Low dose influenza virus challenge in the ferret leads to increased virus shedding and greater sensitivity to oseltamivir. PLoS One 9. https://doi.org/10.1371/journal.pone.0094090

Mclaughlin, R.F., San Francisco, W.S.T., Canada, C.R.O., 1961. Subgross Pulmonary Anatomy in Various. Journal of American Medical Association 175, 694–697.

McManus, J.F.A., 1946. Histological Demonstration of Mucin after Periodic Acid. Nature 158, 202. https://doi.org/10.1038/158202a0

Metersky ML, Masterton RG, Lode H, File TM Jr, Babinchak T. 2012. Epidemiology, microbiology, and treatment considerations for bacterial pneumonia complicating influenza. Int J Infect Dis. 5:e321-31. doi: 10.1016/j.ijid.2012.01.003. Epub 2012 Mar 2. PMID: 22387143.

Mina, M.J., Klugman, K.P., 2014. The role of influenza in the severity and transmission of respiratory bacterial disease. Lancet Respir Med. https://doi.org/10.1016/S2213-2600(14)70131-6

Mohan, H., 2005a. Cell Injury and Cellular Adaptations, in: Textbook of Pathology. Jaypee Brothers Medical Publishers, p. 32.

Mohan, H., 2005b. Cell Injury and Cellular Adaptations, in: Textbook of Pathology. Jaypee Brothers Medical Publishers, pp. 52–53.

Mohan, H., 2005c. Inflammation and healing, in: Textbook of Pathology. Jaypee Brothers Medical Publishers, pp. 171–179.

Mohan, H., 2005d. Haemodynamic disorders, in: Textbook of Pathology. Jaypee Brothers Medical Publishers, p. 109.

Mohan, H., 2005e. The respiratory system, in: Textbook of Pathology. Jaypee Brothers Medical Publishers, p. 469.

Mohan, H., 2005f. Haemodynamic disorders, in: Textbook of Pathology. Jaypee Brothers Medical Publishers, p. 97.

Montoya, M., Foni, E., Solórzano, A., Razzuoli, E., Baratelli, M., Bilato, D., Córdoba, L., del Burgo, M.A.M., Martinez, J., Martinez-Orellana, P., Chiapponi, C., Perlin, D.S., del Real, G., Amadori, M., 2017. Expression dynamics of innate immunity in influenza virus-infected swine. Front Vet Sci 4, 1–13. https://doi.org/10.3389/fvets.2017.00048

Morens, D.M., Taubenberger, J.K., 2010. Historical thoughts on influenza viral ecosystems, or behold a pale horse, dead dogs, failing fowl, and sick swine. Influenza Other Respir Viruses 4, 327–337. https://doi.org/10.1111/j.1750-2659.2010.00148.x

Mori I, Komatsu T, Takeuchi K, Nakakuki K, Sudo M, Kimura Y. 1995a. In vivo induction of apoptosis by influenza virus. J Gen Virol 76:2869 – 2873.

Mori, I., Komatsu, T., Takeuchi, K., Nakakuki, K., Sudo, M., Kimura, Y., 1995b. Viremia induced by influenza virus. Microb Pathog 19, 237–244. https://doi.org/10.1016/S0882-4010(95)90290-2

Morris, D.E., Cleary, D.W., Clarke, S.C., 2017. Secondary bacterial infections associated with influenza pandemics. Front Microbiol 8, 1–17. https://doi.org/10.3389/fmicb.2017.01041

Mueller Brown K, Le Sage V, French AJ, Jones JE, Padovani GH, Avery AJ, Schultz-Cherry S, Rosch JW, Hiller NL, Lakdawala SS. 2022. Secondary infection with Streptococcus pneumoniae decreases influenza virus replication and is linked to severe disease. FEMS Microbes. 3:xtac007. doi: 10.1093/femsmc/xtac007. PMID: 35392116; PMCID: PMC8981988.

Mumford, J.A., Hannant, D., Jessett, D.M., 1990. Experimental infection of ponies with equine influenza (H3N8) viruses by intranasal inoculation or exposure to aerosols. Equine Vet J 22, 93–98. https://doi.org/10.1111/j.2042-3306.1990.tb04217.x

Muranaka, M., Yamanaka, T., Katayama, Y., Niwa, H., Oku, K., Matsumura, T., Oyamada, T., 2012. Time-related pathological changes in horses experimentally inoculated with equine influenza a virus. J Equine Sci 23, 17–26. https://doi.org/10.1294/jes.23.17

Murcia, P.R., Baillie, G.J., Daly, J., Elton, D., Jervis, C., Mumford, J.A., Newton, R., Parrish, C.R., Hoelzer, K., Dougan, G., Parkhill, J., Lennard, N., Ormond, D., Moule, S., Whitwham, A., McCauley, J.W., McKinley, T.J., Holmes, E.C., Grenfell, B.T., Wood, J.L.N., 2010. Intra- and Interhost Evolutionary Dynamics of Equine Influenza Virus. J Virol 84, 6943–6954. https://doi.org/10.1128/jvi.00112-10

Murcia, P.R., Baillie, G.J., Stack, J.C., Jervis, C., Elton, D., Mumford, J.A., Daly, J., Kellam, P., Grenfell, B.T., Holmes, E.C., Wood, J.L.N., 2013. Evolution of Equine Influenza Virus in Vaccinated Horses. J Virol 87, 4768–4771. https://doi.org/10.1128/jvi.03379-12

Murphy, F., Gibbs, E., Horzinek, M., Studdert, M., 1999. Veterinary virology. Veterinary Virology Academic Press, San Diego.

Myers, C., Wilson, W.D., 2006. Equine Influenza Virus. Clinical Techniques in Equine Practice 5, 187–196. https://doi.org/10.1053/j.ctep.2006.03.013

Myers MA, Smith AP, Lane LC, Moquin DJ, Aogo R, Woolard S, Thomas P, Vogel P, Smith AM., 2021. Dynamically linking influenza virus infection kinetics, lung injury, inflammation, and disease severity. Elife.;10:e68864. doi: 10.7554/eLife.68864. PMID: 34282728; PMCID: PMC8370774.

Naficy, K., 1963. Human influenza infection with proved viremia. N Engl J Med 269, 946–6.

Nakamura, M., Matute-Bello, G., Liles, W.C., Hayashi, S., Kajikawa, O., Lin, S.M., Frevert, C.W., Martin, T.R., 2004. Differential response of human lung epithelial cells to Fas-induced apoptosis. American Journal of Pathology 164, 1949–1958. https://doi.org/10.1016/S0002-9440(10)63755-8

Narasaraju T, Ng HH, Phoon MC, Chow VT. MCP-1 antibody treatment enhances damage and impedes repair of the alveolar epithelium in influenza pneumonitis. Am J Respir Cell Mol Biol. 2010 Jun;42(6):732-43. doi: 10.1165/rcmb.2008-0423OC. Epub 2009 Jul 17. PMID: 19617401; PMCID: PMC2891499.

Nayak DP, Twiehaus MJ, Kelley GW, Underdahl NR., 1965. Immunocytologic and histopathologic development of experimental swine influenza infection in pigs. Am J Vet Res. 26(115):1271-83. PMID: 5327087.

Neuhäuser, M. 2011. "Wilcoxon–Mann–Whitney Test." In M. Lovric (Ed.), *International Encyclopedia of Statistical Science*. Springer.

Nishiura, H., Satou, K., 2010. Potential effectiveness of public health interventions during the equine influenza outbreak in racehorse facilities in Japan, 2007. Transbound Emerg Dis. https://doi.org/10.1111/j.1865-1682.2010.01134.x

Numajiri, A., Mibayashi, M., Nagata, K., 2006. Stimulus-Dependent and Domain-Dependent Cell Death Acceleration by an IFN-Inducible Protein, Human MxA. Journal of Interferon & Cytokine Research 26.

Numajiri Haruki, A., Naito, T., Nishie, T., Saito, S., Nagata, K., 2011. Interferon-inducibleantiviral protein MxA enhances cell death triggered by endoplasmic reticulumstress. J Interferon Cytokine Res 31, 847–56.

Nüssing S, Sant S, Koutsakos M, Subbarao K, Nguyen THO, Kedzierska K. 2018. Innate and adaptive T cells in influenza disease. Front Med. 12(1):34-47. doi: 10.1007/s11684-017-0606-8. Epub 2018 Jan 20. PMID: 29352371.

Ogiwara H, Yasui F, Munekata K, Takagi-Kamiya A, Munakata T, Nomura N, Shibasaki F, Kuwahara K, Sakaguchi N, Sakoda Y, Kida H, Kohara M., 2014. Histopathological evaluation of the diversity of cells susceptible to H5N1 virulent avian influenza virus. Am J Pathol. 184(1):171-83.

OIE-WOAH, 2011. Terrestrial Code Online Access - WOAH - World Organisation for Animal Health.

Oikawa, M., Kamada, M., Yoshikawa~, Y., Yoshikawa~, T., 1994. Pathology of Equine Pneumonia Associated with Transport and Isolation of Streptococcus equi subsp. zooepidemicus, J. Comp. Path.

Okahashi N, Sumitomo T, Nakata M, Kawabata S. 2022.Secondary streptococcal infection following influenza. Microbiol Immunol. 66: 253 263. https://doi.org/10.1111/1348-0421.12965

Orlowsky, E.W., Kraus, V.B., 2015. The role of innate immunity in osteoarthritis: When our first line of defense goes on the offensive. Journal of Rheumatology. https://doi.org/10.3899/jrheum.140382

Ottolini MG, Blanco JC, Eichelberger MC, Porter DD, Pletneva L, Richardson JY, Prince GA., 2005. The cotton rat provides a useful small-animal model for the study of influenza virus pathogenesis. *J Gen Virol.*86:2823–2830

Paillot, R., Pitel, P.H., Pronost, S., Legrand, L., Fougerolle, S., Jourdan, M., Marcillaud-Pitel, C., 2019. Florida clade 1 equine influenza virus in France. Veterinary Record 184, 101. https://doi.org/10.1136/vr.l1203

Paillot, R., Prowse, L., Montesso, F., Stewart, B., Jordon, L., Newton, J.R., Gilkerson, J.R., 2013. Duration of equine influenza virus shedding and infectivity in immunised horses after experimental infection with EIV A/eq2/Richmond/1/07. Vet Microbiol 166, 22–34. https://doi.org/10.1016/j.vetmic.2013.04.027

Parrish, C.R., Kawaoka, Y., 2005. THE ORIGINS OF NEW PANDEMIC VIRUSES: The Acquisition of New Host Ranges by Canine Parvovirus and Influenza A Viruses.

Annu Rev Microbiol 59, 553–586. https://doi.org/10.1146/annurev.micro.59.030804.121059

Partin JC, Partin JS, Schubert WK, Jacobs R, Saalfeld K. Isolation of influenza virus from liver and muscle biopsy specimens from a surviving case of Reye's syndrome. 1976. Lancet. 2(7986):599-602. doi: 10.1016/s0140-6736(76)90667-x. PMID: 61342

Patterson-Kane, J.C., Carrick, J.B., Axon, J.E., Wilkie, I., Begg, A.P., 2008. The pathology of bronchointerstitial pneumonia in young foals associated with the first outbreak of equine influenza in Australia. Equine Vet J 40, 199–203. https://doi.org/10.2746/042516408X292214

Pavlovic, J., Zürcher, T., Haller, O., Staeheli, P., 1990. Resistance to influenza virus and vesicular stomatitis virus conferred by expression of human MxA protein. J Virol 64, 3370–3375. https://doi.org/10.1128/jvi.64.7.3370-3375.1990

Payungporn, S., Cynda Crawford, P., Kouo, T.S., Chen, L., Pompei, J., Castleman, W.L., Dubovi, E.J., Katz, J.M., Donis, R.O., 2008. Influenza A Virus (H3N8) in Dogs with Respiratory Disease, Florida. Diseases 14, 902–908.

Peek, S.F., Landolt, G., Karasin, A.I., Slack, J.A., Steinberg, H., Semrad, S.D., Olsen, C.W., 2004. Acute Respiratory Distress Syndrome and Fatal Interstitial Pneumonia Associated with Equine Influenza in a Neonatal Foal. J Vet Intern Med 18, 132–134. https://doi.org/10.1892/0891-6640(2004)18<132:ARDSAF>2.0.CO;2

Perglione, C.O., Gildea, S., Rimondi, A., Miño, S., Vissani, A., Carossino, M., Cullinane, A., Barrandeguy, M., 2016. Epidemiological and virological findings during multiple outbreaks of equine influenza in South America in 2012. Influenza Other Respir Viruses 10, 37–46. https://doi.org/10.1111/irv.12349

Perroncito, E., 1878. Epizoozia tifoide nei gallinacei. Annali della Academia d'Agricoltura di Torino 81, 87–126.

Plopper, C.G., Adams, D.R., 2006. Respiratory System, in: Eurell, J.A., Frappier, B.L. (Eds.), Dellmann's Textbook of Veterinary Histology. Wiley-Blackwell, Oxford, UK, p. 164.

Purves, D., Augustine, G., Fitzpatric, D., 2001. The Olfactory Epithelium and Olfactory Receptor Neurons - Neuroscience - NCBI Bookshelf. Neuroscience.

Radostits, O., Gray, C., Blood, D., Hinchcliff, K., 2003. Equine influenza., in: Radostits OM, Gray CC, Blood DC and Hinchcliff KW (Eds.), Veterinary Medicine, A Text Book of Diseases of Cattle, Sheep, Pigs, Goats and Horses. Elsevier Saunders, New York, NY, pp. 1322–1328.

Rajao, D.S., Anderson, T.K., Gauger, P.C., Vincent, A.L., 2014. Pathogenesis and Vaccination of Influenza A Virus in Swine, in: Compans, R.W., Oldstone, M.B.A. (Eds.), Influenza Pathogenesis and Control - Volume I. pp. 307–327.

Raynard, R.S., Murray, A.G., Gregory, A., 2001. Infectious salmon anaemia virus in wild fish from Scotland. Dis Aquat Organ 46, 93–100. https://doi.org/10.3354/dao046093

Razvi, E.S., Welsh, R.M., 1995. Apoptosis in viral infections. Res., Adv. Virus 45, 1–60.

Read, A.J., Finlaison, D.S., Gu, X., Davis, R.J., Arzey, K.E., Kirkland, P.D., 2011. Application of real-time PCR and ELISA assays for equine influenza virus to determine the duration of viral RNA shedding and onset of antibody response in naturally infected horses. Aust Vet J 89, 42–43. https://doi.org/10.1111/j.1751-0813.2011.00740.x

Reed SE. 1969. Persistent respiratory virus infection in tracheal organ cultures. Br J Exp Pathol. 50(4):378-88. PMID: 4308840; PMCID: PMC2072110

Reuman, P.D., Ayoub, E.M., Small, P.A., 1983. Influenza infection in the infant mouse. Pediatr Res 17, 338–343. https://doi.org/10.1203/00006450-198305000-00006

Reynaud, P., Ahmed, E., Serre, I., Knabe, L., Bommart, S., Suehs, C., Vachier, I., Berthet, J.P., Romagnoli, M., Vernisse, C., Mallet, J.P., Gamez, A.S., Bourdin, A., 2021. Club Cell Loss as a Feature of Bronchiolization in ILD. Front Immunol 12, 1–7. https://doi.org/10.3389/fimmu.2021.630096

Rimmelzwaan GF, Kuiken T, van Amerongen G, Bestebroer TM, Fouchier RA, Osterhaus AD., 2003. A primate model to study the pathogenesis of influenza A (H5N1) virus infection. *Avian Dis.*47:931–933.

Robinson KM, Kolls JK, Alcorn JF. The immunology of influenza virus-associated bacterial pneumonia. 2015. Curr Opin Immunol. 34:59-67. doi: 10.1016/j.coi.2015.02.002. Epub 2015 Feb 24. PMID: 25723597; PMCID: PMC4444379.

Rock, K.L., Kono, H., 2007. The Inflammatory Response to Cell Death. Annual Review of Pathology: Mechanisms of Disease 0, 070817085622001. https://doi.org/10.1146/annurev.pathol.3.121806.151456

Rong, Z., Mai, H., Kapoor, S., Puelles, V.G., Czogalla, J., Schädler, J., Vering, J., Delbridge, C., Steinke, H., Frenzel, H., Schmidt, K., Sehnaz Caliskan, Ö., Martin Wettengel, J., Cherif, F., Ali, M., Ilgin Kolabas, Z., Ulukaya, S., Horvath, I., Zhao, S., Krahmer, N., Tahirovic, S., Önder Yildirim, A., Huber, T.B., Ondruschka, B., Bechmann, I., Ebert, G., Protzer, U., Singh Bhatia, H., Hellal, F., Ertürk, A., 2023. SARS-CoV-2 Spike Protein Accumulation in the Skull-Meninges-Brain Axis: Potential Implications for Long-Term Neurological Complications in post-COVID-19. https://doi.org/10.1101/2023.04.04.535604

Rosas, C., Van de Walle, G.R., Metzger, S.M., Hoelzer, K., Dubovi, E.J., Kim, S.G., Parrish, C.R., Osterrieder, N., 2008. Evaluation of a vectored equine herpesvirus type 1 (EHV-1) vaccine expressing H3 haemagglutinin in the protection of dogs against canine influenza. Vaccine 26, 2335–2343. https://doi.org/10.1016/j.vaccine.2008.02.064

Rossios, C., Pavlidis, S., Gibeon, D., Mumby, S., Durham, A., Ojo, O., Horowitz, D., Loza, M., Baribaud, F., Rao, N., Chung, K.F., Adcock, I.M., 2017. Impaired innate immune gene profiling in airway smooth muscle cells from chronic cough patients. Biosci Rep 37. https://doi.org/10.1042/BSR20171090

Rowe, T., León, A.J., Crevar, C.J., Carter, D.M., Xu, L., Ran, L., Fang, Y., Cameron, C.M., Cameron, M.J., Banner, D., Ng, D.C.K., Ran, R., Weirback, H.K., Wiley, C.A., Kelvin, D.J., Ross, T.M., 2010. Modeling host responses in ferrets during A/California/07/2009 influenza infection. Virology 401, 257–265. https://doi.org/10.1016/j.virol.2010.02.020

Russell, W.M.S., Burch, R.L., 1959. The principles of humane experimental technique. Universities Federation for Animal Welfare.

Sack, A., Cullinane, A., Daramragchaa, U., Chuluunbaatar, M., Gonchigoo, B., Gray, G.C., 2019. Equine influenza virus- A neglected, reemergent disease threat. Emerg Infect Dis 25, 1185–1191. https://doi.org/10.3201/eid2506.161846

Sagiv, A., Bar-Shai, A., Levi, N., Hatzav, M., Zada, L., Ovadya, Y., Roitman, L., Manella, G., Regev, O., Majewska, J., Vadai, E., Eilam, R., Feigelson, S.W., Tsoory, M., Tauc, M., Alon, R., Krizhanovsky, V., 2018. p53 in Bronchial Club Cells Facilitates Chronic Lung Inflammation by Promoting Senescence. Cell Rep 22, 3468–3479. https://doi.org/10.1016/j.celrep.2018.03.009

Salvadori, S., Gansbacher, B., Pizzimenti, a M., Zier, K.S., 1994. Abnormal signal transduction by T cells of mice with parental tumors is not seen in mice bearing IL-2-secreting tumors. J Immunol 153, 5176–5182.

Sameroff, S., Tokarz, R., Jain, K., Oleynik, A., Carrington, C.V.F., Lipkin, W.I., Oura, C.A.L., 2021. Novel quaranjavirus and other viral sequences identified from ticks parasitizing hunted wildlife in Trinidad and Tobago. Ticks Tick Borne Dis. https://doi.org/10.1016/j.ttbdis.2021.101730

Sarasola, P., Taylor, D.J., Love, S., McKellar, Q.A., 1992. Secondary bacterial infections following an outbreak of equine influenza. Veterinary Record 131, 441–442.

Scherzad, A., Hagen, R., Hackenberg, S., 2019. Current understanding of nasal epithelial cell mis-differentiation. J Inflamm Res 12, 309–317. https://doi.org/10.2147/JIR.S180853

Scholtens, R.G., Steele, J.H., Dowdle, W.R., Yarbrough, W.B., Robinson, R.Q., 1964. U.S. Epizootic of Equine Influenza, 1963. Public Health Rep 79, 393–402. https://doi.org/10.2307/4592142

Schorr, E., Hinshaw, V.S., 1994. Use of polymerase chain reaction to detect swine influenza virus in nasal specimens. Am J Vet Res 952–956.

Sell S, Guest I, McKinstry KK, Strutt TM, Kohlmeier JE, Brincks E, Tighe M, Blackman MA, Woodland DL, Dutton RW, Swain SL. 2014. Intraepithelial T-cell cytotoxicity, induced bronchus-associated lymphoid tissue, and proliferation of pneumocytes in experimental mouse models of influenza. Viral Immunol. 27(10):484-96. doi: 10.1089/vim.2014.0077. PMID: 25479178; PMCID: PMC4259197.

Shen P, Fillatreau S. Antibody-independent functions of B cells: a focus on cytokines. Nat Rev Immunol. 2015 Jul;15(7):441-51. doi: 10.1038/nri3857. Epub 2015 Jun 12. PMID: 26065586.

Shubin, A. V, Demidyuk, I. V, Komissarov, A.A., Rafieva, L.M., Kostrov, S. V, 2016. Cytoplasmic vacuolization in cell death and survival.

Siegers JY, Ferreri L, Eggink D, Veldhuis Kroeze EJB, Te Velthuis AJW, van de Bildt M, Leijten L, van Run P, de Meulder D, Bestebroer T, Richard M, Kuiken T, Lowen AC, Herfst S, van Riel D. 2023. Evolution of highly pathogenic H5N1 influenza A virus in the central nervous system of ferrets. PLoS Pathog. Mar 10;19(3):e1011214. doi: 10.1371/journal.ppat.1011214

Singh, R.K., Dhama, K., Karthik, K., Khandia, R., Munjal, A., Khurana, S.K., Chakraborty, S., Malik, Y.S., Virmani, N., Singh, R., Tripathi, B.N., Munir, M., van der Kolk, J.H., 2018. A comprehensive review on equine influenza virus: Etiology, epidemiology, pathobiology, advances in developing diagnostics, vaccines, and control strategies. Front Microbiol 9, 1–26. https://doi.org/10.3389/fmicb.2018.01941

Smyth, G.B., Dagley, K., Tainsh, J., 2011. Insights into the economic consequences of the 2007 equine influenza outbreak in Australia. Aust Vet J 89, 151–158. https://doi.org/10.1111/j.1751-0813.2011.00777.x

Somerville, L., Cardani, A., Braciale, T.J., 2020. Alveolar Macrophages in Influenza A Infection Guarding the Castle with Sleeping Dragons. Infect Dis Ther 1. https://doi.org/10.31038/idt.2020114

Song, D., Kang, B., Lee, C., Jung, K., Ha, G., Kang, D., Park, S., Park, B., Oh, J., 2008. Transmission of Avian Influenza Virus (H3N2) to Dogs. Emerg Infect Dis 14, 741–746.

Sreta D, Kedkovid R, Tuamsang S, Kitikoon P, Thanawongnuwech R. 2009. Pathogenesis of swine influenza virus (Thai isolates) in weanling pigs: an experimental trial. Virol J. 6:34. doi: 10.1186/1743-422X-6-34. PMID: 19317918; PMCID: PMC2678088.

Staeheli, P., 1990. Interferon-induced proteins and the antiviral state. Adv. Virus Res. 38, 147–200.

Stevens, A., Lowe, J., Scott, I., 2009. Core Pathology, 3rd ed. Mosby Elsevier, Edinburgh.

Su, S., Tian, J., Hong, M., Zhou, P., Lu, G., Zhu, H., Zhang, G., Lai, A., Li, S., 2015. Global and quantitative proteomic analysis of dogs infected by avian-like H3N2 canine influenza virus. Front Microbiol 6, 1–15. https://doi.org/10.3389/fmicb.2015.00228

Sun H, Li H, Tong Q, Han Q, Liu J, Yu H, Song H, Qi J, Li J, Yang J, Lan R, Deng G, Chang H, Qu Y, Pu J, Sun Y, Lan Y, Wang D, Shi Y, Liu WJ, Chang KC, Gao GF, Liu J. 2023. Airborne transmission of human-isolated avian H3N8 influenza virus between ferrets. Cell. Sep 14;186(19):4074-4084.e11. doi: 10.1016/j.cell.2023.08.011.

Sutherland, L.M., Edwards, Y.S., Murray, A.W., 2001. Alveolar type II cell apoptosis, Comparative Biochemistry and Physiology Part A.

Sutton, G.A., Viel, L., Suzanne Carman, P., Lynn Boag, B., 1997. Study of the Duration and Distribution of Equine Influenza Virus Subtype 2 (H3N8) Antigens in Experimentally Infected Ponies in vivo. Canadian Journal of Veterinary Research 61, 113–120.

Swain, S.L., McKinstry, K.K., Strutt, T.M., 2012. Expanding roles for CD4 + T cells in immunity to viruses. Nat Rev Immunol 12, 136–148. https://doi.org/10.1038/nri3152

Szabo, S.J., Kim, S.T., Costa, G.L., Zhang, X., Fathman, C.G., Glimcher, L.H., 2000. A novel transcription factor, T-bet, directs Th1 lineage commitment. Cell 100, 655–669. https://doi.org/10.1016/S0092-8674(00)80702-3

Szarek, J.L., Stewart, N.L., Spurlock, B., Schneider, C., 1995. Sensory nerve- and neuropeptide-mediated relaxation responses in airways of Sprague-Dawley rats. J Appl Physiol 78, 1679–1687. https://doi.org/10.1152/jappl.1995.78.5.1679

Tamura S, Iwasaki T, Thompson AH, Asanuma H, Chen Z, Suzuki Y, Aizawa C, Kurata T. Antibody-forming cells in the nasal-associated lymphoid tissue during primary influenza virus infection. J Gen Virol. 1998 Feb;79 (Pt 2):291-9. doi: 10.1099/0022-1317-79-2-291. PMID: 9472613

Tang X., Chong K., 2009. Histopathology and growth kinetics of influenza viruses (H1N1 and H3N2) in the upper and lower airways of guinea pigs Journal of General Virology 90(2), 386-391.

Takizawa, T., Takishima, T., Katori, R., 1965. Structure and function of the lung. Kekkaku(Tuberculosis) 40, 315–336. https://doi.org/10.11400/kekkaku1923.40.8_315

Tang X, Chong KT. 2009. Histopathology and growth kinetics of influenza viruses (H1N1 and H3N2) in the upper and lower airways of guinea pigs. J Gen Virol. 90(Pt 2):386-391. doi: 10.1099/vir.0.007054-0. PMID: 19141447.

Tangwangvivat R, Chaiyawong S, Nonthabenjawan N, Charoenkul K, Janethanakit T, Udom K, Kesdangsakonwut S, Tantilertcharoen R, Thontiravong A, Amonsin A., 2022. Transmission and pathogenicity of canine H3N2 influenza virus in dog and guinea pig models. Virol J. 19(1):162. doi: 10.1186/s12985-022-01888-x.

Taubenberger, J.K., Morens, D.M., 2008. The Patology of Influenza Infections. Annu Rev Pathol 3, 499–522.

Tavares, L.P., Teixeira, M.M., Garcia, C.C., 2017. The inflammatory response triggered by Influenza virus: a two edged sword. Inflammation Research 66, 283–302. https://doi.org/10.1007/s00011-016-0996-0

Tilley, A.E., Walters, M.S., Shaykhiev, R., Crystal, R.G., 2015. Cilia dysfunction in lung disease. Annu Rev Physiol 77, 379–406. https://doi.org/10.1146/annurev-physiol-021014-071931

Timoney, P.J., 1996. Equine influenza. Comp Immunol Microbiol Infect Dis 19, 205–211. https://doi.org/10.1016/0147-9571(96)00006-9

Topham DJ, Tripp RA, Doherty PC., 1997. CD8+ T cells clear influenza virus by perforin or Fas-dependent processes. J Immunol. 1;159(11):5197-200. PMID: 9548456.

Tsuda, Y., Weisend, C., Martellaro, C., Feldmann, F., Haddock, E., 2017. Pathogenic analysis of the pandemic 2009 H1N1 influenza A viruses in ferrets 1453–1460. https://doi.org/10.1292/jvms.16-0619

Tumova, B., Fiserova-Sovinova, O., 1959. Properties of influenza viruses A/Asia/57 and A-equi/Praha/56. I. Agglutination of red blood cells. Bull World Health Organ 20, 445–454.

Tumpey, T.M., Maines, T.R., Van Hoeven, N., Glaser, L., Solórzano, A., Pappas, C., Cox, N.J., Swayne, D.E., Palese, P., Katz, J.M., García-Sastre, A., 2007. A two-amino acid change in the hemagglutinin of the 1918 influenza virus abolishes transmission. Science (1979) 315, 655–659.

van den Brand, J.M.A., Stittelaar, K.J., van Amerongen, G., Rimmelzwaan, G.F., Simon, J., de Wit, E., Munster, V., Bestebroer, T., Fouchier, R.A., Kuiken, T., Osterhaus, A.D., 2010. Severity of pneu- monia due to new H1N1 influenza virus in ferrets is

intermediate between that due to seasonal H1N1 virus and highly pathogenic avian influenza H5N1 virus. Journal of Infectious Diseases 201, 993–999.

van der Sluijs, K.F., van der Poll, T., Lutter, R., Juffermans, N.P., Schultz, M.J., 2010. Bench-to-bedside review: Bacterial pneumonia with influenza - pathogenesis and clinical implications. Crit Care 14.

Van Epps, H.L., 2006. Influenza: Exposing the true killer. Journal of Experimental Medicine 203, 803. https://doi.org/10.1084/jem.2034fta

van Maanen, C., Cullinane, A., 2002. Equine influenza virus infections: An update. Veterinary Quarterly 24, 79–94. https://doi.org/10.1080/01652176.2002.9695127

Van Riel, D., Den Bakker, M.A., Leijten, L.M.E., Chutinimitkul, S., Munster, V.J., De Wit, E., Rimmelzwaan, G.F., Fouchier, R.A.M., Osterhaus, A.D.M.E., Kuiken, T., 2010. Seasonal and pandemic human influenza viruses attach better to human upper respiratory tract epithelium than avian influenza viruses. American Journal of Pathology 176, 1614–1618. https://doi.org/10.2353/ajpath.2010.090949

van Riel D, Rimmelzwaan GF, van Amerongen G, Osterhaus AD, Kuiken T. Highly pathogenic avian influenza virus H7N7 isolated from a fatal human case causes respiratory disease in cats but does not spread systemically. Am J Pathol. 2010 Nov;177(5):2185-90. doi: 10.2353/ajpath.2010.100401. Epub 2010 Sep 16. PMID: 20847292; PMCID: PMC2966778.

Verhelst J, Parthoens E, Schepens B, Fiers W, Saelens X. 2012. Interferon-inducible protein MX1 inhibits influenza virus by interfering with functional viral ribonucleoprotein complex assembly. J Virol. 2012. 86(24):13445-55

Vernau, W., Moore, P.F., 1999. an immunophenotypic study of canine leukaemias and preliminary assessment of clonality by PCR_VetImmImmunopath1999.PDF 69, 145–164.

Vidaña B, Brookes SM, Everett HE, Garcon F, Nuñez A, Engelhardt O, Major D, Hoschler K, Brown IH, Zambon M. 2021. Inactivated pandemic 2009 H1N1 influenza A virus human vaccines have different efficacy after homologous challenge in the ferret model. Influenza Other Respir Viruses. Jan;15(1):142-153. doi: 10.1111/irv.12784.

Voorhees, I.E.H., Glaser, A.L., Toohey-Kurth, K., Newbury, S., Dalziel, B.D., Dubovi, E.J., Poulsen, K., Leutenegger, C., Willgert, K.J.E., Brisbane-Cohen, L., Richardson-Lopez, J., Holmes, E.C., Parrish, C.R., 2017. Spread of canine influenza a(H3N2) virus, United States. Emerg Infect Dis 23, 1950–1957. https://doi.org/10.3201/eid2312.170246

Wang, J., Nikrad, M.P., Phang, T., Gao, B., Alford, T., Ito, Y., Edeen, K., Travanty, E.A., Kosmider, B., Hartshorn, K., Mason, R.J., 2011. Innate immune response to influenza A virus in differentiated human alveolar type II cells. Am J Respir Cell Mol Biol 45, 582–591. https://doi.org/10.1165/rcmb.2010-0108OC

Wang, X., Tan, J., Zoueva, O., Zhao, J., Ye, Z., Hewlett, I., 2014. Novel pandemic influenza A (H1N1) virus infection modulates apoptotic pathways that impact its replication in A549 cells. Microbes Infect 16, 178–186. https://doi.org/10.1016/j.micinf.2013.11.003

Wansleeben, C., Barkauskas, C.E., Rock, J.R., Hogan, B.L.M., 2013. Stem cells of the adult lung: Their development and role in homeostasis, regeneration, and disease. Wiley Interdiscip Rev Dev Biol 2, 131–148. https://doi.org/10.1002/wdev.58

Watson, J., Daniels, P., Kirkland, P., Carroll, A., Jeggo, M., 2011. The 2007 outbreak of equine influenza in Australia: lessons learned Quarantine requirements in Australia Equine influenza in Japan in 2007 Policy and practice of quarantine in Australia Initial events in the 2007 equine influenza outbreak in Australia. Rev. sci. tech. Off. int. Epiz. 30, 87–93.

Watson, C.E., Bell C., Toohey-Kurth. 2017. H3N2 Canine influenza virus infection in a dog. Veterinary Pathology 54(3), 527-530.

Wattrang, E., Jessett, D.M., Yates, P., Fuxler, L., Hannant, D., 2003. Experimental infection of ponies with equine influenza A2 (H3N8) virus strains of different pathogenicity elicits varying interferon and interleukin-6 responses. Viral Immunol 16, 57–67. https://doi.org/10.1089/088282403763635456

Webster, R.G., 1993. Are equine 1 influenza viruses still present in horses? Equine Vet J 25, 537–538. https://doi.org/10.1111/j.2042-3306.1993.tb03009.x

Wencker, M., Turchinovich, G., Di Marco Barros, R., Deban, L., Jandke, A., Cope, A., Hayday, A.C., 2014. Innate-like T cells straddle innate and adaptive immunity by altering antigen-receptor responsiveness. Nat Immunol 15, 80–87. https://doi.org/10.1038/ni.2773

West, J.B., Luks, A.M., 2016. West's respiratory phisiology: the essentials, 10th ed.

Whitley E, Ball J. Statistics review 6: Nonparametric methods. Crit Care. 2002 Dec;6(6):509-13. doi: 10.1186/cc1820. Epub 2002 Sep 13. PMID: 12493072; PMCID: PMC153434.

Whitlock, F., Grewar, J., Newton, R., 2023. An epidemiological overview of the equine influenza epidemic in Great Britain during 2019. Equine Vet J 55, 153–164. https://doi.org/10.1111/evj.13874

Willoughby, R., Ecker, G., McKee, S., Riddolls, L., Vernaillen, C., Dubovi, E., Lein, D., Mahony, J.B., Chernesky, M., Nagy, E., 1992. The effects of equine rhinovirus, influenza virus and herpesvirus infection on tracheal clearance rate in horses. Can J Vet Res 56, 115–121.

Wolf AI, Mozdzanowska K, Quinn WJ 3rd, Metzgar M, Williams KL, Caton AJ, Meffre E, Bram RJ, Erickson LD, Allman D, Cancro MP, Erikson J. Protective antiviral antibody responses in a mouse model of influenza virus infection require TACI. J Clin Invest. 2011 Oct;121(10):3954-64. doi: 10.1172/JCI57362. Epub 2011 Sep 1. PMID: 21881204; PMCID: PMC3195469.

Woolf, N., 1998a. Cell tissue and death, in: Pathology Basic and Systemic. Saunders Elsevier, London, pp. 29–34.

Woolf, N., 1998b. Non-neoplastic disturbances in cell growth and proliferation, in: Pathology Basic and Systemic. Saunders Elsevier, London, p. 240.

Woolf, N., 1998c. Abnormal accumulations of fluid and disturbances of blood distribution, in: Pathology Basic and Systemic. Saunders Elsevier, London, p. 222.

Wu NH, Yang W, Beineke A, Dijkman R, Matrosovich M, Baumgärtner W, Thiel V, Valentin-Weigand P, Meng F, Herrler G. 2016. The differentiated airway epithelium infected by influenza viruses maintains the barrier function despite a dramatic loss of ciliated cells. Sci Rep. 6:39668. doi: 10.1038/srep39668. PMID: 28004801; PMCID: PMC5177954.

Xie H, Zhang R, Guo R, Zhang Y, Zhang J, Li H, Fu Q, Wang X. 2024. Characterization of AI-2/LuxS quorum sensing system in biofilm formation, pathogenesis of Streptococcus equi subsp. zooepidemicus. Front Cell Infect Microbiol. Feb 6;14:1339131

Yamanaka, T., Nemoto, M., Tsujimura, K., Kondo, T., Matsumura, T., 2009. Interspecies transmission of equine influenza virus (H3N8) to dogs by close contact with experimentally infected horses. Vet Microbiol 139, 351–355.

Yamanaka, T., Niwa, H., Tsujimura, K., Kondo, T., Matsumura, T., 2008. Epidemic of equine influenza among vaccinated racehorses in Japan in 2007. Journal of Veterinary Medical Science 70, 623–625. https://doi.org/10.1292/jvms.70.623

Yen, H.-L., Lipatov, A.S., Ilyushina, N.A., Govorkova, E.A., Franks, J., Yilmaz, N., Douglas, A., Hay, A., Krauss, S., Rehg, J.E., Hoffmann, E., Webster, R.G., 2007. Inefficient Transmission of H5N1 Influenza Viruses in a Ferret Contact Model. J Virol 81, 6890–6898. https://doi.org/10.1128/jvi.00170-07

Zens, K.D., Farber, D.L., 2015. Memory CD4 T cells in influenza. Curr Top Microbiol Immunol. https://doi.org/10.1007/82_2014_401

Zhang, L., Zhao, S., Yuan, L.J., Wu, H.M., Jiang, H., Zhao, S.M., Luo, G., Xue, X.D., 2015. Autophagy regulates hyperoxia-induced intracellular accumulation of surfactant protein C in alveolar type II cells. Mol Cell Biochem 408, 181–189. https://doi.org/10.1007/s11010-015-2494-z

Zhirnov, O.P., Konakova, T.E., Wolff, T., Klenk, H.-D., 2002. NS1 Protein of Influenza A Virus Down-Regulates Apoptosis. J Virol 76, 1617–1625. https://doi.org/10.1128/jvi.76.4.1617-1625.2002

Zhou L, Sun H, Song S, Liu J, Xia Z, Sun Y, Lyu Y. H3N2 canine influenza virus and Enterococcus faecalis coinfection in dogs in China., 2019. BMC Vet Res. 15(1):113. doi: 10.1186/s12917-019-1832-x. PMID: 30975135; PMCID: PMC6460796

Zhu Z, Wang W, Jiang Z, Liu Y, Chang K, Ye Y, Xiong J. 2019. Influence of influenza A and B virus infections on human aortic smooth muscle cells and the expressions of cytokines. Journal of Medical Postgraduates. (12): 132-137

Zitzow, L.A., Rowe, T., Morken, T., Shieh, W.-J., Zaki, S., Katz, J.M., 2002. Pathogenesis of Avian Influenza A (H5N1) Viruses in Ferrets. J Virol 76, 4420–4429. https://doi.org/10.1128/jvi.76.9.4420-4429.2002